Recombinant expression and initial characterisation of two *Plasmodium* copper binding proteins

by

David L. Choveaux

BSc (Hons) Biochemistry (UKZN)

Submitted in fulfilment of the
academic requirements for the degree of
Doctor of Philosophy
in
Biochemistry

School of Biochemistry, Genetics and Microbiology
University of KwaZulu-Natal
Pietermaritzburg

May 2011

Preface

The experimental work described in this thesis was carried out in the School of Biochemistry, Genetics and Microbiology, University of KwaZulu-Natal, Pietermaritzburg, South Africa from January 2008 to April 2011, under the supervision of Professor J.P. Dean Goldring. The studies represent original work by the author and have not otherwise been submitted in any form to another University. Where use has been made of the work of others it is duly acknowledged in the text.

David L. Choveaux
May 2011

J.P. Dean Goldring

Declaration – Plagiarism

I, David Choveaux, declare that:

1. The research reported in this thesis, except where otherwise indicated, is my original research.

2. This thesis has not been submitted for any other degree or examination at any other University.

3. This thesis does not contain other persons' data, pictures, graphs or other information, unless specifically acknowledged as being sourced from other persons.

4. This thesis does not contain other persons' writing, unless specifically acknowledged as being sourced from other researchers. Where other written sources have been quoted, then:
    a. Their words have been re-written but the general information attributed to them has been referenced
    b. Where their exact words have been used, then their writing has been placed in italics and inside quotation marks, and referenced

5. This thesis does not contain text, graphics or tables copied and pasted from the internet, unless specifically acknowledged, and the source being detailed in the thesis and in the References sections.

Signed: _____

David L. Choveaux

Abstract

Plasmodium falciparum is a protozoan parasite responsible for the most severe form of human malaria, with infection often resulting in death. Efforts to control malaria have been hindered by an increased spread of parasite resistance to previously effective antimalarial drugs, leading to an intensified search for novel antimalarial drug targets. A group of proteins suggested as potentially effective targets are the integral membrane transport proteins, since they play key roles in *Plasmodium* parasite growth and replication. One such membrane protein recently characterised was the *P. falciparum* copper efflux transporter. Treatment of cultured *P. falciparum* parasites with the intracellular copper chelator neocuproine inhibited parasite growth, suggesting that additional mechanisms for malaria parasite copper homoeostasis are likely to be present. Copper is an essential trace element involved in enzymatic processes requiring redox-chemistry. In higher eukaryotes copper is transported across the plasma membrane via the copper transport protein, Ctr1, and distributed intracellularly by copper metallochaperones. The mechanisms for copper acquisition and distribution in the *Plasmodium* parasite are, however, yet to be characterised.

An *in silico* Basic Local Alignment Search Tool for protein (BLASTp) screen of the *Plasmodium* database (www.plasmodb.org) identified sequences corresponding to a putative copper transporter, and associated copper metallochaperones, in eight species of the *Plasmodium* parasite. Each of the *Plasmodium* copper transport protein sequences was found to contain features common to the well characterised copper transporters. These features included predicted copper-binding motifs in the protein's amino terminus, three membrane spanning domains and the characteristic MxxxM and GxxxG motifs located in the second and third transmembrane domains, respectively. Affinity purified anti-peptide antibodies, generated against an immunogenic peptide (CSDKQSGDDECKPILD) in the amino terminus of a putative malaria parasite copper transporter (PY00413), detected the target protein in murine malaria parasites in association with a parasite membrane. The open reading frames corresponding to the amino terminal domains of one *P. berghei* [PBANKA_130290 (447 bp)] and two *P. falciparum* [PF14_0211 (132 bp) and PF14_0369 (282 bp)] putative copper transport proteins were PCR amplified, ligated into pGEM®-T and then expressed as recombinant fusion proteins with maltose binding protein (MBP). The resulting sizes for the recombinant proteins were 61kDa for MBP-*Pb*CtrNt, 48kDa for MBP-*Pf*Ctr211Nt^{TD} and 55kDa for MBP-*Pf*Ctr369Nt^{TD}, with each protein being recognised by a corresponding anti-peptide antibody. All three recombinant proteins bound copper *in vitro* and *in vivo*, with each having a binding preference for the reduced cuprous ion. This preference has been similarly established for the characterised copper transporters. Although the results supported the expression and copper binding ability of

a *Plasmodium* parasite copper transport protein, the directional transport of copper, by this protein, requires experimental confirmation as does its specific location.

The identification of a *P. falciparum* copper transporter, and other copper dependent proteins, implies a parasite metabolic requirement for copper. Mammalian and yeast cells require a Cox17 metallochaperone for copper delivery to cytochrome-c oxidase. Identification of *P. falciparum* orthologs for Cox17 (PF10_0252) and a number of cytochrome-c oxidase subunits (PF13_0327; PF14_0288; mal_mito_1; mal_mito_2; PFI1365w; PFI1375w), suggests the existence of similar parasite mechanisms for copper delivery. Analysis of the *Plasmodium* Cox17-like sequences identified essential amino acids conserved in the well characterised yeast and mammalian Cox17. This included the identification of six cysteine residues essential for Cox17 function. A homology model of *P. falciparum* Cox17, with human Cox17 as the template [PDB ID: 2RN9 (apoCox17); 2RN8 (Cu^{+}-Cox17)], suggested that *Plasmodium* Cox17 orthologs would adopt a similar structural conformation. The open reading frames for full-length *P. yoelii* [PY03823 (192 bp)] and *P. falciparum* [PF10_0252 (195 bp)] Cox17 were PCR amplified, ligated into pGEM®-T and then expressed as recombinant fusion proteins with either a His_6-tag or glutathione S-transferase (GST)-tag, respectively. The resulting sizes for the recombinant proteins were 11.6kDa for His_6-*Py*Cox17 and 33.5kDa for GST-*Pf*Cox17, with each protein being recognised by a corresponding anti-peptide antibody. Both recombinant Cox17 proteins bound the cuprous ion *in vitro* and *in vivo*, similar to mammalian and yeast Cox17. This supported the likely existence of a mitochondrial copper metallochaperone pathway within the malaria parasite; however, this requires further experimental confirmation. Identification of a parasite copper transport protein, and associated metallochaperones, could provide novel targets for drug-based inhibition of parasite growth. Alternatively, the copper transporter may provide a novel mechanism for drug delivery into the *Plasmodium* parasite. The potential of these malaria parasite proteins being effective drug targets does, however, remain to be confirmed.

Acknowledgements

I would like to express my appreciation toward the following people and organisations for their invaluable contribution to this study:

My supervisor, Professor J.P. Dean Goldring for his expert advice, guidance, patience and for the conference road trips. Also a big thank you for all the help with this thesis.

Professor Theresa H.T. Coetzer for her advice and assistance through the duration of this study.

Charmaine Ahrens and Robyn Hillebrand for all their help with any administrative duties.

My laboratory colleagues and fellow post-graduate students, especially Ikechukwu Achilonu, Jacky Viljoen, Bridgette Cumming, Ramona Hurdayal, Davita Pillay, Philia Vukea, Robert Krause and Melissa Govender.

The National Research Foundation and the University of Kwazulu-Natal for financial assistance.

My mother, Nora Choveaux, and Robert Symons for their help, support and motivation from the beginning to the end of my studies.

To my sisters Ruth, Sarah and Katherine thanks for being there for me.

Last, but not least, to my wife Tarryn Choveaux for all the personal sacrifices, constant support and belief in me that helped get me through to the finish line. Tarry, you've been amazing.

Contents

List of Figures

List of Tables

Abbreviations

2xYT	2 x yeast extract, tryptone
3D	three-dimensional
A_x	absorbance at x nm
ABTS	2,2-azino-di-(3-ethylbenzthiazoline sulfonate)
α-Bu	alpha-butyric acid
AP	alkaline phosphatase
BCA	bicinchoninic acid
Bis	N,N'-methylenebisacrylamide
BLAST	basic logical alignment search tool
bp	base pairs
BSA	bovine serum albumin
CCO	cytochrome-c oxidase
CCS	copper chaperone for superoxide dismutase
cDNA	copy deoxyribonucleic acid
CHCH	coiled-coil-helix-coiled-coil-helix
C-terminal	carboxy terminal
Ctr1	copper transport protein 1
Ctr2	copper transport protein 2
Ctr3	copper transport protein 3
Cu/Zn SOD	Cu/Zn superoxide dismutase
DAPI	4,6-diamidino-2-phenylindole
DDC	diethyldithiocarbamate
DDT	dichloro-diphenyl-trichloroethane
DEPC	diethylpyrocarbonate
dH_2O	distilled water
ddH_2O	double distilled water
DMF	dimethylfluoride
DMSO	dimethylsulfoxide
dNTP	deoxynucleotide triphosphate
DTT	dithiothreitol
ECL	enhanced chemiluminescence
EDTA	ethylenediaminetetra-acetic acid
ELISA	enzyme-linked immunosorbent assay
ESI-MS	electrospray ionization mass spectrometry
FCA	Freund's complete adjuvant

FIA	Freund's incomplete adjuvant
FITC	fluorescein isothiocyanate
GFP	green fluorescent protein
GST	glutathione S-transferase
H_2Asc	ascorbic acid
HEPES	4-(2-hydroxyethyl)-1-piperazineethanesulfonic acid
HPLC	high pressure liquid chromatography
HRP	horseradish peroxidase
ID	identification
IPTG	isopropyl-beta-D-thiogalactopyranoside
kDa	kilo Daltons
LB	Luria Bertani
LDH	lactate dehydrogenase
MBP	maltose binding protein
MBS	M-maleimidobenzoic acid N-hydroxysuccinimide
MCS	multiple cloning site
MEC	molecular exclusion chromatography
N-terminal	amino terminal
NMR	nuclear magnetic resonance
ORF	open reading frame
PAGE	polyacrylamide gel electrophoresis
**Pb*CtrNt	amino terminal domain of *Plasmodium berghei* copper transporter
PBS	phosphate buffered saline
PCR	polymerase chain reaction
PDB	protein data bank
PEG	polyethylene glycol
PEXEL	*Plasmodium* export element
**Pf*Cox17	*Plasmodium falciparum* Cox17
**Pf*Ctr211Nt^{TD}	truncated amino terminal domain of *Plasmodium falciparum* PF14_0211
**Pf*Ctr369Nt^{TD}	truncated amino terminal domain of *Plasmodium falciparum* PF14_0369
PlasmoDB	*Plasmodium* database
PMSF	phenylmethylsulfonylfluoride
PVDF	polyvinylidene difluoride
**Py*Cox17	*Plasmodium yoelii* Cox17
RBC	red blood cell
RT	room temperature
RT-PCR	reverse transcription polymerase chain reaction

SAP	shrimp alkaline phosphatase
SDS	sodium dodecyl sulfate
SH	sulfhydryl group
TAE	Tris-acetate-EDTA
TBS	tris buffered saline
TCA	trichloroacetic acid
TD	truncated
TE	Tris-EDTA
TEMED	N,N,N',N'-tetramethyl ethylene diamine
Tris	2-amino-2-(hydroxymethyl)-1,3-propandiol
UV	ultraviolet
WHO	World Health Organisation
WT	wild type

*abbreviations introduced in this study

CHAPTER 1

Introduction

1.1 Overview of malaria

Malaria is a serious, acute and chronic relapsing infection. Over three billion people, representing approximately 40 percent of the world's population, live at risk of contracting the disease (Tuteja, 2007). Around 250 million malaria cases are reported annually, resulting in approximately a million deaths. More than 90 percent of these deaths are recorded in the sub-Saharan regions of Africa, with the majority being children under the age of five years (Breman *et al.*, 2004). Malaria is caused by a protozoan parasite, belonging to the *Plasmodium* genus, and is transmitted by the bite of the female *Anopheles* mosquito. More than 100 species of *Plasmodium* parasites infect multiple animal species including birds, reptiles and a number of mammals. However, only four species infect humans, namely *Plasmodium falciparum*, *Plasmodium vivax*, *Plasmodium ovalae* and *Plasmodium malariae*, although it was recently established that the primate-infecting *Plasmodium knowlesi* parasite can also infect humans with a potentially fatal outcome (Cox-Singh *et al.*, 2010; Galinski and Barnwell, 2009). In Southeast Asia, malaria caused by *P. knowlesi* is primarily a zoonosis with wild macaques acting as the reservoir hosts (Lee *et al.*, 2011). Symptoms of malaria can develop as soon as six to eight days following a mosquito bite or as late as several months following departure from a malarious area (Tuteja, 2007). Malaria is generally characterised by fever, headache, painful joints, respiratory distress, watery diarrhoea, vomiting and convulsions (Miller *et al.*, 2002). Human mortality, as a result of malaria infection, is predominantly caused by *P. falciparum*. This form of malaria is complex with several pathogenic processes such as jaundice, kidney failure and severe anaemia combining to cause an often fatal outcome (Miller *et al.*, 2002). In malaria endemic countries the severity of malaria is reflected by economic hardship. It is estimated that, on average, malaria causes a 1.3% loss to annual economic growth in endemic countries owing to a reduction in productivity (Sachs and Malaney, 2002). Efforts to prevent and control the disease have, more recently, been hindered by an increased parasite resistance to currently available antimalarial drugs (Crompton *et al.*, 2010; Ekland and Fidock, 2008). This problem underlines the requirement for novel antimalarial drug development (Gamo *et al.*, 2010; Le Roch *et al.*, 2003; Rosenthal, 2003; Staines *et al.*, 2010).

1.1.1 Geographical distribution of malaria

In 2007 the global area at risk of *P. falciparum* malaria infection was 29.73 million km^2, predominantly distributed between the Americas, Africa and Central and South East Asia (Figure 1.1) (Hay *et al.*, 2009). This affected area is largely distributed between the tropics and

subtropics, with many areas of the tropics highly endemic for the disease. The countries of sub-Saharan Africa account for the majority of all recorded malaria cases with the remainder accounted for in India, Brazil, Afghanistan, Sri Lanka, Thailand, Indonesia, Vietnam, Cambodia and China (Tuteja, 2007). In Africa, malaria is highly endemic in western and central countries, particularly around the Congo basin. Disease transmission is largely seasonal with peak infection rates occurring during the rainy season as a result of increased mosquito reproduction (Hay *et al.*, 2009). In more temperate regions, such as Western Europe and the USA, malaria has been successfully eradicated as a result of public health measures and economic development (Tuteja, 2007).

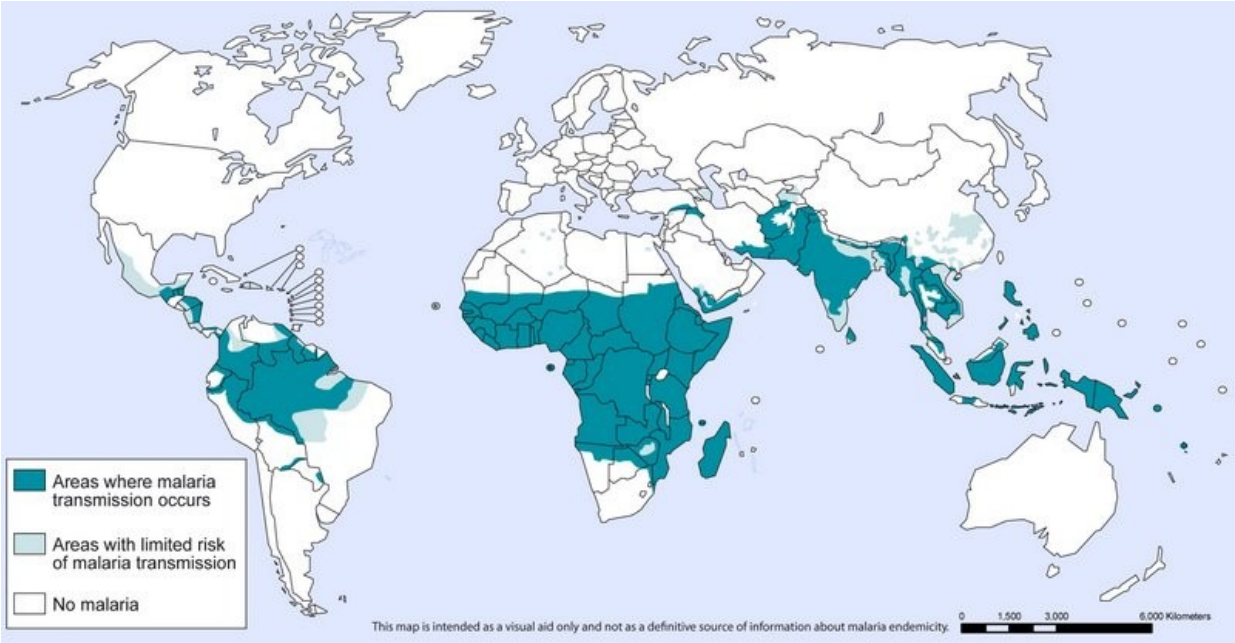

Figure 1.1 Global distribution of malaria

Countries at risk of malaria transmission are highlighted. The severity of disease transmission in Africa is clearly evident. Data is according to the World Health Organisation (WHO).

Malaria transmission in the Southern African countries of Botswana, Namibia, South Africa and Zimbabwe is highly seasonal with a generally lower transmission intensity than the rest of sub-Saharan Africa (World Health Organisation, 2010). In South Africa the main malaria areas are the low-lying parts of the Limpopo province, Mpumalanga province and the north-eastern parts of Kwazulu-Natal. Approximately 10 percent of the South African population lives at risk of malaria and although this disease continues to be a problem, the effects of malaria were much more severe in the early 20th century (Tren and Bate, 2004). Malarial areas during this period extended as far southwards as Port St Johns (Eastern Cape) and as far inland as Pretoria (Gauteng). This area was significantly reduced with the introduction of dichloro-diphenyl-trichloroethane (DDT) (Maharaj *et al.*, 2005). Indoor residual spraying and the use of

artemisinin-based combination therapy, from 2001, has since helped maintain low numbers of malaria cases in South Africa (World Health Organisation, 2010).

1.1.2 A brief history of malaria

Malaria, as a disease, is one of the most ancient infections known to man. However, it was not until the end of the nineteenth century (1880) that Alphonse Laveran, a French army physician, discovered that malaria was not the result of air emanating from swamps, but rather the result of an infection by a parasite belonging to the *Plasmodium* genus (Lavaran, 1881; Tren and Bate, 2004). Thereafter, in 1898, Sir Ronald Ross, a British army surgeon, identified that it was the *Anopheles* mosquito that acted as the parasite vector, transmitting the parasite from one host to the next (Ross, 1899). To this day, malaria remains an economic and social health burden to many developing countries. An effective vaccine is yet to be developed and controlling the disease is made increasingly difficult by the parasite's resistance to an array of previously effective chemotherapeutics (Crompton *et al.*, 2010; Olliaro and Yuthavong, 1999; Rosenthal, 2003).

Early in the 20th century malaria was a severe problem in South Africa, dramatically affecting farming and economic activies (Tren and Bate, 2004). The manifestation of this disease was largely due to the infiltration of labourers carrying the disease, combined with heavy rain fall around the same time. Together these factors created ideal conditions for the breeding of the *Anopheles* vector and thus the spread of malaria (Tren and Bate, 2004). In an effort to control the spread of the disease, testing of insecticides began in KwaZulu-Natal in 1931 and by 1932 a widespread residual house-spraying programme, using pyrethrum, was established. This was soon replaced, in 1946, by the more effective insecticide DDT (Mabaso *et al.*, 2004). Due to environmental safety issues surrounding the use of DDT, this insecticide was replaced by the pyrethroid deltamethrin in 1996. Unfortunately this policy shift resulted in the re-emergence of the *Anopheles funestus* vector, owing to its pyrethroid-resistance, subsequently causing a significant increase in the number of reported malaria cases and deaths (Figure 1.2). As a result, DDT was reintroduced in 2000 causing a significant reduction in the number of malaria cases and deaths reported (Figure 1.2).

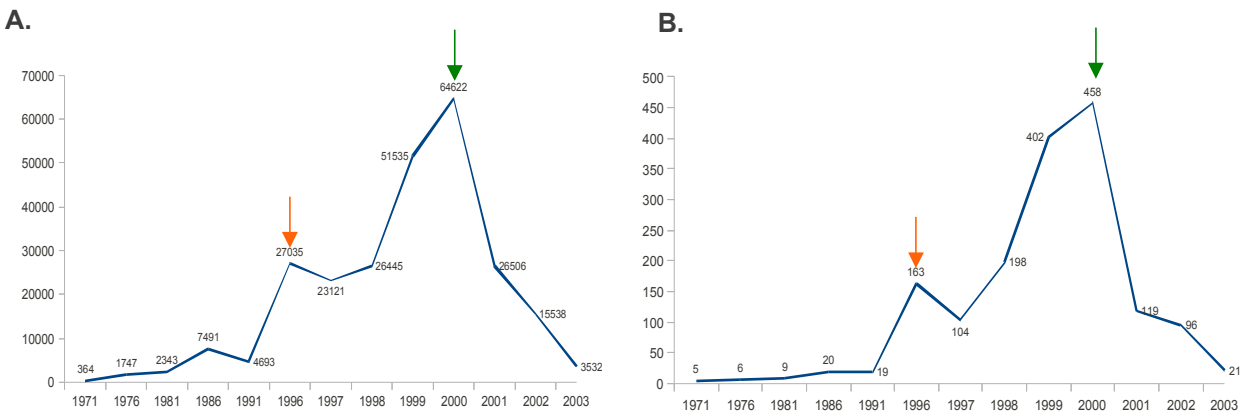

Figure 1.2 Annual number of reported malaria cases and deaths in South Africa

The number of malaria cases (**A**.) and deaths (**B**.) reported in South Africa between 1971 and 2003 are plotted. Data was according to the South African Department of Health. DDT spraying was stopped in 1996 (↓) but then reintroduced in 2000 (↓) (Mabaso *et al*., 2004).

The use of insecticides, such as DDT, controls the spread of malaria by limiting mosquito survival. Although insecticide treatment reduces the number of reported malaria cases and deaths, it has no direct effect on the *Plasmodium* parasite. The malaria parasite still manages to lead a very destructive path amongst humans, especially amongst children who are at the most risk of infection (Rosenthal, 2003). This point is highlighted by the fact that, in South Africa alone, the *Plasmodium* parasite has developed resistance to both chloroquine (by 1985) and sulfadoxine pyrimethamine (by 2000), reaching levels at which these drugs can no longer be used in monotherapy (Guidelines for the prevention of malaria in South Africa, 2003). This, in turn, has lead to changes in chemoprophylaxis and treatment policies in South Africa where artemisinin-based combination therapy is now the preferred method of disease treatment (World Health Organisation, 2010). The requirement for new treatment policies, in South Africa alone, further highlights the necessity for novel drug design and new target identification.

1.1.3 The *Plasmodium* parasite life cycle

The life cycle of the *Plasmodium* parasite is extremely complex with one stage of asexual development in the vertebrate host and a second stage of sexual development within the invertebrate mosquito vector (Figure 1.3). Parasite survival relies on the expression of specialised proteins for the invasion of a variety of cell types and for the evasion of host immune responses (Tuteja, 2007). With a single mosquito bite infective sporozoites are injected into the human host blood stream, where they are slowly released from the site of injection and migrate to the liver (Yamauchi *et al.*, 2007). Once the liver cells have been invaded, *P. falciparum* and *P. malariae* trigger immediate schizogony. On the other hand, *P. vivax* and *P. ovale* can either trigger immediate schizogony or delay this process and pass through the

hypnozoite stage, which are dormant parasites found in the liver (Tuteja, 2007). This stage of asexual replication, known as exo-eryhtrocytic schizogony, gives rise to tens of thousands of merozoites inside the hepatocytes. Each merozoite that is released from the liver is then capable of infecting a new red blood cell. The time taken to complete this tissue stage of development varies between species and is known as the prepatent period. Only after this period, and during the erythrocytic stage of parasite development, do the clinical symptoms and pathology of malaria become evident (White, 1992; van den Ende and van Gompel, 1997).

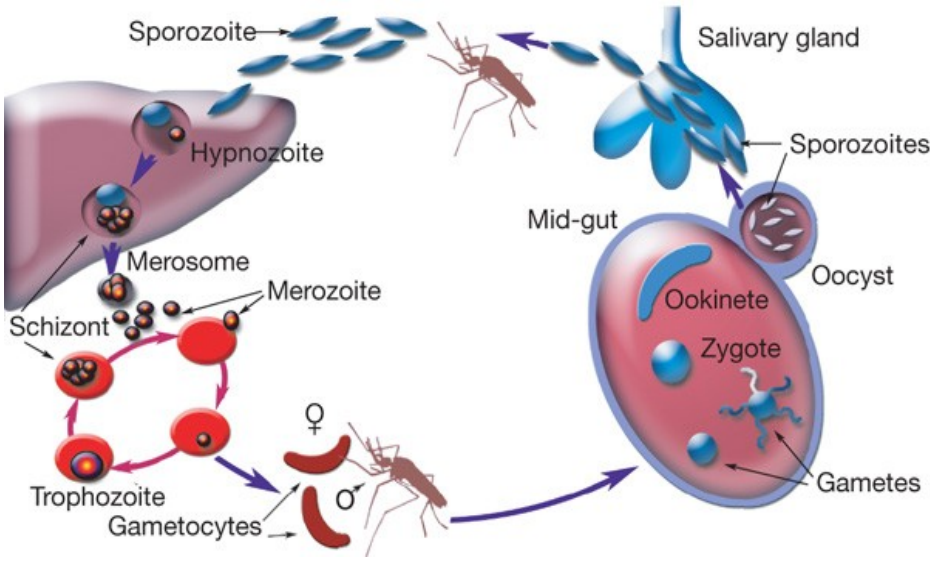

Figure 1.3 Life cycle of the *Plasmodium* parasite

The life cycle of the malaria parasite is complex. One stage of asexual development occurs within the vertebrate host (left side of cycle), whilst the second stage of sexual development occurs within the invertebrate mosquito vector (right side of cycle). Adapted from Winzeler (2008).

Following merozoite release from hepatocytes, the merozoites enter erythrocytes by a complex invasion process that is divided into four distinct phases (Miller *et al.*, 2002). The entry and exposure of merozoites in the blood stream, coupled with the highly specific series of molecular interactions for erythrocyte invasion, has implicated this stage as an attractive target for the development of anti-malarial strategies (Crompton *et al.*, 2010; Frevert *et al.*, 1993). Once inside the erythrocyte the merozoite begins asexual division, with the parasite developing through a number of different stages. These stages progress from the early trophozoite, or ring stage, to the trophozoite and finally the schizont stages of development (Figure 1.3). Each mature schizont contains merozoites that are released following red blood cell lysis and these invade new, uninfected red blood cells. This repetitive cycle of invasion-multiplication-release-invasion continues, taking around 48 h for *P. falciparum, P. ovale* and *P. vivax* infections whilst a *P. malariae* infection cycle takes around 72 h (Tuteja, 2007). Following a variable number of cycles of asexual schizogony, a small proportion of the merozoites do not enter this repetitive cycle of development but rather differentiate into micro- and macrogametocytes (male and

female, respectively). Gametocytes are ingested by the mosquito in a blood meal and these undergo sexual development within the mosquito midgut. The resulting ookinete penetrates the midgut cell wall, transforms into an oocyst and undergoes sporogony, producing numerous sporozoites (Figure 1.3). Sporozoites are then released by rupture and migrate to the salivary glands for onward transmission of the disease (Tuteja, 2007).

1.1.4 Treatment of malaria

Malaria is a curable disease if correctly diagnosed and promptly treated. Appropriate drug treatment of malaria and prophylactic drug treatment of newcomers to malarious areas are integral parts of malaria control (World Health Organisation, 2009). However, antimalarial drug resistance is hindering these efforts. Resistance to chloroquine, a previously effective and safe antimalarial administered as the first line of treatment for *P. falciparum* infections, was first documented five decades ago (Moore and Lanier, 1961). Other commonly used and cheap antimalarials against which the parasite has proven resistant are mefloquine, quinine and sulfadoxine-pyrimethamine (Hakim *et al.*, 1996; Koenderink *et al.*, 2010; Smithius *et al.*, 1997). To overcome the problem of resistance and increase the effective lifespan of antimalarials, combination therapy has been employed in many malaria endemic countries. However, even when used in combination new drugs are not impervious to resistance. Therefore the efficacy of currently used antimalarials is intensely monitored (World Health Organisation, 2009).

The effective action of chloroquine resulted in its global employment for malaria treatment until the emergence of resistance (Muregi and Ishih, 2010; Travassos and Laufer, 2009). Although it is no longer used for the treatment of *P. falciparum* infections, chloroquine is still the drug of choice to treat less severe but recurrent *P. ovale* and *P. vivax* malaria infections (Travassos and Laufer, 2009). *P. falciparum* resistance to chloroquine is mediated by the Chloroquine Resistance Transporter (*Pf*CRT) and is associated with a marked reduction in chloroquine accumulation in the parasite food vacuole (Martin *et al.*, 2009b). Chloroquine acts by inhibiting the parasite mechanism of haematin detoxification in the food vacuole, however, the replacement of *Pf*CRT lysine 76 with a threonine results in chloroquine export from the parasite food vacuole rendering the drug ineffective. This export mechanism is a direct result of the mutation since wild-type *Pf*CRT does not possess a chloroquine transport mechanism (Martin *et al.*, 2009b). Due to widespread chloroquine resistance, sulfadoxine-pyrimethamine was introduced as the replacement drug for malaria treatment. Sulfadoxine-pyrimethamine is composed of two drugs that act on sequential enzymes in the pathway for folate synthesis (Travassos and Laufer, 2009). However, the spread of parasite resistance to sulfadoxine-pyrimethamine was even more rapid than it was for chloroquine (Sibley *et al.*, 2001).

Consequently, the World Health Organisation (WHO) recommended the use of combination therapy that includes an artemisinin derivative for first-line treatment. By the end of 2009, 77 of the 86 *P. falciparum*-endemic countries and territories had adopted this recommendation (World Health Organisation, 2010).

Artemisinins are derived from the Chinese sweet wormwood plant, *Artemisia annua*, and have been used by Chinese herbalists for more than 2000 years (Maude *et al.*, 2010). Artemisinin and its derivatives, artesunate and artemether, are potent antimalarials that act rapidly by killing *Plasmodium* parasites throughout its erythrocytic life cycle (Pukrittayakamee *et al.*, 2004; White, 2008). Although the mechanism of action of artemisinin has not been fully elucidated, it is thought to inhibit a *Plasmodium* parasite sarco/endoplasmic reticulum ATPase (Eckstein-Ludwig *et al.*, 2003). Artemisinin is also thought to reduce malaria transmission since it acts on gametocytes as well (Pukrittayakamee *et al.*, 2004). If used in monotherapy, it is necessary to administer artemisinin over a five to seven day course to avoid the risk of recrudescent infection. Although the recurrent parasites are not resistant to artemisinin, they are capable of evading the short duration of activity exhibited by artemisinin (Ittarat *et al.*, 2003), therefore artemisinins are rather combined with a longer acting partner drug. Currently there are five recommended artemisinin-based combination therapies; artemether plus lumefantrine, artesunate plus amodiaquine, artesunate plus mefloquine, artesunate plus sulfadoxine-pyrimethamine and dihydroartemisinin plus piperaquine (World Health Organisation, 2010).

1.1.5 *Plasmodium* genomics and antimalarial drug discovery

Recent reports of *P. falciparum* resistance to artemisinin treatment (Dondorp *et al.*, 2009; Noedl *et al.*, 2008) highlights the urgent requirement for more selective and effective antimalarials. Identifying effective antimalarials and/or target proteins has been assisted by the sequencing of multiple *Plasmodium* parasite genomes, most recently including *P. vivax* and *P. knowlesi* (Carlton *et al.*, 2002; Carlton *et al.*, 2008; Gardner *et al.*, 2002; Pain *et al.*, 2008). The availability of these genome sequences has the potential to reveal a large number of novel genes and proteins important for parasite biology and pathogenesis. The genomics revolution has, however, yet to result in the development of new antimalarial drugs with target-based lead discovery producing disappointing results thus far. In fact, no new antimalarials have been introduced into clinical practice since 1996 (Gamo *et al.*, 2010). The functional genomics-based approach for target identification has, however, recently gained impetus through the release of a chemical library of *P. falciparum* intraerythrocytic cycle inhibitors from GlaxoSmithKline (Gamo *et al.*, 2010). Access to the chemical structures and associated data of a number of lead

compounds is hoped to help accelerate the pace of drug development for malaria.

An important feature of a candidate drug is that it demonstrates effective inhibition of a target essential to the life cycle of the parasite, resulting in parasite death. Furthermore it is important that the targeted protein does not show significant similarities to any host orthologs (Rosenthal, 2003). Although the availability of a drug repository assists with the identification of new antimalarials (Gamo *et al.*, 2010), novel drug design can follow several strategies, ranging from minor modifications of existing drugs to the design of novel agents (Olliaro and Yuthavong, 1999; Rosenthal, 2003). A group of proteins playing key roles in the growth and replication of the *Plasmodium* parasite are the integral membrane transport proteins (Krishna *et al.*, 2001; Martin *et al.*, 2005; Martin *et al.*, 2009a). Surprisingly though, these parasite proteins remain poorly understood and their potential as antimalarial drug targets remains largely underexploited (Kirk, 2004; Staines *et al.*, 2010). To date, more than 100 known and putative transporter sequences have been identified in the *P. falciparum* genome, with a large number considered to have therapeutic potential (Martin *et al.*, 2005; Martin *et al.*, 2009a; Staines *et al.*, 2010). However, only a few of these proteins have been sufficiently characterised to allow for potential targeting by antimalarials. One well characterised membrane protein is the *P. falciparum* copper efflux protein, *Pf*CuP-ATPase (Rasoloson *et al.*, 2004).

The identification of a novel *P. falciparum* copper efflux protein suggested the likely existence of more elaborate mechanisms for parasite copper homoeostasis, similar to those previously characterised in both yeast and mammalian systems (Kaplan and Lutsenko, 2009; Kim *et al.*, 2008; Lutsenko, 2010). Copper and its associated transport mechanisms have been established as essential to cell metabolism, suggesting copper would be similarly important to the parasite. Targeting parasite proteins required for copper homoeostasis could therefore be of possible therapeutic value. Supporting this idea was the finding that the copper chelators diethyldithiocarbamate (DDC) and neocuproine inhibited the growth of *P. falciparum* parasites *in vitro* (Meshnick *et al.*, 1990; Rasoloson *et al.*, 2004). Interestingly, the complexation of the antimalarials buparvaquone, pyridine-2-carboxamidrazone and 3-arylazo-4-hydroxy-1,2-napthoquinone to copper(II) significantly enhanced their antimalarial properties (Gokhale *et al.*, 2001; Gokhale *et al.*, 2003; Gokhale *et al.*, 2006). Although exact reasons for this enhanced activity were not determined, it was suggested to pertain to the positive reduction potentials of the copper compounds as well as their four-coordinate planar geometry. These properties were proposed to enhance the internalization and efficacy of these compounds (Gokhale *et al.*, 2001; Gokhale *et al.*, 2003). Alternatively, the enhanced activity was thought to be a result of site specific action, of the copper complex, on a component of the electron transport chain (Gokhale *et al.*, 2006). Taken together, these findings support further investigation of putative

Plasmodium spp. copper transport and distribution pathways for potential antimalarial targets.

1.2 Biological and physiological importance of copper

Copper is essential to life because of the catalytic and structural roles it plays in numerous proteins. The ability of copper to cycle between the stable oxidized Cu(II) and unstable reduced Cu(I) redox states is the property harnessed by cuproenzymes involved in various redox reactions. However, if not correctly managed, it is this same property that makes copper potentially toxic to cells (Camakaris *et al.*, 1999; Dameron and Harrison, 1998). As a result, cellular systems have evolved elaborate mechanisms to regulate intracellular copper concentrations and ensure targeted copper delivery to the necessary intracellular enzymes (Figure 1.4). Enzymes requiring copper as a cofactor are generally involved in fundamental biological processes necessary for cellular growth and development. These processes include iron transport, oxidative stress protection, peptide hormone production, skin pigmentation, blood clotting as well as connective tissue formation (Bertinato and L'Abbe, 2004; Lutsenko, 2010; Nose *et al.*, 2006; Puig and Thiele, 2002; Sharp, 2003). The average daily copper intake of an adult human ranges from 0.6 to 1.6 mg, with the main sources being grains, nuts, beans, shellfish and liver (Linder and Hazegh-Azam, 1996; Tapiero *et al.*, 2003). In normal human blood plasma, non-toxic concentrations of free copper ions are estimated to be in the order of 10^{-18} to 10^{-13} M (Linder and Hazegh-Azam, 1996), whilst a normal erythrocyte has about 20 μM copper, 70% of which is contained in Cu/Zn superoxide dismutase (Cu/Zn SOD) (Hatano *et al.*, 1982; Rasoloson *et al.*, 2004; Shields *et al.*, 1961). In excess of these normal cellular concentrations copper can, however, prove to be cytotoxic.

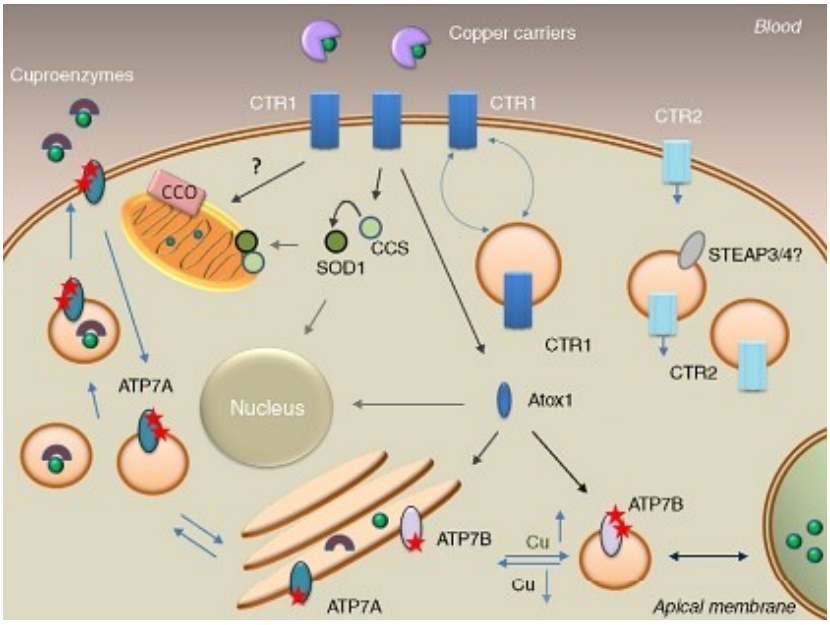

Figure 1.4 Copper acquisition and distribution in a generalised mammalian cell

Mechanisms of copper homoeostasis within a mammalian cell are both sophisticated and diverse. Following extracellular copper acquisition, by CTR1 or CTR2, entering copper is retrieved by copper chaperones having multiple functions: CCS distributes copper to SOD1 in the cytosol and mitochondria, Atox1 transfers copper to the secretory pathway and nucleus whilst an ensemble of proteins appear to deliver copper to cytochrome-c oxidase in mitochondria. CTR2 is predominantly localised intracellularly (for mobilisation of copper stores) but is also found associated with the plasma membrane. STEAP3/4 are presumed to act as intracellular reductases that facilitate copper transport across lysosomal membranes. ATP7A and ATP7B transport copper to the secretory pathway for incorporation into metalloenzymes and mediate copper excretion by sequestering excess copper in vesicles. Stars (★) represent phosphorylation of the Cu-ATPases, which is essential for protein trafficking between locations. CTR2 Adapted from Lutsenko (2010).

Copper, similar to iron, can undergo Fenton chemistry resulting in the production of the highly damaging hydroxyl radical ($Cu^{+} + H_2O_2 \rightarrow Cu^{2+} + \bullet OH + OH^{-}$). Hydroxyl radicals can cause membrane lipid peroxidation, direct oxidation of proteins and cleavage of both DNA and RNA (Halliwell and Gutteridge, 1984). Furthermore, excess free copper ions have been shown to exert a toxic effect by displacing other essential metal co-factors, such as zinc, from metalloenzymes thereby rendering these enzymes inactive (Predki and Sarkar, 1992). However, cellular systems avoid these negative effects through the evolution of sophisticated homoeostatic mechanisms (Figure 1.4). These mechanisms involve the influx and efflux of copper as well as processes whereby copper is delivered to various subcellular locations via specific copper metallochaperones (Kaplan and Lutsenko, 2009; Kim *et al.*, 2008; Leary *et al.*, 2009; Lutsenko, 2010; Rosenzweig, 2002). The importance of these mechanisms is perhaps best highlighted by Menkes and Wilson's diseases, which are human diseases caused by mutations to the *ATP7A* and *ATP7B* genes, respectively (Mercer, 2001; Shim and Harris, 2003). Both diseases are generally characterised by severe neurological disorders caused by copper imbalances and associated toxicity (Shim and Harris, 2003). Although not causally associated, imbalances in cellular copper concentrations have also been linked with Alzheimer's diseases (Kim *et al.*, 2008; Tapiero *et al.*, 2003).

Cu-ATPase-mediated excretion of excess copper has been proposed to be the main factor controlling cellular copper homoeostasis (Tapiero *et al.*, 2003). Equally important is the mechanism of copper acquisition and uptake, which is mediated by the integral membrane copper transport protein, Ctr1, in yeast and mammalian cells (Dancis *et al.*, 1994; Lee *et al.*, 2002; Zhou and Gitschier, 1997). The importance of Ctr1 to mammalian growth and development has been demonstrated in two independent gene-targeting studies in mice. The production of a *Ctr1*$^{-/-}$ phenotype, through gene knock-out experiments, resulted in the termination of embryonic development midway through gestation thereby supporting an essential role for this protein (Kuo *et al.*, 2001; Lee *et al.*, 2001). A similar observation was made following gene knock-out of the *Drosophila melanogaster Ctr1B* gene, which also resulted in developmental defects and arrest (Zhou *et al.*, 2003). Once transported into the cell, copper is distributed to specific destinations via dedicated copper metallochaperone proteins. These proteins include CCS, which distributes copper to Cu,Zn superoxide dismutase in the cytosol and mitochondria, Atox1, which transfers copper to the secretory pathway and nucleus, whilst an ensemble of proteins delivers copper to cytochrome-c oxidase in mitochondria (Kim *et al.*, 2008; Lutsenko, 2010; Rosenzweig, 2002). With regards to the *Plasmodium* parasite, currently there is limited research focussed on identifying mechanisms of copper homoeostasis. To date, a mechanism for copper efflux, by the *Pf*CuP-ATPase protein, has been proposed (Rasoloson *et al.*, 2004); however, mechanisms of copper acquisition and distribution remain uncharacterised.

1.2.1 Acquisition of copper and the copper transport protein

In eukaryotic cells the copper transport protein, Ctr1, plays a key role in copper uptake. Depending on cell type, this integral membrane protein can be found associated with either the plasma membrane or intracellular vesicles (Figure 1.4). This has been hypothesised to be reflective of a protective post-translational control mechanism against the accumulation of excessive intracellular copper concentrations (Klomp *et al.*, 2002; Ooi *et al.*, 1996). A single Ctr1 polypeptide is characterised by three transmembrane domains, a methionine-rich amino terminus and an essential MxxxM motif in the second transmembrane domain (Puig *et al.*, 2002a) (Figure 1.5). This conserved and essential methionine motif has been implicated in modulating the protein's affinity for copper and the rate of its transport by Ctr1 (Eisses and Kaplan, 2005; Puig *et al.*, 2002a). Genetic, biochemical as well as recent two- and three-dimensional crystallographic studies indicate that Ctr1 is present in the membrane as a homotrimer (Aller *et al.*, 2004; Aller and Unger, 2006; De Feo *et al.*, 2009; Lee *et al.*, 2002) with the translocation pore or pathway formed at its centre (Aller and Unger, 2006; De Feo *et al.*,

2009). Protein oligomerisation is essential to Ctr1 function, with stable oligomer formation dependent on a GxxxG motif (Figure 1.5) in the third transmembrane domain (Aller *et al.*, 2004; Eisses and Kaplan, 2002) as well as a cysteine residue in the carboxy terminus (Eisses and Kaplan, 2005; Lee *et al.*, 2007).

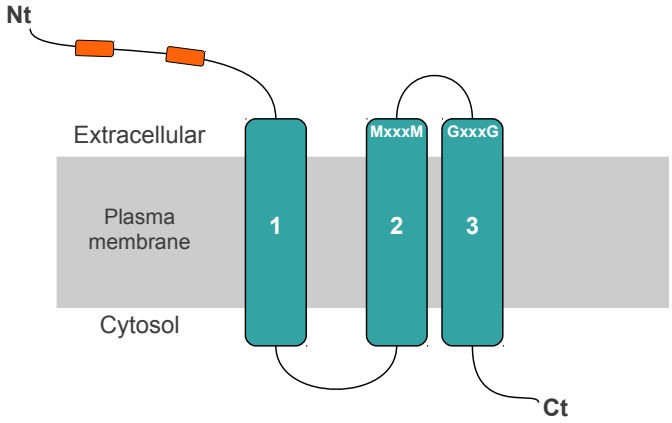

Figure 1.5 Schematic representation of the features characteristic of the copper transport proteins

Copper transport proteins are characterised by three transmembrane domains (1 – 3) resulting in a topology that places the amino terminus (Nt) extracellularly and the carboxy terminus (Ct) intracellularly. Methionine motifs (—) are found in the Nt for initial copper acquisition. The two most important motifs for function and oligomeric structure are MxxxM and GxxxG, located in the second and third transmembrane domains, respectively.

The mechanism by which Ctr1 transports copper is likely to be passive since Ctr1 function is unaffected by metabolic inhibitors (Lee *et al.*, 2002). Additionally, Ctr1 protein sequences lack an identifiable ATP-binding domain. In yeast, copper uptake via Ctr1 is dependent upon the Cu^{2+}/Fe^{3+} metalloreductases Fre1 and Fre2 for maximal activity (Georgatsou *et al.*, 1997; Hassett and Kosman, 1995; Rees and Thiele, 2007), with Cu^{+} presumed to be the transported species. In agreement with this, was the finding that in human cells divalent metal ions do not inhibit copper uptake whereas isoelectric and similar sized Ag^{+} ions block hCtr1-mediated copper uptake (Bertinato *et al.*, 2010; Lee *et al.*, 2002). Furthermore, the reductant ascorbic acid has been shown to enhance ^{64}Cu uptake in both yeast and human cell lines (Puig *et al.*, 2002a). In addition, it has been established that the Cu^{+} ion is the preferred species for intracellular distribution. This was supported by a study demonstrating the efficient and rapid transfer of Cu^{+} ions from a recombinant yeast copper transport protein carboxy terminus to the Atx1 metallochaperone (Xiao and Wedd, 2002). Transfection studies and copper uptake assays, with yeast and mammalian cells, have established that Ctr1 has a Michaelis-Menten K_M for copper in the low micromolar range (1-5 μM) (Dancis *et al.*, 1994; Lee *et al.*, 2002).

A second copper transport protein, identified in both yeast and human cells, is Ctr2 (Rees *et al.*, 2004; Zhou and Gitschier, 1997). Ctr2 is a low-affinity copper transporter that is largely

intracellular in human cells (van den Berghe *et al.*, 2007) and is predicted to function in releasing copper from vacuole compartments in yeast cells (Rees *et al.*, 2004). A small fraction of overexpressed human Ctr2 does, however, appear to localise at the plasma membrane where it can mediate copper uptake (Bertinato *et al.*, 2008). Reasons for this location are unknown, however, it is thought to perhaps help facilitate copper import when Ctr1 is downregulated (Lutsenko, 2010). Similar to Ctr1, Ctr2 functions in tandem with a reductase to convert Cu^{2+} to Cu^{+} for translocation across the membrane of the lysosome (Rees and Thiele, 2007). Since lysosomes are predicted to have an oxidising environment compared to the cytosol, the action of a reductase is required to maintain copper in the reduced form for successful translocation (Lutsenko, 2010). Due to structural similarities it is also presumed that Ctr2 would possess a similar biochemical mechanism to Ctr1 for the transport of copper across a membrane. However, further investigations into the role and mechanism of Ctr2, in mammalian cells, are still required.

1.2.2 Structural requirements for copper uptake

In general, membrane-bound transport proteins are of two possible orientations. The more commonly observed orientation is one where the protein has a sufficiently large enough monomeric structure capable of forming an independent translocation pore across the lipid bilayer (Aller and Unger, 2006). The alternative orientation is referred to as having a “half-transporter” architecture where a substrate is transported between the interface of two subunits. An example of such a protein is the *Escherichia coli* multidrug resistance efflux transporter EmrE (Ma and Chang, 2004). These transport proteins are thought of as being a hybrid between the classical transporter structure and the channel proteins, for example the potassium channels (Figure 1.6). Another class of proteins displaying a similar hybrid structure, is the Ctr1 family of proteins. The transporter function of Ctr1 is dependent on trimeric oligomerisation (Aller *et al.*, 2004) with its overall architecture lying somewhere between that of a traditional monomeric transporter and that of a channel (Figure 1.6).

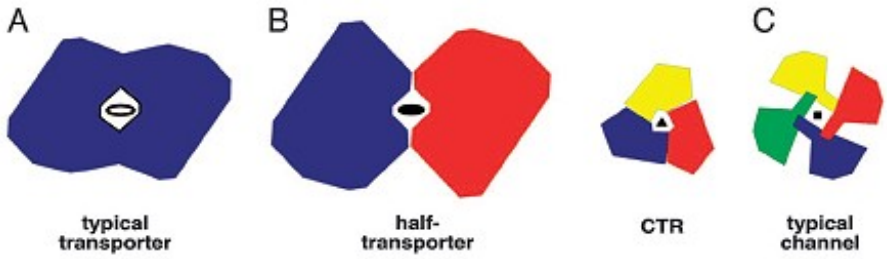

Figure 1.6 General structural orientation of transport and channel proteins

The majority of "typical" transport proteins contain a permeation pathway within a single monomer displaying pseudo twofold symmetry (**A**.). Half-transporter type proteins are generally composed of two subunits (**B**.). Each subunit contains 6-10 transmembrane domains that dimerise to form a pore through which substrates can be transported. In contrast, hCtr1 monomers are too small to form a pore, thus making oligomerisation essential for function (**C**.) This structure appears to be a hybrid of typical transporter and channel proteins. Adapted from Aller and Unger (2006).

The three-dimensional structure of Ctr1 was recently determined and yielded the first insights into the general organisation and operating principles of this family of proteins (Aller and Unger, 2006; De Feo *et al*., 2009). Despite their importance to cell physiology, the Ctr1 family of proteins vary greatly in primary sequence and length. Thus, it appears to be the overall design and architecture of the proteins rather than sequence identity that is key to their mechanism of transport. Indeed, it has been proposed that the first transmembrane domain of Ctr1 serves as an adaptor allowing evolutionarily distant copper transport proteins to adopt a similar, but not identical, overall structure (De Feo *et al*., 2010). Further supporting the conservation of protein structure for function, was the finding that human Ctr1 is functional in *Drosophila* cells (Hua *et al*., 2010). From the solved structure, it was proposed that copper uptake occurs along the central threefold axis of the copper transporter trimer where the second transmembrane domain, with contributions from the first and third domains, creates a copper-permeable pore through the membrane (De Feo *et al*., 2009). This orientation was strongly supported by a tryptophan scan of human Ctr1 and yeast Ctr3 (De Feo *et al*., 2010). However, the precise mechanism by which copper is moved across the membrane, by Ctr1, remains only partially defined.

An improved model mechanism for copper translocation across the membrane was recently proposed (Aller and Unger, 2006; De Feo *et al*., 2009; De Feo *et al*., 2010). Due to its channel-like architecture, it was presumed that for Ctr1 to function correctly it would require a gating mechanism to control the influx of Cu^{+} ions. This was proposed to be achieved extracellularly through the amino terminus or intracellularly through interactions with residues of the second transmembrane domain (Eisses and Kaplan, 2005). Numerous lines of biochemical evidence have, in fact, largely implicated the MxxxM motif in controlling the gating and selectivity of

copper. In addition to this, it was suggested that the transport mechanism involves a conformational change of the protein during transport (De Feo et al., 2009). This idea was supported by an carbon-alpha trace model study of hCtr1, which suggested that copper ions are transported one at a time through the pore with the transmembrane subunits of the trimer alternating between four confirmations (Figure 1.7) (Schushan *et al*., 2010). Currently the favoured model for the Ctr1 transport mechanism is one in which copper is acquired by the extracellular amino terminus, transferred to the MxxxM motif thereby causing a conformational change allowing the copper ion to be transferred through the pore via a chain of copper exchange reactions between defined Cu^{+}-binding sites (De Feo *et al*., 2009; Schushan *et al*., 2010). The proposed kinetic control of copper movement through Ctr1 would also explain the protein's independence from an ATP-hydrolysis mechanism for transport (De Feo *et al*., 2009). To what extent the cytoplasmic carboxy terminus is involved is not yet fully understood, however, it is believed to regulate the entry of copper into the cytoplasm for transfer to the intracellular copper metallochaperones (Xiao and Wedd, 2002).

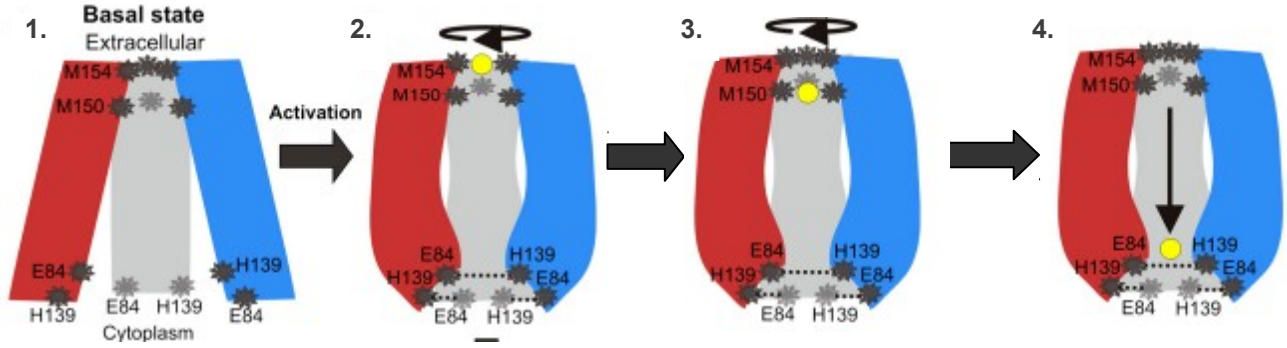

Figure 1.7 Proposed mechanism of transport for the human copper transport protein

The three Ctr1 subunits are shown in red, blue and grey with residues of interest depicted in dark grey and the copper ion in yellow. Step **1**: In its basal state no copper is bound to the transmembrane domains, with the Met154 triad serving as an external gate. Unprotonated His139 remains separate from Glu84. Step **2**: Activation, resulting from a pH shift or ion binding, causes a conformational change at the cytoplasmic end along with rotational movement at the extracellular end. Protonated His139 and Glu84 interact to stabilise the conformation. Step **3**: With a second conformational shift at the extracellular end the copper ion is passed from the Met154 triad to the Met150 triad. Met154 triad returns to blocking the pore entrance. Step **4**: The copper ion is then passed through the polar pore, although how the ion is passed to the carboxy tail remains to be determined. Adapted from Schushan *et al*. (2010).

1.3 Intracellular copper trafficking

Once copper enters the cell, soluble Cu^{+}-binding metallochaperones bind the ion and deliver it to target proteins through protein-protein interactions (Rosenzweig, 2002). Although it is not clear how these chaperones are loaded with Cu^{+}, it is thought to perhaps be through a direct interaction with the Ctr1 transporter (Xiao *et al*., 2004). Well characterised pathways of copper delivery include those for CCS (Copper Chaperone for Superoxide dismutase), which delivers

copper to Cu,Zn superoxide dismutase (SOD), as well as for Atox1, which transfers copper to the membrane-bound, copper transporting P-type ATPases in the secretory pathway (Figure 1.4) (Kim *et al*., 2008; Leary *et al*., 2009; Lutsenko, 2010). Copper is also required in the mitochondrion for the maturation and activity of cytochrome-c oxidase and Cu,Zn superoxide dismutase. In this regard, the copper metallochaperones Cox11, Cox17, Cox19, Sco1 and Sco2 are essential for the formation of a functional cytochrome-c oxidase complex (Cobine *et al*., 2006a; Leary *et al*., 2009). The mechanism by which copper is delivered to the mitochondrion does, however, require further elucidation (Kim *et al*., 2008; Lutsenko, 2010; Rees and Thiele, 2004).

1.3.1 Copper trafficking to the mitochondrion

Based on the localisation of Cox17 to the cytosol and mitochondrial intermembrane space, it was originally believed that this small, cysteine-rich protein was responsible for the delivery of copper to the mitochondrion (Beers *et al*., 1997; Glerum *et al*., 1996). The simple prediction was that Cox17 would shuttle Cu^{+} ions into the intermembrane space for use in the assembly of cytochrome-c oxidase. This idea was supported by the finding that purified Cox17 could bind copper (Heaton *et al*., 2001; Palumaa *et al*., 2004; Srivastava *et al*., 1997). However, by tethering Cox17 to the mitochondrial inner membrane only it was established that the *cox17Δ* cells displayed normal cytochrome-c oxidase activity, thereby reversing the expected respiratory defect. This therefore suggested that perhaps the function of Cox17 was spatially restricted to the intermembrane space (Maxfield *et al*., 2004). Consequently, it was proposed that Cox17 was still required for the delivery of copper to cytochrome-c oxidase, but it may not be metallated until reaching the intermembrane space. This was supported by the finding that a deletion of *COX17* did not decrease the total mitochondria-associated copper levels (Carr and Winge, 2003). It was found that the bulk of mitochondrial copper was localised within the matrix in a soluble, low molecular weight complex (Figure 1.8). This complex contains Cu^{+}, is resistant to proteinase K or trypsin digestion, is anionic and is eluted in a monodisperse fraction on reverse phase HPLC (Cobine *et al*., 2004). Furthermore, it was found that the complex could be depleted of Cu^{+} by two heterologously expressed copper binding proteins, human SOD1 or yeast Crs5 metallothionein, suggesting it could be involved in a copper delivery mechanism (Cobine *et al*., 2006b).

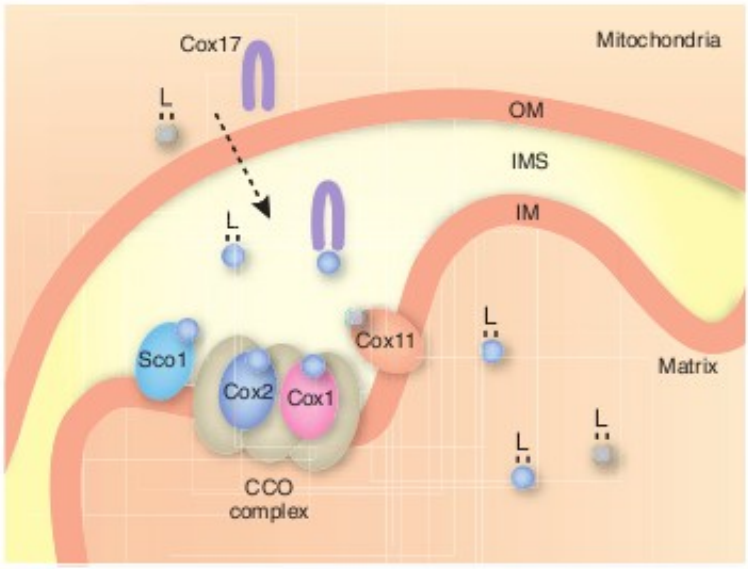

Figure 1.8 Metallochaperone-mediated loading of copper into mitochondrial cytochrome-c oxidase

Copper is shuttled from the cytoplasm to the mitochondrion by an as yet incompletely characterised mechanism. It is thought that a small ligand (denoted L) binds cytosolic copper and delivers it to the mitochondrial intermembrane space (IMS). The Cu^{+} ions are then bound by Cox17 for transfer to Sco1, which transfers copper to the Cox2 subunit, or to Cox11, which delivers copper to the Cox1 subunit of cytochrome-c oxidase (CCO). The novel copper ligand is thought to perhaps be involved in mitochondrial copper storage as well. Adapted from Kim *et al*. (2008).

Although the precise mechanism of copper delivery to the mitochondrion remains to be fully elucidated, the importance of copper to cytochrome-c oxidase assembly and function remains well documented (Cobine *et al*., 2006a; Kim *et al*., 2008; Leary *et al*., 2009). Copper is one of the catalytic cofactors in cytochrome-c oxidase, therefore copper insertion into this enzyme is essential for its function (Tsukihara *et al*., 1996). A number of accessory factors are important for the copper metallation of cytochrome-c oxidase. These include Cox11, Cox17, Sco1 and Sco2 (Figure 1.8), although Sco2 is not required in yeast cells (Cobine *et al*., 2006a). Three copper ions are inserted into two sites of cytochrome-c oxidase; a single ion into the Cu_B site and two ions into the Cu_A site. These sites are located in the Cox1 and Cox2 subunits respectively, which form part of the core cytochrome-c oxidase enzyme. The insertion of copper into the Cu_A and Cu_B sites is likely to occur in the intermembrane space with Sco1 and Cox11 implicated as the respective donor molecules (Carr *et al*., 2002; Hiser *et al*., 2000; Lode *et al*., 2000). These two co-metallochaperones obtain copper ions from Cox17 through transient interactions mediated by distinct structural interfaces (Horng *et al*., 2004). Copper transfer from Cox17 to Sco1 was also found to be coupled with a transfer of electrons, which was thought to perhaps assist with selective copper delivery (Banci *et al*., 2008a). The essential requirement for Cox17-mediated copper delivery is perhaps best highlighted by embryonic lethality in Cox17 null mice (Takahashi *et al*., 2002). Additionally yeast cells lacking Cox17 are respiratory deficient due to a lack of cytochrome-c oxidase activity, however, this mutant phenotype can be

suppressed by the addition of high copper salt concentrations to the growth medium (Glerum *et al*., 1996).

1.3.2 Structural features of Cox17

The Cox17 metallochaperone can readily adopt multiple oligomeric states and is thus capable of forming a number of distinct Cu^{+} conformers (Arnesano *et al*., 2005; Heaton *et al*., 2001; Voronova *et al*., 2007a). However, in the intermembrane space the bioactive conformer of Cox17 appears to consist of a single Cu^{+} ion coordinated to a monomeric protein stabilised by two disulfide bonds (Abajian *et al*., 2004; Banci *et al*., 2008b; Voronova *et al*., 2007b). This was supported by the finding that, *in vitro*, the partially oxidised state of Cox17 ($Cox17_{2S\text{-}S}$), containing a single copper ion, and not the fully oxidised form, containing four copper ions, transfers Cu^{+} to apoWT-hSco1 (Banci *et al*., 2007). In this active state, human Cox17 is structurally organised in a coiled-coil-helix-coiled-coil-helix (CHCH) structural motif with a flexible amino terminal tail. The single copper ion bound to this conformer is coordinated by two consecutive cysteine residues at positions C22 and C23 (Banci *et al*., 2008b). The additional Cox17 cysteine residues are organised in a twin CX_9C motif, located at the amino and carboxy-terminal ends of each helix of the CHCH motif, which form two interhelical disulfide bonds (Banci *et al*., 2008b). It has, however, been suggested for yeast Cox17 that only three of the six conserved cysteine residues are essential for *in vivo* function (Heaton *et al*., 2000; Punter and Glerum, 2003). These three essential cysteine residues are present in a $C^{23}CxC^{26}$ motif and are involved in copper coordination (Abajian *et al*., 2004; Heaton *et al*., 2000).

The import of Cox17, into the mitochondrial intermembrane space, is dependent on an oxidative folding mechanism. This is achieved by the TOM complex through a Mia40/Erv1 disulfide-relay process (Mesecke *et al*., 2005). Mia40 and Erv1 are located within the intermembrane space and mediate the import of small, cysteine-rich Tim proteins in addition to Cox17 (Rissler *et al*., 2005). Erv1 catalyses the formation of disulfides in Mia40 allowing it to transiently capture imported proteins, containing reduced thiolates, by forming interchain disulfide bonds. The bound polypeptides are then released by disulfide exchange reactions resulting in disulfide bond formation within the imported protein (Mesecke *et al*., 2005). Due to the highly reducing conditions of the cell cytosol, it is presumed that Cox17 exists in this environment in its fully reduced molten globule state, since this is necessary for its import into the intermembrane space (Mesecke *et al*., 2005). The two CX_9C motifs present in Cox17 are also present in Mia40 (Chacinska *et al*., 2004), thus it is presumed that the similar folds found in these proteins could be involved in the protein-protein recognition process that occurs during

Cox17 entrapment in the intermembrane space (Banci *et al*., 2008b). Once in the intermembrane space Cox17 is predominantly matured into the $Cox17_{2S\text{-}S}$. This state is presumed to predominate as a result of the more oxidative redox environment of the intermembrane space compared to the cytosol (Voronova *et al*., 2007b). This redox environment would allow for the reduction of the easily reducible disulfide bond, between the cysteine residues involved in copper binding, whilst the two disulfides in the CHCH motif are highly stable toward reduction and therefore unaffected (Banci *et al*., 2008b). $Cox17_{2S\text{-}S}$ would subsequently be loaded with copper in the intermembrane space for transfer to the two co-metallochaperones Sco1 and Cox11. These proteins then load copper into the Cu_A and Cu_B sites of cytochrome-c oxidase.

1.4 Outline of study

The ever increasing development of *Plasmodium* parasite resistance to previously effective antimalarial drugs, coupled to recent reports of reduced susceptibility to artemisinins in western Cambodia (Dondorp *et al*., 2009; Noedl *et al*., 2008), highlights the urgent need for new drugs. The advent of the genomics era was hoped to stimulate target-based lead discovery, however, to date this has yielded disappointing results (Gamo *et al*., 2010). In an effort to overcome these shortcomings, a web-based system was recently developed where researchers can mine information on malaria proteins, predict ligands, as well as perform comparisons to human and mosquito host protein characteristics. The resulting system, termed Discovery, has aimed at allowing the identification of putative protein targets as well as potential lead compounds (Joubert *et al*., 2009). Although the Discovery system offers a good starting platform, the development of new antimalarial drugs can still follow alternate strategies ranging from modifications of existing drugs to the design of novel agents against new targets (Rosenthal, 2003). In terms of new target identification, a largely under-exploited group of parasite proteins are the integral membrane proteins (Staines *et al*., 2010).

An attractive property of parasite membrane transporters, as drug targets, is the fact that the structure of these proteins, as well as their transport mechanisms, appear to be significantly different to host membrane proteins thus providing the potential for selective chemotherapeutics (Martin *et al*., 2009a; Rosenthal, 2003; Staines *et al*., 2010). The characterisation of a parasite membrane bound transporter, involved in copper ion efflux and localised to the parasite and erythrocyte membranes (Rasoloson *et al*., 2004), suggested the exploration of parasite copper metabolic pathways for novel targets. Targeting proteins involved in parasite copper homoeostasis is supported by the finding that the copper chelators

diethyldithiocarbamate and neocuproine inhibit *P. falciparum* growth *in vitro* (Meshnick *et al*., 1990; Rasoloson *et al*., 2004). Apart from the identification of the parasite P-type ATPase copper efflux protein (Rasoloson *et al*., 2004), limited data exists on parasite copper acquisition and distribution. The aim of the current study was to identify and characterise a novel membrane-bound copper transporter as well as an associated intracellular copper chaperone within the *Plasmodium* genus. Using both computational and biochemical methodology, each protein was assessed for its ability to potentially bind copper. The expression and localisation of each native protein was to be determined using anti-peptide antibodies. An expanded understanding of the *Plasmodium* parasite's copper metabolic pathways could help lead to the identification of novel antimalarial drug targets.

A BLASTp search of PlasmoDB lead to the identification of several copper-requiring protein orthologs, thus supporting the likely parasite requirement for cellular copper (Chapter 3). One of these protein orthologs identified corresponded with the intracellular copper metallochaperone Cox17. The identification of this and the other copper dependent proteins suggested the potential for a dedicated mechanism for parasite copper acquisition. A subsequent BLASTp search of the *Plasmodium* database was therefore employed and identified sequences for a copper transporter in eight species of the parasite (Chapter 3). A thorough *in silico* analysis of the putative *P. falciparum* copper transporter and Cox17 sequences was used to support the predicted function of each protein. In an effort to confirm native protein expression, the Predict7^{TM} computer algorithm (Cármenes *et al*., 1989) was used to identify immunogenic regions in each protein from both the murine and human malaria parasites (Chapter 3).

To establish the copper binding abilities of the parasite copper transporter and metallochaperone, significant amounts of purified protein was required. To this end, the coding domain for the predicted amino terminus of the copper transporter was PCR amplified and cloned (Chapter 4), whilst the full-length Cox17 metallochaperone was similarly amplified and cloned (Chapter 5). In both instances the coding domains were amplified from a rodent malaria parasite source as well as *P. falciparum*. Sequencing of the inserted products confirmed identity and supported the presence of a native parasite coding domain for each respective protein. Each protein was expressed in *Escherichia coli* and the recombinant proteins purified for functional studies. The ability of each recombinant protein to bind copper was tested both *in vitro* and *in vivo*. Copper was detected using the copper specific bicinchoninic acid assay (Brenner and Harris, 1995). Additionally, the *in vitro* copper binding ability of each respective recombinant protein was tested using the ascorbic acid oxidation assay (Chapter 4 and 5). To

establish native parasite protein expression and location, anti-peptide antibodies were raised in chickens (Chapter 4 and 5) and used in western blotting and immunofluorescent microscopy studies.

CHAPTER 2

Materials and methods

2.1 Introduction

This chapter describes the biochemical, immunochemical, parasitological and molecular biology techniques used in this study.

2.2 Materials

The following reagents and antibodies were purchased from Sigma-Aldrich-Fluka (Steinheim, Germany): 2-mercaptoethanol, 4-chloro-1-naphthol, acrylamide, ampicillin, avidin, Biomax® X-ray film, bisacrylamide, bromophenol blue, Coomassie Brilliant Blue G-250, Coomassie Brilliant Blue R-250, Ellman's Reagent, formamide, Freund's complete adjuvant, Freund's incomplete adjuvant, Giemsa stain, glycine, isopropyl β-D-1-thiogalactopyranoside (IPTG), L-cysteine, kanamycin, maleimidobenzoyl-*N*-hydroxysuccinimide ester (MBS), N-laurylsarcosine, ovalbumin, *p*-iodophenol, polyvinypyrrolidine, Ponceau S, rabbit serum albumin, saponin, Sephadex G-25, Sephadex G-10, *N,N,N',N'*-tetramethyethylenediamine (TEMED), Triton X-100, tryptone, Tween-20, urea and yeast extract. Bovine serum albumin was purchased from Roche (Mannheim, Germany). Equipment purchased from BioRad (California, USA): Poly Prep® affinity column, low range protein molecular weight marker, Mini Protean II™ vertical PAGE unit and the VersaDoc™ imaging system. The following were purchased from Fermentas (Vilinius, Lithuania): agarose, 10× T4 DNA ligase buffer, T4 DNA ligase, DNA MassRuler™, dNTP mix, *Eco*RI, molecular biology grade DTT, *Not*I, Buffer O™, shrimp alkaline phosphatase (SAP) and an unstained protein molecular weight marker. The pMal expression system and broad range protein molecular weight marker were purchased from New England BioLabs (Massachusetts, USA). Molecular biology reagents were purchased from Solis Biodyne (Tartu, Estonia), which included the 10× PCR buffer ($MgCl_2$ and detergent-free), PCR $MgCl_2$ stock solution (25 mM) and *Taq* polymerase. The *Escherichia coli* host cells, plasmids and antibodies purchased from Novagen (Damstadt, Germany) were BL21 (glycerol stock), BL21 (DE3) (glycerol stock), JM109 (glycerol stock) and JM103 (glycerol stock) cells; pET-23a and pET-28a plasmids; mouse monoclonal anti-His-Tag IgG, rabbit polyclonal anti-glutathione S-transferase IgG and peroxidase-conjugated sheep monoclonal anti-mouse IgG. Polyethylene glycol 6000 was purchased from Merck Biosciences (Damstadt, Germany). di-Ammonium 2,2'-azino-bis(3-ethybenzothiazoline-sulfonate) (ABTS) was purchased from Boehringer (Mannheim, Germany). An orbital shaking incubator was purchased from New Brunswick Scientific (New Jersey, USA). SulfoLink™ Coupling Gel and Snake skin™ dialysis membrane were purchased from Pierce

Perbio Science (Erembodegem, Belgium). pGEX-4T-1, Hybond-C™ Extra nitrocellulose membrane and the Ultraspec 2100*pro* UV/visible spectrophotometer were purchased from GE Healthcare (Buckinghamshire, England). Peroxidase-conjugated rabbit anti-IgY, peroxidase-conjugated rabbit anti-mouse IgG and peroxidase-conjugated goat anti-rabbit IgG antibodies were from Jackson Immunochemicals (Pennsylvania, USA). Ni-NTA® metal affinity resin was purchased from Qiagen (Duesseldorf, Germany). Improm II® Reverse Transcription System was purchased from Promega (Wisconsin USA). Oligonucleotide primers for the *P. yoelii* copper transport protein coding domain were synthesized by Whitehead Scientific (Johannesburg, South Africa). Oligonucleotide primers for the *P. falciparum* copper transport protein and Cox17 coding domains as well as *P. yoelii* Cox17 coding domain were synthesized by the Molecular and Cell Biology synthetic DNA unit at the University of Cape Town (Cape Town, South Africa). Synthetic peptides for all three copper transport proteins were synthesized by Auspep (Melbourne, Australia), whilst those for the two Cox17 metallochaperones were synthesized by GL Biochem (Shanghai, China). VersaMax™ ELISA plate reader was purchased from Molecular Devices Corporation (California, USA). Nunc Maxi Sorp™ 96-well ELISA plates were from Nunc products (Roskilde, Denmark). The DNA purification kit was purchased from PEQLAB Biotechnologie (Erlangen, Germany). An Avanti™ J-26 XPI centrifuge was from Beckman Coulter (California, USA). GeneAmp™ PCR thermocyler was from Applied Biosystems (California, USA). The Virosonic™ cell disruptor was purchased from VirTis (New York, USA).

2.3 Bioinformatics methods

This section describes the bioinformatics tools used in this study.

2.3.1 Sequence identification and analysis

Copper transport protein

To establish a parasite requirement for copper, the *P. falciparum* proteome (www.plasmodb.org) was BLASTp searched for the presence of copper-requiring protein orthologues (Table 3.1). The identification of a number of copper-requiring enzymes within the *P. falciparum* proteome suggested a need for copper for parasite metabolic function. Sequences for a putative *Plasmodium* copper transport protein were similarly identified by a Basic Logical Alignment Search Tool search for proteins (BLASTp) of PlasmoDB, using the *Theileria parva* (Muguga stock) polymorphic immunodominant molecule (PIM) (GenBank: AAA99499). Putative copper transport protein sequences were identified for eight species of the *Plasmodium* parasite. Each sequence was retrieved and saved as a text file in FASTA format. In an effort to support sequence identity, each retrieved *Plasmodium* spp. sequence was aligned with sequences of

characterised copper transport proteins using the ClustalW™ server (Thompson *et al.*, 1994). The characterised sequences included were for the *Homo sapiens* (Accession No. NP_001850), *Arabidopsis thaliana* (GenBank: BAE98928) and *Saccharomyces cerevisiae* (GenBank: AAB68064) copper transport proteins. To identify the presence of three characteristic transmembrane domains in the retrieved *Plasmodium* spp. sequences, each was submitted to both the HMMTOP (Tusnády and Simon, 2001) and TMHMM 2.0 (Krogh *et al.*, 2001) topology prediction servers. The presence of potential signal sequences in each protein was established using the TMHMM server as well as the SignalP 3.0 program (Center for Biological Sequence Analysis, Lyngby, Denmark). The presence of parasite specific targeting signals was determined using the PlasmoAP and PlasmoMit servers found at PlasmoDB as well as the PSEApred2 server for PEXEL motif prediction. The genome organisation of the two *P. falciparum* copper transport protein coding domains were constructed from information retrieved from PlasmoDB and the nucleotide database of the National Center for Biotechnology Information (NCBI). *P. falciparum* expression data for lactate dehydrogenase, S-adenosylhomocysteine hydrolase, Cox11 and cytochrome-c oxidase subunit I were retrieved from PlasmoDB.

Cox17

The sequence of a putative *Plasmodium* spp. Cox17 copper chaperone was identified from the BLASTp search of PlasmoDB for copper-requiring protein orthologues. The specific sequence used to search PlasmoDB was the *H. sapiens* Cox17 sequence (GenBank: AAA98114). As with the identification of a putative *Plasmodium* spp. copper transport protein sequence, a putative Cox17 sequence was identified in the same eight species of the parasite. To identify characteristic Cox17 features in each retrieved sequence, they were aligned with characterised Cox17 sequences using the ClustalW™ server (Thompson *et al.*, 1994). The characterised sequences included were the *H. sapiens* (GenBank: AAA98114), *A. thaliana* (Accession No. NP_566508) and *S. cerevisiae* (GenBank: CAA97453) Cox17 proteins. This alignment revealed the conservation of six cysteine residues known to be essential for Cox17 function. As with the copper transport proteins, the presence of potential signal sequences in each protein was established using the TMHMM server as well as the SignalP 3.0 server (Center for Biological Sequence Analysis, Lyngby, Denmark). The presence of parasite specific targeting signals was determined using the PlasmoAP and PlasmoMit servers found at PlasmoDB as well as the PSEApred2 server for PEXEL motif prediction. The genome organisation of the *P. falciparum* Cox17 protein coding domain was constructed from information retrieved from PlasmoDB and the nucleotide database of the National Center for Biotechnology Information (NCBI).

2.3.2 Homology modelling

A homology model of the putative *P. falciparum* Cox17 metallochaperone (PF10_0252) was constructed using the NMR-solved structures of *Homo sapiens* Cox17, with and without copper bound [Protein Data Bank (PDB) ID's: 2RN8 (plus Cu^{+}) and 2RN9 (minus Cu^{+})] (Banci *et al*., 2008b). Each of these structures were used individually to produce a *Pf*Cox17 model using the Swiss-pdb DeepView program (Guex and Peitsch, 1997). Once the desired *Hs*Cox17 structure was loaded into the DeepView program, the *Pf*Cox17 sequence was loaded for subsequent mapping. This was achieved by aligning the *Pf*Cox17 sequence to the *Hs*Cox17 sequence (AAA98114) with the assistance of a ClustalW™ alignment (Thompson *et al.*, 1994). Sequence insertions in the alignment resulted in unsolved gaps in the hypothetical *Pf*Cox17 structure. These were accounted for by inserting a fold that placed the least structural strain on the protein model. The predicted folds are derived from solved protein structures having similar amino acid sequence arrangements. The final hypothetical protein model was checked for amino acid side chain or backbone clashes and corrected as necessary.

2.3.3 Phylogenetic tree construction

For phylogenetic analysis of the retrieved sequences, the same approach was adopted for both the putative *Plasmodium* spp. copper transport protein and Cox17 sequences. The eight *Plasmodium* sequences, for each respective protein, were aligned with the relevant sequences from the organisms listed in Table 2.1. Sequences were aligned using the ClustalW™ server (Thompson *et al.*, 1994) and a phylogenetic tree constructed from this alignment. The resulting tree diagram was copied as a JPEG image and edited, if necessary, with the GIMP™ image editor software.

Table 2.1 Accession numbers of sequences used for copper transport protein and Cox17 phylogenetic tree construction

Organism	Accession number	
	Copper transport protein	Cox17
Homo sapiens	NP_001850	AAA98114
Mus musculus	NP_780299	BAB32486
Rattus norvegicus	NP_598284	NP_445992
Danio rerio	NP_991280	NP_001004652
Arabidopsis thaliana	BAE98928	NP_566508
Saccharomyces cerevisaie	AAB68064	CAA97453
Theileria parva	AAA99499	EAN30678

2.3.4 Predict7™ antigenic peptide prediction

The production of synthetic peptide antigens for antibody production relies on the precise prediction of antigenic sites on a protein molecule (Saravanan and Kumar, 2009). Immunogenic regions on the proteins encoded by PY00413, PY03823, PF10_0252, PF14_0211 and PF14_0369 were identified using the Predict7™ programme (Cármenes *et al.*, 1989). The programme calculates various features of an amino acid sequence, namely antigenicity (Welling *et al.*, 1985), hydrophilicity (Hopp and Woods, 1983), flexibility (Karplus and Schulz, 1985), surface probability (Emini *et al.*, 1985), hydropathy, secondary structure and N-glycosylation sites. For this particular study, the respective protein sequences (saved as text files) were uploaded into Predict7™ and regions satisfying the more important criteria of hydrophilicity, surface probability and side chain flexibility were selected (Saravanan and Kumar, 2009). Furthermore, when selecting a peptide it was important that the selected sequence did not contain more than two lysine residues since multiple lysines can interfere with peptide specific antibody production due to their long side chains. For the copper transport proteins, peptide sequences were specifically chosen from the amino-terminal domain due to its extracellular location, presumably making it more accessible to antibodies. The prediction file for each protein was saved as a .xls file and the graphics of the three desirable properties plotted using Microsoft Excel™ graphing software. Protein-protein BLAST searches were carried out on the selected peptides to ensure the sequence was absent in all *G. gallus* (antibody production host), *H. sapiens* (*P. falciparum* host) and *M. musculus* (*P. yoelii* host) native proteins. If necessary a cysteine residue was added to the amino-terminus of those peptide sequences lacking a native cysteine at this position. The cysteine residue enables conjugation to a carrier molecule and Sulfolink® affinity resin. The specific peptides selected for antibody production are shown in Table 2.2.

Table 2.2 Peptide sequences selected for anti-peptide antibody production in chickens

Protein name	PlasmoDB identifier	Peptide sequence[a]
P. yoelii copper transport protein	PY00413	CSDKQSGDDECKPILD
P. yoelii Cox17	PY03823	**C**PLNTTEESKTα-Bu(C)A[b]
P. falciparum copper transport protein I	PF14_0211	CHSKNDDGVMLPMY
P. falciparum copper transport protein II	PF14_0369	**C**NLQKEEDTVVQLQD
P. falciparum Cox17	PF14_0252	**C**PINNTNEANKGE

[a] Cysteines represented by a bold 'C' are indicative of residues added for coupling, whilst underlined three letter codes indicate the name by which the peptide is referred to
[b] α-Bu is the abbreviation for α-butyric acid, which is used to substitute any internal cysteine residues

2.4 Biochemical and immunochemical techniques

This section describes the biochemical and immunochemical techniques used in this study.

2.4.1 Sodium dodecyl sulfate polyacrylamide gel electrophoresis

Discontinuous sodium dodecyl sulfate polyacrylamide gel electrophoresis (Laemmli, 1970) was used to analyse (i) *Plasmodium yoelii* or *Plasmodium falciparum* infected red blood cell lysates, (ii) recombinant protein expression and (iii) steps in the purification of recombinant proteins.

2.4.1.1 Materials

Monomer solution [30% (w/v) acrylamide, 2.7% (w/v) bis-acrylamide]. Acrylamide (73 g) and bis-acrylamide (2 g) were dissolved and made up to 250 ml with distilled water. The solution was stirred, filtered though Whatman No. 1 filter paper and stored in an amber coloured bottle at 4°C.

Separating gel buffer [1.5 M Tris-HCl, pH 8.8]. Tris (45.37 g) was dissolved in 200 ml of distilled water, titrated to pH 8.8 with HCl and the volume made up to 250 ml with distilled water. The solution was filtered through Whatman No. 1 filter paper and stored at 4°C.

Stacking gel buffer [500 mM Tris-HCl, pH 6.8]. Tris (3 g) was dissolved in 40 ml of distilled water, titrated to pH 6.8 with HCl and the volume made up to 50 ml with distilled water. The solution was filtered with Whatman No. 1 filter paper and stored at 4°C.

10% (w/v) Sodium dodecyl sulfate (SDS). SDS (10 g) was dissolved, with gentle heating, and made up to 100 ml with distilled water. The solution was stored at room temperature (RT).

Initiator reagent [10% (w/v) ammonium persulfate]. Ammonium persulfate (0.1 g) was dissolved in 1 ml of distilled water and stored at 4°C.

Tank buffer [250 mM Tris-HCl, 192 mM glycine, 0.1% (w/v) SDS, pH 8.3]. Tris (6 g) and glycine (28.8 g) were dissolved in approximately 1 ℓ of distilled water with stirring. Before use, 10 ml of 10% SDS was added to a litre of buffer.

Reducing treatment buffer [125 mM Tris-HCl, pH 6.8, 4% (w/v) SDS, 20 % (v/v) glycerol, 10% (v/v) 2-mercaptoethanol]. Stacking gel buffer (2.5 ml), 10% SDS (4 ml) and glycerol (2 ml) were made up to 9 ml with distilled water. Bromophenol blue (35 µg) was added as a tracking dye and, before use, 2-mercaptoethanol was added at a 1:10 dilution. The solution was stored at RT.

Non-reducing sample buffer [125 mM Tris-HCl, 4% (w/v) SDS, 20 % (v/v) glycerol, pH 6.8]. Stacking gel buffer (2.5 ml), 10% SDS (4 ml) and glycerol (2 ml) were made up to 10 ml with distilled water. Bromophenol blue (35 µg) was added as tracking dye and the solution stored at RT.

Stain stock solution [1% (m/v) Coomassie blue R-250]. Coomassie blue R-250 (2 g) was dissolved in 200 ml distilled water with ≥ 1 h stirring at RT. The solution was filtered through Whatman No. 1 filter paper and stored at RT.

Staining solution [0.125% (m/v) Coomassie blue R-250, 50% (v/v) methanol, 10% (v/v) acetic acid]. Stain stock (62.5 ml) was mixed with methanol (250 ml) and acetic acid (50 ml) and made up to 500 ml with distilled water.

Destaining solution I [50% (v/v) methanol, 10% (v/v) acetic acid]. Methanol (500 ml) was mixed with acetic acid (100 ml) and made up to 1 ℓ with distilled water.

Destaining solution II [7% (v/v) acetic acid, 5% (v/v) methanol]. Acetic acid (70 ml) was mixed with methanol (50 ml) and made up to 1 ℓ with distilled water.

2.4.1.2 Method

Reducing or non-reducing SDS-PAGE was carried out as described by Laemmli (1970) using a Bio-Rad Mini Protean II™ vertical slab electrophoresis apparatus. Separating and stacking gels were prepared according to the recipes shown in Table 2.3. The gel-casting unit was assembled according to the manufacturers' instructions and the prepared gels submersed in tank buffer in a Bio-Rad Mini Protean II™ vertical slab electrophoresis apparatus.

Table 2.3 Recipe for two Laemmli SDS-polyacrylamide gels

Reagent	Separating gel		Stacking gel
	12.50%	10.00%	4.00%
Monomer solution	6.25 ml	5.00 ml	940 µl
Separating gel buffer	3.75 ml	3.75 ml	-
Stacking gel buffer	-	-	1.75 ml
10% SDS	150 µl	150 µl	70 µl
Distilled water	4.75 ml	6.00 ml	4.30 ml
Initiator reagent	75 µl	75 µl	35 µl
TEMED	7.5 µl	7.5 µl	15 µl

Samples were loaded into the wells and electrophoresis was carried out at 36 mA (18 mA per gel slab). The gels were removed and stained with Coomassie Blue R-250 staining solution for ≥ 1 h and then destained with successive changes of destain I and II. Once destained the gel was imaged with the BioRad VersaDoc™ image documentation system. The molecular weight of the desired protein band(s) were determined using a graph of log molecular weight of the standards versus distance migrated (mm) into the separating gel. The molecular weight standards used were representative of either a BioRad low molecular weight marker [Phosphorylase B (97,400 Da); Serum albumin (66,200 Da); Ovalbumin (45,000 Da); Carbonic anhydrase (31,000 Da); Trypsin inhibitor (21,500 Da); Lysozyme (14,000 Da)] or a Fermentas unstained protein molecular weight marker [β-galactosidase (116,000 Da); Bovine serum albumin (66,200 Da); Ovalbumin (45,000 Da); Lactate dehydrogenase (35,000 Da); Rease Bsp98I (25,000 Da); β-lactoglobulin (18,400 Da); Lysozyme (14,400 Da)].

2.4.2 Tricine-SDS-PAGE

Tricine sodium dodecyl sulfate polyacrylamide gel electrophoresis (Schägger, 2006) was used to analyse (i) *Plasmodium yoelii* or *Plasmodium falciparum* infected red blood cell lysates and (ii) steps in the purification of recombinant His_6-*Py*Cox17.

2.4.2.1 Materials

Acrylamide-bisacrylamide (AB)-3 stock solution [49.5% (w/v) acrylamide, 3% (w/v) bis-acrylamide]. Acrylamide (48 g) and bis-acrylamide (1.5 g) were dissolved and made up to 100 ml with distilled water. The solution was stirred, filtered through Whatman No. 1 filter paper and stored in an amber coloured bottle at 7 – 10°C.

Gel buffer (3x) [3 M Tris-HCl, 0.3% (w/v) SDS, pH 8.45]. Tris (36.33 g) and SDS (0.3 g) were dissolved in 90 ml distilled water, titrated to pH 8.45 with HCl and made to a final volume of 100 ml with distilled water. The solution was stored at RT.

Initiator reagent [10% (w/v) ammonium persulfate]. Ammonium persulfate (0.1 g) was dissolved in 1 ml of distilled water and stored at 4°C.

Anode buffer [0.1 M Tris-HCl, pH8.9]. Tris (12.11 g) was dissolved in 950 ml distilled water, titrated to pH 8.9 with HCl and made to a final volume of 1 ℓ with distilled water. The solution was stored at 4°C.

Cathode buffer [0.1 M Tris-HCl, 0.1 M Tricine, 0.1% (w/v) SDS, pH 8.25]. Tris (12.11 g), tricine (17.92 g) and SDS (1 g) were dissolved in in 950 ml distilled water. The pH of the solution should be close to 8.25 and should not be titrated (Schägger, 2006). The buffer was made to a final volume of 1 ℓ with distilled water and stored at RT.

Reducing treatment buffer (4x) [0.15 M Tris-HCl, pH 7, 12% (w/v) SDS, 30% (w/v) glycerol, 6% (v/v) 2-mercaptoethanol, 0.05% (w/v) Coomassie blue G-250]. Tris (0.908 g), SDS (6 g), glycerol (15 g) and 2-mercaptoethanol (3 ml) were dissolved in 25 ml distilled water and titrated to pH 7 with HCl. Coomassie blue G-250 (0.025 g) was added to the solution and dissolved. The solution was then made to a final volume of 50 ml with distilled water.

2.4.2.2 Method

Reducing Tricine-SDS-PAGE was carried out as described by Schägger (2006) using a Bio-Rad Mini Protean II™ vertical slab electrophoresis apparatus. Separating and stacking gels were prepared according to the recipes shown in Table 2.4. The gel-casting unit was assembled according to the manufacturers' instructions and the prepared gels submersed in tank buffer in a Bio-Rad Mini Protean II™ vertical slab electrophoresis apparatus.

Table 2.4 Recipe for two Tricine-SDS polyacrylamide gels

Reagent	Separating gel (10%)	Stacking gel (4%)
AB-3	3.00 ml	500 µl
Gel buffer	5.00 ml	1.5 ml
Glycerol	1.5 g	-
Distilled water	6.00 ml	3.95 ml
Initiator reagent	75 µl	45 µl
TEMED	7.5 µl	4.5 µl

Electrophoresis was initially carried out at 30 V until the dye front entered the separating gel. The voltage was then increased to 90 V and electrophoresis continued until the dye front was approximately 0.5 cm from the bottom of the separating gel. The gels were removed and stained with Coomassie Blue R-250 staining solution for ≥ 1 h followed by destaining with successive changes of destain I and II. Destained gels were imaged with the BioRad VersaDoc™ image documentation system. The molecular weight of the desired protein band(s) were determined using a graph of log molecular weight of the standards versus distance migrated (mm) into the separating gel. The molecular weight standards used were representative of a New England Biolabs broad range protein marker [Myosin (212,000 Da); MBP-β-galatosidase (158,194 Da); β-galatosidase (116,351 Da); Phosphorylase b (97,184 Da); Serum albumin (66,409 Da); Glutamic dehydrogenase (55,561 Da); MBP2 (42,710 Da); Thioredoxin reductase (34,622 Da); Triosephosphate isomerase (26,972 Da); Trypsin inhibitor (20,100 Da); Lysozyme (14,313 Da); Aprotinin (6,517 Da); Insulin A (3,400 Da); B chain (2,340 Da)].

2.4.3 Western blot

Proteins resolved by SDS-PAGE gel electrophoresis can be electro-transferred onto a solid membrane such as nitrocellulose, PVDF or nylon for detection with protein-specific antibodies. The western blot method used in this study was conducted in accordance with the protocol described by Towbin *et al.* (1979). This technique was employed for the detection of recombinant proteins in *Escherichia coli* cell lysates and native proteins in *Plasmodium* cell lysates that were resolved by SDS-PAGE.

2.4.3.1 Materials

Transfer buffer [50 mM Tris, 200 mM glycine, 20% (v/v) methanol]. Tris (6.051 g), glycine (14.4 g) and methanol (200 ml) were made up to 1 ℓ with distilled water and stored at 4°C.

Ponceau S stain [0.2% (w/v) Ponceau S in 1% (v/v) acetic acid]. Ponceau S (20 mg) was resuspended in 1 ml of glacial acetic acid. The volume was made up to 100 ml with distilled water and stored at RT.

Tris buffered saline (TBS) [20 mM Tris-HCl, pH 7.4, 200 mM NaCl]. Tris (2.42 g) and NaCl (11.69 g) were dissolved in 950 ml of distilled water, titrated to pH 7.4 with HCl and the volume made up to 1 ℓ with distilled water. The solution was stored at RT.

Blocking solution [5% (w/v) non-fat powdered milk in TBS]. Locally sourced (Elite®) fat-free powdered milk (5 g) was suspended in 100 ml of TBS. This solution was freshly prepared.

BSA-TBS [0.5% (w/v) BSA in TBS]. BSA (0.5 g) was dissolved in 100 ml TBS. This solution was freshly prepared.

Substrate reagent [0.06% (w/v) 4-chloro-1-naphthol, 0.0015% (v/v) H_2O_2, 20% (v/v) methanol in TBS]. A stock solution of 4-chloro-1-naphthol was prepared by dissolving 30 mg in methanol (10 ml). Two ml of this stock solution was made up to 10 ml with TBS and H_2O_2 (4 µl of a 30% solution) was added, ensuring the solution was exposed to minimal light. This working solution was freshly prepared.

2.4.3.2 Method

Following a SDS-PAGE run, one gel was stained with Coomassie blue R-250 as a reference gel whilst the other gel was electro-blotted to nitrocellulose. The nitrocellulose membrane-gel “sandwich” was placed in a blotting apparatus containing blotting buffer with the nitrocellulose membrane towards the anode. Protein was transferred to the membrane [(13 V, 40 mA, 16 h) or (70 V, 250 mA, 2 h)], visualised on the nitrocellulose with Ponceau S stain and the molecular weight marker proteins marked with a pencil. The Ponceau S stained nitrocellulose membrane was destained and unoccupied sites on the membrane blocked with blocking solution for 1 h. The nitrocellulose membrane was then washed three times with TBS (5 min/wash), followed by a 2 h incubation with the required dilution of the desired primary antibody in BSA-TBS. The nitrocellulose membrane was again washed three times in TBS (5 min/wash) and then incubated for 1 h in the appropriate dilution of secondary antibody in BSA-TBS. The nitrocellulose membrane was washed a further three times in TBS (5 min/wash) followed by addition of the substrate reagent. The membrane was incubated in substrate until a band(s), suggestive of the targeted protein, became apparent. The image was captured with the VersaDoc imaging system and the blot stored.

2.4.4 Bradford standard protein assay

2.4.4.1 Materials

Bradford dye reagent [0.06% (w/v) Coomassie Brilliant Blue G-250 in 2% (v/v) perchloric acid]. Coomassie Brilliant Blue G-250 (0.3 g) was resuspended in 500 ml of 2% (v/v) perchloric acid in distilled water. The solution was stirred for 1 h at RT and filtered through Whatman No.1 filter paper. The solution was stored in an amber glass bottle at RT.

Phosphate buffered saline (PBS), pH 7.2. NaCl (8 g), KCl (0.2 g), Na_2HPO_4 (0.917 g) and KH_2PO_4 (0.2 g) were dissolved in 950 ml of distilled water, titrated to pH 7.2 with HCl and made up to 1 ℓ with distilled water and stored at 4°C.

Ovalbumin stock solution [1.0 mg/ml]. Ovalbumin (1 mg) was dissolved in 1 ml of PBS and used to set up a standard curve from 0 to 50 µg. This curve was used for determination of unknown concentrations.

Protein standards [0 – 50 µg ovalbumin/100 µl of buffer]. Proteins standards were prepared from the ovalbumin stock by resuspending 10 to 50 µg ovalbumin in 100µl of buffer. Standards were prepared in 10 µg increments.

2.4.4.2 Method

In a 1.5 ml microfuge tube, dye reagent (900 µl) was mixed with the protein standard solutions (0.1 ml) and incubated at RT for 15 min. Each protein standard was prepared in triplicate and the absorbance value for each solution determined at 595 nm. The mean absorbance value for each standard was recorded and plotted against the amount of protein in an *x-y* scatter plot. Solutions having an unknown protein concentration were prepared in a similar manner to the protein standards, with the resulting protein concentration derived by extrapolation on the standard curve.

2.4.5 Coupling synthetic peptides to rabbit albumin carrier for antibody production

Synthetic peptides derived from the copper transport and Cox17 proteins (*P. yoelii* and *P. falciparum*) were coupled to rabbit albumin and injected into chickens for anti-peptide antibody production. Peptides are coupled to a carrier protein due to their relatively small sizes. The molecular weight of the peptides ranged from 1500 – 2000 Da and were thus unlikely to be able to elicit a host immunogenic response alone (Saravanan and Kumar, 2009). The peptides were designed and synthesized with a terminal cysteine residue to provide a functional sulfhydryl

(SH) group for covalent attachment to the carrier protein and affinity matrix. Prior to coupling, peptides were treated with dithiothreitol (DTT) to produce free terminal SH residues, whilst the rabbit albumin carrier was activated with 3-maleimidobenzoic acid *N*-hydroxysuccinimide (MBS). MBS is a heterobifunctional reagent that cross links peptides to carrier proteins through cysteines and free amino groups (Harlow and Lane, 1988). Reduced peptides were separated from DTT on a Sephadex G-10 resin and the MBS-rabbit albumin complex separated from unreacted MBS on a Sephadex G-25 resin.

2.4.5.1 Materials

Phosphate buffered saline (PBS), pH 7.2. As per Section 2.4.4.1

MEC Buffer [0.1 M NaH_2PO_4, pH 7.0, 0.02% (w/v) NaN_3, 1 mM Na_2-EDTA]. NaH_2PO_4 (11.998 g), Na_2-EDTA (0.372 g) and sodium azide (0.2 g) were dissolved in 950 ml of distilled water, titrated to pH 7.0 with NaOH and made up to 1 ℓ with distilled water.

Peptide reducing buffer [0.1 M Tris-HCl, pH 8.0, 1 mM Na_2-EDTA]. Tris (2.24 g) and Na_2-EDTA (0.372 g) were dissolved in 150 ml of distilled water, titrated to pH 8.0 with HCl and made up to 200 ml with distilled water.

Ellman's reagent buffer [0.1 M Tris-HCl, pH 8.0, 1 mM Na_2-EDTA, 0.1% (w/v) SDS]. Tris (1.21 g), Na_2-EDTA (0.372 g) and SDS (1 ml of 10% SDS) were dissolved in 90 ml of distilled water, titrated to pH 8.0 with HCl and made up to 100 ml with distilled water.

Dithiothrietol [10 mM]. Dithiothrietol (7.71 mg) was dissolved in 5 ml of peptide reducing buffer.

2.4.5.2 Method

It has previously been determined that 4 mg of a synthetic peptide is sufficient to produce 4 to 10 mg of affinity purified polyclonal antibodies, 12 to 15 weeks after a schedule of four immunisations in a chicken (Goldring and Coetzer, 2003).

Calculations:

Peptides were coupled to rabbit albumin carrier at a peptide:carrier ratio of 40:1. The amount of rabbit albumin carrier to be coupled to 4 mg of synthetic peptide was determined by the

formula:

$$68200 \times \frac{1}{40} \times \frac{4 \times 10^{-3} g\ (peptide)}{Mw\ (peptide)} \times 1000 = carrier\ (mg)$$

68200 is the molecular mass of rabbit albumin in Daltons.

Rabbit albumin carrier was activated with MBS at a carrier:MBS ratio of 1:40. The amount of MBS required for activation of the calculated amount of rabbit albumin was determined by the formula:

$$314.26 \times 40 \times \frac{carrier\ (mg)}{68200} \times 1000 = MBS\ (mg)$$

Where 314.26 is the molar mass of MBS.

Activating the carrier with MBS:

The calculated quantity of MBS was dissolved in 100 µl of dimethylfluoride (DMF)and made up to 500 µl with PBS. This was combined with an equal volume of PBS containing the calculated quantity of rabbit albumin. The solution was mixed gently for 30 min at RT with a rotary mixer. The solution was then loaded onto a Sephadex G-25 size exclusion chromatography resin pre-equilibrated with MEC buffer. The MBS-rabbit albumin complex was eluted with MEC buffer and the eluted fractions collected in 1 ml volumes. The A_{280} of each collected fraction was determined and those with an absorbance ≥ 0.3 were pooled together.

Reducing the peptide with DTT:

Peptide (4 mg) was solubilised in 50 µl of dimethylsulfoxide (DMSO) and the volume was made up to 500 µl with peptide reducing buffer. DTT reagent (500 µl) was combined with the peptide solution and this solution was incubated at 37°C for 90 min. The reduced peptide solution was then loaded onto a Sephadex G-10 size exclusion chromatography resin pre-equilibrated with MEC buffer. Reduced peptide fractions of 500 µl were collected and the presence of free SH groups determined with Ellman’s reagent (10 µl of eluted fraction + 10 µl of Ellman’s reagent). The set of fractions producing an intense yellow colour, with Ellman's reagent, were pooled together.

Reacting the reduced peptide with the MBS-activated carrier:

The pooled MBS-rabbit albumin fractions were combined with the pooled fractions of reduced peptide. This mixture was then incubated at RT for 3 h, with gentle stirring. Following incubation, the solution was aliquoted into four equal volumes and stored at -20°C.

2.4.6 Preparation of immunogen for immunisation in chickens

For the initial immunisation, the peptide-carrier complex was emulsified in Freund's complete adjuvant (FCA) and thereafter Freund's incomplete adjuvant (FIA) was used. FCA is made up of heat attenuated *Mycobacterium tuberculosis* mixed in mineral oil to elicit cell-mediated immunity, resulting in the production of antibodies against the peptide and carrier. On the other hand, FIA is mineral oil without heat attenuated *M. tuberculosis*.

2.4.6.1 Method

The peptide-carrier complex solution was removed from -20°C and thawed at RT. Once thawed it was dispensed into a 20 ml scintillation vial and combined with an equal volume of FCA or FIA. The mixture was triturated, using a 2.5ml syringe, until a relatively viscous emulsion formed. This emulsion was subsequently loaded into the 2.5ml syringe. Chickens were immunised intra-muscularly, in the large breast muscles, with 400 µl to 500 µl of the immunogen containing ~ 125 µg of the synthetic peptide. As mentioned, the first immunisation was prepared in FCA whilst the three subsequent booster immunisations were prepared with FIA. Immunisations were carried out at two-week intervals. Eggs from each chicken were collected daily, labelled and stored at 4°C until the antibodies were isolated.

2.4.7 Isolation of immunoglobulin Y (IgY) from chicken egg yolk

The solubility of proteins in an aqueous environment depends largely on the surface availability of hydrophilic amino acids. These hydrophilic amino acids form hydrogen bonds with water molecules in the hydration shell of the protein. Dextran and polyethylene glycol (PEG) can disrupt this interaction and are therefore widely used as protein precipitation agents. Dextran and PEG are preferentially excluded from the hydration shell around proteins bringing the protein solution to its solubility limit (Chun *et al.*, 1967; Ingham, 1984; Polson *et al.*, 1985). PEG is a linear, water-soluble, non-ionic polymer with a molecular weight varying from 200 to 20 000 Da depending on the extent of polymerization. PEG can be used to extract proteins at room temperature without causing protein denaturation (Ingham, 1984; Polson *et al.*, 1985). PEG, with a molecular weight of 4 000 to 6000 Da, is routinely used in protein precipitation. Polymers larger than this offer no advantage, since their solutions are more viscous (Atha and Ingham, 1981; Ingham, 1984). Since PEG has a minimal effect on protein stability and precipitates protein in a relatively short time, it is the molecule of choice for protein isolation particularly compared to organic solvents and ammonium sulphate.

In this study, PEG 6000 (Mw ~ 6 kDa) precipitation was used to isolate IgY from eggs produced by chickens immunised with the synthetic peptide-rabbit albumin complex. IgY was isolated using the method of Polson *et al.* (1985). Chickens were housed and cared for at the University of KwaZulu-Natal farms at Ukulinga, Pietermaritzburg. The use of chickens for this study was approved by the University's ethical committee, with the ethical clearance project number: AE/Goldring/05 for 2005 – 2006; 004/07/Animal for 2007; 025/08/Animal for 2008 and 003/10/Animal for 2010.

2.4.7.1 Materials

IgY isolation buffer [100 mM NaH_2PO_4, pH 7.6, 0.02% (w/v) NaN_3]. NaH_2PO_4 (11.998 g) and NaN_3 (0.2 g) were dissolved in 950 ml of distilled water, titrated to pH 7.6 with NaOH and made up to 1 ℓ with distilled water.

IgY Storage Buffer [100 mM NaH_2PO_4, pH 7.6, 0.1% (w/v) NaN_3]. NaH_2PO_4 (11.998 g) and NaN_3 (1 g) were dissolved in 950 ml of distilled water, titrated to pH 7.6 with NaOH and made up to 1 ℓ with distilled water.

2.4.7.2 Method

Egg yolks were separated from albumin and carefully washed under slow running tap water to help remove the albumin. Yolk sacks were punctured and the yolk contents gently squeezed into a measuring cylinder to determine the total yolk volume. Isolation buffer, equivalent to two yolk volumes, was added to the yolk contents and mixed by stirring. Solid PEG was added to 3.5% (w/v) and stirred continuously to ensure all the PEG dissolved. The precipitated vitellin fraction was removed by centrifugation (4420 *g*, 30 min, RT). The resulting supernatant was filtered through non-absorbent cotton wool and the filtrate volume determined. Solid PEG was added to the filtrate at 8.5% (w/v) and, as before, this was stirred thoroughly. The solution was centrifuged (12000 *g*, 10 min, RT) to pellet the precipitate, with the resulting supernatant being discarded. The pellet was dissolved in a volume of buffer equivalent to the original egg yolk volume and 12% (w/v) PEG added. This was again stirred thoroughly and then centrifuged (12000 *g*, 10 min, RT). The supernatant was again discarded and the final pellet dissolved in a volume of buffer equivalent to one-sixth of the original yolk volume. The final IgY concentration was determined using the extinction coefficient $E\,\frac{1\,mg/ml}{280\,nm} = 1.25$ (Coetzer, 1985).

2.4.8 Preparation of peptide-specific affinity matrices and purification of anti-peptide IgY

Affinity purification offers separation of biomolecules based on unique biological interactions. The matrix generally consists of polyacrylamide, dextran or agarose polymerized beads. The matrix is insoluble and is usually commercially synthesized to acquire specific functional groups such as aldehyde, carboxylic acid, hydroxyl, amine, or sulfhydryl groups. The ligand is immobilized on the matrix by means of several specific coupling reactions. Molecules to be purified, adsorb to the immobilized ligands when passed though the affinity matrix. The remaining components in the mixture are generally washed off the matrix with several washes of the appropriate column buffer. A buffer of low pH or high ionic strength, or a specific reagent, is used to disrupt the affinity-based interactions between the adsorbed molecules and ligand to elute the desired products.

SulfoLink® Coupling Gel is a 6% beaded agarose that has been derived to have an iodoacetyl group spaced by a 12-atom structure (Pierce SulfoLink manual). This enables the covalent bonding of molecules, such as peptides and proteins with free SH functional groups, to the iodoacetyl group on the agarose gel matrix. The 12-atom spacer is designed to decrease steric hindrance between the coupled ligand and the affinity-bound molecule, enhancing the binding of the molecule to its ligand. The molecule to be coupled must be in monomeric form without disulfide linkage. Thus the molecule is reduced with DTT to acquire free -SH reactive functional groups prior to coupling. The reducing agent (DTT) is then removed, by size exclusion chromatography, to prevent it from out-competing the peptide for binding to the iodoacetyl functional groups. The -SH group specifically reacts with the iodide, on the iodoacetyl functional group, to form a stable thioether bond.

2.4.8.1 Materials

Coupling buffer [50 mM Tris-HCl, pH 8.5, 5 mM Na_2-EDTA]. Tris (12.1 g) and Na_2-EDTA (3.72 g) were dissolved in 950 ml of distilled water, titrated to pH 8.5 with HCl and the volume made to 1 ℓ with distilled water.

Blocking solution [50 mM L-cysteine in coupling buffer]. L-cysteine (2.2 g) was dissolved in 250 ml of coupling buffer.

Wash solution [1 M NaCl]. NaCl (58.44 g) was dissolved in 1 ℓ of distilled water.

Equilibration buffer [100 mM NaH_2PO_4, pH 7.6, 0.1% (w/v) NaN_3]. NaH_2PO_4 (11.998 g) and NaN_3 (1 g) were dissolved in 950 ml of distilled water, titrated to pH 7.6 with NaOH and the

volume made up to 1 ℓ with distilled water.

Affinity column-washing buffer [100 mM NaH_2PO_4, pH 6.5, 0.02% (w/v) NaN_3]. NaH_2PO_4 (11.998 g) and NaN_3 (0.2 g) were dissolved in 950 ml of distilled water, titrated to pH 6.5 with NaOH and the volume made up to 1 ℓ with distilled water.

Elution buffer [100 mM glycine, pH 2.8, 0.02% (w/v) NaN_3]. Glycine (0.75 g) and NaN_3 (0.02 g) were dissolved in 80 ml of distilled water, titrated to pH 2.8 with HCl and the volume made up to 100 ml with distilled water.

Neutralising buffer [1 M NaH_2PO_4, pH 8.5, 0.02% (w/v) NaN_3]. NaH_2PO_4 (11.998 g) and NaN_3 (0.02 g) were dissolved in 80 ml of distilled water, titrated to pH 8.5 with NaOH and the volume made up to 100 ml with distilled water.

2.4.8.2 Method

Coupling of peptides to SulfoLink™ affinity matrix

For coupling of peptides to the SulfoLink™ resin, 7.5 mg of the peptide was reduced as described in Section 2.4.5. SulfoLink™ resin (2 ml of 50% slurry = 1 ml column volume) was dispensed into a BioRad Poly-Prep® affinity column. The resin was equilibrated with 5 column volumes of coupling buffer. The buffer was allowed to flow through the matrix until the meniscus was just above the matrix. The reduced peptide solution was added to the equilibrated resin and the column capped to close the inlet and outlet. The suspension was mixed on a rotary mixer (15 min, RT), and then incubated in a stationary, upright position (30 min, RT). The caps were removed and the outlet opened to allow the reaction by-products and uncoupled peptides to elute. The resin was washed with 5 column volumes of the coupling buffer, the outlet capped and 1 ml of the blocking buffer added to the matrix and the inlet capped. The suspension was mixed again on a rotary mixer (15 min, RT) and then allowed to stand (30 min, RT). The column was uncapped to allow the buffer to drain out. The matrix was washed with 5 column volumes of the wash solution and equilibrated with 5 column volumes of the equilibration buffer. The affinity matrix was stored at 4°C until use.

Affinity purification

Prior to purification, the affinity resin was equilibrated with 20 column volumes of washing buffer. The isolated IgY (Section 2.4.7) was pooled and filtered through Whatman No.1 filter paper to remove insoluble materials that could clog the affinity column. The filtrate was cycled

through the resin overnight, in a reverse direction. Unbound antibodies were subsequently washed off the column with 20 column volumes of affinity column-washing buffer in a forward direction. Bound antibodies were eluted with elution buffer and 1 ml fractions collected in microfuge tubes containing 100 µl of neutralizing buffer. The A_{280} of collected fractions was determined and the elution profile of A_{280} against elution volume plotted. Fractions with $A_{280} \geq 0.2$ were pooled together and protein concentration determined. The affinity purified polyclonal anti-peptide IgY was stored at 4°C.

2.4.9 Enzyme linked immunosorbent assay for anti-peptide IgY titre

In this study, an indirect enzyme linked immunosorbent assay (ELISA) was used to determine the weekly anti-peptide IgY titres for each immunised chicken.

2.4.9.1 Materials

Phosphate buffered saline (PBS), pH 7.2. As per Section 2.4.4.1

Blocking solution [0.5% (w/v) bovine serum albumin-PBS]. BSA (0.5 g) was dissolved in 100 ml of PBS.

Tween-PBS washing solution [0.1% (v/v) Tween-PBS]. Tween-20 (1 ml) was made up to 1 ℓ with PBS.

0.15 M citrate-phosphate buffer, pH 5.0. A solution of citric acid monohydrate (21.0 g/ℓ) was titrated with a solution of Na_2HPO_4 (28.4 g/ℓ) to pH 5.0.

Substrate solution [0.05% (w/v) ABTS and 0.0015% (v/v) H_2O_2 in citrate-phosphate buffer]. ABTS (7.5 mg) and H_2O_2 (7.5 µl) were dissolved in citrate-phosphate buffer (15 ml).

2.4.9.2 Method

A 96-well microtitre plate (Nunc Maxi Sorp™) was coated with 150 µl of a 1 µg/ml solution of peptide in PBS for 3 h at 37°C and then overnight at 4°C. Following incubation the peptide solution was discarded, the plate rinsed with Tween-PBS and then blocked with blocking solution (200 µl, 1 h, 37°C). After blocking, the plate was washed three times with Tween-PBS. Weekly isolates of immune IgY were prepared in blocking solution (100 µg/ml) and the plate incubated with 150 µl of these preparations. Included, as a control, was crude IgY isolated from pre-immune eggs. These primary antibody samples were incubated for 2 h at 37°C followed by

three washes with Tween-PBS. A rabbit-anti-chicken IgY-Horse Raddish Peroxidase (HRP) conjugated secondary antibody was prepared in blocking solution (1:15 000 dilution), added to each well (150 µl) and incubated (1 h, 37°C). Following incubation, the plate was again washed three times with Tween-PBS. Substrate solution was prepared and added to each well (150 µl). The plate was incubated at RT, in the dark, until colour sufficiently developed. The absorbance of the substrate solution was recorded at 405 nm with the VersaMax™ ELISA plate reader.

2.5 Parasitological techniques

The rodent malaria parasites *P. yoelii, P. berghei, P. vinckei* and *P. chabaudi*, provide useful models for laboratory studies of the *Plasmodium* parasite's biology (Carlton *et al.*, 2002). All four rodent malaria parasites can infect and be propagated in mice. These infections can be used to study the interaction between the host and erythrocytic stage of parasite development. This highlights just one of the aspects that make mouse malaria infections useful models for studying immunological, molecular and biochemical aspects of the *Plasmodium* parasite (Sanni *et al.*, 2002). Variation does, however, exist between species and strains of the rodent-infecting parasites in terms of virulence. For example, certain strains of *P. yoelii* are lethal to mice (e.g. 17XL), following infection, whilst other strains are non-lethal (e.g. 17XNL).

This section describes techniques used for the propagation, isolation and purification of *P. yoelii* and *P. berghei*. In these studies, the lethal *P. yoelii* 17XL and *P. berghei* ANKA strains were used. Parasites were propagated in 6 – 8 week old male BALB/c mice obtained from National Health Laboratory Services, Johannesburg, South Africa, through intraperitoneal injection of 100 µl of stabilate containing 1 x 10^7 parasitised mouse red blood cells (Burns *et al.*, 1989). Mice used in this study were kept in the university animal housing facility at a constant temperature of 19 – 22°C. Each animal was housed in an individual cage having a plastic bottom and steel mesh lid. Cages, saw dust, water and food were autoclaved prior to use. Food and water was provided *ad libitum.* Parasitemia was analysed every second day, post infection, by light microscopy of methanol-fixed, Giemsa-stained thin blood smears of tail blood (Warhurst and Williams, 1996).

2.5.1 Propagation of *P. yoelii* and *P. berghei* parasites in BALB/c mice and cryo-preservation

2.5.1.1 Materials

Phosphate buffered saline (PBS), pH 7.2. As per Section 2.4.4.1

Cryo-preservative [10% (v/v) glycerol-PBS]. Glycerol (1 ml) was dissolved in 9 ml of PBS and

autoclaved.

2.5.1.2 Method

Parasites were propagated in male BALB/c mice by intra-peritoneal injection of parasite stabilate (1 x 10^7 parasitised mouse red blood cells). The lower abdomen was cleaned with 70% ethanol and the mouse held upside down for the organs to partially drop. The syringe (insulin syringe, 1 cc) was inserted ~ 0.5 cm into the skin and the stabilate slowly injected into the mouse. The syringe was slowly withdrawn, with rotation, to help prevent the stabilate from exuding following injection. The mouse was immediately returned to its cage and monitored for 5 – 10 min post injection. Parasitemia was monitored daily by Giemsa staining of a thin smear of tail blood. The thin blood smear was air-dried, fixed in methanol for 1 min at RT and then left to dry at RT. The smear was stained with Giemsa for 20 – 30 min at RT, washed under slow running water, air-dried and viewed at 1000× magnification (oil immersion). The number of infected RBC was expressed as a percentage of non-infected RBC. Once parasitemia reached a suitable level, mice were bled and the blood collected in a heparin-treated vacuum glass tube. Parasite infected red blood cells were preserved in 10%-glycerol-PBS at 1 x 10^7 parasitised-RBC (pRBC) per 100 µl of stabilate. The stabilate was labelled, flash-frozen and immediately stored in a liquid nitrogen cryo-tank.

2.5.2 Isolation of *P. yoelii* and *P. berghei* parasites from infected mouse red blood cells

2.5.2.1 Materials

Phosphate buffered saline (PBS), pH 7.2. As per Section 2.4.4.1

Saponin-PBS [0.05% (w/v) saponin in PBS]. Saponin (5 mg) was dissolved in 10 ml of PBS and kept on ice prior to use.

2.5.2.2 Method

At 30 – 40% parasitemia, an infected mouse was sacrificed and the blood collected into a heparin-treated vacuum tube and kept on ice. The blood was diluted with ice cold PBS (1:4) and passed through a Plasmodipur® filter to remove host white blood cells. The filtrate was centrifuged (800 *g*, 15 min at 4°C) to pellet the infected RBC. The pelleted cells were washed three times with ice cold PBS (five times the pelleted RBC volume) and then resuspended in five volumes of saponin-PBS. The cell suspension was incubated at RT for 30 min to allow for complete hemolysis, as indicated by a dark red colour. The suspension was centrifuged (3500 *g*, 15 min at 4°C) to pellet the liberated, mixed stage parasites. The supernatant was carefully

aspirated, leaving behind only a small volume of the supernatant so as not to disturb the parasite pellet. The parasite pellet was washed a further two times with five volumes of ice-cold PBS. This final pellet was resuspended in an equal volume of PBS, divided into aliquots and stored at -20°C. Parasite protein lysate was prepared from these isolated parasites by subjecting the sample to three freeze-thaw cycles, between 37°C and -196°C (liquid nitrogen for 2 min), following the addition of Triton X-100 (1%), EDTA (5 mM) and PMSF (1mM). Samples were further disrupted by sonication on ice (5 cycles, 15 sec/cycle, 1 min on ice between cycles). The total parasite lysate was then centrifuged at 100,000 *g* for 1 h so as to separate the lysate into soluble and insoluble material. The respective fractions were separated from one another and used for western blotting studies.

2.5.3 Immunofluorescence microscopy

2.5.3.1 Materials

Sodium carbonate-bicarbonate coating buffer [0.02 M Na_2CO_3, 0.02 M $NaHCO_3$, 0.2% NaN_3, pH 9.7]. Na_2CO_3 (0.168 g) was made up to 100 ml with distilled water (solution A), whilst $NaHCO_3$ (0.105 g) and NaN_3 (0.01 g) were made up to 50 ml with distilled water (solution B). Solution A was titrated against solution B to pH 9.7.

Isotonic Tris buffer [0.15 M Tris-HCl, pH 7.5]. Tris (0.908 g) was dissolved in 40 ml of distilled water, titrated to pH 7.5 with HCl and made to a final volume of 50 ml with distilled water. The solution was sterilised by filtration through a 0.22 µm syringe filter prior to use.

0.9% NaCl. NaCl (0.9 g) was dissolved in 10 ml distilled water. The solution was sterilied by filtration through a 0.22 µm syringe filter prior to use.

Hank's balanced salt solution. Hank's balanced salt (0.475 g) and Na_2CO_3 (0.0175 g) were dissolved in 45 ml of distilled water, titrated to pH 7 and made up to a final volume of 50 ml with distilled water. The solution was sterilised by filtration through a 0.22 µm syringe filter prior to use.

THS solution. Isotonic Tris buffer (5 ml), Hank's balanced salt solution (50 ml) and 0.9% NaCl (45 ml) were combined under sterile conditions and stored in a sterile bottle.

Phosphate buffered saline (PBS), pH 7.2. As per Section 2.4.4.1

Glutaraldehyde-PBS [1% (v/v) glutaraldehyde in PBS]. Glutaraldehyde (200 µl of a 50%

solution) was made up to 5 ml with PBS.

BSA-PBS solution [2% (w/v) BSA in PBS]. BSA (0.2 g) was dissolved in PBS (10 ml).

DAPI solution [5 µg/ml in PBS]. DAPI (2.5 µl of a 2 mg/ml solution) was made up to 1 ml with PBS and kept away from light.

2.5.3.2 Method

Pre-treatment of *P. yoelii*-infected red blood cells (pRBC)

Infected mouse blood was collected in a heparin-treated tube, an aliquot removed (100 µl) and centrifuged (800 *g*, 5 min, 4°C). The plasma was discarded and the packed cells resuspended in 100 µl of THS solution. Cells were again collected by centrifugation, the supernatant removed and the cells washed a further four times with 100 µl of THS (800 *g*, 5 min, 4°C). The packed cells were resuspended to 1% haematocrit (30 µl packed cell volume in 3 ml of THS solution) and kept on ice.

Preparation of slides and fixing of pRBC

A 12-well slide was incubated with 20 µl of the coating buffer per well (30 min, RT) and the solution then aspirated. A small volume of the cell suspension was added to each well (~20 µl) and the cells were left to settle for 30 min at RT. Unbound cells were washed off the slide by inverting and rinsing the slide in a Petri dish containing THS solution. Bound cells were fixed by covering each well with glutaraldehyde-PBS (10 sec, RT). The fixing solution was removed by aspiration and the fixing step repeated. The slides were washed with distilled water, air-dried and stored desiccated at -20°C.

Immuno-detection of the *P. yoelii* putative copper transport protein and lactate dehydrogenase

A slide was removed from storage at -20°C and allowed to equilibrate to RT inside a humidified Petri dish. BSA-PBS (20 µl) was added to each well and incubated at RT to block non-specific sites (1 h). The BSA-PBS solution was vacuum-aspirated and a solution of the desired primary antibody (20 µl of 1 µg/ml anti-peptide IgY or pre-immune IgY, in BSA-PBS) added to the respective wells and incubated for 2 h at RT. The primary antibody solution was vacuum-aspirated and wells washed three times with PBS. All wells were incubated with a donkey anti-IgY-FITC conjugated secondary antibody (20 µl of a 1:5000 dilution, in BSA-PBS) for 1 h at RT (in the dark). The secondary antibody solution was vacuum-aspirated and the wells washed three times with PBS (in the dark). Cells were finally stained with DAPI solution, followed by three washes with PBS (in the dark). The slide was stored at 4°C overnight, in a desiccated

vacuum chamber, away from light and then viewed with an Olympus AX70 fluorescent microscope using green and UV filters for FITC and DAPI, respectively. Images were captured with the CC12 Soft Imaging System™ colour camera and processed with analySIS™ software.

2.6 Molecular biology methods

This section describes the methods used to isolate *Plasmodium* parasite nucleic acids used for down stream applications. These applications included the polymerase chain reaction (PCR), ligation and cloning, subcloning, analysis of expression by reverse transcriptase-PCR (RT-PCR) and expression of recombinant *P. yoelii*, *P. berghei* and *P. falciparum* proteins. The design of oligonucleotides used to PCR amplify the desired coding domains were based on sequences published on the PlasmoDB web site (www.plasmodb.org).

2.6.1 Agarose gel electrophoresis

2.6.1.1 Materials

Na_2EDTA [0.5 M, pH 8.0]. Na_2EDTA (18.6 g) was dissolved in 80 ml of distilled water, titrated to pH 8.0 and the volume made up to 100 ml with distilled water.

50× TAE electrophoresis buffer. Tris (242 g) was dissolved in 500 ml of distilled water, with the addition of 0.5 M Na_2EDTA solution (100 ml) and glacial acetic acid (57.1 ml). The solution was made up to 1 ℓ with distilled water and stored at RT.

Ethidium bromide staining reagent [10 mg/ml in 1× TAE]. Ethidium bromide (0.1 g) was resuspended in 1× TAE and stirred at RT for 30 min. The dye solution was filtered with Whatman No.1 filter paper and stored in an amber bottle at RT.

10× sample loading buffer. Bromophenol blue (0.25 g) was resuspended in 33 ml of 1× TAE, glycerol added (60 ml) and the solution made up to 100 ml with 1× TAE. The reagent was stored at RT.

2.6.1.2 Method

For a 1% agarose gel, 0.3 g of agarose was weighed out and suspended in 30 ml of 1× TAE buffer. The agarose was completely melted and once the solution had cooled ethidium bromide was added to a final concentration of 0.5 µg/ml. The gel was poured and once set it was placed into an agarose gel electrophoresis tank containing 1× TAE buffer. The desired samples were combined with loading buffer (9:1; sample:10× sample loading buffer) and loaded into the sample wells. Electrophoresis was carried out at 80 V and an image of the gel captured with

the VersaDoc™ gel documentation system under ultraviolet light. The size of the DNA bands of interest were determined from a graph of log DNA standards (bp) against distance migrated (mm) from the well. The DNA standards used were representative of either a Promega 1 kb DNA stepladder (10,000 bp; 9,000 bp; 8,000 bp; 7,000 bp; 6,000 bp; 5,000 bp; 4,000 bp; 3,000 bp; 2,000 bp; 1,000 bp) or a Fermentas MassRuler™ DNA ladder mix (10,000 bp; 8,000 bp; 6,000 bp; 5,000 bp; 4,000 bp; 3,000 bp; 2,500 bp; 2,000 bp; 1,500 bp; 1,031 bp; 900 bp; 800 bp; 700 bp; 600 bp; 500 bp; 400 bp; 300 bp; 200 bp; 100 bp; 80 bp).

2.6.2 Isolation of *P. berghei* total RNA

2.6.2.1 Materials

DEPC-treated TE buffer [10 mM Tris (pH 8), 1 mM EDTA]. Tris (10 ml of 1 M solution, pH 8) was mixed with EDTA (2 ml of 0.5 M solution, pH 8). The volume was made up to 1 ℓ with distilled water. DEPC was added to 0.1% (v/v), incubated at 37°C overnight and autoclaved to remove residual DEPC.

Formamide gel-loading buffer. Formamide (160 µl) was mixed with DEPC-treated TE buffer (40 µl) and bromophenol blue dye was added.

2.6.2.2 Method

For this study parasite RNA was isolated to confirm transcription of the amino terminal coding domain of putative *P. berghei* copper transport protein. The amplified product was to subsequently be ligated into an expression vector and used for recombinant protein expression. *P. berghei* RNA was isolated using the Qiagen RNeasy® Plus Mini kit. The kit is designed to purify RNA from animal cells or tissues and is compatible with a wide range of cell types. The kit offers efficient purification of high-quality RNA with the selective removal of double-stranded DNA. Samples are lysed in a denaturing lysis buffer, to ensure inactivation of all RNases, and the lysate passed through a spin column to eliminate genomic DNA. Importantly, for this study, the procedure provides an enrichment of mRNA. Parasites were isolated from red blood cells, as per Section 2.5.2, and used for RNA isolation. Prior to isolation, the designated working area, equipment and accessories were thoroughly cleaned and sterilised to minimise the introduction of unwanted RNases. In addition, all polypropylene microfuge tubes used were certified RNAse and DNAse free. All steps for the isolation procedure were as per the manufacturer's instruction. Isolated RNA was stored in aliquots at -70°C. The purity of the isolated RNA was analysed by electrophoresis on a 1% agarose gel. The RNA sample (5 µl) was mixed with formamide gel-loading buffer (10 µl) and incubated at 65°C for 10 min to denature the RNA. Agarose gel electrophoresis was subsequently performed. After

electrophoresis the gel image was captured with the VersaDoc™ gel documentation system under ultraviolet light.

2.6.3 Isolation of *P. yoelii* and *P. falciparum* genomic DNA

In this study, genomic DNA was isolated for molecular cloning of PCR-amplified fragments. For this reason the Fermentas™ DNA purification kit was used with slight modification to produce higher DNA yields. This isolation kit is designed to isolate genomic DNA from various sources, such as whole blood, cell and tissue culture or bacterial culture. The kit is based on one step lysis and selective precipitation of genomic DNA under alkaline conditions. Although the kit is capable of extracting DNA from whole blood, purified *P. yoelii* or *P. falciparum* parasites were used. For *P. yoelii* genomic DNA isolation, infected mouse blood was collected in a microfuge tube containing 0.5 ml of PBS, according to the manufacturer's instruction. The blood cells were washed three times with PBS before isolating the parasites (Section 2.5.2). For the isolation of *P. falciparum* DNA a similar approach was adopted for parasite preparation, however, since these were cultured parasites it was not necessary to use a Plasmodipur® filter step. *P. falciparum* parasitised red blood cells were pelleted, washed with PBS and parasites liberated by saponin treatment (Section 2.5.2). DNA isolation was followed as per the manufacturer's instruction with a slight modification of the DNA precipitation step, which was carried out at -20°C for 30 min to enhance precipitation. The final DNA pellet was resuspended in sterile double distilled water (50 µl) and stored in aliquots at -70°C. DNA yield and purity was analysed by spectrophotometry and standard 0.5% agarose gel electrophoresis.

2.6.4 Primers for PCR-based amplification of PBANKA_130290, PY03823, PF10_0252, PF14_0211 and PF14_0369

Primers were derived from published sequences of the partially sequenced *P. yoelii* and completely sequenced *P. berghei* and *P. falciparum* genomes, in the *Plasmodium* database. Web-based bioinformatics software was used to assist with primer design (Primer3 - http://frodo.wi.mit.edu/primer3/). Primers were engineered with relevant restriction sites used for cloning and expression of the desired PCR products. Secondary structures such as hair pin formation were explicitly avoided when designing primers. Table 2.5 lists primers used in this study.

Table 2.5 Primers designed for PCR amplification

Primer name	Sequence (5'→3')	Derived from (PlasmoDB ID)	Application
PyCtrFL-fwd	ATG AAT ATA TGG AAA ATT ATA TAT ATT G	PY00413	PCR and nested-PCR analysis to support the presence of a full-length PY00413 coding domain. The expected size of the amplicon is 1791 bp, including introns
PyCtrFL-rev	TCA TAG ATG AAA AGC ATC CCC CCC C	PY00413	
PyCtrNe-fwd	CAG TTT CGA TGA TCA ATG TGG AAT GAT TGC	MALPY00116	Nested PCR analysis to support the existence of the full-length PY00413 coding domain. Expected size of amplicon is 2700 bp
PyCtrNe-rev	GCA AAT AAG TCC CCC AAA ATT GTA ATG	MALPY00116	
PbCtrNt-fwd[a]	*at*G AAT TCA TGA ATA TAT GGA AAA TTA TAT ATA TTG	PBANKA_130290	RT-PCR analysis of the transcription of PBANKA_130290 mRNA. Amplicon is to be used for cloning and recombinant expression of the putative amino-terminal domain. Expected size of amplicon is 447 bp
PbCtrNt-rev[b]	*ca*G CGG CCG CTT CCC AAA ATT TGA ATA AAA TAA TAG	PBANKA_130290	
PfCtr211FL/Nt-fwd[a]	*at*G AAT TCT TCA CTT TCG ATT TTG TGA GC	PF14_0211	PCR analysis to support the presence of a full-length PF14_0211 coding domain. Expected size of the amplicon is 423 bp (no introns)
PfCtr211FL-rev	AGA TAA GCA GAA GAA AGA CC	PF14_0211	
PfCtr211Nt-rev[c]	*ca*C TGC AGT TAA TTC TTT ACT TGA AAT ATG TC	PF14_0211	PCR amplification of the putative amino terminal domain of PF14_0211, in conjunction with the forward primer above. Amplicon is to be used for cloning and recombinant expression. Expected size of the amplicon is 132 bp
PfCtr369FL/Nt-fwd[a]	*at*G AAT TCG ACA AAA GCG ACA ATA GTA TTT G	PF14_0369	PCR analysis to support the presence of a full-length PF14_0369 coding domain. Expected size of the amplicon is 920 bp, including introns
PfCtr369FL-rev	ACA TCC ACA ACA AGC TGG ATC	PF14_0369	
PfCtr369Nt-rev[c]	*ca*C TGC AGT TAC GAT TTG GTT TCC CAT TTG	PF14_0369	PCR amplification of the putative amino terminal domain of PF14_0369, in conjunction with the forward primer above. Amplicon is to be used for cloning and recombinant expression. Expected size of the amplicon is 282 bp
Py/PfLDH-fwd	GGA TCT GGT ATG ATT GGA GGT GTT ATG GCC	PY03885	Positive control in PCR and RT-PCR analysis. Expected size of the amplicon is 850 bp.
Py/PfLDH-rev	TTC GAT TAC TTG TTC TAC ACC ATT ACC ACC	PY03885	

Table 2.5 continued

Primer name	Sequence (5'→3')	Derived from (PlasmoDB ID)	Application
PyCox17-fwd[a]	*at*G AAT TCA TGG GAT TAG GTT TAA CTA AG	PY03823	PCR analysis to support the presence of a full-length coding domain for a putative *P. yoelii* copper chaperone, Cox17. Amplicon is to be used for cloning and recombinant expression. Expected size of the amplicon is 192 bp
PyCox17-rev[b]	*ca*G CGG CCG CAT CAA ACC CTT CAT TTC TTA GG	PY03823	
PfCox17-fwd[d]	*at*G GAT CCA TGG GTA TGA GCT TGA ACA AAC	PF10_0252	PCR analysis to support the presence of a full-length coding domain for a putative *P. falciparum* copper chaperone, Cox17. Amplicon is to be used for cloning and recombinant expression. Expected size of the amplicon is 195 bp
PfCox17-rev[b]	*ca*G CGG CCG CAT CAA AAC CTT CAC TCC TTA AAC	PF10_0252	

[a] underlined and highlighted bases indicate an *Eco*RI restriction site
[b] underlined and highlighted bases indicate a *Not*I restriction site
[c] underlined and highlighted bases indicate a *Pst*I restriction site
[d] underlined and highlighted bases indicate a *Bam*HI restriction site

2.6.5 Polymerase chain reaction (PCR)

For all PCR amplification experiments FIREPol® *Taq* polymerase was employed as the enzyme of choice. *Taq* polymerase was selected since it introduces adenine (A) overhangs during amplification, which are ideal for TA cloning into a relevant cloning vector. PCR was optimised for each set of primers (Table 2.6). Parameters such as annealing temperature, $MgCl_2$ concentration and cycle number (limited to 35 cycles) were optimised over a broad range. The initial denaturation temperature was 94°C for 5 min with a slightly altered extension temperature of 60°C used for all amplifications. The final elongation temperature was 72°C for 7 min. For all reactions 100 µM of dATP, dCTP, dGTP and dTTP mix was used along with 1.0 U of FIREPol® *Taq* DNA polymerase. These conditions were similarly used for nested PCR, where a second PCR product is amplified from the product of the first reaction. For this technique the first product was amplified using primers PyCtrNe-fwd and PyCtrNe-rev, with a second product amplified from this using PyCtrFL-fwd and PyCtrFL-rev. Table 2.6 illustrates the optimised PCR conditions determined for each set of primers used in this study. The 10× PCR buffer used was detergent and $MgCl_2$ free. PCR products of interest were separated on an agarose gel and purified (Section 2.6.7) before cloning.

Table 2.6 Primer properties, $MgCl_2$ concentration and thermal cycling conditions used for PCR

Primer name	T_m (°C)	[Primer] (µM)	[$MgCl_2$] (µM)	Thermal cycle conditions [°C (time)]	Cycles
PyCtrFL-fwd	44.8	0.5	2.5	94 (30 s) → 40 (30 s) → 60 (2 min)	35
PyCtrFL-rev	61.8	0.5			
PyCtrNe-fwd	58.9	0.7	2.5	94 (30 s) → 50 (30 s) → 60 (2 min)	35
PyCtrNe-rev	55.2	0.7			
PbCtrNt-fwd	53.1	0.5	2.5	94 (30 s) → 45 (30 s) → 60 (2 min)	30
PbCtrNt-rev	62.2	0.5			
PfCtr211FL/Nt-fwd	58.7	0.8	2.5	94 (30 s) → 40 (30 s) → 60 (2 min)	30
PfCtr211FL-rev	42.7	0.8			
PfCtr211Nt-rev	55	0.8			
PfCtr369FL/Nt-fwd	58.9	0.8	2.5	94 (30 s) → 40 (30 s) → 60 (2 min)	30
PfCtr369FL-rev	52.2	0.8			
PfCtr369Nt-rev	63.9	0.8			
PyCox17-fwd	56	0.8	2.5	94 (30 s) → 50 (30 s) → 60 (2 min)	30
PyCox17-rev	70.8	0.8			
PfCox17-fwd	63	0.8	2.5	94 (30 s) → 50 (30 s) → 60 (2 min)	30
PfCox17-rev	70.1	0.8			
Py/PfLDH-fwd	61.8	0.5	2.5	94 (30 s) → 50 (30 s) → 60 (2 min)	30
Py/PfLDH-rev	58.2	0.5			

2.6.6 Reverse transcriptase polymerase chain reaction for the analysis of PBANKA_130290 expression

Reverse transcription polymerase chain reaction (RT-PCR) was carried out with Promega's Improm II™ Reverse Transcription System kit according the manufacturer's instruction. *P. berghei* total RNA isolated from purified parasites (Section 2.6.2) was used as template. The first strand cDNA synthesis was amplified, according to the manufacturer's instructions, with the provided oligodT or random oligonucleotide hexamers. The reverse transcriptase cDNA product, from both oligodT and random oligonucleotide hexamers, was subsequently used for PCR amplification using the following primers: PbCtrNt-fwd, PbCtrNt-rev, PyLDH-fwd and PyLDH-rev (Table 2.5). The conditions for PCR were as per those described in Section 2.6.5 and Table 2.6. The amplified PCR product was resolved on a 1% agarose gel and an image captured with the VersaDoc™ image documentation system under ultraviolet light.

2.6.7 Purification of DNA from agarose gel

In this study, purification of the desired PCR products and restriction endonuclease-digested expression vectors was carried out using the peqGOLD™ gel extraction kit. The extraction kit is designed to rapidly purify DNA fragments, resolved by agarose gel electrophoresis, using mini-spin columns containing a silica membrane. The kit is based on the capability of guanidine thiocyanate to denature the agarose gel, at 60 – 65°C, and extract the DNA fragment. The extracted DNA is then tightly bound to the silica membrane whilst the remaining reaction by-products, buffer ions and solubilised agarose gel flow through. Following washing with an ethanol-based wash solution, the bound DNA fragment is concentrated into a smaller volume by elution with TE buffer or sterile distilled water as per the manufacturer's instruction. The approximate concentration of the purified sample was then determined by agarose gel electrophoresis. This was achieved by comparing the intensity of the purified band to those of the Fermentas DNA MassRuler™ molecular weight standards, whose concentrations are known. Excision of the desired DNA fragment was achieved by viewing the agarose gel under UV light for ≤20 sec. This short exposure was adhered to so as to prevent UV-mediated cutting of DNA fragment.

2.6.8 Ligation of purified cDNA fragments into a pGEM®-T cloning vector

The pGEM®-T cloning vector (Figure 2.1) is a 3000 bp linearised vector with a single 3´-terminal thymidine overhang at both ends. These overhangs improve the efficiency of PCR product ligation by preventing recircularisation of the vector and providing compatible overhangs for PCR products generated by the thermostable FIREPol® *Taq* polymerase. This vector is high

copy number and contains the T7 and SP6 RNA polymerase promoters, which flank the multiple cloning site (MCS) within the α-peptide coding region of the enzyme β-galactosidase. Insertion of a PCR product within this site results in the inactivation of the α-peptide, thereby allowing identification of recombinants by blue/white colony screening on indicator plates. To further assist with the selection of vector transformed cells, pGEM®-T contains the gene for ampicillin resistance (β-lactamase). In this study, gene fragments derived from RT-PCR amplification of *P. berghei* total RNA as well as PCR amplification of *P. yoelii* and *P. falciparum* genomic DNA (primers for amplification of putative amino-terminal coding domains and Cox17 described in Table 2.5) were gel purified and ligated into pGEM®-T. Plasmids containing the gene of interest were subsequently propagated, purified and the gene excised from the recombinant plasmid using the relevant restriction enzymes. The generated gene fragments, containing non-cohesive 5' and 3' overhangs, were used for subcloning into the desired expression vectors (Section 2.6.11).

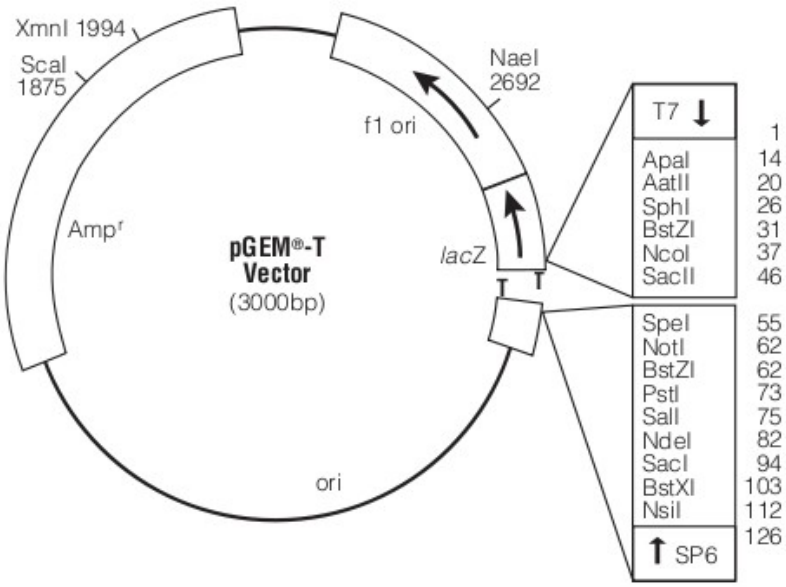

Figure 2.1 Map of the pGEM®-T cloning vector

The pGEM®-T vector contains the *lac*Z gene, encoding the enzyme β-galactosidase, which forms the basis of blue:white colony screening used for the identification of positive colonies. The desired insert is ligated into the region between *Sac*II and *Spe*I, where the thymidine overhangs are located. Also included, for targeted vector selection, is the ampicillin resistance gene (Amp^r) (*Adapted from pGEM®-T and pGEM®-T easy systems technical manual*).

2.6.9 cDNA ligation using T4 DNA ligase

DNA ligation is a biochemical reaction specifically catalysed by DNA ligase. This technique enables the ligation of PCR products or excised genomic DNA fragments into a plasmid vector that are in turn either used for recombinant expression of the protein encoded by the inserted DNA fragment or for the creation of a cDNA library (Sambrook *et al.*, 1989a). The T4 DNA

ligase and 10× T4 DNA ligase buffer used in these experiments were obtained from Fermentas™.

2.6.9.1 Materials

10× T4 DNA ligase buffer, T4 DNA ligase, gel-purified PCR or RT-PCR amplicons, linearised and purified expression plasmid DNA and sterile double distilled water (ddH_2O) were used.

2.6.9.2 Method

The desired cDNA insert was obtained by restriction endonuclease-digestion of the pGEM-T cloning vector and purified from an agarose gel as described in Section 2.6.7. As before, the approximate concentration of the purified insert was determined by comparison to the Fermentas DNA MassRuler™. The final volume of the ligation reaction was 10 µl, with the purified cDNA insert and plasmid DNA added at a ratio of 4:1 (insert:plasmid). The additional components added to the ligation reaction are shown in Table 2.7. Prior to overnight incubation at 4°C, the reaction components were mixed with gentle flicking followed by a brief centrifugation step. The reaction mix was used directly for transformation of competent *E. coli* cells, without deactivation of the enzyme.

Table 2.7 Reaction parameters for DNA ligation

Component	Quantity
10× T4 ligase buffer	1.0 µl
Purified cDNA	4× [plasmid]
Expression plasmid	0.25× [insert DNA]
T4 DNA ligase	2.5 U
Sterile ddH_2O	Variable
Total volume	10 µl

2.6.10 Isolation of plasmid DNA

Plasmid DNA was isolated by the phenol-chloroform-isoamyl alcohol method (Sambrook *et al.*, 1989b). The method is based on the principle that chromosomal and plasmid DNA, found in a bacterial lysate, can be differentially precipitated. Purity of the isolated plasmid was evaluated by agarose gel electrophoresis.

2.6.10.1 Materials

GTE solution [50 mM glucose, 25 mM Tris-HCl pH 8, 10 mM EDTA]. Glucose (1 g), Tris (0.3 g) and Na_2EDTA (0.37 g) were dissolved in 80 ml of distilled water, titrated to pH 8 with HCl and

made to a final volume of 100 ml with distilled water. The solution was autoclaved and stored at 4°C.

Lysis solution [1% (w/v) SDS, 0.2 M NaOH]. NaOH (0.08 g) and SDS (0.1 g) were dissolved in 10 ml of distilled water. This solution was stored at 4°C and made fresh weekly.

Potassium acetate [3 M KOH, pH 4.8]. KOH pellets (16.8 g) were dissolved in 25 ml of acetic acid, the pH checked after neutralisation and adjusted to 4.8 with acetic acid as necessary. The solution was made up to a final volume of 100 ml with distilled water and stored at 4°C.

Phenol-chloroform-isoamyl alcohol [25:24:1 (v/v)]. Liquefied phenol (50 ml), chloroform (48 ml) and isoamyl alcohol (2 ml) were mixed together and stored at RT in an amber bottle.

Chloroform-isoamyl alcohol [24:1 (v/v)]. Chloroform (48 ml) and isoamyl alcohol (2 ml) were mixed together and stored at RT.

Sodium acetate [3 M NaOH, pH 5.5]. NaOH pellets (12 g) were dissolved in 25 ml of acetic acid, the pH checked after neutralisation and adjusted to 5.5 with acetic acid. The solution was made up to a final volume of 100 ml with distilled water and stored at 4°C.

70% (v/v) ethanol. Absolute ethanol (70 ml) was made up to 100 ml with distilled water and stored at -20°C.

2.6.10.2 Method

E. coli cells (50 ml overnight culture) containing the desired plasmid were pelleted by centrifugation (4000 *g*, 15 min, 4°C) and the resulting pellet resuspended in GTE solution ($1/100^{th}$ of the original culture volume). RNAse (50 µg/ml) and lysis solution (0.5 ml) were subsequently added and the cells mixed at RT for 5 min to help effect complete cell lysis. Potassium acetate (1 ml) was added, mixed for 5 min and then centrifuged (11 500 *g*, 30 min, RT). The supernatant was carefully removed and transferred to a fresh DNAse-free tube. An equal volume of phenol-chloroform-isoamyl alcohol was added and mixed gently for 5 min. The mixture was centrifuged (11 500 *g*, 30 min, RT) and the upper aqueous phase carefully transferred to a fresh tube. An equal volume of chloroform-isoamyl alcohol was added and this was mixed for 2 min at RT. The mixture was again centrifuged (11 500 *g*, 30 min, RT) and the upper aqueous phase transferred to a fresh tube. Sodium acetate ($1/10^{th}$ the volume of aqueous supernatant) and ice-cold absolute ethanol (2.5 volume of the aqueous supernatant)

were added to the aqueous supernatant, mixed and incubated at -20°C (1 h). The precipitated plasmid was pelleted by centrifugation (11 500 *g*, 30 min, 4°C), washed twice with ice-cold 70% ethanol and resuspended in sterile 1× TE buffer (50 µl). The purity of the isolated plasmid DNA was evaluated by agarose gel electrophoresis.

2.6.11 Expression plasmids used in the study

pET-23a

The pET-23a plasmid (Figure 2.2) was the initial expression vector used for the recombinant expression of the amino terminal domain of the putative *P. berghei* copper transport protein (*Pb*CtrNt). The 447bp gene fragment containing the amino terminal domain was ligated into the vector at the *Eco*RI and *Not*I restriction sites. The product was expected to have an addition of approximately 23 amino acid residues due the position of the insert relative to the start codon, which is situated at the *Nde*I restriction site (bp 238 on the plasmid). The host strain used for pET-23a expression was the *E. coli* BL21(DE3) pLysS strain. The recombinant construct is from here on referred to as pT-*Pb*CtrNt.

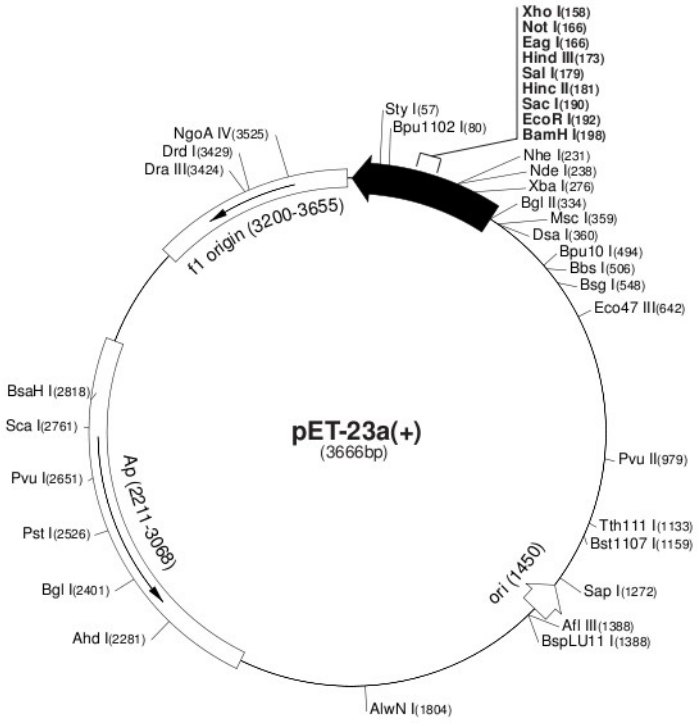

Figure 2.2 Map of the pET-23a expression plasmid

The figure illustrates the restriction sites and important features of the pET-23a plasmid including the ampicillin resistant gene (Ap) and the multiple cloning region. The genes of interest were either inserted in the *Eco*RI and *Not*I (*Pb*CtrNt; *Py*Cox17) or *Bam*HI and *Not*I (*Pf*Cox17) sites. Genes were inserted in frame with the C-terminal His_6-tag and transcribed in the direction indicated by the solid black arrow (➡) housing the multiple cloning site (*Adapted from Novagen manual*).

In addition to the above, the pET23a construct was utilised for the recombinant expression of both the *P. yoelii* and *P. falciparum* putative Cox17 proteins. The *P. yoelii* gene (192bp) was

ligated into the vector at the *Eco*RI and *Not*I restriction sites, whilst the *P. falciparum* gene (195bp) was ligated into the *Bam*HI and *Not*I restriction sites. As stated above, both products were expected to have an additional 23 amino acid residues. The host strain used for pET-23a expression of the Cox17 constructs was the *E. coli* BL21(DE3) strain. The recombinant constructs for *P. yoelii* and *P. falciparum* are referred to as pT23-*Py*Cox17 and pT23-*Pf*Cox17, respectively.

pET-28a

In this study, pET-28a (Figure 2.3) was used for the recombinant expression of both the *P. yoelii* and *P. falciparum* putative Cox17 copper chaperones. The 192bp *P. yoelii* gene was ligated into the vector at the *Eco*RI and *Not*I sites, whilst the 195bp *P. falciparum* gene was ligated into the *Bam*HI and *Not*I sites. Both products were expected to have the addition of approximately 41 amino acid residues due the position of the insert relative to the start codon, which is situated at the *Nco*I restriction site (bp 296 on the plasmid). The host strain used for pET-28a expression in this study was the *E. coli* BL21(DE3) strain. As with the pET23a constructs, the *P.* yoelii and *P. falciparum* pET28a constructs are from here on referred to as pT28-*Py*Cox17 and pT28-*Pf*Cox17, respectively.

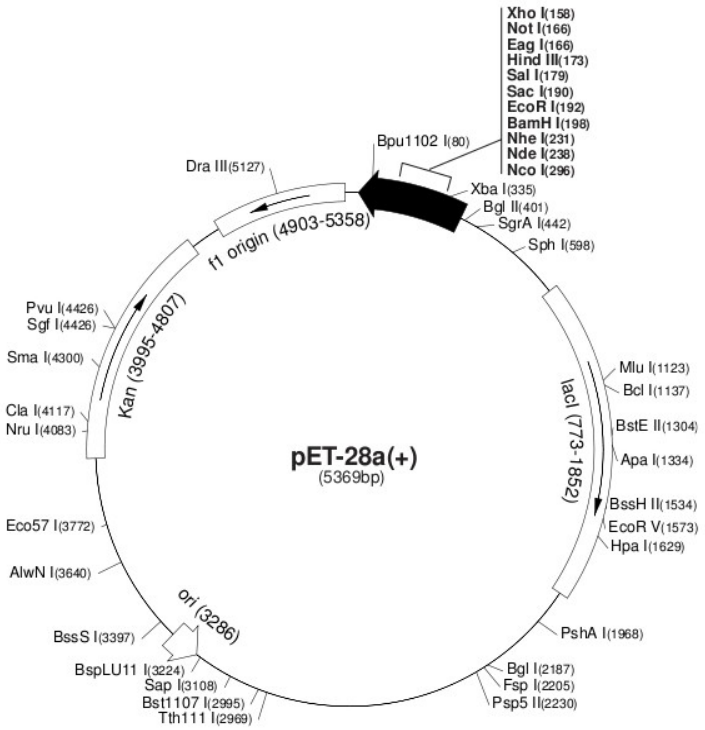

Figure 2.3 Map of the pET-28a expression plasmid

The figure illustrates restriction sites and important features of the pET-28a plasmid including the kanamycin resistant gene (kan) and the multiple cloning region. The genes of interest were either inserted in the *Eco*RI and *Not*I (*Py*Cox17) or *Bam*HI and *Not*I (*Pf*Cox17) sites. Inserts were inserted in frame with the N-terminal His_6-tag and transcribed in the direction indicated by the solid black arrow (➡) housing the multiple cloning site . (*Adapted from Novagen manual*).

pGex-4T-1

pGex-4T-1 (Figure 2.4) was initially used for the recombinant expression of *Pb*CtrNt in an effort to overcome insoluble recombinant protein production. The 447bp gene fragment, coding for the putative *P. berghei* amino terminal domain, was ligated into the vector at the *Eco*RI and *Not*I sites in frame with the N-terminal GST protein. The host strain used for expression was *E. coli* BL21. The construct is referred to as pGx-*Pb*CtrNt. In addition to this, the pGex-4T-1 vector was used for the recombinant expression of *Pf*Cox17, following unsuccessful attempts with the two pET vectors described above. The 195bp *Pf*Cox17 gene was ligated into the *Bam*HI and *Not*I sites in frame with the N-terminal GST protein. The host strain used for expression was *E. coli* BL21. The Cox17 construct is referred to as pGx-*Pf*Cox17.

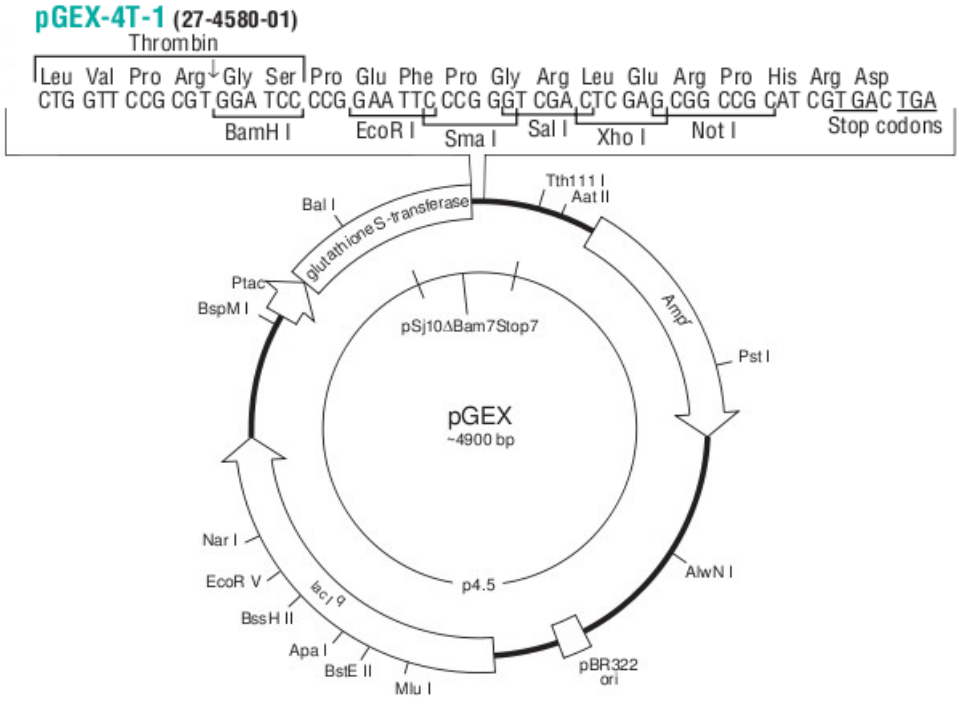

Figure 2.4 Map of pGEX-4T-1 expression plasmid

The figure illustrates the restriction sites of the multiple cloning region and other important features of the plasmid. These features include the glutathione S-transferase (GST) gene, the ampicillin resistant gene (Amp^r) and the inducible P_{tac} promoter. The genes of interest were either inserted in the *Eco*RI and *Not*I sites (*Pb*CtrNt) or the *Bam*HI and *Not*I sites (*Pf*Cox17), in frame with the GST gene. (*Adapted from GE Health care manual*).

pMal-c2X and pMal-p2X

The pMal-2 series of expression vectors (Figure 2.5) were initially used for the same purpose as the pGex-4T-1 vector, to try to overcome the expression of insoluble *Pb*CtrNt. Both pMal-2 vectors contain the *malE* gene, encoding the highly soluble maltose binding protein (MBP). The difference between pMal-c2X and -p2X lies in the removal of the *malE* signal sequence in the pMal-c2X vector, resulting in cytoplasmic expression of the recombinant protein. The retention

of the *malE* signal sequence in the pMal-p2X vector results in targeting of the expressed recombinant protein to the cell periplasm. The 447bp gene fragment, coding for the putative *P. berghei* amino terminal domain, was ligated into both the pMal-c2X and -p2X vectors at the *Eco*RI and *Pst*I sites, in frame with the N-terminal MBP. The host strain used for recombinant expression was *E. coli* JM103 or BL21. The pMal-c2X construct is referred to as pMc-*Pb*CtrNt and the pMal-p2X construct as pMp-*Pb*CtrNt

In addition to the above, the pMal-2 series of vectors were also used for the recombinant expression of the amino-terminal domains of the two putative *P. falciparum* copper transport proteins (PF14_0211 and PF14_0369). An identical approach was adopted for these two proteins where the respective gene fragments (132bp for PF14_0211 and 282bp for PF14_0369) were ligated into both the pMal vectors at the *Eco*RI and *Pst*I sites, in frame with the N-terminal MBP. The host strain used for recombinant expression was *E. coli* JM103. The pMal-c2X constructs are referred to as pMc-*Pf*Ctr211Nt and pMc-*Pf*Ctr369Nt for PF14_0211 and PF14_0369, respectively. Similarly the pMal-p2X constructs are referred to as pMp-*Pf*Ctr211Nt and pMp-*Pf*Ctr369Nt for PF14_0211 and PF14_0369, respectively.

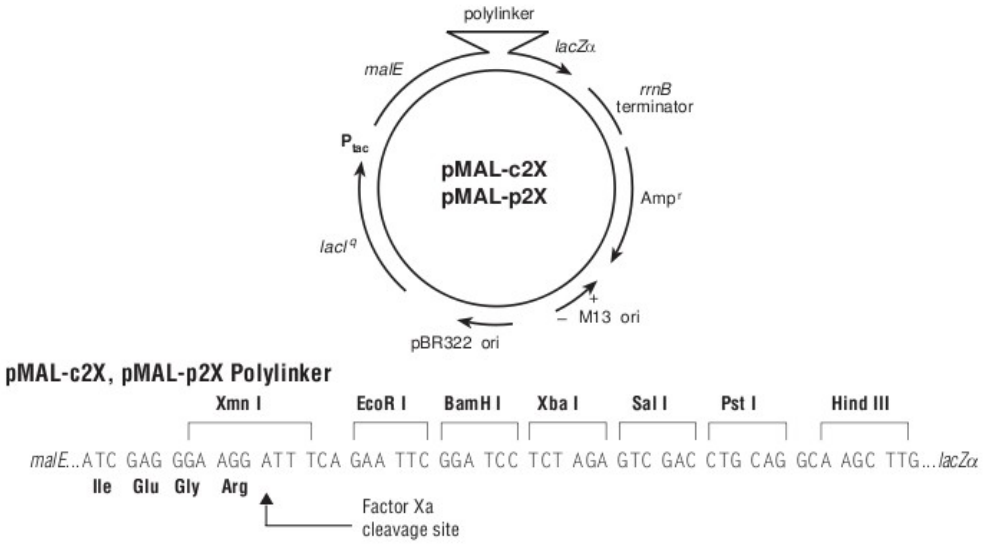

Figure 2.5 Map of the pMal-2x expression plasmids

The figure illustrates the restriction sites of the polylinker region and other important features of the plasmid. These features include the *malE* gene, the ampicillin resistant gene (Amp^r) and the inducible P_{tac} promoter. The genes of interest were inserted in the *Eco*RI and *Pst*I sites, in frame with the *malE* gene for fusion to a maltose binding carrier protein (*Adapted from the NEB pMAL™ protein fusion and purification manual*).

2.6.12 Restriction endonuclease digestion of plasmids

For insertion of the desired gene fragment into an expression vector it was necessary to prepare the expression plasmids by restriction digestion. This was achieved with the two

enzymes used to liberate the relevant fragment from the pGEM®-T cloning vector. The enzymes utilised for each respective preparation were specifically selected to create non-cohesive 5' and 3' overhangs that insure correct orientation and in frame ligation of the gene of interest. Digestion of the plasmid does, however, result in the creation of free 5'-phosphate groups. The presence of this group allows for an undesirable re-circularisation of the plasmid when DNA ligase is introduced for gene product ligation. This unwanted result is avoided by dephosphorylating the digested plasmid with shrimp alkaline phosphatase (SAP) prior to ligation. Restriction enzyme digestion of the expression plasmid was confirmed by agarose gel electrophoresis, following which the digested plasmid was gel purified (Section 2.6.7). Linearised plasmids were purified prior to ligation to eliminate nucleic acid fragments, buffer components, enzymes and nucleotides that can compromise the insertion of a target gene into the plasmid. The desired gene fragment, to be subcloned into an expression plasmid, was initially ligated into the pGEM®-T vector (Section 2.6.8) for propagation in *E. coli*. This strategy reduces the likelihood of PCR-introduced mutations being carried into an expression vector following direct ligation of PCR products. The inserts are liberated from the cloning vector using the relevant restriction enzymes described in section 2.6.11. As previously mentioned, liberated gene fragments were gel purified prior to ligation for reasons mentioned above.

2.6.12.1 Materials

*EcoR*I, *Bam*HI, *Not*I and *Pst*I restriction enzymes, shrimp alkaline phosphatase (SAP), Fermentas 10× Orange Buffer™ (Buffer O) and recombinant/non-recombinant super coiled plasmid DNA were used.

2.6.12.2 Method

A single *E. coli* colony harbouring the desired expression plasmid or cloning vector plus inserted fragment was used to inoculate 10 ml of LB medium plus antibiotic. This culture was grown overnight at 37°C with shaking (200 rpm). Cells were pelleted by centrifugation (4000 *g*, 15 min, 25°C) and plasmid DNA isolated as described in Section 2.6.10. Once purified the plasmid was digested as follows: 10× Buffer O (5 µl), plasmid DNA (44 µl) and the first (*EcoR*I/*Bam*HI) restriction enzyme (1 µl) followed by incubation at 37°C (2 h). The first enzyme was deactivated (65°C, 20 min) and digestion confirmed by agarose gel electrophoresis (Section 2.6.1). If the digestion was successful 1 µl of the second enzyme (*Not*I/*Pst*I) was added directly to the mix and incubated (RT, overnight). Following this second incubation the enzyme was again deactivated (85°C, 15 min). For preparation of the expression vectors, shrimp alkaline phosphatase (SAP) (1 µl) was added to the digestion mix and immediately incubated (37°C, 30 min). Gene fragments liberated from the cloning vector were not

dephosphorylated with SAP. The dephosphorylated plasmid and liberated DNA fragment were subsequently purified from an agarose gel (Section 2.6.7) before proceeding with the ligation reaction.

2.6.13 *E. coli* hosts used for cloning and expression of recombinant proteins

Table 2.8 *E. coli* host cell genotypes used for cloning and expression of recombinant proteins

***E. coli* strain**	**Genotype**	**Application**
JM109	F´ *traD36 proA⁺B⁺ lacI^q Δ(lacZ)M15/ Δ(lac-proAB) glnV44 e14⁻ gyrA96 recA1 relA1 ndA1 thi hsdR17(rK⁻mK⁺)*	Maintenance and propagation of recombinant plasmids for transformation into expression cells
BL21[p]	*F⁻ ompT hsdS$_B$ (r$_B$⁻ m$_B$⁻)gal dcm*	Expression of recombinant pGEX-4T-1
BL21(DE3)[p]	*F⁻ ompT hsdS$_B$ (r$_B$⁻ m$_B$⁻)gal dcm (DE3)*	Expression of recombinant pET-23a and pET-28a containing the putative copper chaperone Cox17
BL21(DE3) pLysS[p]	*F⁻ ompT hsdS$_B$ (r$_B$⁻ m$_B$⁻)gal dcm (DE3) pLysS (CamR)*	Expression of recombinant pET-23a vector containing *Pb*CtrNt
JM103	endA1 glnV44 sbcBC rpsL thi-1 Δ(lac-proAB) F'[traD36 proAB⁺ lacI^q lacZΔM15]	Expression of recombinant pMal-c2X and pMal-p2X

[p] deficient in lon protease

2.6.14 Transformation and culturing of *E. coli* transformants

2.6.14.1 Materials

Super Optimal broth with Catabolite repression (SOC medium) [2% (w/v) tryptone, 0.5% (w/v) yeast extract, 10 mM NaCl, 2.5 mM $MgCl_2$, 10 mM $MgSO_4$ and 20 mM Glucose]. Tryptone (0.5 g), NaCl (0.015 g) and yeast extract (0.125 g) were dissolved in 25 ml of double distilled water and autoclaved. The medium was cooled to ~ 55°C and $MgCl_2.6H_2O$ (125 µl), $MgSO_4$ (500 µl) and glucose (1 ml) added. The final volume of the solution was made up to 50 ml with sterile (autoclaved) double distilled water. The media was aliquoted into sterile microfuge tubes and stored at -20°C.

$MgCl_2.6H_2O$ [1 M]. $MgCl_2.6H_2O$ (2.03 g) was dissolved in a final volume of 10 ml with double distilled water and filter sterilised through a 0.22 µm syringe filter. The solution was used for SOC medium.

$MgSO_4$ [1 M]. $MgSO_4$ (1.2 g) was dissolved in a final volume of 10 ml with double distilled water and filter sterilised through a 0.22 µm syringe filter. The solution was used for SOC medium.

Glucose [1 M]. Glucose monohydrate (1.98 g) was dissolved in a final volume of 10 ml with double distilled water and filter sterilised through a 0.22 µm syringe filter. The solution was used for SOC medium.

LB-agar [1% (w/v) tryptone, 0.5% (w/v) yeast extract, 1.5% (w/v) agar, 0.5% (w/v) NaCl, pH 7.4]. Tryptone (10 g), yeast extract (5 g) and NaCl (5 g) were resuspended and dissolved in 900 ml distilled water. The pH was adjusted to 7.4 with NaOH, agar (15 g) added and the volume made up to 1 ℓ with distilled water. The medium was autoclaved (121°C, 20 min), cooled to ~55°C and the desired antibiotic added to the working concentration indicated in Table 2.9. The media was dispensed into sterile plastic culture plates, allowed to solidify and then sealed with Parafilm™. Plates were stored inverted at 4°C.

LB medium [1% (w/v) tryptone, 0.5% (w/v) yeast extract, 0.5% (w/v) NaCl, pH 7.4]. Tryptone (10 g), yeast extract (5 g) and NaCl (5 g) were resuspended and dissolved in 900 ml distilled water. The pH was adjusted to 7.4 with NaOH and the volume made up to 1 ℓ with distilled water. The medium was autoclaved (121°C, 20 min), cooled to ~ 55°C and the desired antibiotic added to the working concentration indicated in Table 2.9. The desired volume of medium was dispensed into sterile Erlenmeyer flasks and used to culture *E. coli* cells.

Potassium acetate [1 M, pH 7.5]. Potassium acetate (9.8 g) was dissolved in 60 ml of double distilled water, titrated to pH 7.5 with KOH and the volume made up to 100 ml. The solution was sterilised by filtration through a 0.22 µm syringe filter. This reagent was used in frozen stock buffer and DTT-DMSO reagents.

Frozen stock buffer (FSB) [100 mM KCl, 45 mM $MnCl_2.4H_2O$, 10 mM $CaCl_2.2H_2O$, 3 mM hexamine cobalt chloride ($HACoCl_3$) 10 mM potassium acetate and 10% (w/v) glycerol, pH 6.2]. Potassium acetate (1 ml), KCl (0.74 g), $MnCl_2.4H_2O$ (0.98 g), $CaCl_2.2H_2O$ (0.15 g), $HACoCl_3$ (80 mg) and glycerol (10 g) were dissolved in 80 ml of double distilled water, titrated to pH 6.2 and the volume made up to 100 ml. The buffer was sterilised by filtration through a 0.22 µm syringe filter and used immediately for the preparation of competent *E. coli* cells.

DTT-DMSO [1 M DTT, 10 mM potassium acetate and 90% (v/v) DMSO]. Molecular biology grade DTT (1.54 g), potassium acetate (0.1 ml) and DMSO (9 ml) were made up to 10 ml with sterile double distilled water. This reagent was either used immediately or stored at -20°C.

2.6.14.2 Method

Preparation of competent cells

A single *E. coli* colony was grown overnight in 10 ml LB medium (37°C) and then diluted 1:100 in fresh medium. This culture was grown at 37°C to an OD_{600} between 0.4 – 0.6 following which cells were pelleted (4000 *g*, 15 min, 4°C), drained thoroughly and gently resuspended in ice-cold frozen stock buffer (1/10th of culture volume). This cell suspension was incubated on ice for 15 min and then pelleted (4000 *g*, 15 min, 4°C). The cells were again gently resuspended in ice-cold frozen stock buffer (1/50th of culture volume) and 17.5 µl of DTT-DMSO added. This was gently mixed and then incubated on ice for 10 min. A further 17.5 µl of DTT-DMSO was added to the cell suspension, mixed gently and the suspension incubated on ice for 20 min. Aliquots of 50 µl were dispensed into cold, sterile microfuge tubes and the cells snap-frozen in liquid nitrogen (2 min). Aliquots were stored at -70°C until required.

Transformation of competent *E. coli* cells

Ligation mix (5 µl) or plasmid DNA was added to an aliquot of competent cells, incubated on ice for 30 min and then heat shocked at 42°C for 60 sec. The cells were immediately returned to ice and incubated for 2 min. Following this, SOC medium (450 µl) was added to the cells and incubated at 37°C for 60 min with shaking. The cells were plated on duplicate LB-agar plates containing the desired antibiotic and incubated inverted, overnight at 37°C.

2.6.15 Antibiotics used for positive selection and maintenance of *E. coli* transformants

Stock solutions of the ampicillin and kanamycin were prepared in double distilled water, whilst chloramphenicol was prepared in methanol. All solutions were sterilised by filtration through a 0.22 µm syringe filter and aliquotted into sterile microfuge tubes, in a sterile environment, for storage at -20°C. Chloramphenicol was dissolved in methanol due to its insolubility in water. Table 2.9 illustrates the applications as well as the concentration of the stock and working solutions of the antibiotics used in this study.

Table 2.9 Concentration and applications of the selective antibiotics used

Antibiotic	[Stock] (mg/ml)	[Working] (µg/ml)	Application
Ampicillin	50	100	Used in LB-agar plates as well as overnight and outgrowth cultures of *E. coli* cultures with ampicillin-encoded expression vectors pET-23a, pGEX-4T-1, pMal-c2X and pMal-p2X. It was similarly used for the selection of cells containing the pGEM®-T vector.
Chloramphenicol	35[a]	100	Used in LB-agar plates as well as overnight and outgrowth cultures of *E. coli* BL21(DE3) pLysS cells with the pLysS encoded plasmid. pLysS is used for tight regulation of IPTG induced expression of the recombinant protein.
Kanamycin	30	30	Used in LB-agar plates as well as overnight and outgrowth cultures of *E. coli* cells containing the recombinant pET-28a vector for expression.

[a] Stock solution prepared in 100% methanol

2.7 Recombinant protein expression and purification

This section describes all techniques employed for the recombinant expression and purification of *Pb*CtrNt, *Pf*Ctr211Nt, *Pf*Ctr369Nt, *Py*Cox17 and *Pf*Cox17. The protocol used to establish copper binding to each of the respective recombinant proteins is also described. SDS-PAGE analysis and western blotting techniques are described in Sections 2.4.1 and 2.4.3, respectively.

2.7.1 Expression of pET, pGex-4T-1 and pMal-2 vector encoded recombinant proteins

2.7.1.1 Materials

2xYT medium [1.6% (w/v) tryptone, 1% (w/v) yeast extract, 0.5% (w/v) NaCl, pH 7.2]. Tryptone (16 g), yeast extract (10 g) and NaCl (5 g) were dissolved in 900 ml distilled water. The pH was adjusted to 7.2 with NaOH and the volume made up to 1 ℓ with distilled water. The medium was autoclaved (121°C, 20 min), cooled to ~55°C and the desired antibiotic added to the working concentration indicated in Table 2.9. The desired volume of medium was dispensed into sterile Erlenmeyer flasks and used to culture *E. coli* cells.

M9 minimal medium [50 mM Na_2HPO_4, 20 mM KH_2PO_4, 20 mM NH_4Cl, 10 mM NaCl, 2 mM $MgSO_4$, 100 µM $CaCl_2$, 0.2% glucose]. Na_2HPO_4 (6.8 g), KH_2PO_4 (3.0 g), NaCl (0.5 g) and NH_4Cl (1.0 g) were dissolved in 990 ml of distilled water and autoclaved. The medium was cooled to ~55°C and $MgSO_4$ (2 ml), $CaCl_2$ (100 µl) and glucose (10 ml) were added. The desired antibiotic was then added to the working concentration indicated in Table 2.9 and the required volume of medium dispensed into sterile Erlenmeyer flasks for *E. coli* cell culture.

$MgSO_4$ [1 M]. $MgSO_4$ (1.2 g) was dissolved in a final volume of 10 ml double distilled water and filter sterilised through a 0.22 µm syringe filter. The solution was used for M9 minimal medium .

$CaCl_2$ [1 M]. $CaCl_2$ (1.11 g) was dissolved in a final volume of 10 ml double distilled water and filter sterilised through a 0.22 µm syringe filter. The solution was used for M9 minimal medium.

Glucose [20%]. Glucose monohydrate (2.0 g) was dissolved in a final volume of 10 ml double distilled water and filter sterilised through a 0.22 µm syringe filter. The solution was used for M9 minimal medium.

0.1 M PMSF stock solution. PMSF (0.174 g) was dissolved in 100% isopropanol (10 ml), aliquotted and stored at -20°C.

0.5 M Na_2EDTA, pH 8. Na_2EDTA (g) was dissolved in 90 ml of distilled water, titrated to pH 8 with HCl and made to a final volume of 100 ml with distilled water.

10% (w/v) NaN_3 stock solution. NaN_3 (5 g) was dissolved in 50 ml distilled water and stored at RT.

Cell resuspension buffer 1 [50 mM NaH_2PO_4, 300 mM NaCl, 10 mM Imidazole, 5% (v/v) glycerol, 1 mM PMSF, 0.01% (w/v) NaN_3, pH 8]. NaH_2PO_4 (0.6 g), NaCl (1.754 g), imidazole (0.068 g) and glycerol (5 ml) were dissolved in 90 ml of distilled water. The solution was titrated to pH 8 with NaOH followed by the addition of NaN_3. The buffer was made up to a final volume 100 ml with distilled water. Following cell resuspension and just prior to cell disruption, PMSF was added to a final concentration of 1 mM.

Cell resuspension buffer 2 [100 mM NaH_2PO_4, 300 mM NaCl, 10 mM Imidazole, 12 mM 2-mercaptoethanol, 5% (v/v) glycerol, 1 mM PMSF, 0.01% (w/v) NaN_3, pH 8]. NaH_2PO_4 (1.2 g), NaCl (1.754 g), imidazole (0.068 g), 2-mercaptoethanol (100 µl) and glycerol (5 ml) were dissolved in 90 ml of distilled water. The solution was titrated to pH 8 with NaOH followed by the addition of NaN_3. The buffer was made up to a final volume 100 ml with distilled water. Following cell resuspension and just prior to cell disruption, PMSF was added to a final concentration of 1 mM.

Phosphate buffered saline (PBS), pH 7.2. As per Section 2.4.4.1

pMal column buffer [100 mM NaH_2PO_4, 200 mM NaCl, 1 mM EDTA, 0.01% (w/v) NaN_3, pH 7.4]. NaH_2PO_4 (11.998 g), NaCl (11.668 g) and EDTA (2 ml of 0.5 M Na_2EDTA) were dissolved in 950 ml of distilled water, titrated to pH 7.4 with NaOH and NaN_3 added. The buffer was made to a final volume of 1 ℓ with distilled water.

Tris/sucrose buffer [200 mM Tris, 20% (w/v) Sucrose, pH 8]. Tris (12.11 g) and sucrose (100 g) were dissolved in 350 ml distilled water, titrated to pH 8 with HCl and made to a final volume of 500 ml.

2.7.1.2 Method

Expression of His_6-*Pb*CtrNt, His_6-*Py*Cox17, GST-*Pb*CtrNt, GST-*Pf*Cox17, MBP-*Pb*CtrNt, MBP-*Pf*Ctr211Nt^{TD} and MBP-*Pf*Ctr369Nt^{TD}

Table 2.10 Culture conditions used for recombinant expression of constructs prepared for this study

Construct	*E. coli* host cell	Antibiotics*	Growth medium	Cultivation temperature (°C)	IPTG concentration (mM)	Induction time (h)
pT-*Pb*CtrNt	BL21(DE3) pLysS	Ampicillin and chloramphenicol	LB	30	0.4	5
pT23-*Py*Cox17	BL21(DE3)	Ampicillin	2xYT	37	0.4	5
pT28-*Py*Cox17	BL21(DE3)	Kanamycin	2xYT	37	1	5
pT23-*Pf*Cox17	BL21(DE3)	Ampicillin	2xYT	37	0.4	5
pT28-*Pf*Cox17	BL21(DE3)	Kanamycin	2xYT	37	1	5
pGx-*Pb*CtrNt	BL21	Ampicillin	LB	37	0.5	4
pGx-*Pf*Cox17	BL21	Ampicillin	LB	37	0.5	4
pMc-*Pb*CtrNt	JM103/BL21	Ampicillin	LB	30	0.3	4
pMc-*Pf*Ctr211Nt	JM103	Ampicillin	LB	30	0.3	4
pMc-*Pf*Ctr369Nt	JM103	Ampicillin	LB	30	0.3	4
pMp-*Pb*CtrNt	JM103	Ampicillin	LB	30	0.3	16
pMp-*Pf*Ctr211Nt	JM103	Ampicillin	LB	30	0.3	16
pMp-*Pf*Ctr369Nt	JM103	Ampicillin	LB	30	0.3	16

* Refer to table 2.9 for antibiotic concentrations

The following describes a generic protocol followed for the expression of the five respective recombinant proteins being studied. Each construct was transformed (Section 2.6.14) into a selected *E. coli* host cell (Table 2.10) and positive colonies identified. A colony containing the desired plasmid construct was selected and prepared as a three-way steak on a LB-agar plate

supplemented with the relevant antibiotic/s (Table 2.9 and 2.10). Agar plates were inverted and cells grown overnight at 37°C. A single colony was selected and inoculated into bacterial growth medium (5 ml), supplemented with the relevant antibiotic(s) (Table 2.9 and 2.10), and incubated overnight (16 h) at the desired temperature (Table 2.10) with shaking. The overnight culture was diluted (1:100) in fresh medium, with antibiotic(s), and incubated at the relevant temperature with shaking. The culture was grown until an optical density between 0.4 and 1.0, at 600 nm, was reached. Recombinant protein expression was induced with IPTG (Table 2.10) and ampicillin was added at the point of induction and every 2 h post-induction. This maintains a selective pressure, since ampicillin is metabolised and depleted from the medium by *E. coli* cells. In an effort to improve the soluble expression of correctly folded MBP-*Pb*CtrNt, numerous alterations to the expression conditions were tested (Table 2.11). Following the period of induction, cells were harvested by centrifugation (4000 *g*, 15 min, 4°C).

Table 2.11 Variations to the culture conditions used for the recombinant expression of MBP-*Pb*CtrNt

Culture condition	Expression medium	LB
		2xYT
		M9 Minimal Medium
	Temperature	15°C*
		22°C
		30°C*
	OD_{600}	~0.6
		≥ 2.0*

*Induction of MBP-*Pb*CtrNt expression post-log growth phase ($O.D._{600} \geq 2.0$) was examined at both 15°C and 30°C.

Cells expressing His_6-*Pb*CtrNt or His_6-*Py*Cox17 were resuspended in cell resuspension buffer 1 and 2, respectively. The volume of buffer used was equivalent to 1/20th the original culture volume. Egg white lysozyme (1 mg/ml) was added to cell resuspension buffer 2 only and this was incubated on ice (30 min). Cells expressing GST-fusion proteins were similarly resuspended in 1/20th the original culture volume but in this instance with PBS containing egg white lysozyme (1 mg/ml) and incubated on ice (30 min). MBP-fusion proteins, expressed from pMal-c2 plasmids, were resuspended in 1/20th the original culture volume with chilled pMal column buffer. Various buffer conditions were also tested for the purification of MBP-*Pb*CtrNt (Table 2.12), in an attempt to reduce the purification of aggregated multimers. *E. coli* lysate was prepared by subjecting the cell suspension to three freeze-thaw cycles, between 37°C and -196°C (liquid nitrogen for 2 min), followed by further disruption with sonication on ice (10 cycles, 30 sec/burst, 1 min between bursts). Triton X-100 was added to suspensions containing GST-fusion proteins, to a final concentration of 1%, and this was incubated on ice (30 min). The

total cell lysate was separated into soluble and insoluble fractions by centrifugation (12000 *g*, 30 min, 4°C) and all samples analysed for expression by SDS-PAGE/Tricine-SDS-PAGE and western blotting.

MBP-fusion proteins exported to the periplasm were isolated as per the method of French *et al*. (1996). This method required that the cell pellet be resuspended in a volume of Tris/sucrose buffer equivalent to 1/5th the original culture volume. Both chicken egg white lysozyme (500 µg/ml) and EDTA (400 µl of 0.5 M EDTA) were added to the resuspended pellet and incubated at RT with gentle agitation (15 min). An equivalent volume of ice-cold distilled water was then added. This was incubated on ice with stirring (15 min), following which spheroplasts and unlysed cells were removed by centrifugation (13 000 *g*, 15 min, 4°C). As before, the isolated samples were analysed for expression by SDS-PAGE and western blotting.

Table 2.12 Variations to the lysate buffer conditions used to isolate and purify MBP-*Pb*CtrNt

Lysate preparation	Buffer species	Acetate$^{\vdash}$
		Phosphate$^{\blacklozenge\dashv}$
		Tris$^{\dashv}$
	Buffer additives	1-50 mM DTT$^{\#}$
		0.1% Triton X-100$^{\#}$
		8 M Urea
	Buffer pH	4$^{\vdash}$
		5.8$^{\blacklozenge}$
		7.4$^{\blacklozenge\dashv}$
		8$^{\blacklozenge\dashv}$

$^{\vdash}$, $^{\blacklozenge}$ and $^{\dashv}$ indicate the corresponding pH at which the buffer species were used.
$^{\#}$DTT and Triton X-100 were tested separately as well as in combination with each other.

2.7.2 Purification of recombinant malaria parasite proteins

2.7.2.1 Materials

<u>His_6-tagged proteins</u>:

<u>Wash buffer [100 mM NaH_2PO_4, 300 mM NaCl, 20 mM imidazole, 12 mM 2-mercaptoethanol, 5% (v/v) glycerol, 0.01% (w/v) NaN_3, pH 8]</u>. NaH_2PO_4 (1.2 g), NaCl (1.754 g), imidazole (0.136 g), 2-mercaptoethanol and glycerol were dissolved in 90 ml of distilled water. The solution was titrated to pH 8 with NaOH followed by the addition of NaN_3 and made up to a final volume 100 ml with distilled water.

His_6-elution buffer [100 mM NaH_2PO_4, 300 mM NaCl, 250 mM imidazole, 12 mM 2-mercaptoethanol, 0.01% (w/v) NaN_3, pH 8]. NaH_2PO_4 (1.2 g), NaCl (1.754 g), imidazole (1.70 g) and 2-mercaptoethanol were dissolved in 90 ml of distilled water. The solution was titrated to pH 8 with NaOH followed by the addition of NaN_3 and made up to a final volume of 100 ml with distilled water.

GST-fusion proteins:

PBS-T [PBS plus 1% Triton X-100]. PBS was prepared as per Section 2.4.4.1 and Triton X-100 added to 100 ml of PBS.

GST-elution buffer [50 mM Tris-HCl, 10 mM reduced glutathione, pH 8]. Tris (0.303 g) and reduced glutathione (0.154 g) were dissolved in 45 ml distilled water, titrated to pH 8 with HCl and made to a final volume of 50 ml.

MBP-fusion proteins:

MBP-elution buffer [100 mM NaH_2PO_4, 200 mM NaCl, 1 mM EDTA, 10 mM Maltose, 0.01% (w/v) NaN_3, pH 7.4]. NaH_2PO_4 (1.2 g), NaCl (1.167 g), maltose (0.360 g) and EDTA (200 µl of 0.5 M Na_2EDTA) were dissolved in 90 ml of distilled water, titrated to pH 7.4 with NaOH and NaN_3 added. The buffer was made to a final volume of 100 ml with distilled water.

2.7.2.2 Method

All recombinant proteins produced in this study were purified by affinity chromatography, using the appropriate resin. His_6-tagged proteins were purified using Ni-NTA resin, GST-fusions using glutathione-agarose and MBP-fusions using an amylose resin. Resin (~1 ml) was placed into a BioRad affinity column and pre-equilibrated with 10 column volumes of buffer. The Ni-NTA resin was equilibrated with cell resuspension buffer 2, glutathione agarose with PBS-T and amylose resin with pMal column buffer. Soluble bacterial lysate was filtered through Whatman No. 1 and then circulated over the affinity matrix (Figure 2.6) in a forward direction (flow-rate 0.5 $ml.min^{-1}$), at 4°C. The resins were then washed with 20 column volumes of buffer (Figure 2.6) or until the A_{280} of the flow through reached a steady absorbance ≤ 0.01. Ni-NTA resin was washed with wash buffer, glutathione agarose with PBS-T and amylose resin with pMal column buffer. Bound protein was eluted (0.5 $ml.min^{-1}$, 1 ml/fraction, 12 fractions) using the required elution buffer (Figure 2.6) and the A_{280} of each eluted fraction was recorded. Fractions with an A_{280} ≥

0.4 were pooled together and the purification profile analysed by SDS-PAGE (Section 2.4.1) or Tricine-SDS-PAGE (Section 2.4.2), as necessary. Purified protein pools were stored for short periods at 4°C or for longer periods at -20°C. The final protein concentration was estimated by the method of Bradford (Section 2.4.4).

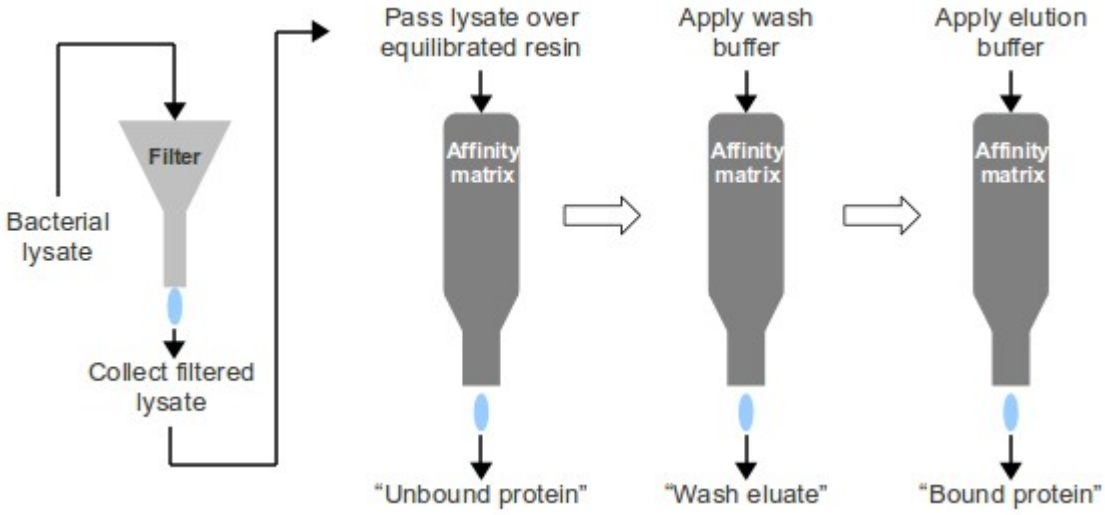

Figure 2.6 Strategy used for the purification of the recombinant malaria parasite proteins

2.7.3 Fractionation of MBP-*Pb*CtrNt by molecular exclusion chromatography

2.7.3.1 Materials

Sephacryl S-100 resin

Sephacryl S-300 resin

MEC buffer [100 mM NaH_2PO_4, 200 mM NaCl, 0.01% NaN_3, pH7.5]. NaH_2PO_4 (11.998 g) and NaCl (11.700 g) were dissolved in 950 ml distilled water and the buffer titrated to pH 7.5 with NaOH. NaN_3 was added and the buffer made to a final volume of 1000 ml with distilled water.

2.7.3.2 Method

For protein fractionation either the Sephacryl S-100 or S-300 resin was packed into a glass column and equilibrated with two column volumes of MEC buffer (flow rate ≈ 0.5 ml.min^{-1}). The column was calibrated using blue dextran (2000 kDa), bovine serum albumin (66 kDa), ovalbumin (45 kDa) and myoglobin (18 kDa) dissolved in MEC buffer (flow rate ≈ 0.5 ml.min^{-1}; collected 5 ml fractions). The calibrated MEC resins were used for MBP-*Pb*CtrNt fractionation. An affinity purified sample of MBP-*Pb*CtrNt (5.5 mg, 4 ml) was applied to the resin and eluted with MEC buffer (flow rate ≈ 0.5 ml.min^{-1}; collected 5 ml fractions). Affinity purified MBP-*Pb*CtrNt

samples containing either 1 mM DTT or 0.2% Triton X-100 were also fractionated using the Sephacryl S-100 resin, following the method described above.

2.7.4 Copper binding studies and the bicinchoninic acid assay

Copper binding and the oxidation state of copper bound to the recombinant proteins was assessed using the bicinchoninic acid (BCA) release assay. For this assay protein-copper complexes are disrupted by acid denaturation and the released copper detected in solution (Brenner and Harris, 1995). BCA is highly sensitive and specific for reduced copper, Cu(I), forming an intense violet complex detectable at 354 nm (extinction coefficient, $\varepsilon = 4.58 \pm 0.1 \times 10^4$ M^{-1} cm^{-1} at 354.5 nm). If oxidized copper, Cu(II), is present in solution then ascorbic acid must be added to the sample, following acid denaturation, to yield the Cu(I)-BCA complex. The formation of the Cu(I)-BCA complex in the absence of ascorbic acid, suggests the protein-bound copper ions were already in the reduced state. Recombinant proteins were also tested for their ability to reduce copper-catalysed ascorbic acid oxidation.

2.7.4.1 Materials

Ascorbic acid solution [100 mM Ascorbic acid]. Ascorbic acid (88 mg) was dissolved in 5 ml distilled water and stored at RT.

Copper stock solution 1 [10 mM $CuCl_2$]. $CuCl_2.2H_2O$ (8.5 mg) was dissolved in 5 ml distilled water and stored at RT. This solution was used for *in vitro* copper binding studies.

Copper stock solution 2 [1 M $CuCl_2$]. $CuCl_2.2H_2O$ (0.852 g) was dissolved in 5 ml distilled water and sterilised by filtration through a 0.22 µm syringe filter. This solution was used for *in vivo* copper binding studies.

Na-P buffer [0.1 M NaH_2PO_4, 0.01% NaN_3, pH 7.5]. NaH_2PO_4 (11.998 g) was dissolved in 950 ml distilled water, titrated to pH 7.5 with NaOH and NaN_3 added (1 ml of a 10% solution). The buffer was made to a final volume of 1 ℓ.

Reagent A [30% (w/v) Trichloroacetic acid]. Trichloroacetic acid (15 g) was dissolved in distilled water and made to a final volume of 50 ml. This reagent was stable at RT for up to 6 months.

Reagent B [2 mM Ascorbic acid]. Ascorbic acid (3.5 mg) was dissolved in 10 ml distilled water. This reagent was prepared fresh before use.

Reagent C [0.15mM Bicinchoninic acid, 0.9 M NaOH, 0.2 M HEPES]. Purified bicinchoninic acid disodium salt (6 mg), NaOH (3.6 g) and HEPES (15.6 g) were dissolved in distilled water and made to a final volume of 100 ml. This reagent was stable at RT for up to 6 months.

H_2Asc solution [240 µM ascorbic acid, pH 4.5]. Ascorbic acid (2.2 mg) was dissolved in 45 ml distilled water, titrated to pH 4.5 with NaOH and made to a final volume of 50 ml

2.7.4.2 Method

BCA release assay

The BCA release assay makes use of a HEPES-buffered BCA solution (Reagent C) with NaOH included to neutralise the TCA and bring the pH of the solution close to 7 (Brenner and Harris, 1995). For the assay, the desired protein solution (750 µl) was pipetted into a 2.0 ml microfuge tube and Reagent A added (250 µl). This solution was vortexed, to ensure mixing, and centrifuged (12 000 *g*, 2 min) to pellet the protein precipitate. The resulting supernatant was aliquotted (4 x 250 µl) into fresh microfuge tubes. For this particular study Reagent B (50 µl) was added to two of the tubes, whilst the remaining two tubes received an equivalent volume of distilled water. This solution was mixed and Reagent C (200 µl) then added to each tube, mixed and allowed to incubate at RT (2 min) before reading absorbance at 354 nm. Standards and blanks were prepared in the same final volume (500 µl).

In vitro copper binding

Each purified recombinant protein was used at 10 µM for *in vitro* copper binding studies. For copper binding, duplicate samples of each protein were prepared and each was mixed with a volume of copper stock solution 1, equivalent to a 20-fold molar excess. To one of the samples ascorbic acid solution was added to a final concentration of 10 mM, whilst the other sample received an equivalent volume of distilled water. Samples were mixed by brief vortex and incubated at RT (15 min) with occasional agitation. Unbound copper was removed by dialysis against three changes of Na-P buffer (> 100-fold volume excess) at 4°C, two by 2 h and one overnight. Following dialysis, protein samples were collected and bound copper measured using the BCA release assay, described above. Solutions of $CuCl_2$ (Na-P buffer), with or without the addition of ascorbic acid, were used as standards and affinity-purified MBP served as a negative control. The statistical significance of copper binding was determined by Student's t-test.

In vivo copper binding

To test the ability of the respective proteins to bind copper *in vivo,* cells harbouring the relevant recombinant plasmid were induced in the presence of 0.5 mM $CuCl_2$. This concentration of a copper salt has previously been shown to have no significant effect on the growth rate of *E. coli* cells (Lutsenko *et al.*, 1997). Copper stock solution 2 was specifically added to recombinant *E. coli* cultures 1 h post-IPTG-induced expression, to a final concentration of 0.5 mM. Standard procedures for optimal recombinant protein expression were followed (Section 2.7.1) and proteins were purified under identical conditions to the proteins expressed in the absence of copper (Section 2.7.2). Following purification, pooled His_6-*Py*Cox17 and GST-*Pf*Cox17 proteins were dialysed against three changes of Na-P buffer (>100-fold volume excess) at 4°C, two by 2 h and one overnight. MBP-fusion proteins were analysed for copper binding directly proceeding purification. All proteins were adjusted to a concentration of 10 μM, for consistency, and then analysed for bound copper using the BCA release assay described above. The statistical significance of copper binding and the effect of copper on recombinant protein yield were determined by Student's t-test.

Ascorbate oxidation assay

The ability of each recombinant protein to reduce the copper-catalysed oxidation of ascorbic acid was tested *in vitro*. In a typical experiment a mixture was prepared containing H_2Asc solution to a final concentration of 120 μM (500 μl), copper stock solution to a final concentration of 8 μM (0.8 μl) and 5 μM recombinant protein (variable) made to a final volume of 1 ml with distilled water. The absorbance of this solution was monitored at 255 nm with readings taken every 5 s for 300 s. Reactions were carried out at RT.

CHAPTER 3

Bioinformatic studies and antigenic peptide selection for the putative *Plasmodium* spp. copper transport and metallochaperone proteins

3.1 Introduction

Bioinformatics is the term attributed to the use of applied mathematics, statistics and computer science to help solve biological problems and queries. The field incorporates programmes aimed at: (i) solving DNA and protein sequence alignments; (ii) identifying novel genes; (iii) assisting with genome assembly; (iv) solving and predicting protein structure; (v) predicting gene expression and potential protein-protein interactions and (vi) modelling the path of evolution (Claverie and Notredame, 2003). This chapter describes the bioinformatic techniques used for the identification and preliminary characterisation of novel copper-requiring proteins in the *Plasmodium* proteome. To assist with protein characterisation, antibodies were raised against antigenic epitopes of a putative copper transport protein and copper metallochaperone from the *P. yoelii* and *P. falciparum* parasites.

It has previously been shown that *P. falciparum* requires a copper efflux protein (*Pf*CuP-ATPase) for control of cellular copper (Rasoloson *et al.*, 2004). This suggested a requirement of copper for parasite metabolic function, however, how the parasite acquires extracellular copper remains to be confirmed. The current model suggests copper is acquired through the ingestion and digestion of host erythrocyte Cu/Zn superoxide dismutase (Cu/Zn SOD). This mechanism was based on the assumption that an observed decrease in host erythrocyte Cu/Zn SOD content was a result of parasite consumption. Digestion of Cu/Zn SOD would result in the release of bioavailable copper for the parasite (Rasoloson *et al.*, 2004). Another possible, but unexplored mechanism, is copper uptake via a dedicated copper transport protein. Such a mechanism has previously been characterised in yeast, plant, human and other related mammalian systems (Dancis *et al.*, 1994; Kampfenkel *et al.*, 1995; Mackenzie *et al.*, 2004; Zhou and Gitschier, 1997; Zhou *et al.*, 2003). To establish the potential of the parasite utilising such a mechanism, a bioinformatics approach was employed. Additional copper binding proteins were also searched for. One of these proteins, the Cox17 metallochaperone, has been implicated in copper delivery to yeast cell mitochondria (Beers *et al.*, 1997) for the activation of cytochrome-c oxidase (Horng *et al.*, 2004).

The *in silico* identification of *Plasmodium* proteins involved in copper metabolism suggests native expression; however, this requires confirmation using biochemical means. The approach adopted for this study was based on the successful characterisation of *P. falciparum* protein

kinases with anti-peptide antibodies (Dorin *et al.*, 2005; Nunes *et al.*, 2007). When selecting a suitable epitope for anti-peptide antibody production, the following criteria were analysed: (i) surface probability (Emini *et al.*, 1985; Janin and Wodak, 1978) (ii) hydrophilicity (Hopp and Woods, 1983) and (iii) flexibility (Karplus and Schulz, 1985). Flexibility is of particular importance as this property increases the probability of the selected peptide assuming a similar spatial orientation to that found in the native protein. On the other hand, antigenicity (Welling *et al.*, 1985) is of less importance since it is a combination of a peptide's hydrophilicity and surface probability. It is also desirable that the selected epitope lacks potential N-glycosylation sites since polysaccharides can mask the selected region on the native protein. Also of consideration, particularly with regard to *Plasmodium* parasite proteins, is that the number of lysine residues in the selected peptide are limited. Antibodies raised against peptides with multiple lysine residues may cross-react with multiple *Plasmodium* proteins since a number of parasite proteins are lysine-rich.

A BLASTp search of PlasmoDB, for a putative copper transport protein, identified coding domains for two potential transporters in most of the available parasite genomes. Examples of these were *P. berghei* (PBANKA_102150 and PBANKA_130290) and *P. falciparum* (PF14_0211 and PF14_0369). *P. yoelii* appeared to be one of the exceptions, only encoding a single copper transporter (PY00413). Searches for other copper-dependent proteins identified the presence of another gene encoding a putative metallochaperone, Cox17, in all the aforementioned parasite proteomes. Suitable antigenic epitopes were identified in five of the identified parasite proteins using the Predict7™ epitope prediction algorithm (Cármenes *et al.*, 1989). For each of the copper transport proteins, peptide sequences were selected from the extracellular amino-terminal domain. Selected peptides were ensured to exclude regions showing sequence similarity to proteins in the chicken, mouse and human proteomes so as to avoid potential recognition of host proteins by the antibodies. The synthesised peptides were coupled to a carrier protein and injected into chickens for antibody production. The resulting antibodies were affinity purified and used for the detection of native parasite proteins.

3.2 Results

3.2.1 Putative copper requiring proteins of *P. falciparum*

Within mammalian and yeast cellular systems copper is an essential cofactor for the correct functioning of a number of enzymes (Puig and Thiele, 2002; Sharp, 2003). One of these enzymes, cytochrome-c oxidase (CCO), is a key catabolic enzyme consisting of 13 subunits, in the mammalian isoform, that is located in the inner membrane of the mitochondrion (Tsukihara *et al.*, 1996). Cytochrome-c oxidase functions as a terminal electron transfer complex in the

mitochondrial respiratory chain, transferring electrons from cytochrome-c to molecular oxygen (Ferguson-Miller and Babcock, 1996). The enzyme contains three functionally important copper ions located at its binuclear Cu_A and mononuclear Cu_B sites (Tsukihara *et al.*, 1996). Copper, as a reactive metal, cannot freely access cytochrome-c oxidase with the metallation of the Cu_A and Cu_B sites requiring the copper chaperones Cox17, Sco1 and Cox11 (Horng *et al.*, 2004). Identification of these particular copper chaperones and other copper-requiring protein orthologues, within the *P. falciparum* proteome, would support a requirement for copper, as previously suggested (Rasoloson *et al.*, 2004). Following a BLASTp search of the *Plasmodium* database (www.plasmodb.org), ten such orthologs were identified (Table 3.1). These were Cox11, Cox17, Cox19, Sco1, cytochrome-c oxidase subunits I, II, III, Vb and VIb as well as S-adenosyl-L-homocysteine hydrolase (SAHH). In terms of cytochrome-c oxidase and copper binding, the identification of cytochrome-c oxidase subunits I and II seems most significant since these contain the mononuclear Cu_B and binuclear Cu_A sites that require copper as a essential cofactor (Tsukihara *et al.*, 1996).

The *Plasmodium* genome appears to lack an identifiable class of metallothioneins as well as a Cu/Zn superoxide dismutase ortholog (Table 3.1). In yeast and mammalian cells, these proteins are essential for copper storage and free radical detoxification, respectively (Kim *et al.*, 2008; Puig and Thiele, 2002; Sharp, 2003) Their apparent absence from the parasite genome suggests one of two possibilities. Either the *Plasmodium* parasite evolved unique mechanisms to deal with the aforementioned cellular situations thereby losing the necessity for these proteins, or alternately, the sequence features of potential *Plasmodium* orthologs were not of sufficient similarity to be identified by the mammalian and yeast sequences used to search PlasmoDB. The absence of a Cu/Zn superoxide dismutase metallochaperone does, however, suggests that an alternative parasite mechanism could exist for free radical detoxification. An absence of dopamine-β-monooxygenase and peptidylglycine monooxygenase orthologs from the *Plasmodium* genome (Table 3.1) was not unexpected since these enzymes are involved in processes specific to mammalian organisms (Friedman and Kaufman, 1965; Murthy *et al.*, 1986).

Table 3.1 Copper-dependent protein orthologs identified in the *P. falciparum* proteome

Enzyme name	Accession number	Protein function	*P. falciparum* orthologue identified	PlasmoDB protein identifier
Copper chaperone for superoxide dismutase (CCS)	CAG46726	Activates cytosolic Cu/Zn superoxide dismutase	No	N/A
Cu/Zn Superoxide dismutase	AAB05661	Free radical detoxification	No	N/A
Dopamine-β-monooxygenase	PO9172	Catecholamine production	No	N/A
Peptidylglycine monooxygenase	P19021	Bioactivation of peptide hormones	No	N/A
Metallothionein	AAP97267	Storage of excess copper and other divalent metals	No	N/A
Copper transport protein (Ctr1)	L41833	Required for cellular copper import	**Yes**	PF14_0211 PF14_0369
S-adenosyl-L-homocysteine hydrolase	P23526	Catalyses the reversible hydrolosis of S-adenosylhomocysteine to adenosine and L-homocysteine	**Yes**	PFE1050w
Cox11	CAG46636	Implicated in the formation of the Cu_B site of cytochrome-c oxidase	**Yes**	PF14_0721
Cox17	AAA98114	Transfers copper to Cox11 and Sco1 in the intermembrane space of mitochondria	**Yes**	PF10_0252
Cox19	AAY35062	Required for cytochrome-c oxidase assembly and activation in the mitochondrial intermembrane space	**Yes**	PFL0090c
Sco1	O75880	Implicated in the formation of the Cu_A site of cytochrome-c oxidase	**Yes**	PF07_0034
Cytochrome-c oxidase subunit I	ACR77861	Part of the functional core of the enzyme complex, specifically forming the catalytic subunit	**Yes**	mal_mito_2
Cytochrome-c oxidase subunit II	ABU47824	Part of the functional core of the enzyme complex, transfers electrons from cytochrome-c to the bimetallic centre of subunit I	**Yes**	PF14_0288 (IIa) PF13_0327 (IIb)
Cytochrome-c oxidase subunit III	ABJ99455	Part of the functional core of the enzyme complex and one of the main transmembrane subunits of cytochrome-c oxidase	**Yes**	mal_mito_1
Cytochrome-c oxidase subunit Vb	AAA52060	Zinc binding site of cytochrome-c oxidase	**Yes**	PFI1365w
Cytochrome-c oxidase subunit VIb	AAP35591	Potential haem-binding subunit of cytochrome-c oxidase	**Yes**	PFI1375w

3.2.2 Identification of a putative *Plasmodium* spp. copper transport protein

The identification of copper binding proteins within the *P. falciparum* proteome (Table 3.1) supports the likely parasite requirement for copper. A mechanism for copper acquisition does, however, remain to be identified. As mentioned, the current hypothesis is that copper is acquired via the ingestion and digestion of host erythrocyte Cu/Zn superoxide dismutase (Cu/Zn SOD). A mechanism not yet considered is copper acquisition via a dedicated copper transport protein. To identify a putative *Plasmodium* copper transporter sequence, PlasmoDB

was BLASTp searched with the *Theileria parva* polymorphic immunodominant molecule (PIM) sequence, which possesses copper transport protein features. Sequences corresponding to a copper transporter were identified for eight *Plasmodium* species (spp.), including *falciparum*, *vivax*, *yoelii*, *berghei, chabaudi*, *galinaceum*, *reichenowi* and *knowlesi*. All retrieved sequences were aligned with sequences of other characterised copper transport proteins (Ctr1), using the ClustalW™ server (Thompson *et al.*, 1994), to identify features common to and characteristic of these transporters (Figure 1.5). These features include three transmembrane domains, copper-binding methionine motifs within the extracellular amino-terminus and most importantly MxxxM (MX_3M) and GxxxG (GX_3G) motifs located in the second and third transmembrane domains respectively (Figure 1.5). Sequence alignment identified both the MX_3M and GX_3G motifs in the *Plasmodium* sequences (Figure 3.1), as well as an important methionine residue located approximately 20 amino acids from the first putative transmembrane domain (data not shown) (Puig *et al.*, 2002a).

```
Hs              SFPHLLQTVLHIIQVVISYFLMLIFMTYNGYLCIAVAAGAGTGYFLFS-----WKKAVVV 183
Ms              SFPHLLQTVLHIIQVVISYFLMLIFMTYNGYLCIAVAAGAGTGYFLFS-----WKKAVVV 189
Tp              LLTHLFLFLIALCAYALDFLLMLVVMTFNVGVFFAVILGYSVGYVLSSLAYSTLRTQPNR 531
Cp              IKVICTNVLLTILYYFMHYLLMLIAMTFNWGLFFSVIIGLSIGYGIFELGSITKNECSCN 169
Pf_0211         PCQNVNYGFLSFLHYTIDYLLMLIVMTFNPYIFLSIMTGLSSAYLFYGHLI--------- 160
Pf_0369         FKNNSYRMLLSFVIYSWDYLLMLIVMTFNVGLFVAVVLGLSFGFFIFGNKFVSSKKCSPD 218
Pv              FKNNLTRSLLSFIIYSWDYLLMLIVMTFNVGLFFAVVVGLSIGFFLFGHKFVTCGKSSTD 339
Py              FKNNTIRMILSFIIYSWDYLLMLIVMTFNVGLFFAVILGLSFGYFLMGGKFVTCTNTSHS 259
Pb              FKNNMIRMILSFIIYSWDYLLMLIVMTFNVGLFFAVILGLSFGYFLMGEKFVACTKSSKC 221
Pc              FKHNTIRMILSFIIYSWDYLLMLIVMTFNVGLFFAVILGLSFGYFLMGNNFVSCTQNSNC 196
Pg              FKNNTIRMILAFIIYSWDYLVMLIVMTFNVGLFFSVIFGLAFGFFLFGSHFVTSKKCATT 199
Pk              FKNNLTRSALSFIIYSWDYLLMLIVMTFNVGLFVAVVVGLSIGFFLFGHKFVTCGSNSTD 289
Pr              FKNNSYRMLLSFVIYSWDYLLMLIVMTFNVGLFVAVVLGLSFGFFIFGNKFVSSKKCSPD 170
                         : :      :::*: *:*  : .::  * . .: :
```

Figure 3.1 Alignment of essential protein motifs in human, mouse, *Theileria* and *Cryptosporidium* copper transporter sequences with the *Plasmodium* sequences

Alignment of the essential copper transporter MX_3M and GX_3G motifs. Sequences are as follows: Hs = *Homo sapiens*; Ms = *Mus musculus*; Tp = *Theileria parva*; Cp = *Cryptosporidium parvum*; Pf_0211 = *Plasmodium falciparum* PF14_0211; Pf_0369 = *P. falciparum* PF14_0369; Pv = *P. vivax*; Py = *P. yoelii*; Pb = *P. berghei*; Pc = *P. chabaudi*; Pg = *P. galinaceum*; Pk = *P. knowlesi*; Pr = *P. reichenowi* (Refer to Section 2.3 for the sequence accession numbers). Conserved residues are indicated by *, whilst : represents a conserved substitution and . a semi-conserved substitution. Underlined amino acids, in the *H. sapiens* sequence, indicate the approximate position of transmembrane domains two and three, respectively.

Each of the *Plasmodium* sequences was analysed using the TMHMM (Krogh *et al.*, 2001) and HMMTOP (Tusnády and Simon, 2001) transmembrane domain prediction servers. At least three putative transmembrane domains were identified in each retrieved sequence. Figure 3.2 is representative of the results obtained from the TMHMM server (Krogh *et al.*, 2001) and depicts the predicted topology for the *P. falciparum* (PF14_0211) (Figure 3.2a) and *P. berghei* (Figure 3.2b) sequences in relation to the known topology of the *Saccharomyces cerevisiae*

copper transport protein (ScCtr1) (Figure 3.2c). As previously indicated (Figure 1.5), the presence of three predicted transmembrane domains would presumably result in an orientation whereby the amino-terminus is extracellular and the carboxy-terminus intracellular. This prediction is in close agreement with the established topology of ScCtr1 and other known copper transport proteins, such as hCtr1 (Aller and Unger, 2006). It is, however, important to note the presence of a fourth predicted transmembrane domain in the *P. falciparum* plot (Figure 3.2a), within the first 30 amino acids of the protein sequence. According to the TMHMM server, a transmembrane domain predicted within the amino terminus of a protein is suggestive of a signal sequence (Krogh *et al.*, 2001). This prediction was supported by submitting the PF14_0211 sequence to the SignalP server (data not shown), a signal peptide cleavage site prediction program (Emanuelsson *et al.*, 2007). A similar signal peptide was identified for the other *Plasmodium* sequences. Interestingly, analysis of each sequence for an apicoplast targeting signal (PlasmoAP server) indicated that only *P. falciparum* PF14_0369 contained such a sequence.

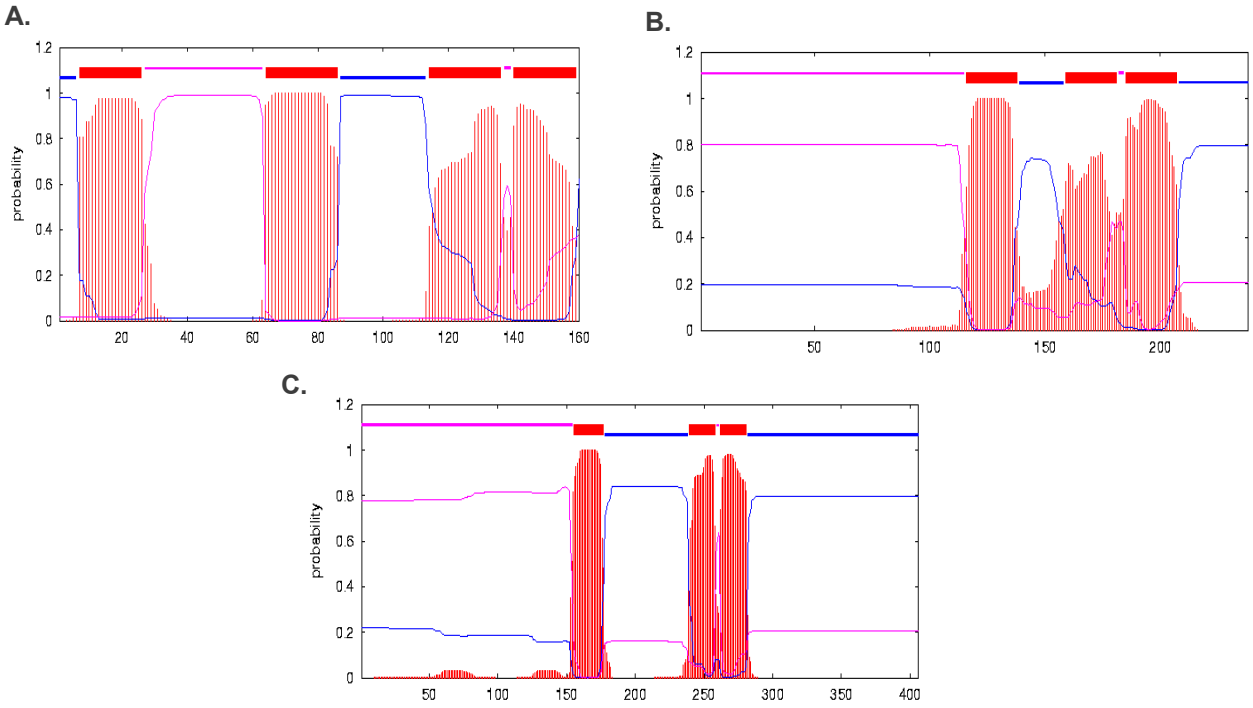

Figure 3.2 Topology prediction for two putative *Plasmodium* sp. copper transport proteins compared to the known topology of the *S. cerevisiae* copper transport protein.

TMHMM plots for *P. falciparum* PF14_0211 (**A**), *P. berghei* (**B**) and *S. cerevisiae* (**C**) copper transporter sequences are depicted. Represented in all panels are regions of the protein sequence predicted to be extracellular (—), regions predicted to form transmembrane domains (▬) and regions predicted to be cytosolic (—).

3.2.3 Analysis of the coding sequences for two putative *P. falciparum* copper transport proteins

Identification of a putative copper transport protein sequence, within the *Plasmodium* proteome, required a preliminary characterisation of the protein sequence. Further *in silico* characterisation involves an analysis of the gene organisation of *P. falciparum* chromosome 14 since it harbours the coding domains for both predicted *P. falciparum* copper transport proteins. In general it has been noted that *P. falciparum* chromosomes vary considerably in length with most variation occurring in the subtelomeric regions (Gardner *et al.*, 2002). This variation is due to the fact that subtelomeric domains typically contain gene families encoding proteins essential to host-pathogen interactions and antigenic variation. These include the *var*, *rif* and *stevor* families (Cheng *et al.*, 1998; Kyes *et al.*, 1999; Marti *et al.*, 2004). However, it has also been demonstrated that there is a central "core" region within the 14 *P. falciparum* chromosomes that contain a number of gene orthologs conserved in the three rodent-infecting *Plasmodium* species (Hall *et al.*, 2005; Kelly *et al.*, 2006). These conserved *P. falciparum* gene orthologs collectively totalled 4391 genes and in general the gene pairs were found to be under purifying selective pressure (Hall *et al.*, 2005). Based on the finding that the gene encoding LDH is found within the "core" region of *P. falciparum* chromosome 13 (data not shown), it was presumed that coding domains found within the "core" region of other chromosomes could infer the protein has a potentially important function. With this is mind the location of the *P. falciparum* copper transporter coding domains was evaluated (PF14_0211 and PF14_0369).

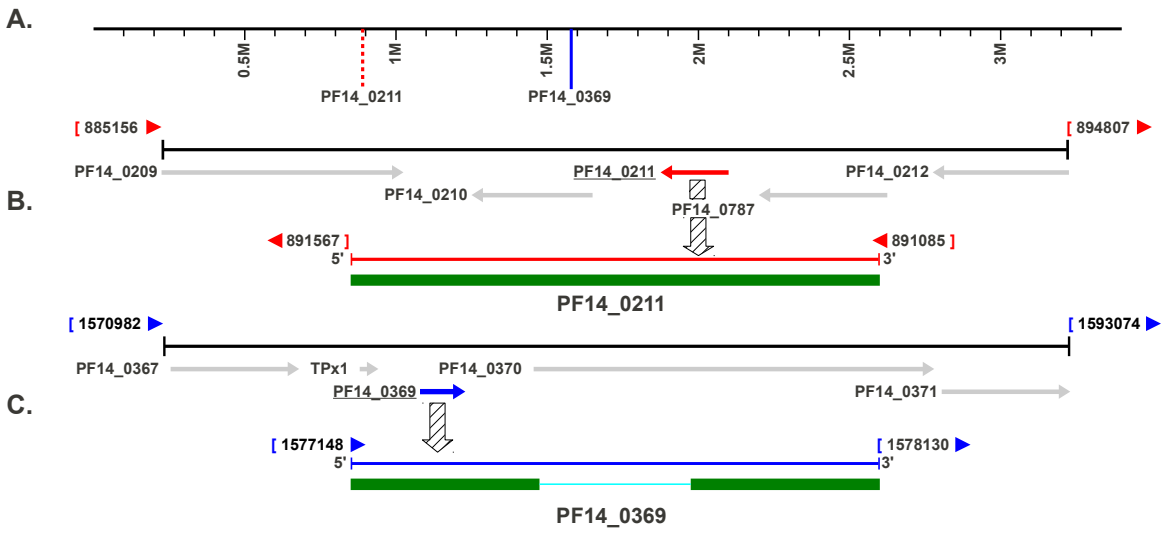

Figure 3.3 Location of the copper transporter coding domains on *P. falciparum* chromosome 14

Chromosomal location of PF14_0211 (---) and PF14_0369 (—) coding domains on *P. falciparum* chromosome 14 (**A**) plus an exploded view of chromosome 14 gene organisation, relative to PF14_0211 (**B**) and PF14_0369 (**C**). In panels **B** and **C** the upper image represents gene organisation whilst the lower image highlights the presence of introns (—) and exons (■) within each respective coding domain. The corresponding base pair numbers (adjacent to the coloured arrowheads) are shown above the 5' and 3' termini for each coding domain.

Chromosome 14 (Figure 3.3) has been predicted to contain a centromere at approximately 1,15 Mbp from the left-hand telomere (Kelly *et al.*, 2006). As seen in figure 3.3, the sequences encoding the two copper transport proteins are located relatively close to this predicted centromere, at approximately 0.89 Mbp and 1.57 Mbp for PF14_0211 and PF14_0369 respectively. Although localisation of the centromere is not definitive of the central "core" conserved region, of chromosome 14, it is nevertheless suggestive of where this region might be. The PF14_0211 coding domain is also located amongst a number of hypothetical, but importantly, conserved proteins according to PlasmoDB annotation (Figure 3.3). Similarly for PF14_0369 it was noted that the surrounding gene organisation (Figure 3.3) appears to be conserved across the *Plasmodium* species thus far annotated (data not shown). This trend of conserved organisation has been previously documented for a number of other *Plasmodium* proteins (van Lin *et al.*, 2001).

The PF14_0211 and PF14_0369 coding domains displayed clear differences between their respective intron/exon organisation. Whilst PF14_0211 contains a single exon and no introns (Figure 3.3b), PF14_0369 contains two exons and a single intron (Figure 3.3c). This intron/exon organisation was also present in the corresponding orthologous coding domains of other *Plasmodium* spp. The one exception was for the *P. yoelii* coding domain (PY00413), which was composed of two introns and three exons (data not shown). This conservation of gene organisation and chromosomal localisation, for the *Plasmodium* copper transport protein, suggests a likely role for this protein in parasite metabolic activity.

3.2.4 Identification of a putative *Plasmodium* spp. Cox17 copper metallochaperone

The copper metallochaperone Cox17 has been implicated in the delivery of copper to the mitochondrion in yeast and mammalian cells (Cobine *et al.*, 2006a; Leary *et al.*, 2009). Characterisation of the Cox17 metallochaperone has made use of the *S. cerevisiae* model, although mammalian isoforms have also been characterised. To date, a Cox17 chaperone has not yet been annotated or characterised in any Apicomplexan organism. To identify a *Plasmodium* Cox17 ortholog, the *Arabidopsis thaliana* Cox17 sequence was used to BLASTp search PlasmoDB. This particular sequence was selected since the *A. thaliana* genome appears closely related to the *Plasmodium* genome (Gardner *et al.*, 2002) This search revealed a putative Cox17 sequence in the genomes of *P. falciparum*, *vivax*, *yoelii*, *berghei, chabaudi*, *galinaceum*, *reichenowi* and *knowlesi*. These were the same species predicted to encode a copper transporter. A ClustalW™ alignment of all retrieved parasite Cox17 sequences, with the sequences of known Cox17 proteins (Figure 3.4), was constructed to identify conserved amino acids.

```
Hs  MPGLVDS-----NPAPPE------SQEKKPLK-PCCACPETKKARDACIIEKGE--EHCGHLIEAHKECMRALGFKI---- 63
Sc  MTETDKK-------QEQEN-----HAECEDKPKPCCVCKPEKEERDTCILFNGQDSEKCKEFIEKYKECMKGYGFEVPSAN 69
At  MTDQPAQN-GLIPPPTSEPSKAAASAETKPKKRICCACPDTKKLRDECIVEHGE--SACTKWIEAHKICLRAEGFNV---- 74
Pf  MGMSLNK------PINNTN---EANKGEVKKKKICCVCLETKKLRDECIVKLGE--EQCKKFIDDHNKCLRSEGFDIK--- 67
Py  MGLGLTK------PLNTT----EESKTCAKKKKICCVCLDTKKLRDECIVNLGE--EQCKKYINDHNQCLRNEGFDIK--- 66
Pv  MGFF-NW------PSKNTS---EEAKGGAAKKKICCVCLETKKLRDECIVKLGE--EQCRKYIEDHNQCLRDEGFDVK--- 66
Pb  MGLSLTK------PLNTT----EENKTCAKKKKICCVCLDTKKLRDECIVNLGE--EKCKKYIDEHNQCLRNEGFDIK--- 66
Pk  MGFFSNW------PFKNTS---EEAKGGAPKKKICCVCLETKKLRDECIVKLGE--EQCRKYIEDHNQCLRNEGFDVK--- 67
Pc  MGSSLT-------ILNTT----DESKTGAPKKKICCVCLDTKKLRDECIVKYGE--KKCKKYIDDHNRCLRNEGFDIK--- 65
Pg  MGTFLNK------PIKNTN---EEIKGE-KKKKICCVCLETKKLRDECIVKLGE--EQCKKFIDDHNQCLRNEGFDIK--- 66
Pr  MGMSLNK------PINNPN---EANKGEVKKKKICCVCLKTKKLKDECIVKLGE--KQCKKFIDDHNKCLRSEGFDIK--- 67
    *                                **.*   *: :* **   *:  . * . *: :: *::  ** :
```

Figure 3.4 Alignment of conserved amino acids in human, yeast and *Arabidopsis* Cox17 sequences with the *Plasmodium* sequences

Cox17 sequences aligned are for *Homo sapiens* (Hs), *Saccharomyces cerevisiae* (Sc), *Arabidopsis thaliana* (At), *P. falciparum* (Pf), *P. yoelii* (Py), *P. vivax* (Pv), *P. berghei* (Pb), *P. knowlesi* (Pk), *P. chabaudi* (Pc), *P. galinaceum* (Pg) and *P. reichenowi* (Pr) (Refer to Section 2.3 for the sequence accession numbers). Essential residues are highlighted by colour. Conserved residues are indicated by *****, whilst **:** represents a conserved substitution and **.** a semi-conserved substitution. The underlined sequence on the Hs and Sc sequences represents the Cox17 copper binding site.

A mutagenic study on more than two-thirds of the *S. cerevisiae* Cox17 protein sequence identified that only one-sixth of these mutants produced a respiration-deficient phenotype (Punter and Glerum, 2003). Surprisingly, only 40% of the conserved residue mutations had an adverse effect on Cox17 function. The conserved residues that were affected by mutation are Cys-23, Cys-24, Cys-26, Arg-33, Asp-34, Cys-47 and Cys-57 (Punter and Glerum, 2003). Alignment of the eight retrieved *Plasmodium* spp. sequences with the human and yeast Cox17 sequences, established that these essential residues were conserved (Figure 3.4). The one exception was for the *P. reichenowi* sequence where a conserved substitution replaced Arg-33 for a Lys residue. Considering sequencing of the *P. reichenowi* genome is incomplete this difference could be the result of a sequencing error or artefact. It is important to note the conservation of the CysCysXaaCys motif at amino acids 23 to 26 (*S. cerevisiae* numbering) in all the *Plasmodium* sequences. This motif forms part of the Cox17 copper binding domain (underlined sequence in Figure 3.4) and is essential to its function (Abajian *et al.*, 2004; Heaton *et al.*, 2000; Punter and Glerum, 2003).

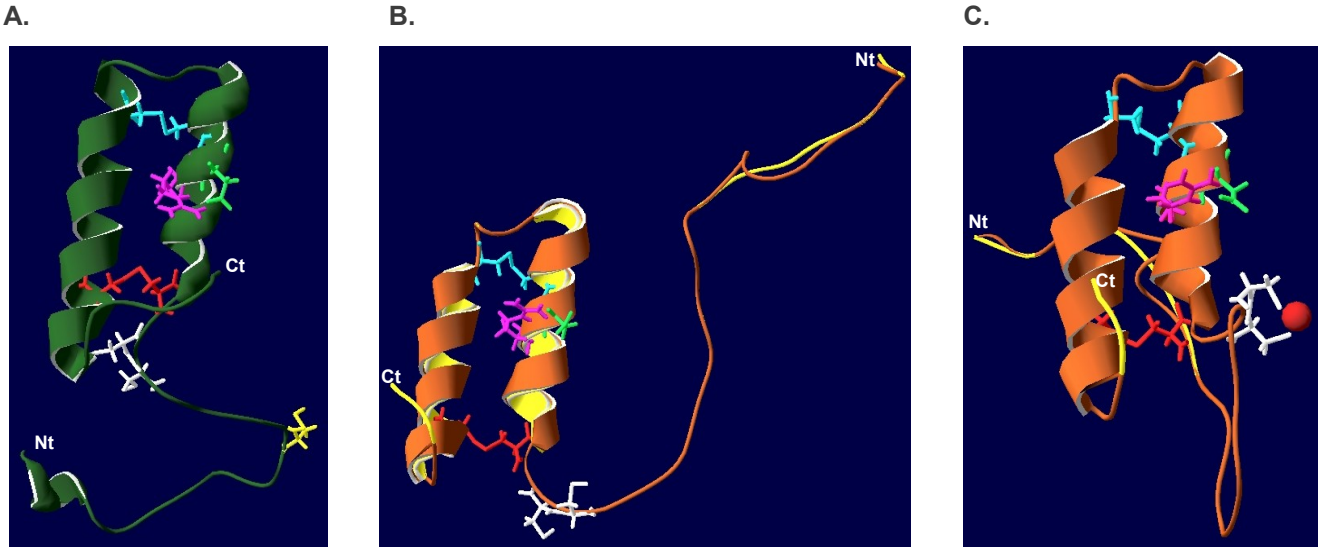

D.

```
HsCox17         MPGLVDS---NPAPPESQEKKPLKPCCACPETKKARDACIIEKGEEHCGHLIEAHKECMR 57
PfCox17         MGMSLNKPINNTNEANKGEVKKKKICCVCLETKKLRDECIVKLGEEQCKKFIDDHNKCLR 60
                *   ::.   *.  .:. * *  * **.* **** ** **:: ***:* ::*: *::*:*

HsCox17         ALGFKI- 63
PfCox17         SEGFDIK 67
                : **.*
```

Figure 3.5 *P. falciparum* Cox17 homology model

The *Saccharomyces cerevisiae* Cox17 structure (green) (Arnesano *et al*., 2005) is included for comparison (**A**). *P. falciparum* Cox17 (brown) was modelled against the NMR-solved structure of *Homo sapiens* Cox17 (yellow) without (**B**) or with (**C**) copper bound (Banci *et al*., 2008). The model was constructed by sequence alignment (**D**). In panels **A** to **C** the amino (Nt) and carboxy (Ct) termini are labelled. Coloured residues, in all three panels, are shown as stick representations and correspond to the residues highlighted in **D**, although residue numbers differ in panel **A** as does an additional cysteine residue (coloured yellow). The underlined cysteine doublet in **D** is coloured white in all panels. Copper in panel **C** is shown by the red sphere (●).

To understand *Plasmodium* Cox17 function, the *Homo sapiens* Cox17 (hCox17) NMR structure (Banci *et al.*, 2008b) was used as a template to model the hypothetical structure of *P. falciparum* Cox17 (*Pf*Cox17) (Figure 3.5) with the Swiss-pdb DeepView program (Guex and Peitsch, 1997). Both yeast and human Cox17 have a coiled coil-helix-coiled coil helix structural motif (Figure 3.5) (Abajian *et al.*, 2004; Arnesano *et al.*, 2005; Banci *et al.*, 2008b), which is predicted to be common to the related mitochondrial proteins Cox19 (Nobrega *et al.*, 2002) and Cox 23 (Barros *et al.*, 2004). From the homology model of *Pf*Cox17 this structural motif appears to be conserved, with a close resemblance observed between *Pf*Cox17 and both the apo and Cu-loaded forms of hCox17 (Figure 3.5b and c, respectively). Located at the amino and carboxyl terminal ends of each helix are four conserved cysteine residues that form two interhelical disulfide bonds in yeast and human Cox17 (Figure 3.5, red and cyan highlighted residues). These conserved residues are also present in *Pf*Cox17 (Figure 3.5d) and appear to map closely to the corresponding residues in both apo and Cu-loaded hCox17 (Figure 3.5b and c, respectively). The conserved and essential Arg-32 and Asp-34 residues in hCox17 are also

closely mapped by the corresponding residues in *Pf*Cox17 (Figure 3.5b and c). Copper binding to hCox17 results in local structural rearrangements around the two copper-coordinating cysteine residues (Figure 3.5b and c, white highlighted residues) causing the normally unstructured and flexible amino terminus (Figure 3.5b) to become more structured and less flexible (Figure 3.5c) (Banci *et al*., 2008b). *Pf*Cox17 appears to closely resemble these changes in protein structure. The one clear difference between *Pf*Cox17 and hCox17 is the insertion of three amino acids in the unstructured amino terminus (Figure 3.5b and d). However, this appears to have little bearing on the structure predicted for *Pf*Cox17.

3.2.5 Analysis of the putative *P. falciparum* Cox17 metallochaperone coding sequence

Candidate *P. falciparum* chromosomal centromeres were identified by etoposide-mediated topisomerase-II cleavage of the 14 chromosomes. Identified centromeres were classified as regions of ~2 kb in length with extremely high A+T content (>97%) and imperfect short tandem repeats (Kelly *et al.*, 2006). For chromosome 10 the candidate centromere was suggested to be located 1.1 Mb from the left-hand telomere, however, this site lacked an apparent AT-rich domain. Although localisation of the *P. falciparum* chromosome 10 centromere was not confirmed, the suggested location was used as a reference for the analysis of the putative *P. falciparum* Cox17 coding domain (PF10_0252). The PF10_0252 coding domain is predicted to be localised between bases 1 088 212 and 1 088 415 of chromosome 10 (Figure 3.6). This is in close association with the candidate centromere. As previously suggested, conservation of a protein coding domain within the apparent "core" region of a chromosome could be suggestive of metabolic importance (Section 3.2.3). Analysis of the PF10_0252 intron/exon structure indicated the presence of a single 204bp exon with an absence of introns (Figure 3.6b). A similar gene organisation was observed for all retrieved *Plasmodium* Cox17 sequences (data not shown).

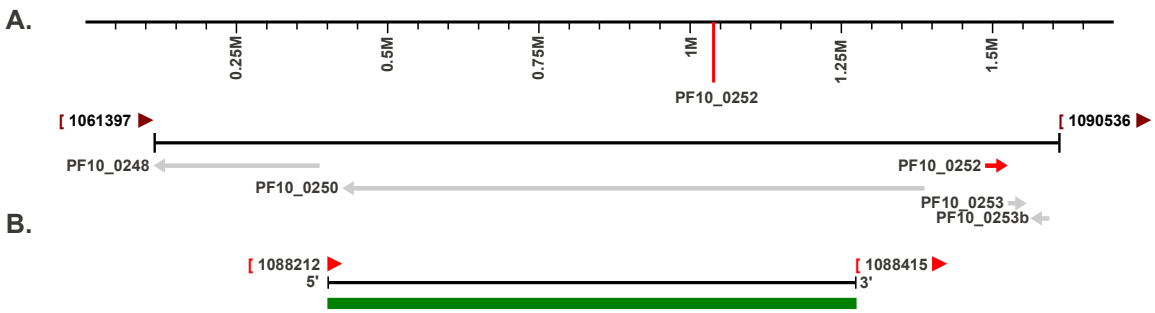

Figure 3.6 Localisation of the Cox17 coding domain in *P. falciparum* chromosome 10

PF10_0252 (---) coding domain localisation on *P. falciparum* chromosome 10 (**A**). An exploded view of chromosome 10 gene organisation relative to PF10_0252 (**B**); the upper image depicts surrounding genes whilst the lower image depicts the intron (—)/exon (■) structure of the PF14_0252 coding domain. The corresponding base pair numbers (adjacent to the coloured arrowheads) are shown above the 5' and 3' termini.

3.2.6 Transcription levels of a *P. falciparum* copper transporter and metallochaperone

Each stage of the *P. falciparum* parasite's developmental life cycle was examined for the expression of each copper transporter, as well as for those proteins related to cytochrome-c oxidase, and compared to lactate dehydrogenase (LDH) expression (Figure 3.7). Analysis of the LDH data indicated relatively consistent expression throughout the erythrocytic stages of the parasite's life cycle, although expression did appear to decrease slightly during the latter stages of development (Figure 3.7a). LDH expression is lowest during the gametocyte stage, whilst expression in sporozoites is relatively comparable to expression during the erythrocytic stages of development (Figure 3.7a). Compared to LDH, the two copper transporters (PF14_0211 and PF14_0369) showed reduced levels of expression with an apparent peak in expression during schizont development (Figure 3.7b and Figure 3.7c). Expression of both copper transporters during sporozoite and gametocyte development was very similar, but at a lower levels compared to peak protein expression. Expression of cytochrome-c oxidase subunit I showed a similar trend to the copper transporters, peaking at the schizont stage (Figure 3.7e). Unlike copper transporter expression, however, cytochrome-c oxidase peak expression did not decrease during the gametocyte stage but did decrease during the sporozoite stage of development (Figure 3.7e). Similar to LDH, Cox17 expression was relatively consistent through all stages of the erythrocytic life cycle. This consistency in Cox17 expression was also evident for the sporozoite and gametocyte stages of development (Figure 3.7d). However, in contrast to LDH, Cox17 was expressed at significantly reduced levels for all stages of development. A similar expression pattern, to Cox17, was noted for the related Cox11 and Sco1 copper metallochaperones (data not shown). Taken together, this expression data supports a parasite requirement for copper acquisition, distribution and utilisation through the different stages of parasite development.

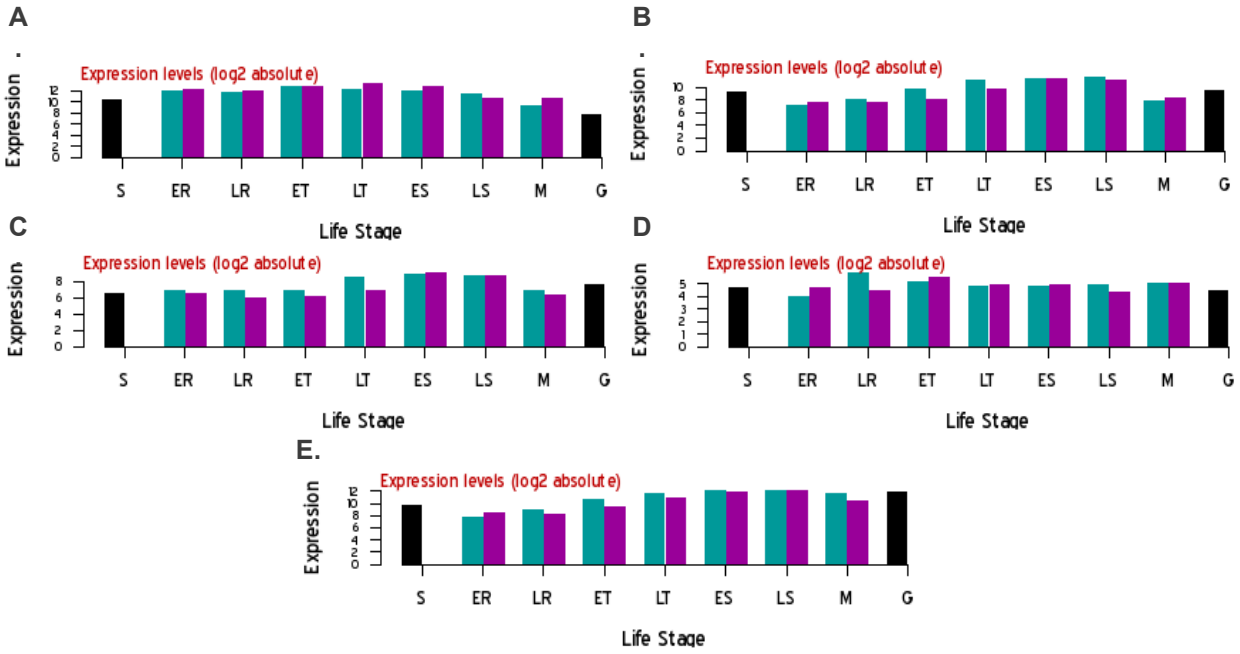

Figure 3.7 Relative expression of *P. falciparum* copper-dependent protein orthologs compared to lactate dehydrogenase.

mRNA expression profiles for *P. falciparum* **A** lactate dehydrogenase (PF13_0141), **B** PF14_0211 copper transporter, **C** PF14_0369 copper transporter, **D** Cox17 (PF10_0252) and **E** cytochrome-c oxidase subunit I (mal_mito_2). For each graph the y-axis represents the affymetrix MOID expression value normalized by experiment (www.plasmodb.org). Labels on the x-axis are: S = sporozoites, ER = early rings, LR = late rings, ET = early trophozoites, LT = late trophozoites, ES = early schizonts, LS = late schizonts, M = merozoites and G = gametocytes. Parasites were synchronised by sorbitol or temperature. Data for gametocyte samples represents synchronisation by sorbitol only whilst data for sporozoites represents the average of two replicates. The represented data is in accordance with the dataset determined by Le Roch *et al.* (2003).

3.2.7 Phylogenetic analysis of the *Plasmodium* copper transporter and Cox17 protein sequences

Phylogenetic trees were generated by aligning the eight *Plasmodium* copper transporter or Cox17 protein sequences with the sequences of seven characterised copper transporter (Figure 3.9) or Cox17 (Figure 3.10) proteins, respectively. In both trees all eight *Plasmodium* species were found to form a related cluster. For the copper transporters this cluster included *Theileria parva* whilst the same was not true for Cox17. Although displaying slight differences between proteins, the close relation between *Plasmodium* parasites and *T. parva* is expected considering both parasites belong to a large monophyletic assemblage of entirely parasitic organisms, the Apicomplexans (Escalante and Ayala, 1995). Interestingly, an event of divergence was noted for the *P. falciparum* PF14_0211 sequence from the other *Plasmodium* copper transporters. Although evidently related to one another, the divergence of PF14_0211 from PF14_0369 in particular suggests these proteins share a similar mechanism but could possibly perform their roles at separate cellular destinations. The identification of an apicoplast targeting signal in the PF14_0369-encoded protein, and not the PF14_0211-encoded protein, also supports this possibility. The idea of copper transporters sharing a similar mechanism but

being targeted to different locales in a cell has previously been established for the human copper transporters Ctr1 and Ctr2 (Rees *et al.*, 2004; van den Berghe *et al.*, 2007).

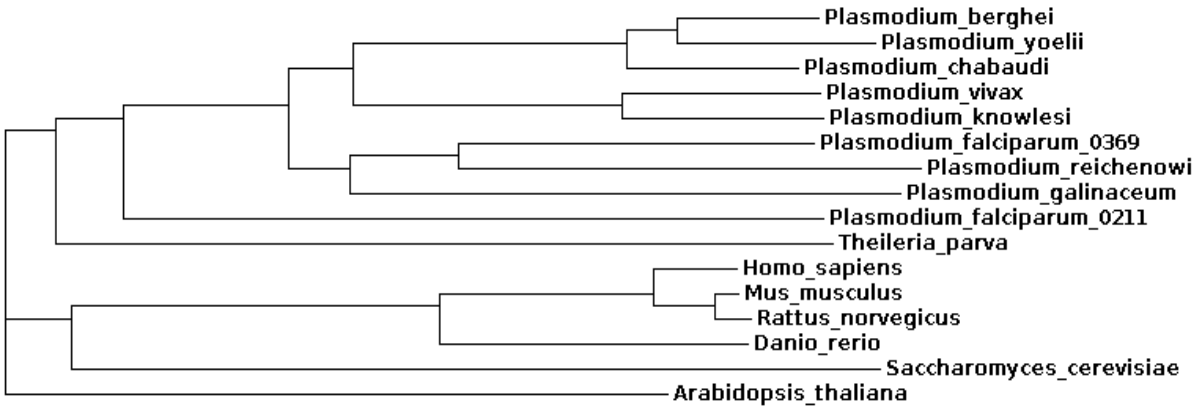

Figure 3.8 Phylogenetic analysis of the *Plasmodium* copper transport protein sequences with mammalian, yeast, plant and Apicomplexan parasite copper transporter sequences

Eight *Plasmodium* copper transport protein sequences were aligned with the sequences of seven previously identified copper transport proteins from *H. sapiens, M. musculus, R. norvegicus, D. rerio, S. cerevisiae, A. thaliana and T. parva* (Refer to Section 2.3 for the sequence accession numbers). All 15 sequences were aligned using the ClustalW™ server (Thompson *et al.*, 1994) and a phylogenetic tree constructed.

For both the copper transporter (Figure 3.8) and Cox17 (Figure 3.9) trees, the three rodent malaria parasites cluster together as *P. vivax* does with *P. knowlesi* and *P. falciparum* with *P. reichenowi* and *P. galinaceum*. Similar evolutionary relationships have previously been observed from the phylogenetic analysis of the cytochrome b and small subunit rRNA sequences (Rathore *et al.*, 2001). The last of the aforementioned clusters has also been similarly noted for the small subunit rRNA sequences (Escalante and Ayala, 1994). These various clusters collectively indicate the relatedness of the sequences, with the events of divergence suggesting probable adaptations to accommodate for specific host conditions. As expected, all *Plasmodium* species show a relatively distant relation to the mammalian, yeast and plant reference species used. Similar results were obtained for a phylogenetic analysis of LDH sequences (data not shown).

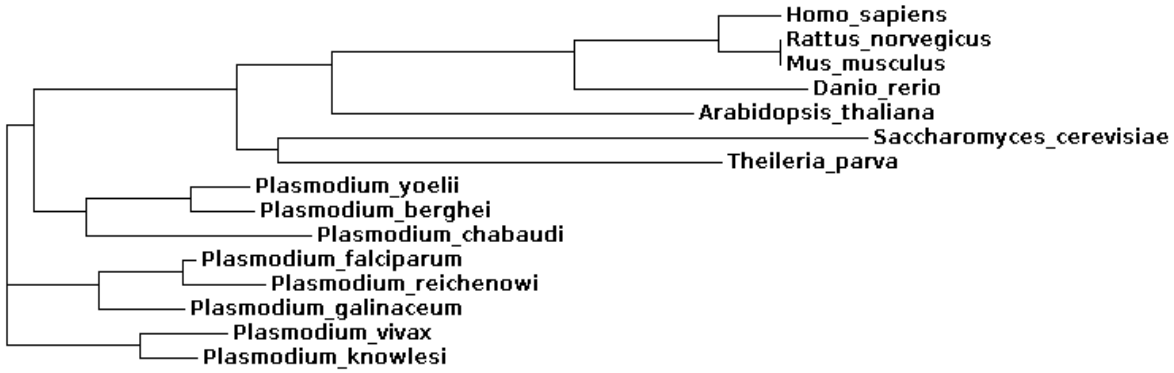

Figure 3.9 Phylogenetic analysis of the *Plasmodium* Cox17 metallochaperone sequences with mammalian, yeast, plant and Apicomplexan parasite Cox17 metallochaperones

Cox17 metallochaperone sequences from eight *Plasmodium* species were aligned with the sequences of seven previously identified Cox17 metallochaperones from *H. sapiens, R. norvegicus, M. musculus, D. rerio, A. thaliana, S. cerevisiae, and T. parva* (Refer to Section 2.3 for the sequence accession numbers). All 15 sequences were aligned using the ClustalW™ server (Thompson *et al.*, 1994) and a phylogenetic tree produced using the same server.

3.2.8 Selection of immunogenic peptides for antibody production in chickens

To demonstrate the native expression of each parasite protein being studied, a protein-specific antibody-based approach was adopted (Martin *et al.*, 2009a). Anti-peptide antibodies were raised against peptides from the parasite copper transport protein and Cox17 metallochaperone. Peptides were identified using the Predict7™ program (Cármenes *et al.*, 1989) and subsequently synthesised. Peptides were selected from the single *P. yoelii* and two *P. falciparum* copper transport proteins, as well as the *P. yoelii* and *P. falciparum* Cox17 metallochaperones. For each of the three copper transport proteins, peptide sequences were selected from the amino-terminal domain as this is predicted to be extracellular (Figure 3.2) and thus likely to be more accessible to antibodies in its native state. Cox17 is a soluble protein localised to the cell cytoplasm and inner-mitochondrial space (Beers *et al.*, 1997) providing a greater number of accessible epitopes.

Predict7™ analysis of the copper transport protein sequences (Figure 3.10) identified the following peptides: CSDKQSGDDECKPILD for the *P. yoelii* protein, CHSKNDDGVMLPMY for PF14_0211 and CNLQKEEDTVVQLQD for PF14_0369. Peptides identified for the Cox17 sequences (Figure 3.11) were CPLNTTEESKTCA, for the *P. yoelii* protein, and CPINNTNEANKGE, for the *P. falciparum* protein (For each peptide the three underlined amino acids represent the abbreviated laboratory reference name of the peptide and corresponding antibodies). For the *P. yoelii* Cox17-specific peptide (KTC), the internal cysteine residue was substituted for an α-aminobutyric acid group so as to avoid the formation of internal disulfide bonds and allow for specific amino terminal cross-linking to rabbit albumin. Each peptide sequence was subjected to a BLASTp search against the *Gallus gallus*, *Mus musculus*, *Homo*

sapiens and *Plasmodium* parasite proteomes, with no significant matches identified (data not shown). This search was performed to ensure antibodies would be generated in the chicken host and that the resulting antibodies would be specific to the target protein, meaning they would not bind to other parasite or host proteins.

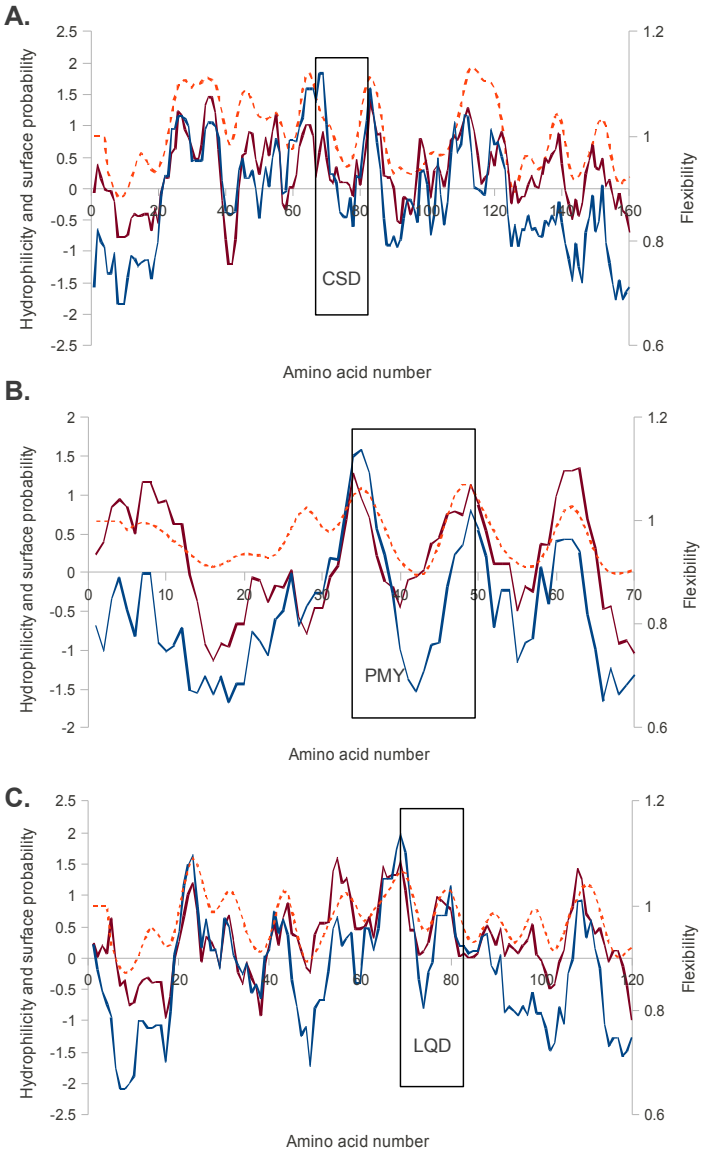

Figure 3.10 Selection of immunogenic peptides from the amino-terminal domains of three putative *Plasmodium* copper transport proteins

Predict7™ analysis of the amino-terminal sequences of a *P. yoelii* (**A**) and two *P. falciparum* copper transport proteins, PF14_0211 (**B**) and PF14_0369 (**C**). The selected peptides are identified by the boxed region in each panel. For each Predict7™ analysis hydrophilicity (—), surface probability (—) and flexibility (---) are plotted.

MBS coupling of peptides requires a terminal cysteine residue. This can either be native to the sequence or included during peptide synthesis. For the copper transport protein peptides, the *P. yoelii* and PF14_0211 amino terminal cysteine residues are native to the protein, whereas a cysteine residue was added to the amino terminus of PF14_0369. It was also necessary to add

a cysteine residue to the amino terminus of both Cox17 peptides. Peptides conjugated to the rabbit albumin carrier were then injected into chickens.

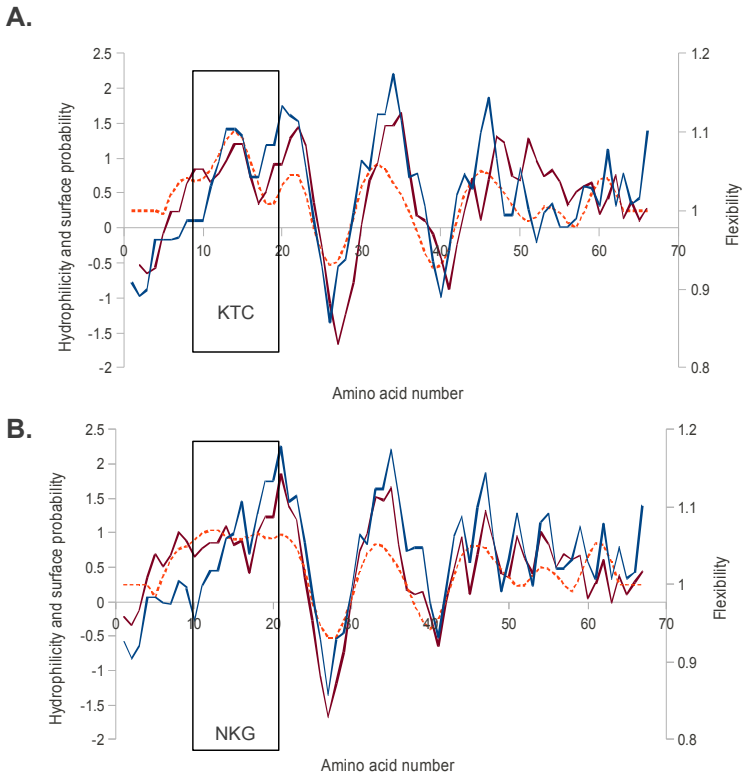

Figure 3.11 Selection of immunogenic peptides from the *Plasmodium* metallochaperone Cox17

Predict7™ analysis of the putative Cox17 metallochaperone sequences for *P. yoelii* (**A**) and *P. falciparum* (**B**). The selected peptides are identified by the boxed region in each panel. For each Predict7™ analysis hydrophilicity (—), surface probability (—) and flexibility (---) are plotted.

3.3 Discussion

Proteins involved in copper import and export are associated with a number of pathway-specific copper metallochaperones that deliver copper to specific targets in a cell (O'Halloran and Culotta, 2000; Rosenzweig, 2001; Kim *et al.*, 2008). To date, mechanisms for copper homoeostasis have not been extensively characterised for the malaria parasite. What has been established is that the parasite expresses a copper P-type ATPase (*Pf*CuP-ATPase) for the efflux of excess copper (Rasoloson *et al.*, 2004). Rasoloson *et al*. (2004) also suggested that more elaborate copper homeostatic pathways, particularly for copper acquisition and distribution are likely to be present. The current study explored these potential pathways using a bioinformatics analysis of the *Plasmodium* database (PlasmoDB).

3.3.1 Identification of a putative *Plasmodium* spp. copper transport protein and Cox17

A BLASTp search of PlasmoDB was executed using the sequences of previously identified and characterised copper-dependent proteins. This yielded positive results for some, but not all, of

the sequences used (Table 3.1). Perhaps one of the more important proteins identified was a subunit of a cytochrome-c oxidase complex that requires copper for the formation of the active protein (Table 3.1). In the presence of oxygen, energy production in eukaryotic cells is predominantly generated by mitochondrial oxidative phosphorylation (Iwata *et al.*, 1995). This process is driven by an electron-transport chain composed of a number of complex mitochondrial membrane proteins, of which cytochrome-c oxidase is the terminal enzyme (Cobine *et al.*, 2006a). Deficiencies in cytochrome-c oxidase activity have been linked to a number of human diseases including encephalomyopathies, Leigh syndrome, hypertrophic cardiomyopathies and fatal lactic acidosis (Diaz, 2010). This highlights the importance of this enzyme to human cells and suggests the possibility that this enzyme is likely to be important in *Plasmodium* metabolism. This is supported by the identification of Cox11, Cox17, Cox19 and Sco1 metallochaperone orthologs, which transfer and insert copper into the cytochrome-c oxidase complex. The identification of a copper-requiring S-adenosyl-L-homocysteine hydrolase ortholog was also significant since this protein has been established as being important to parasite survival since enzyme inhibition interferes with parasite proliferation (Bujnicki *et al.*, 2003; Creedon *et al.*, 1994). Taken together, these results suggest a parasite requirement for copper.

A physiological role for copper, in the *Plasmodium* parasite, has previously been suggested from studies using the intracellular copper chelator neocuproine. Treatment of an *in vitro* parasite culture with nanomolar concentrations of neocuproine inhibited parasite transition from rings to trophozoites (Rasoloson *et al.*, 2004). However, the mechanism by which the parasite acquires copper has not yet been established. Two possible mechanisms exist. The first is copper acquisition via parasite ingestion and digestion of host erythrocyte Cu/Zn SOD (Rasoloson *et al.*, 2004), whilst the other is via a dedicated copper transport protein, similar to that identified in yeast and mammalian cells (Dancis *et al.*, 1994; Lee *et al.*, 2000; Lee *et al.*, 2002). Following extensive research, characteristic sequence features have been identified for this family of proteins. The most notable features include a methionine-rich amino terminus, three transmembrane domains and essential MX_3M and GX_3G motifs in the second and third transmembrane domains respectively (Aller *et al.*, 2004; Puig *et al.*, 2002a) (Figure 1.5). A BLASTp search of PlasmoDB identified candidate copper transporter sequences for eight species of the *Plasmodium* parasite. Alignment of the retrieved sequences with sequences of known copper transporters identified the essential and largely definitive MX_3M and GX_3G motifs in all eight *Plasmodium* species (Figure 3.1). Methionine motifs were also identified in the predicted amino terminal domain of these proteins. These motifs are important for protein function (Eisses and Kaplan, 2005; Guo *et al.*, 2004; Puig *et al.*, 2002a) but are not unique to the copper transport proteins.

A topological analysis of each sequence identified the presence of three putative membrane-spanning domains (Figure 3.2). This too is considered a definitive feature of the copper transport proteins (Dancis *et al.*, 1994). It is, however, important to note that three transmembrane domains are unable to form a functional channel or pore through which ions can be transported (Nose *et al.*, 2006). It was therefore proposed, and subsequently verified, that copper transport protein monomers create a channel by associating in a homotrimeric complex (Aller and Unger, 2006; De Feo *et al.*, 2009). This copper-permeable pore consequently forms a pathway that permits the controlled movement of copper across the membrane and into the cell. Given the importance of trimer formation to protein function (Aller *et al.*, 2004), a similar formation is likely to exist for the *Plasmodium* copper transporters. Supporting this likelihood, was the recent finding that the first transmembrane domain of the copper transporter serves as an adaptor that allows evolutionarily distant copper transport proteins to adopt a similar, but not identical, overall structure (De Feo *et al.*, 2010).

The presence of a putative *Plasmodium* copper transport protein sequence suggests a dedicated system for copper acquisition in the parasite. This is supported by the presence of sequences for orthologs of cytochrome-c oxidase and its associated metallochaperones Cox11, Cox17 and Sco1 (Table 3.1). Cox17 is of particular interest since this protein localises to the cell cytoplasm and inner mitrochondrial space and is thought to be involved in shuttling copper from the copper transporter to the mitochondrion (Beers *et al.*, 1997). This mechanism has been re-evaluated (Cobine *et al.*, 2006a; Lutsenko, 2010), however, the importance of Cox17 to cell survival (Takahashi *et al.*, 2002) has not been disputed. To better understand parasite copper pathways and homoeostasis, the Cox17 sequence was studied. Eight species of the *Plasmodium* parasite contained Cox17 metallochaperone sequences, suggesting a conserved presence and role for this protein. ClustalW™ alignment of the *Plasmodium* sequences, with other Cox17 sequences, highlighted essential and conserved motifs that are important to protein function (Figure 3.4). These include the CysCysXaaCys motif, which coordinates the cuprous ion to Cox17 (Abajian *et al.*, 2004), plus additional cysteine residues required for structural disulfide bond formation (Figure 3.5). From the homology model for *Pf*Cox17 it appears that these conserved cysteine residues adopt a similar conformational orientation to the corresponding residues in human Cox17, resulting in *Pf*Cox17 forming a coiled coil-helix-coiled coil helix structural motif (Figure 3.5b and c). This is a common feature of related mitochondrial proteins (Barros *et al.*, 2004; Nobrega *et al.*, 2002), which suggests that *Plasmodium* Cox17 is likely to be involved in copper delivery to the parasite mitochondrion. This modelling project was, however, prepared on a rudimentary level and thus requires further analysis to confirm the observed and inferred result.

Each *Plasmodium* Cox17 sequence was further examined for the presence of potential signal sequences and transmembrane regions. Characterisation of *S. cerevisiae* Cox17 found the protein to be localised to the cell cytosol as well as the inner mitochondrial space (Beers *et al.*, 1997). A signal sequence directing the protein to the inner mitochondrial space is, however, absent raising the question as to how Cox17 is directed to the mitochondrion. Only recently was a possible mechanism behind this targeting action identified. Through a unified electrospray ionization mass spectrometry (ESI-MS) based strategy it was demonstrated that Cox17, amongst other copper chaperones, is driven toward its partner proteins by exploiting gradients of increasing copper binding affinity (Banci *et al.*, 2010). Thus an absence of a signal peptide in the retrieved *Plasmodium* sequences would, to some degree, support the likelihood of these proteins being representative of Cox17 metallochaperones. Additionally, Cox17 is not known to anchor to cell or mitochondrial membranes, therefore the absence of long hydrophobic stretches of amino acids was expected. Each sequence was systematically analysed by SignalP, PlasmoAP, PlasMit (Bender *et al.*, 2003), TMHMM and HMMTOP. As predicted, none of the retrieved sequences returned a positive result for any of the above evaluations. Overall, the presence of both the Cox17 copper chaperone and copper transport protein supports a physiological need for copper by the malaria parasite.

3.3.2 Chromosomal location of the copper transporter and Cox17 coding domains

Due to the considerable length variation of *P. falciparum* chromosomes, the majority of research has focussed on elucidating subtelomeric structure and function as well as the roles of the encoded proteins (Kyes *et al.*, 2001). Consequently, the remainder of the chromosome is left relatively poorly defined (Gardner *et al.*, 2002; Kooij *et al.*, 2005). Recently, though, candidate centromeres were identified for all 14 *P. falciparum* chromosomes. Centromeres were defined as regions approximately 2 kb long, with extremely high A+T content (>97%) and imperfect short tandem repeats (Kelly *et al.*, 2006). The location of the candidate centromeres was inferred as being indicative of the probable “core” region of each parasite chromosome. This “core” region has been found to contain a number of conserved gene orthologs in other parasite species, suggesting an important role for these proteins in parasite metabolism (Hall *et al.*, 2005). For example, the coding domain for the essential enzyme lactate dehydrogenase is found in the “core” region of *P. falciparum* chromosome 13. The relative position of this coding domain appeared to be conserved within a predicted “core” of other *Plasmodium* species' chromosomes (data not shown), thereby supporting the notion that gene conservation within the chromosome “core” suggests importance to parasite metabolism. The chromosomal location of the copper transporter and Cox17 coding domains was therefore assessed to see if

they reside in the “core” of the respective chromosomes to which they are localised.

For the *P. falciparum* parasite, both copper transporter coding domains are localised to chromosome 14 (Figure 3.3) whereas the Cox17 coding domain is found on chromosome 10 (Figure 3.6). For these respective chromosomes the candidate centromere of chromosome 14 was more confidently identified than that for chromosome 10 (Kelly *et al.*, 2006). The respective coding domains, for both copper transporters and Cox17, were found to be in close proximity to the predicted centromeres. This gene localisation appeared conserved amongst the other *Plasmodium* species analysed. As indicated, the chromosomal position of a selected *Plasmodium* parasite gene can serve to indicate the potential importance of the protein for the parasite. Localisation to the subtelomeric or telomeric domains is suggestive of a gene encoding a protein necessary for antigenic variation and therefore undergoing a high turnover rate. On the other hand, genes with a more centromeric localisation are presumed to encode for metabolically essential proteins. Through this reasoning it was inferred that the localisation of both *P. falciparum* copper transporter and Cox17 coding domains suggests an important role for these proteins to the parasite.

3.3.3 Phylogenetic analysis of the *Plasmodium* copper transporter and Cox17 amino acid sequences

Phylograms of the copper transporter and Cox17 sequences showed that in both instances the *Plasmodium* species formed a distinct clade (Figure 3.8 and 3.9), confirming their affiliation to the same genus. This was, however, more apparent for the copper transport proteins since the rodent-infecting parasites form a separate, but closely related branch for the analysis of Cox17 (Figure 3.9). A similar observation has been made for other parasite proteins, suggesting that these species do not cluster closely with other *Plasmodium* related clades (Escalante and Ayala, 1994). Rodent-infecting *Plasmodium* species are, however, known to show a monophyletic relation with respect to one another (Perkins and Schall, 2002), as was observed for both analyses. Regarding the relationships seen for the other species, it was noted that the results for the copper transporter and Cox17 were similar to results obtained from studies of the *Plasmodium* small subunit rRNA (Rathore *et al.*, 2001; Escalante and Ayala, 1994). From these studies it was identified that *P. falciparum* is monophyletic with *P. reichenowi* but shares a distant common ancestor with the avian parasite *P. galinaceum*. Furthermore it was found that *P. vivax* is only distantly related to *P. falciparum* and generally clusters with monkey-infecting species *P. knowlesi* (Rathore *et al.*, 2001; Escalante and Ayala, 1994), which is again similar to the results seen from both analyses. A close relationship between *P. vivax* and *P. knowlesi* is also in agreement with the recent findings that *P. knowlesi* can infect humans with a potentially

fatal outcome (Cox-Singh *et al.*, 2010).

The respective *Plasmodium* sequences were also compared to other copper transporter or Cox17 metallochaperone protein sequences from an unrelated organism. Considering the *Apicomplexan* parasites are evolutionarily distant from the Chordates (Templeton *et al.*, 2004), it was not surprising that shown on a separate and distantly related branch was a cluster containing *H. sapiens*, *M. musculus*, *R. norvegicus* and *D. rerio* (Figure 3.8 and 3.9). This is also in agreement with the taxonomic relationships established between these organisms, by both morphological and sequence comparisons (Baldauf *et al.*, 2000; Gardner *et al.*, 2002). Both phylograms also suggest a close evolutionary relationship between the *A. thaliana* Copt1 sequence and the *Plasmodium* species (Figure 3.8), supporting the suggestion that the genome of *P. falciparum* is more similar to that of *A. thaliana* than to other taxa (Gardner *et al.*, 2002). However, this relationship was less evident from an analysis of Cox17 (Figure 3.9). For the copper transporter sequences (Figure 3.8) a direct relation was seen between the *Plasmodium* species and another Apicomplexan parasite, *T. parva*. The Cox17 sequences showed a slightly differing result (Figure 3.9), but both parasites still indicated a close relationship.

3.3.4 Peptide selection

It has previously been demonstrated that a novel protein can be identified through an initial *in silico* analysis, followed by a biochemical and genetic characterisation (Reininger *et al.*, 2005; Dorin *et al.*, 2005). To assist with the characterisation of the identified proteins, anti-peptide antibodies were to be generated. By using the Predict7™ algorithm (Cármenes *et al.*, 1989), peptides were selected from each of the three putative copper transport proteins (Figure 3.10) as well as the two Cox17 metallochaperones (Figure 3.11). The synthesised peptides were conjugated to a rabbit albumin carrier protein for injection into chickens. The resulting antibodies were to be used for immunolocalisation of the respective proteins. Establishing protein location will be important to understanding protein function, particularly for the *P. falciparum* copper transporters, since each transporter is predicted to be located in different parasite membranes. PF14_0211 is predicted to be targeted to the parasite membrane whereas PF14_0369 is predicted to be targeted to the apicoplast membrane. This difference, in predicted location, suggests PF14_0211 could function to acquire extracellular copper whilst PF14_0369 might be involved in mobilising copper stores. Similar roles have been predicted for the human copper transporters Ctr1 and Ctr2 (Rees *et al.*, 2004; van den Berghe *et al.*, 2007). In addition, establishing the membrane orientation of the copper transporters will help determine the directional transport of each protein. This could be achieved by generating

antibodies against a peptide from the transporter's carboxyl terminus to be used in conjunction with the anti-peptide antibodies generated against the peptide selected from the amino terminus. A similar approach has been used to establish the orientation of human Ctr1 (Klomp *et al.*, 2003).

Mechanisms for *Plasmodium* parasite copper homoeostasis were suggested following the identification of a *P. falciparum* copper efflux protein (Rasoloson *et al.*, 2004). Until now a dedicated mechanism for parasite copper acquisition has not been established. A BLASTp search of PlasmoDB identified sequences corresponding to putative copper transport proteins in eight species of the *Plasmodium* parasite. Each of these sequences was found to contain sequence features common to other copper transporters. Also identified, from a BLASTp search, were a number of putative metallochaperone proteins, including Cox17. An analysis of the parasite Cox17 metallochaperone sequences identified amino acids conserved amongst the characterised yeast and mammalian Cox17 proteins suggesting a conservation of protein function. To establish native expression and localisation, of these copper-requiring parasite proteins, anti-peptide antibodies were to be raised against peptides selected from the identified *P. yoelii* and *P. falciparum* protein orthologs. Establishing putative protein function was to be achieved by recombinantly expressing the amino terminal domain of the putative *Plasmodium* copper transporter to determine its ability to bind copper. A similar copper binding study was to be carried out using a recombinant form of the full-length *Plasmodium* Cox17 ortholog.

CHAPTER 4

The *Plasmodium* spp. putative copper transport protein: Native protein expression and copper binding studies with the recombinant amino-terminal domain

4.1 Introduction

The high redox activity of copper has resulted in mammalian and yeast cells developing complex systems to maintain and control cellular copper levels (Kim *et al.*, 2008; Rae *et al.*, 1999; Rosenzweig, 2002). *In silico* identification of a putative *Plasmodium* copper transport protein and associated metallochaperones (Chapter 3) suggests that similar pathways may be present to maintain *Plasmodium* parasite copper homeostasis. PCR amplification and sequencing of the genes predicted to encode each parasite protein enables recombinant expression of these proteins for functional studies. Successful PCR amplification also suggests the presence of a native coding domain for the corresponding protein. Native protein expression, in the parasite, can then be confirmed through specific anti-peptide antibody recognition. This approach has proven successful for the characterisation of *Plasmodium* protein kinases (Dorin *et al.*, 2005; Merckx *et al.*, 2003), lactate dehydrogenase (Hurdayal *et al.*, 2010) and membrane-bound transport proteins (Narum *et al.*, 2001; Rasoloson *et al.*, 2004).

The structural properties and function of a protein, having a hypothetical function, can only be confidently inferred from biochemical and cell biological experimentation. This requires relatively large quantities of the protein, which are difficult to obtain from a native cell by standard protein isolation methods. Consequently systems have been developed for the heterologous expression of target proteins. One expression system, which still remains one of the most attractive, is the Gram-negative bacterium *Escherichia coli*. The attraction of *E. coli* is its ability to rapidly multiply to high cell densities on inexpensive substrates, its well characterised genetics and the availability of numerous plasmid vectors and mutant host strains (Baneyx, 1999). The *E. coli* system has also been successfully used for the characterisation of numerous *Plasmodium* protein kinases (Dorin *et al.*, 2005; Merckx *et al.*, 2003; Nunes *et al.*, 2007), glycolytic enzymes (Brady and Cameron, 2004; Turgut-Balik *et al.*, 2004; Winter *et al.*, 2003) and surface-related proteins (Narum *et al.*, 2001; Rasoloson *et al.*, 2004; Rodrigues *et al.*, 2003).

Identification of the genes encoding mammalian copper transport proteins made use of a yeast functional complementation system (Lee *et al.*, 2000; Zhou and Gitschier, 1997). This system employs mutant *S. cerevisiae* cells lacking high affinity copper uptake due to *Ctr1* and *Ctr3*

gene inactivation (Lee *et al.*, 2000; Zhou and Gitschier, 1997). Hence a restoration of normal cell growth to mutant cells, transfected with the candidate gene, confirmed the gene encoded a protein functioning as a copper transporter. Using a similar approach it would seem likely that the function of the protein encoded by the candidate *Plasmodium* copper transporter gene could be confirmed. However, a setback to this approach is the finding that heterologous expression of full length *Plasmodium* membrane proteins is difficult (Krishna *et al.*, 2001; Martin *et al.*, 2009a; Vedadi *et al.*, 2007). Consequently the recombinant expression of the amino terminal copper-binding domain of the *Plasmodium* copper transporter was selected. This extracellular domain is predicted to be important for copper acquisition as well as for copper access to and from the pore of the characterised copper transporters (De Feo *et al.*, 2009; Jiang *et al.*, 2005; Larson *et al.*, 2010).

Knowledge of the pathways for copper homoeostasis in the *Plasmodium* parasite is limited. It has, however, been demonstrated that the parasite requires intracellular copper for survival (Meshnick *et al.*, 1990; Rasoloson *et al.*, 2004). A dedicated mechanism for copper acquisition has, however, not yet been characterised. Through an *in silico* based approach, a sequence corresponding to a putative *Plasmodium* copper transport protein was identified (Section 3.2.2). These proteins are known to function as the primary regulators of copper access into cells (Dancis *et al.*, 1994; Lee *et al.*, 2000; Zhou and Gitschier, 1997). This study therefore aimed to confirm the presence of native *P. berghei* and *P. falciparum* copper transporter coding domains, and their corresponding proteins, using PCR and anti-peptide antibody based approaches, respectively. Furthermore protein function was to be inferred from *in vitro* and *in vivo* copper-binding studies using a recombinant amino-terminal domain of both the *P. berghei* and *P. falciparum* proteins.

4.2 Results

4.2.1 Confirmation of a putative *Plasmodium* copper transporter coding domain sequence

Initial attempts at identifying a parasite copper transporter coding domain, as well as the encoded native protein, made use of the rodent-infecting malaria parasite model. This model parasite serves as a useful comparative tool as it is capable of reproducing much of the biology of human malaria parasites (Carlton *et al.*, 2002; Hall *et al.*, 2005; van Lin *et al.*, 2001). In the first instance, *P. yoelii* parasite DNA was isolated from parasitised BALB/c mouse blood and used as a template for amplification of the putative copper transporter's full-length coding domain by PCR. The target sequence was predicted to contain two introns and three protein-coding exons (data not shown), producing a sequence approximately 1791 bp long. Agarose

gel analysis of the PCR amplicons revealed a product approximately 1800 bp in size (Figure 4.1a), corresponding to the predicted size. PCR amplification of the LDH coding domain was included as a positive control with an amplification product approximately 815 bp in size (Figure 4.1a). This amplicon was in agreement with the predicted size of the targeted LDH coding domain region. As a further control, DNA was isolated from uninfected BALB/c mouse blood and used as a template for PCR amplification. All reactions using this template DNA returned negative results (data not shown).

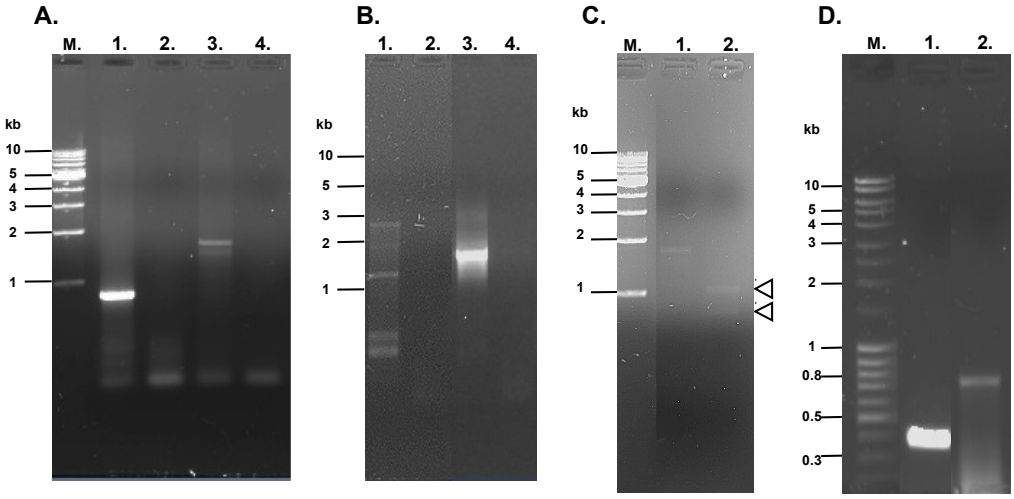

Figure 4.1 PCR and reverse transcriptase-PCR amplification of the coding domains for putative *P. yoelii* and *P. berghei* copper transporters

A PCR amplification, from *P. yoelii* genomic DNA, of the coding domains for lactate dehydrogenase (lane 1) and the putative copper transport protein (lane 3). Lanes 2 and 4 are controls using DNA isolated from uninfected mouse blood. **B** Nested PCR of the putative *P. yoelii* copper transport protein coding region. Lane 1 primary PCR product, lane 3 secondary PCR from lane 1. Lanes 2 and 4 negative controls. **C** *Bam*HI digestion to support *P. yoelii* amplicon identity. Lane 1, gel purified amplicon of the putative *P. yoelii* copper transporter coding region. Lane 2, *Bam*HI digestion of lane 1 amplicon with arrows highlighting digested products. The upper arrow in lane 2 is 1050 bp, lower arrow 750 bp. **D** Reverse transcriptase-PCR amplification, from *P. berghei* RNA, of the coding domains for the amino terminus of a putative *P. berghei* copper transporter (lane 1) and for LDH (lane 2). All PCR products were analysed on 1% (w/v) agarose gels. Molecular mass markers (**M**) are on the left of each gel (see materials and methods for details).

The identity of the *P. yoelii* 1800bp amplicon was supported by nested PCR (Figure 4.1b) and *Bam*HI enzyme digestion (Figure 4.1c). For nested PCR, a 2700bp region encompassing the predicted copper transporter coding domain was amplified from genomic DNA and from this the 1800bp product was amplified (Figure 4.1b). The 1800bp amplicon was subsequently gel purified and digested with *Bam*HI. *Bam*HI digestion yielded two products (Figure 4.1c), of 1050bp and 750bp, which corresponded well with the predicted sizes. For functional studies of the murine malaria parasite's copper transporter, the predicted amino terminus was to be recombinantly expressed and its copper binding ability assessed. Since the number of copper transporters encoded by the *P. berghei* and *P. falciparum* genomes is similar, *P. berghei* was selected as the murine malaria parasite model organism. The relevant portion of the *P. berghei*

copper transporter's coding domain was therefore amplified by reverse transcription-PCR (RT-PCR) from a *P. berghei* RNA pool. Amplification yielded a 450bp product (Figure 4.1d), indicating native transcription of the targeted coding domain. As before, amplification of the LDH coding domain served as a positive control and yielded a product of the expected size. The putative copper transporter amino terminal amplicon was ligated into the pGEM®-T vector and sequenced. Sequencing data correlated well with the *P. berghei* nucleotide sequence available at PlasmoDB, showing 99% identity (Figure 4.2). *In silico* translation of this sequence yielded an amino acid sequence with 98% identity to the PlasmoDB sequence (data not shown).

```
PbCtrNt_vect      ATGAATATATGGAAAATTATATATATTGTTTTAATTATAAACTCTTCATTTGTGGTGAAT 60
PbCtrNt_plas      AAGAATATATGGAAAATTATATGCATTGTTTTAATTATAAACTCTTCATTTGTGGTAAAT 60
                  * ********************  ******************************** ***

PbCtrNt_vect      GTAAATTGTGAGTCCAATGATAAAAATGATGATACTAAAAACAACAAAAATATGGGTTGT 120
PbCtrNt_plas      GTAAATTGTGAGTCCAATGATAAAAATGATGATACTAAAAACAACAAAAATATGGGTTGT 120
                  ************************************************************

PbCtrNt_vect      GGTGGTGGTACTAATAAATCACTGCCATCCGTAAACAAACCGCTAAATAGTTGTTGCAGT 180
PbCtrNt_plas      GGTGGTGGTACTAATAAATCACTGCCATCCGTAAACAAACCGCTAAATAGTTGTTGCAGT 180
                  ************************************************************

PbCtrNt_vect      GGTAAACGATCGGGAAATGATGAGTGCAAACCAATATTAGATCTCAATCACATAGGAAGT 240
PbCtrNt_plas      GGTAAACGATCGGGAAATGATGAGTGCAAACCAATATTAGATCTCAATCACATAGGAAGT 240
                  ************************************************************

PbCtrNt_vect      GAAGGCAAAAACAAAATTCCATTTATTTACAAATGCTGTATAAATCATGATACATATGAA 300
PbCtrNt_plas      GAAGGCAAAAACAAAATTCCATTTATTTACAAATGCTGTATAAATCATGATACATATGAA 300
                  ************************************************************

PbCtrNt_vect      AACATAATTAATGAGCACTTTAATGAAGAAAATCAAAACAATGCAACCGATGCCCCCAAA 360
PbCtrNt_plas      AACATAATTAATGAGCACTTTAATGAAGAAAATCAAAACAATGCAACCGATGCCCCCAAA 360
                  ************************************************************

PbCtrNt_vect      AAATTGAATATGATGATGAGTGATTTATCTATGCCTATGTCATTTCAGAATACTACCCAT 420
PbCtrNt_plas      AAATTGAATATGATGATGAGTGATTTATCTATGCCTATGTCATTTCAGAATACTACCCAT 420
                  ************************************************************

PbCtrNt_vect      ACTATTATTTTATTCAAATTTTGGGAA 447
PbCtrNt_plas      ACTATTATTTTATTCAAATTTTGGGAA 447
                  ***************************
```

Figure 4.2 Alignment of the RT-PCR amplified putative *P. berghei* copper transporter's amino terminus coding sequence with the PlasmoDB sequence

The sequenced *P. berghei* copper transport protein amino-terminus (PbCtrNt_vect) and PlasmoDB sequence [PbCtrNt_plas (PBANKA_130290)] were aligned with the ClustalW program (http://www.ebi.ac.uk/Tools/msa/clustalw2/).

Using a similar approach, the putative *P. falciparum* copper transporter coding domain was amplified. Here, both the full length and amino terminus coding domains were targeted, whilst amplification of the LDH coding domain served as a positive control. A LDH product was

amplified from the *P. falciparum* genome that was approximately 820bp in size (Figure 4.3), which was similar to the results obtained for *P. yoelii* and *P. berghei* (Figure 4.1). Having identified that two potential copper transport proteins are expressed by *P. falciparum* (Section 3.2.2), it was necessary to probe for the presence of both coding domains (PF14_0211 and PF14_0369) in the parasite genome. Agarose gel analysis of the respective PCR reactions indicated amplification products of approximately 410bp for the full length PF14_0211 domain and 890bp for the full length PF14_0369 domain (Figure 4.3). The size of each PCR product corresponded well with the predicted sizes of each coding domain, which were 423bp for PF14_0211 and 920bp for PF14_0369. Since *P. falciparum* DNA was isolated from cultured parasites, the PCR control used in this instance was a reaction containing no template. These control reactions produce no amplicons (data not shown).

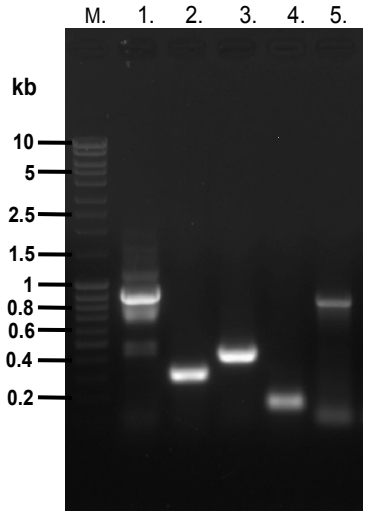

Figure 4.3 PCR amplification of the coding sequences for two putative *P. falciparum* copper transport proteins and their predicted amino termini

The full-length and amino terminus coding domains for PF14_0211 (lanes 3 and 4, respectively) and PF14_0369 (Lanes 1 and 2, respectively) were PCR amplified from *P. falciparum* genomic DNA and analysed on a 1% (w/v) agarose gel. Lane 5 is the *P. falciparum* LDH control. Molecular mass markers (**M**) are shown to the left of the gel (See materials and methods for details).

To confirm the identity of the *P. falciparum* amplicon, the amplicons corresponding to the amino termini of the putative *P. falciparum* copper transporters were cloned and sequenced. The PF14_0211 amplicon was approximately 150bp and the PF14_0369 amplicon 290bp (Figure 4.3), which was in agreement with the predicted sizes. Sequencing of each product identified that both amplicons corresponded well with the respective PlasmoDB sequences, with 98% identity for PF14_0211 and 100% for PF14_0369 (Figure 4.4). *In silico* translation of these sequences yielded amino acid sequences with 97% and 100% identity to the PlasmoDB sequences for PF14_0211 and PF14_0369, respectively (data not shown).

A.

```
PfCtr211Nt_vect      TTCACTTTCGATTTTGTGAGCAGCAGTTGTTGTCATTCAAAAAATGACGATGGAGTTATG 60
PfCtr211Nt_plas      TTCACTTTCGATTTTGTGAGCAGCAGTTGTTGTCATTCAAAAAATGACGATGGAGTTATG 60
                     ************************************************************

PfCtr211Nt_vect      TTACCTATGTATTTTTCAAATAATGGAAATATAAAAATGTTATTTGACATATTTCAAGTA 120
PfCtr211Nt_plas      TTACCTATGTATTTTTCAAATAATGAAAATATAAAAATGTTATTTGACATATTTCAAGTA 120
                     ************************ ********************************

PfCtr211Nt_vect      AAAAAT 126
PfCtr211Nt_plas      AAGAAT 126
                     ** ***
```

B.

```
PfCtr369Nt_vect      GACAAAAGCGACAATAGTATTTGTAAACCTTCTGTTAAAATATCATGTGCTCACAATTGT 60
PfCtr369Nt_plas      GACAAAAGCGACAATAGTATTTGTAAACCTTCTGTTAAAATATCATGTGCTCACAATTGT 60
                     ************************************************************

PfCtr369Nt_vect      TGTAAGAATAAATTATCTTTTATGTATAATTGTTGGAAACACTATGATAAATATAGTAAT 120
PfCtr369Nt_plas      TGTAAGAATAAATTATCTTTTATGTATAATTGTTGGAAACACTATGATAAATATAGTAAT 120
                     ************************************************************

PfCtr369Nt_vect      ATAATAAAAGATAATTTACAAAAAGAAGAAGATACAGTTGTTCAATTACAAGATCATGAT 180
PfCtr369Nt_plas      ATAATAAAAGATAATTTACAAAAAGAAGAAGATACAGTTGTTCAATTACAAGATCATGAT 180
                     ************************************************************

PfCtr369Nt_vect      AATATTGATATTGTCGAACATGTTGAAACTATGCCAATGTCCTTTCAGCTGACTACACAC 240
PfCtr369Nt_plas      AATATTGATATTGTCGAACATGTTGAAACTATGCCAATGTCCTTTCAGCTGACTACACAC 240
                     ************************************************************

PfCtr369Nt_vect      ACAATTATTTTATTTAACAAATGGGAAACCAAATCG 276
PfCtr369Nt_plas      ACAATTATTTTATTTAACAAATGGGAAACCAAATCG 276
                     ************************************
```

Figure 4.4 Alignment of the sequenced amplicons for PF14_0211 and PF14_0369 putative copper transport protein amino terminus coding domains with the PlasmoDB sequences

A PF14_0211 (PfCtr211Nt_vect) and **B** PF14_0369 (PfCtr369Nt_vect) amino termini amplicons. PlasmoDB sequences are PfCtr211Nt_plas and PfCtr369Nt_plas, respectively. Sequences were aligned using the ClustalW program (http://www.ebi.ac.uk/Tools/msa/clustalw2/).

4.2.2 Immunolocalisation of the murine and human malaria parasite putative copper transporters

Detection of the native parasite copper transport protein employed antibodies generated against peptides designed in Section 3.2.8 (Figure 3.10).

4.2.2.1 Anti-peptide antibody production

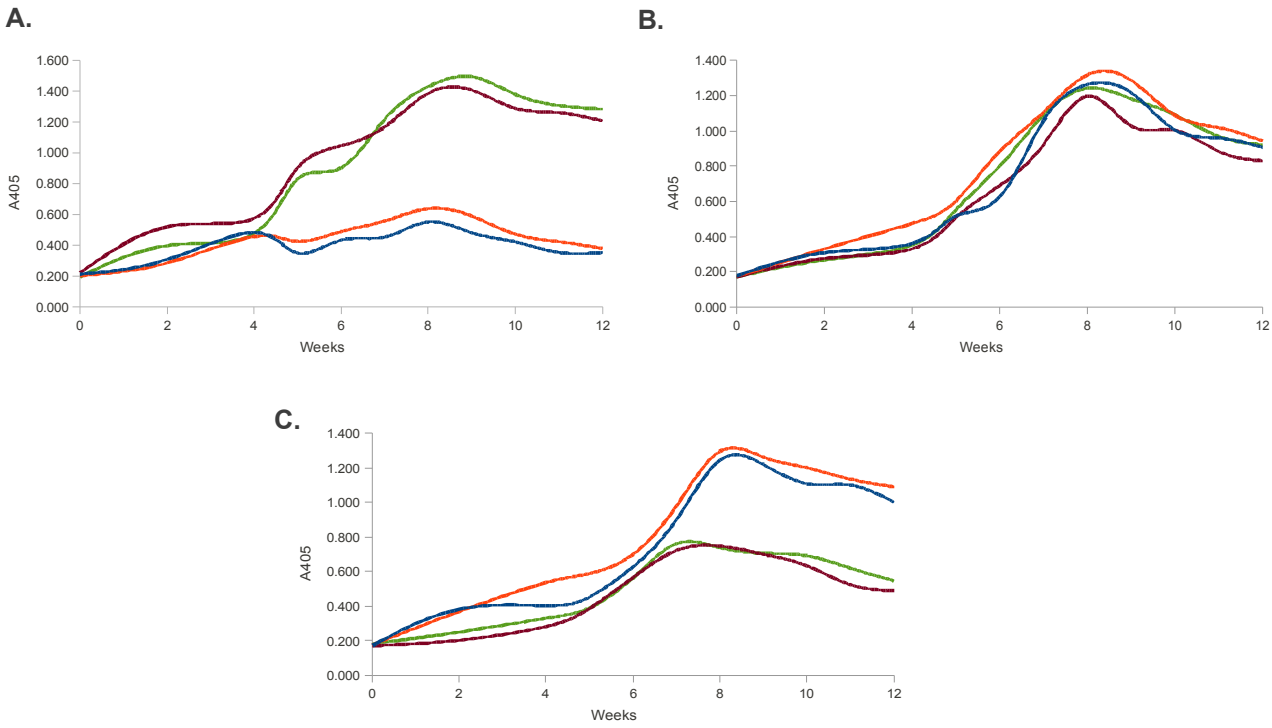

Figure 4.5 Anti-peptide antibody responses against the CSD, PMY and LQD peptides over 12 weeks

Anti-peptide antibody production against the CSD (**A**), PMY (**B**), and LQD (**C**) peptides was monitored by ELISA over a 12 week period. In all panels peptide-specific antibody production is shown for for chicken 1 (—) and chicken 2 (—). Also shown is the antibody production against the rabbit albumin carrier for chicken 1 (—) and chicken 2 (—).

Antibody titres against each peptide were monitored by ELISA over a 12-week period. For both the CSD (Figure 4.5a) and LQD (Figure 4.5c) peptide conjugates, one chicken was found to produce a poor antibody response. For the PMY peptide conjugate both immunised chickens appeared to produce similar and relatively strong antibody responses (Figure 4.5b). For all three peptides, the antibody response was detectable around week four, peaking at week eight and tailing off by the end of week twelve (Figure 4.5). Anti-peptide antibody titres followed a similar pattern to the antibody titres against the rabbit albumin carrier protein. Following antibody production the chicken antibodies were isolated from egg yolks, pooled and affinity purified on a peptide-specific matrix. Bound antibodies were eluted from the matrix (Figure 4.6) and pooled for each respective peptide. Antibodies generated against the putative *P. yoelii*

copper transporter peptide (CSD) were also expected to recognise the corresponding *P. berghei* protein, since only three of the 16 amino acids in this peptide are not conserved between species. The final yield for the copper transporter antibodies was 3.78 mg for anti-CSD, 12.1 mg for anti-PMY and 13.4 mg for anti-LQD antibodies.

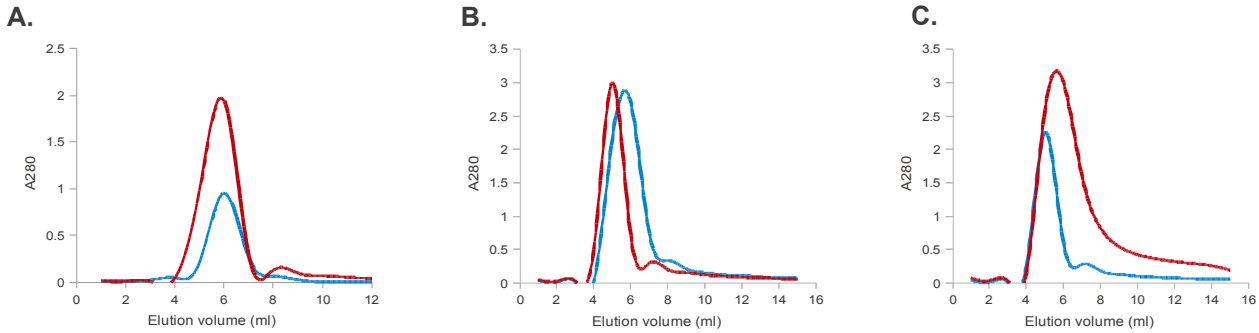

Figure 4.6 Affinity purification profiles for anti-CSD, -PMY, and -LQD antibodies

Representative purification profiles of antibodies raised against the CSD (**A**), PMY (**B**) and LQD (**C**) peptides are shown above. Shown in all panels are the purification profiles for antibodies purified from eggs collected 4 to 8 weeks post-inoculation of chicken 1 (—) and chicken 2 (—).

4.2.2.2 Detection and localisation of the malaria parasite copper transporters

The amplification of putative murine malaria parasite copper transporter coding domains (Figure 4.1), in particular the RT-PCR amplification and sequencing of a portion of the *P. berghei* coding domain, supports the idea of native expression of a malaria copper transport protein. It is, however, important to confirm expression through detection of the native protein. As mentioned, this was to be achieved using anti-peptide antibodies produced for this study (Section 4.2.2.1). Infected red blood cell lysate was prepared and separated into soluble and insoluble fractions (Section 2.5.2), separated on a 10% SDS-polyacrylamide gel and transferred to a nitrocellulose membrane (Figure 4.7). As a control, a pan-specific anti-peptide antibody against parasite LDH was used to probe the soluble, “cytoplasmic” fraction. The anti-LDH antibody detected a band in the soluble fraction at approximately 35 kDa, which corresponded with its predicted size and location (Figure 4.7b). For detection of a putative murine malaria parasite copper transporter, a blot of *P. yoelii* lysate was probed with anti-CSD antibodies generated against a peptide in the protein's amino terminus. A prominent protein band was detected at approximately 32 kDa (Figure 4.7c), corresponding well with the predicted size of the putative transporter. In contrast to LDH, the band corresponding to a putative copper transporter was only present in the insoluble fraction. This suggests a membrane association for the transport protein. Importantly neither protein was detected in the uninfected mouse red blood cell lysate.

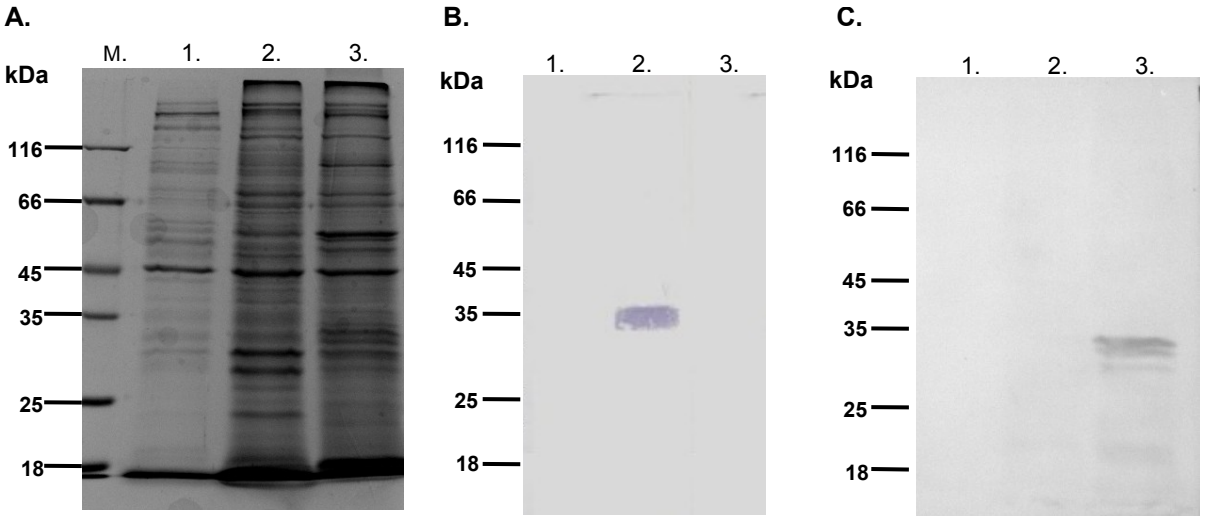

Figure 4.7 Anti-peptide antibody detection of lactate dehydrogenase and the putative copper transport protein in *P. yoelii* infected mouse red blood cell lysate.

P. yoelii infected BALB/c mouse red blood cell lysate was separated into soluble (lane 2) and insoluble (lane 3) fractions and analysed with uninfected lysate (lane 1) by 10% SDS-PAGE (**A**). Western blot of **A** probed with a pan-specific LDH anti-peptide antibody (**B**) or the copper transporter specific (CSD) anti-peptide antibody (**C**). Molecular mass markers (**M**) are indicated on the left of each image (see materials and methods for details).

To confirm native expression and verify localisation of this putative transporter, the anti-CSD anti-peptide antibodies were used for immunofluorescent microscopy studies (Figure 4.8). Murine malaria parasites were again used as the initial model organism, with the pan-specific anti-LDH antibodies providing a reference and internal control. For LDH, the green fluorescent signal appears to be localised to the parasite cytoplasm (Figure 4.8a) whereas the putative copper transporter signal appears to be associated with the periphery of the parasite (Figure 4.8b). The stage of parasite development captured for LDH appears to be representative of the trophozoite stage of parasite development (Bannister *et al.*, 2000). Expression of LDH at this stage is predicted to be relatively abundant (Figure 3.8a) and the strong fluorescent signal obtained supports this. For the copper transport protein, the fluorescent signal was predominantly visible at the ring and trophozoite stages of parasite development. This clear difference in the signals obtained for LDH and the transporter, suggests different sites of protein localisation. Localisation of the putative copper transporter's fluorescent signal to the periphery of the parasite suggests a probable association with a parasite membrane. Such an association could be predicted since three putative transmembrane domains were identified in the protein's amino acid sequence (Figure 3.3). However, the location of the putative copper transporter could not be confirmed since another antibody, specific to a well characterised membrane-bound transport protein, was not available. The blue fluorescent signal, visible in all panels of figure 4.8, is a result of DAPI staining of parasite genomic DNA. Control experiments using non-immune antibodies produced no detectable fluorescent signal (data not shown).

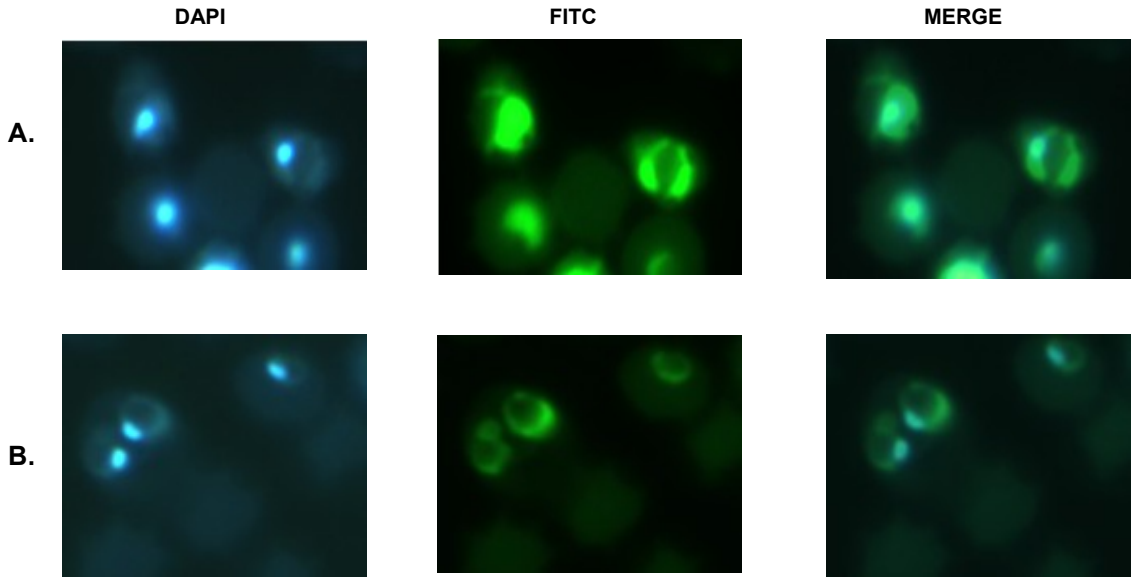

Figure 4.8 Anti-peptide antibody localisation of lactate dehydrogenase and the putative copper transport protein in *P. yoelii* infected mouse blood by immunofluorescent microscopy

A Localisation of lactate dehydrogenase (LDH) and **B** the putative copper transport protein in *P. yoelii* infected mouse red blood cells. LDH was detected with pan-specific anti-peptide antibodies and the copper transporter with anti-CSD anti-peptide antibodies. Primary antibodies were detected with a donkey anti-chicken IgY antibody conjugated to fluorescein isothiocyanate (FITC). Nuclear material was stained with 4,6-diamidino-2-phenylindole (DAPI).

Since the rodent-infecting *Plasmodium* species serve as useful research models (Carlton *et al.*, 2002; Hall *et al.*, 2005; van Lin *et al.*, 2001), detection and localisation of a putative copper transporter within the *P. yoelii* parasite infers the expression of the *P. falciparum* ortholog. Anti-peptide antibodies raised against the two *P. falciparum* copper transporters (Section 4.2.2.1) were therefore used in blotting and immunofluorescent microscopy studies to confirm protein expression and location. However, attempts to detect the native *P. falciparum* copper transporters by western blot proved unsuccessful *(P. falciparum* D10 frozen parasite culture was obtained from Professor P.J. Smith, Division of Clinical Pharmacology, University of Cape Town, South Africa). Even when the more sensitive enhanced chemiluminescence (ECL) assay was employed, a positive signal was not attainable. Similarly, detection of the native proteins by immunfluorescence was not possible since a *P. falciparum* culture has not established in the research facilities used for this study.

4.2.3 Recombinant expression of the putative *P. berghei* and *P. falciparum* copper transport protein amino terminal domains

The approach adopted in this study was to recombinantly express the amino terminal domain of the putative *Plasmodium* copper transport protein for use in copper binding experiments. This domain was selected since it is essential for extracellular copper acquisition and uptake (De

Feo *et al.*, 2009; Larson *et al.*, 2010), particularly under copper-limiting conditions (Eisses and Kaplan, 2002; Puig *et al.*, 2002a). A similar approach was also adopted for the characterisation of human and *P. falciparum* proteins predicted to function in the efflux of excess intracellular copper (Lutsenko *et al.*, 1997; Ralle *et al.*, 2004; Rasoloson *et al.*, 2004). These studies demonstrated the ability of a recombinant amino terminus to bind copper, thereby supporting the protein's predicted function. The steps involved in the preparation of the expression vectors used in this study are summarised in Figure 4.9.

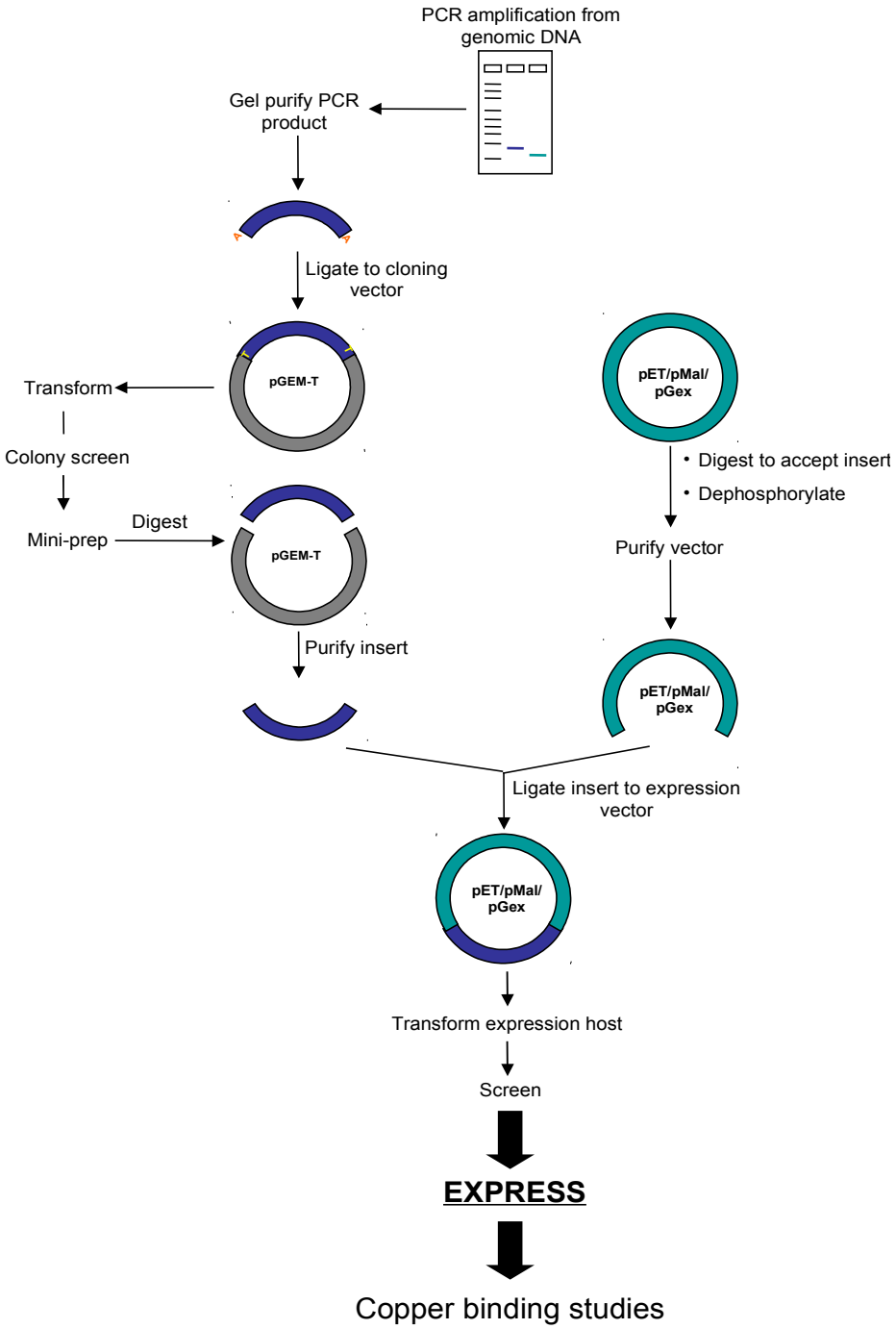

Figure 4.9 Cloning and sub-cloning strategies for the recombinant expression of *Plasmodium* spp. proteins

For the recombinant expression of the putative *P. berghei* copper transport protein's amino terminus (*Pb*CtrNt), a 447bp product was amplified by RT-PCR (Figure 4.1d), gel purified and ligated into the pGEM®-T cloning vector (Figure 4.9). Following transformation into *E. coli* JM109 cells, positive colonies were identified by blue:white colony screening and confirmed by colony PCR. Positive colonies were grown in Luria-Bertani (LB) broth, the plasmid isolated and the insert excised by restriction digestion with either *Eco*RI and *Not*I (pET23a/pGex-4T-1) or *Eco*RI and *Pst*I (pMal-c2/-p2). The excised fragment was gel purified and ligated into an expression vector digested with the appropriate restriction enzymes. Initial attempts at recombinant expression of *Pb*CtrNt made use of the pET23a vector transformed into *Escherichia coli* BL21(DE3)pLysS cells. Successful recombinant protein expression was confirmed from an analysis of the fractionated cell lysate on a SDS-polyacrylamide gel and western blot (Table 4.1). Although expression was successful, the expressed product was found in bacterial inclusion bodies. This result indicates protein misfolding and therefore required that the recombinant protein be refolded *in vitro* to obtain a soluble product. Refolding is, however, considered relatively undesirable due to poor recovery, the necessity for extensive optimisation of refolding conditions and the possibility that the resolubilisation procedure may affect the integrity of the refolded protein (Sørensen and Mortensen, 2005b). Consequently, recombinant expression using the soluble glutathione S-transferase (GST) and maltose binding protein (MBP) fusion partners was a more desirable option.

Table 4.1 Recombinant expression of the amino terminal domain of the putative *P. berghei* copper transport protein yielded predominantly insoluble products

Expression vector	*Escherichia coli* host cell	Recombinant protein			Western blot detection			
		Soluble	Insoluble	Periplasmic	α-CSD	α-His	α-GST	α-MBP
pET23a	BL21(DE3) pLysS	No	Yes	n/a	+	+	n/a	n/a
pGex-4T-1	BL21	No	Yes	n/a	+	n/a	+	n/a
pMal-c2	JM103/BL21	Yes	Partial	n/a	+	n/a	n/a	+
pMal-p2	JM103	Yes	Partial	No	+	n/a	n/a	+

Although the pMal-c2 and pMal-p2 *Pb*CtrNt MBP-fusions were predominantly produced as soluble products (Table 4.1 and Figure 4.10), fusion of *Pb*CtrNt to GST was still produced as an insoluble product (Table 4.1). However, expression of the pMal-p2 construct produced an unexpected result. Expression of a fusion protein using the pMal-p2 vector is expected to result in protein targeting to the cell periplasm (NEB pMal Manual). In this instance, however, the expressed protein (MBP-*Pb*CtrNt) was retained in the cell cytoplasm (Table 4.1). For this reason, the pMal-c2 expressed protein was selected for further analysis. Small-scale experiments indicated that a 61kDa MBP-*Pb*CtrNt product was purified and was recognised by

both the anti-CSD and anti-MBP antibodies (Figure 4.10). Although designed against the *P. yoelii* protein, the anti-CSD anti-peptide antibodies were expected to recognise the *P. berghei* homolog since there is only a difference of three amino acids between the respective peptides. The estimated size of the expression construct was also found to correspond well with the construct's predicted size of 60kDa. However, there was a significant amount of protein degradation as highlighted by the presence of protein bands that appear to be less than 61kDa in size (Figure 4.10b). The addition of a range of protease inhibitors, in the process of protein isolation, did not impact on the amount of protein degradation detected. This suggested that either truncated products were synthesised or that the transcribed product was degraded within the *E. coli* cell cytoplasm, prior to purification.

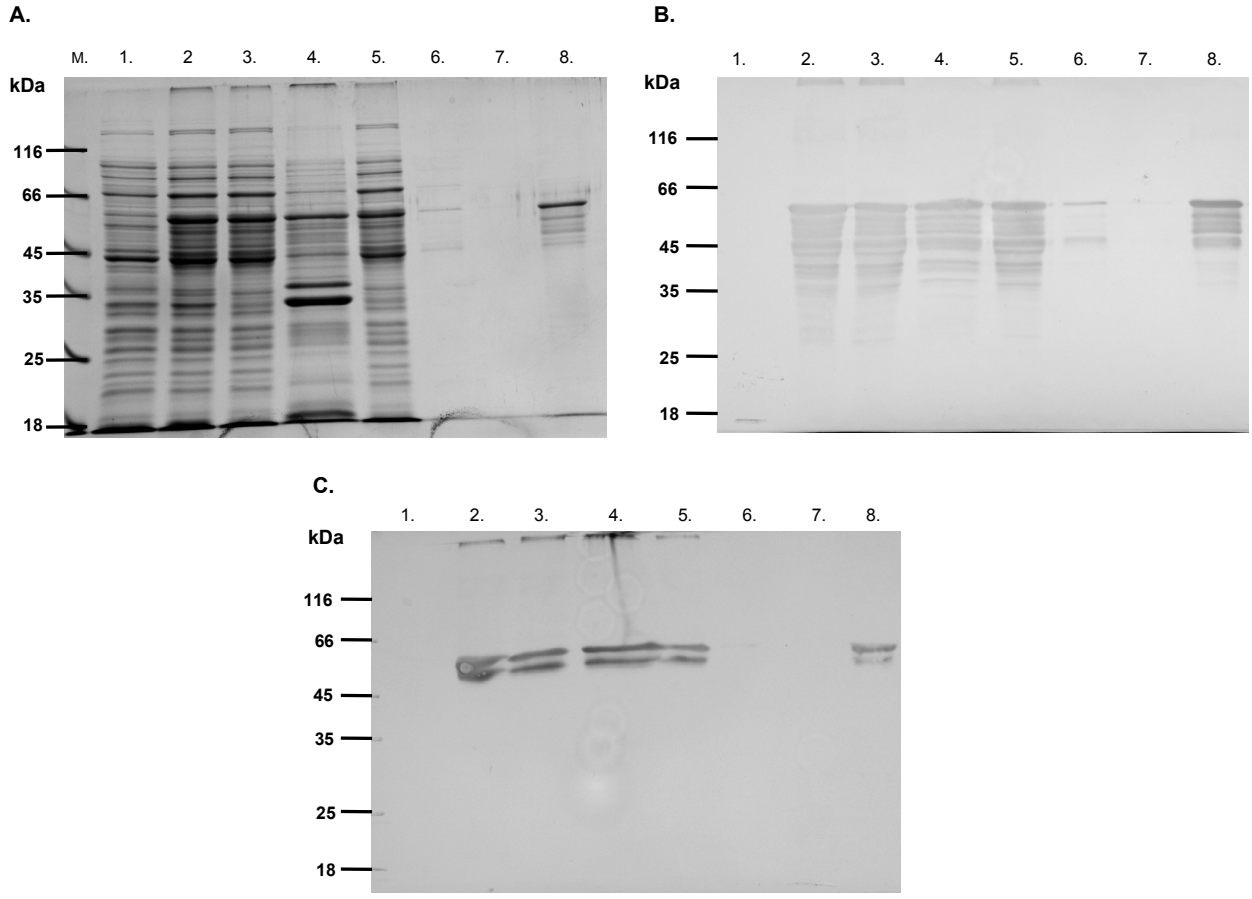

Figure 4.10 Recombinant expression of the putative *P. berghei* copper transport protein's amino terminus fused to the maltose binding protein (MBP-*Pb*CtrNt)

Small-scale expression and purification of MBP-*Pb*CtrNt, analysed by 10% SDS-PAGE (**A**). Recombinant MBP-*Pb*CtrNt was probed with anti-MBP (**B**) and anti-CSD (**C**) antibodies. In all three panels: lane 1, uninduced *E. coli*; lane 2, IPTG induced total cell protein; lane 3, soluble fraction; lane 4, insoluble fraction. Lanes 5 to 8 are fractions from amylose affinity chromatography: lane 5, unbound amylose resin eluate; lane 6 and 7, wash steps; lane 8 amylose-bound MBP-*Pb*CtrNt. Molecular mass markers (**M**) are indicated on the left of each image (see materials and methods for details).

In an effort to reduce possible protein degradation, the *E. coli* BL21 strain was used as the host cell. As with the addition of protease inhibitors, this made no noticeable improvement to the

expression of MBP-*Pb*CtrNt (Figure 4.11). This was particularly evident from a comparison of the anti-MBP blots of MBP-*Pb*CtrNt expressed in *E. coli* JM103 and BL21 cells (Figure 4.11). Interestingly, MBP-*Pb*CtrNt expressed and purified from both JM103 and BL21 cells also produced a high molecular weight product having a size that appears to be greater than 116kDa (Figure 4.11). As with the 61kDa MBP-*Pb*CtrNt product, the high molecular weight species was recognised by both anti-MBP (Figure 4.11b/d) and anti-CSD antibodies (data not shown). Therefore, in an attempt to eliminate the degraded products and high molecular weight aggregates, of MBP-*Pb*CtrNt, a number of variables affecting expression and purification were tested for their effect on the purity of the recombinant protein (Table 4.2).

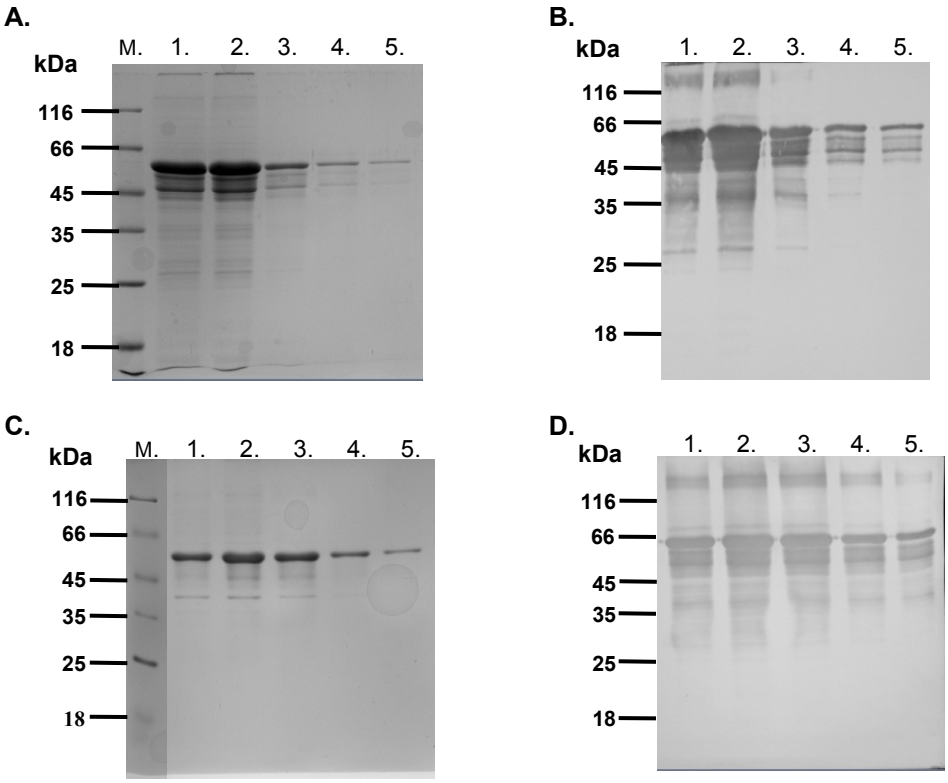

Figure 4.11 Expression of recombinant MBP-*Pb*CtrNt in *Escherichia coli* JM103 and protease deficient BL21 cells

MBP-*Pb*CtrNt expressed and purified from *E. coli* JM103 cells was analysed by 10% SDS-PAGE (**A**) and western blotting with anti-MBP antibodies (**B**). Similarly, MBP-*Pb*CtrNt expressed and purified from protease deficient *E. coli* BL21 cells was analysed by 10% SDS-PAGE (**C**) and western blotting with anti-MBP antibodies (**D**). In all panels, lanes 1 to 5 represent five amylose purified samples. Molecular mass markers (**M**) are indicated on the left of each image (see materials and methods for details).

A variety of culture conditions can affect proteolytic activity and protein expression (Makrides, 1996). To test these variables, *E. coli* BL21 host cells transformed with the pMc-*Pb*CtrNt construct were used and three different growth media tested. These were M9 minimal medium, Luria-Bertani broth and 2xYT broth. Each of these media contain different concentrations of defined carbon and nitrogen sources, with the M9 minimal medium being the most simple.

However, these media made no observable improvement or alteration to the expression of MBP-*Pb*CtrNt (Table 4.2). Following pMal-2 manual recommendations, LB broth was selected for subsequent analyses. Another important factor affecting recombinant protein expression is cultivation temperature. Expression of MBP-*Pb*CtrNt was therefore tested at 15°C, 22°C (room temperature) and 30°C following initial tests at 37°C. Changes to the cultivation temperature were, however, found to make no noticeable improvement to the quality of the amylose purified samples, regardless of the temperature employed (Table 4.2). A further factor that affects expression is the host cell density at which expression is induced. Changes to this variable were therefore tested.

Table 4.2 Culture conditions tested for the expression and purification of MBP-*Pb*CtrNt

Condition altered			Purified MBP-*Pb*CtrNt analysis			Result
			10% SDS-PAGE	α-CSD	α-MBP	
Expression	Expression medium	LB	✔	✔	✔	**NONE** of the tested conditions were found to improve the observed banding pattern of purified MBP-*Pb*CtrNt▲
		2xYT	✔	n/d	✔	
		M9 Minimal Medium	✔	n/d	✔	
	Temperature	15°C*	✔	n/d	✔	
		22°C	✔	n/d	✔	
		30°C*	✔	✔	✔	
	OD_{600}	~0.6	✔	n/d	✔	
		≥ 2.0*	✔	✔	✔	
Purification	Buffer species	Acetate├	✔	n/d	✔	
		Phosphate♦┼	✔	✔	✔	
		Tris┼	✔	✔	✔	
	Buffer additives	1-50 mM DTT#	✔	n/d	✔	
		0.1% Triton X-100#	✔	n/d	✔	
		8 M Urea▲	✔	✔	n/d	
	Buffer pH	4├	✔	✔	✔	
		5.8♦	✔	✔	✔	
		7.4♦┼	✔	✔	✔	
		8♦┼	✔	✔	✔	

✔ indicates that the method listed in the corresponding column was used to analyse the MBP-*Pb*CtrNt samples
*Induction of MBP-*Pb*CtrNt expression post-log growth phase ($O.D._{600}$ ≥ 2.0) was examined at both 15°C and 30°C.
├, ♦ and ┼ indicate the corresponding pH at which the buffer species were used.
#DTT and Triton X-100 were tested separately as well as in combination with each other.
▲The chaotropic agent urea was the only additive affecting the MBP-*Pb*CtrNt multimers.

Initiation of recombinant protein expression post-log growth phase (OD_{600}≥ 2.0) has been found to produce increased amounts of soluble, high quality protein (Flick *et al.*, 2004). The effect of

initiating MBP-*Pb*CtrNt expression post-log phase was therefore tested for cells grown at both 15°C and 30°C (Table 4.2). Initial experiments made use of the more standard growth temperature of 30°C combined with the initiation of expression at OD_{600}≥ 2.0 instead of 0.6. Western blot analysis of the amylose purified protein established this alteration again made no clear improvement to the quality of the final product. Therefore in an attempt to establish whether expression of MBP-*Pb*CtrNt could be improved by significantly decelerating cell growth, expression in host cells was induced at a temperature of 15°C when the OD_{600} was ≥ 2.0. Unfortunately, this approach made no discernible difference compared to the experiment carried out at 30°C. Taken together, these results suggest that alterations to the cell culture conditions, affecting MBP-*Pb*CtrNt expression, make no improvements to the amylose purified product.

To determine the effect the buffering species could have on protein purification, phosphate, Tris and acetate buffers were tested. The phosphate buffer was tested at pH 5.8, 7.4 and 8 whilst the Tris buffer was tested at pH 7.4 and 8, due to its pKa. The acetate buffer was used to test the lowest pH value of 4 (Table 4.2). Tris and phosphate buffers are common lysis buffer components generally used between pH 7 and 8, hence their selection. Use of a pH 5.8 phosphate buffer and pH 4 acetate buffer was based on the finding that the human copper transport protein shows increased rates of copper uptake under low extracellular pH conditions (Lee *et al.*, 2002). Additionally a MBP-fusion with the amino-terminal domain of a *Cryptosporidium parvum* ATPase was successfully purified at pH 6 (LaGier *et al.*, 2001). Hence the effects a similar pH might have on purification of the recombinant amino terminus of the *P. berghei* copper transport protein were examined. However, none of these three buffers were found to improve the quality of purified MBP-*Pb*CtrNt. Following pMal-2 manual recommendations, the Tris buffer was chosen as the standard buffer for further experiments.

A second concern with the final product, was the presence of high molecular weight multimers (Figure 4.11). Reducing agents, such as dithiothreitol (DTT), are often included in lysis buffers to prevent protein oxidation and thus prevent the formation of recombinant protein aggregates and multimers upon cell lysis (Gräslund *et al.*, 2008). To test whether reducing agents could disrupt MBP-*Pb*CtrNt multimers, DTT, ranging in concentration from 1 to 50 mM, was included in the Tris buffer (Table 4.2). However, even at concentrations as high as 50 mM, DTT did not disrupt MBP-*Pb*CtrNt multimers. For this reason, Triton X-100 was also tested in the lysis buffer since it can assist with recombinant protein solubilisation and reduces non-specific binding to the affinity resin (The *QIAexpressionist*, 2001). A concentration limit of 0.2% was selected for Triton X-100 and was tested alone as well as in combination with 1 mM DTT. Neither of the conditions examined were found to make an observable difference.

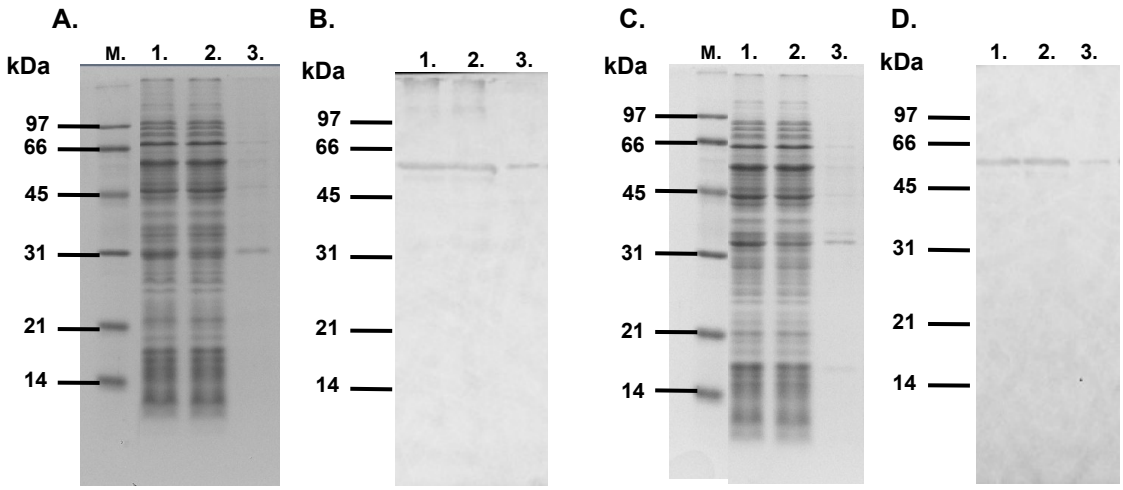

Figure 4.12 Disruption of MBP-*Pb*CtrNt aggregates under reducing conditions following urea solubilisation

MBP-*Pb*CtrNt cell lysates were analysed on 12.5% SDS-PAGE gels under non-reducing (**A**) and reducing conditions (**C**). Samples were blotted and probed with anti-CSD antibodies for non-reducing (**B**) and reducing conditions (**D**). In all panels lane 1 represents total cell protein, lane 2 the soluble fraction and lane 3 the insoluble fraction. Molecular mass markers (**M**) are indicated on the left of each image (see materials and methods for details).

The formation of recombinant protein aggregates and multimers has previously been observed for other MBP-fusion proteins. When fused to MBP, the human papillomavirus E6 oncoprotein (MBP+E6) was produced as a soluble, but misfolded protein aggregate that could only be solubilised by 6 M guanidinium chloride or 9 M urea (Nominé *et al.*, 2001b). To test whether similar conditions could help with MBP-*Pb*CtrNt purification, the cell lysate was prepared in the presence of 8 M urea (Table 4.2), following expression, and the resulting cellular fractions analysed on a SDS-PAGE gel under both non-reducing and reducing conditions and blotted onto nitrocellulose (Figure 4.12). Blots of the samples examined under reducing conditions, indicated that the addition of urea disrupts the high molecular weight protein aggregates (Figure 4.12d). Under non-reducing conditions these aggregates were not disrupted (Figure 4.12b), suggesting that disulfide bonds were involved in aggregate formation. This is likely since the amino terminal domain of the putative *P. berghei* copper transport protein is predicted to contain eight cysteine residues (Figure 4.13a).

A.

M N I W K I I Y I V L I I N S L F V V N V N C E S N
D Q N D G T T S N K K N T G C C G G T N K P L P S V
N K P L K S C C S D K Q S G D D E C K P I L D L N H
I G S K G K N K I P F I Y K C C I N H D I Y E S I I
N E H F S E E N Q S N T T G G P E K L N *M* *M* *M* G N L
S *M* *P* *M* S F Q N T T H T I I L F K F W E

B.

F T F D F V S S S C C H S K N D D G V *M* *L* *P* *M* Y F S
N N E N I K M L F D I F Q V K N R Y

C.

D K S D N S I C K P S V K I S C A H N C C K N K L S
F M Y N C W K H Y D K Y S N I I K D N L Q K E E D T
V V Q L Q D H D N I D I V E H V E T *M* *P* *M* S F Q L T
T H T I I L F N K W E T K S A L

Figure 4.13 Highlighted cysteine residues in *Pb*CtrNt, *Pf*Ctr211Nt^{TD} and *Pf*Ctr369Nt^{TD}

Cysteine residues are underlined and highlighted in the recombinant amino terminal domain for the putative *P. berghei* copper transporter (**A**) and the two truncated amino terminal domains of the putative *P. falciparum* copper transporters, PF14_0211 (**B**) and PF14_0369 (**C**).

The MBP-*Pb*CtrNt multimers, predominantly evident in blots of purified protein (Figure 4.11), appears to be a result of protein aggregate formation. To test whether the multiple MBP-*Pb*CtrNt related products could be separated, an amylose purified sample was fractionated by molecular exclusion chromatography (MEC) on both Sephacryl^{TM} S-100 and S-300 resins (Figure 4.14). Both MEC experiments showed identical results, with MBP-*Pb*CtrNt eluting in a single peak corresponding with the void volume of the resin (Figure 4.14b). Analysis of the eluted sample, by both SDS-PAGE and western blot, confirmed that the multiple protein species present in the purified MBP-*Pb*CtrNt sample had not been fractionated (Figure 4.14). Similar to previous results (Table 4.2), the addition of 1 mM DTT or 0.2% Triton X-100 had no effect (data not shown). From the Sephacryl^{TM} S-300 chromatogram, the protein aggregate appears to be greater than 1.5 x 10^6 Da suggesting that the MBP-*Pb*CtrNt aggregate consists of a minimum of 25 protein monomers. Taking the problems encountered with the recombinant expression of MBP-*Pb*CtrNt into consideration, the truncated amino terminal domains of two putative *P. falciparum* copper transport proteins were prepared for recombinant expression.

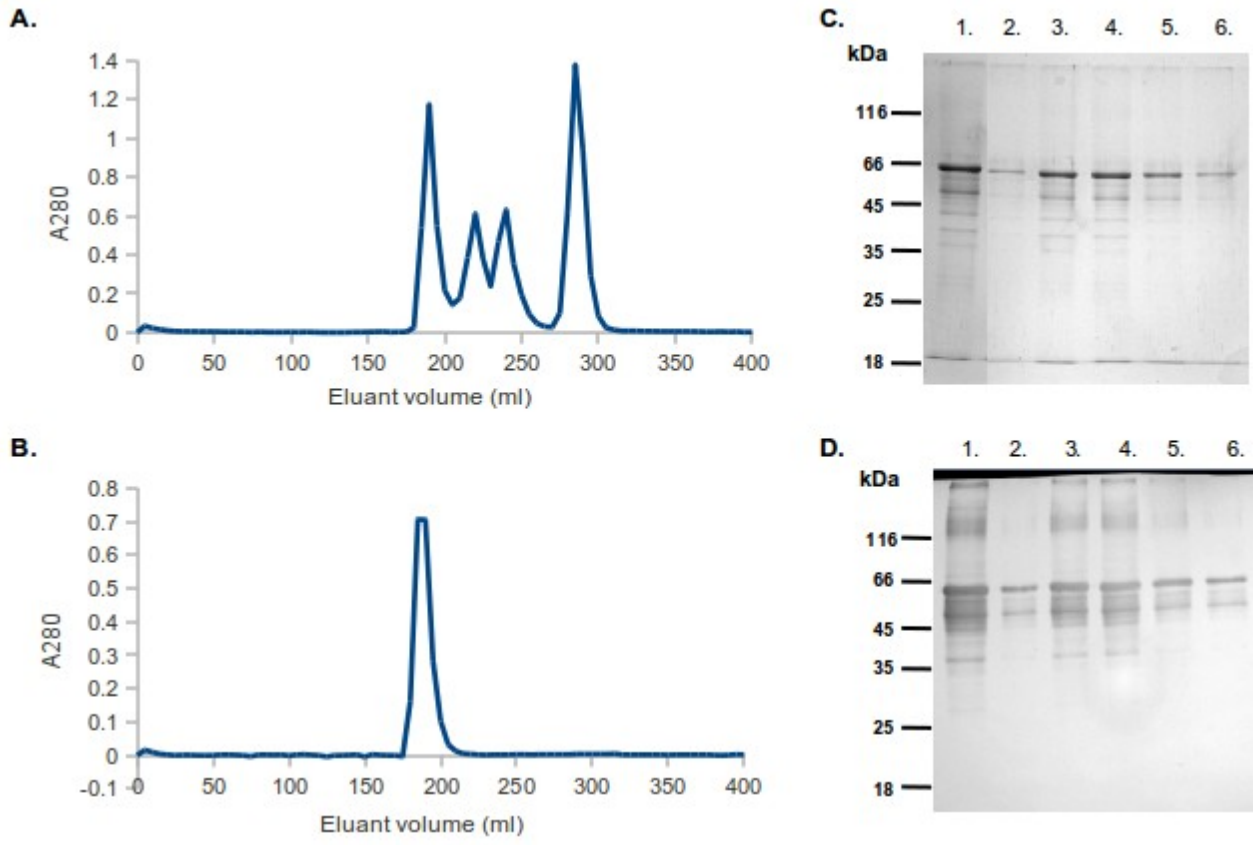

Figure 4.14 Fractionation of MBP-*Pb*CtrNt aggregates by molecular exclusion on a Sephacryl™ S-100* resin

A Resin calibration using blue dextran (peak 1; 2 x 10^6 Da), bovine serum albumin (peak 2; 66000 Da), ovalbumin (peak 3; 45000 Da) and myoglobin (peak 4; 17000 Da). **B** Elution profile for MBP-*Pb*CtrNt. **C** MBP-*Pb*CtrNt fractions analysed by 10% SDS-PAGE, transferred to nitrocellulose and probed with anti-MBP antibodies (**D**). For gel and blot analysis, lane 1 contained the amylose purified starting sample, whilst lanes 2 – 6 contained the eluted fractions containing protein (180 to 200 ml eluant). Shown to the left of the gel and blot images are the molecular mass markers (see materials and methods for details). *Fractionation of amylose purified MBP-*Pb*CtrNt on a Sephacryl™ S-300 resin produced the same result.

The coding sequences, used for expression of the *P. falciparum* proteins, were PCR amplified with the exclusion of predicted signal sequences found within the first 60 nucleotides. A similar approach to that taken for the expression of the putative *P. berghei* copper transport protein's amino terminus was adopted (Figure 4.9). The PCR amplicons corresponding to the coding domains of the truncated (TD) amino terminus of PF14_0211 and PF14_0369 (Figure 4.3) were gel purified and ligated into the pGEM®-T cloning vector (Figure 4.9). The constructs were transformed into a cloning cell, positive colonies identified and cultivated, plasmids isolated and the insert excised by *Eco*RI and *Pst*I digestion (Figure 4.9). For the recombinant expression of the *P. falciparum* proteins the pMal-2 expression system was again used. Both pMal-c2 and pMal-p2 constructs were prepared and transformed into JM103 host cells for expression of the truncated PF14_0211 and PF14_0369 amino terminal domains.

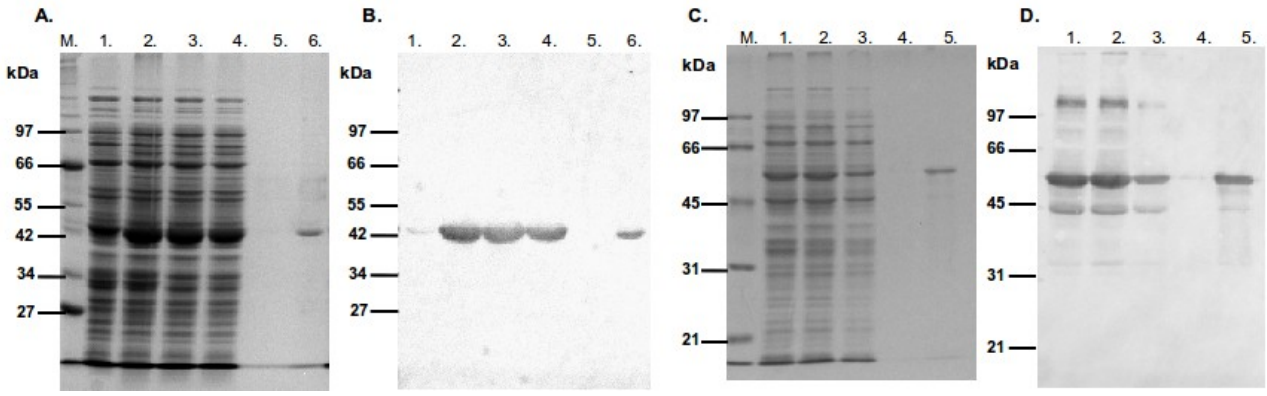

Figure 4.15 Recombinant expression and purification of the amino terminal domain of two putative *P. falciparum* copper transport proteins fused to maltose binding protein

The amino terminal domains of PF14_0211 (**A** and **B**) and PF14_0369 (**C** and **D**) were expressed as recombinant MBP fusion proteins from the pMal-c2X vector and analysed by 10% SDS-PAGE (**A** and **C**)**.** Samples were blotted to nitrocellulose and probed with anti-MBP antibodies (**B** and **D**). In panels A and B: lane 1, uninduced total cell protein; lane 2, total cell protein; lane 3, soluble fraction; lane 4, unbound protein eluate; lane 5, the wash fraction; lane 6, amylose bound protein. In panels C and D: lane 1, total cell protein; lane 2, soluble fraction; lane 3, unbound protein eluate; lane 4, the wash fraction; lane 5, amylose bound protein. Molecular mass markers (**M**) are indicated on the left of each image (see materials and methods for details).

Following induction of both PF14_0211 (MBP-*Pf*Ctr211Nt^{TD}) and PF14_0369 (MBP-*Pf*Ctr369Nt^{TD}) expression, the bacterial cell lysates were analysed by SDS-PAGE and western blot (Figure 4.15). Positive expression of both constructs was evident from SDS-PAGE analysis of a small-scale purification, with a 46kDa product purified for MBP-*Pf*Ctr211Nt^{TD} (Figure 4.15b) and a 55kDa product purified for MBP-*Pf*Ctr369Nt^{TD} (Figure 4.15d). These sizes corresponded well with the predicted sizes of 48kDa for MBP-*Pf*Ctr211Nt^{TD} and 54kDa for MBP-*Pf*Ctr369Nt^{TD}. The additional 42kDa product present in the purified MBP-*Pf*Ctr369Nt^{TD} fraction (Figure 4.15d and 4.16d) is likely to be MBP lacking the fused protein. This could have been caused by fusion protein degradation, leaving a stable MBP-sized breakdown product (pMal manual). An anti-MBP blot of the relevant samples also indicated the presence of high molecular weight aggregates (Figure 4.15), similar to those observed for MBP-*Pb*CtrNt (Figure 4.11). These were particularly evident for MBP-*Pf*Ctr369Nt^{TD} samples (Figure 4.15d). Although aggregation appears less prevalent in the images captured from the MBP-*Pf*Ctr211Nt^{TD} analysis (Figure 4.15b), faint bands, presumably representative of aggregates, were evident in the original blots. These results suggest that removal of the signal peptide alone did not reduce or inhibit aggregation of the recombinant proteins. A sequence property believed to have affected MBP-*Pb*CtrNt expression was the presence of eight cysteine residues (Figure 4.13a). Analysis of the truncated *P. falciparum* amino terminal sequences identified that PF14_0211 contained two cysteines (Figure 4.13b) whereas PF14_0369 contained five cysteines (Figure 4.13c). Since disulfide bond dependent folding of heterologous proteins can be actively catalysed in the *E. coli* cell periplasm (Baneyx, 1999), MBP-*Pf*Ctr211Nt^{TD} and MBP-*Pf*Ctr369Nt^{TD} expression was

targeted to this compartment using the *malE* leader sequence of pMal-p2X.

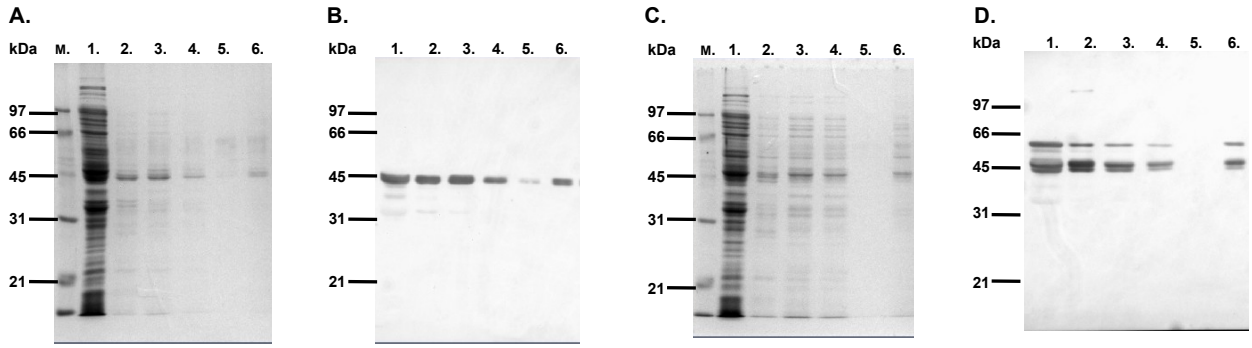

Figure 4.16 Recombinant expression and purification of the amino terminal domain of two *P. falciparum* copper transport proteins fused to maltose binding protein containing the *malE* leader sequence

Periplasmic expression and purification of MBP-*Pf*Ctr211Nt^{TD} (**A**) and MBP-*Pf*Ctr369Nt^{TD} (**C**) analysed by 10% SDS-PAGE. MBP-*Pf*Ctr211Nt^{TD} (**B**) and MBP-*Pf*Ctr369Nt^{TD} (**D**) samples were blotted to nitrocellulose and probed with anti-MBP antibodies. In all panels: lane 1, total cell protein; lane 2, supernatant following sucrose treatment; lane 3, periplasmic contents; lane 4, unbound amylose resin eluate; lane 5, wash fraction; lane 6, amylose bound protein. Molecular mass markers (**M**) are indicated on the left of each image (see materials and methods for details).

Following MBP-*Pf*Ctr211Nt^{TD} and MBP-*Pf*Ctr369Nt^{TD} periplasmic expression, the contents of the *E. coli* periplasm was isolated by osmotic shock and analysed. Western blot analysis confirmed the export of both recombinant proteins to the periplasm with an apparent absence of protein aggregation (Figure 4.16b and 4.16d). In addition, each sample indicated a reduction in recombinant protein degradation when expressed in the periplasm (Figure 4.16). Therefore, in contrast to the difficulties faced with cytoplasmic expression, targeting MBP-*Pf*Ctr211Nt^{TD} and MBP-*Pf*Ctr369Nt^{TD} expression to the cell periplasm appeared to reduce both recombinant protein aggregation and degradation. Furthermore, the successful periplasmic expression of MBP-*Pf*Ctr211Nt^{TD} and MBP-*Pf*Ctr369Nt^{TD}, compared to unsuccessful attempts for MBP-*Pb*CtrNt, suggested that amino terminal signal peptides of *Plasmodium* proteins can interfere with *E. coli* targeting of heterologous proteins to the periplasm. Importantly, these initial small-scale experiments confirmed that MBP-*Pf*Ctr211Nt^{TD} and MBP-*Pf*Ctr369Nt^{TD} could be purified from the osmotic shock fluid using amylose affinity chromatography. Both the MBP-*Pf*Ctr211Nt^{TD} and MBP-*Pf*Ctr369Nt^{TD} constructs were therefore prepared for large-scale expression and purification.

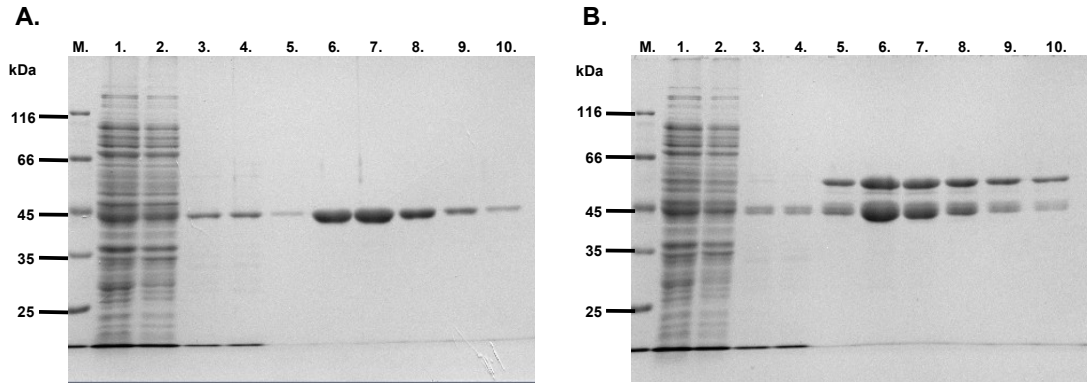

Figure 4.17 Amylose affinity purification of MBP-*Pf*Ctr211Nt^{TD} and MBP-*Pf*Ctr369Nt^{TD} from the periplasm of *E. coli* JM103 cells

Steps in the purification of MBP-*Pf*Ctr211Nt^{TD} (**A**) and MBP-*Pf*Ctr369Nt^{TD} (**B**) analysed by 10% SDS-PAGE. Lane 1, total cell suspended in Tris/sucrose buffer; lane 2, total cell protein diluted in distilled water; lane 3, the periplasmic fraction; lane 4, unbound amylose resin eluate; lanes 5 – 10, eluted fractions. Molecular mass markers (**M**) are indicated on the left of each image (see materials and methods for details).

Optimal conditions for MBP-*Pf*Ctr211Nt^{TD} expression were determined to be induction with 0.3 mM IPTG at 30°C, whilst MBP-*Pf*Ctr369Nt^{TD} expression was induced using the same concentration of IPTG but at room temperature. Both recombinant proteins were expressed overnight at the respective temperatures. The periplasmic contents of the host cells was subsequently released using a simple, two-step osmotic shock method described by French *et al.* (1996). Each protein was purified by amylose affinity chromatography with reduced protein degradation and no protein aggregates (Figure 4.17). Each recombinant protein was also recognised by the respective anti-peptide antibodies (Figure 4.18). The anti-peptide antibody blot for MBP-*Pf*Ctr369Nt^{TD} also supports the notion that the 42kDa band in the purified sample is likely to be representative of MBP which results from fusion protein degradation. Considering the predicted function of the *P. falciparum* proteins is the same as that for MBP-*Pb*CtrNt, each of these recombinant proteins was tested for copper binding *in vivo* and *in vitro*.

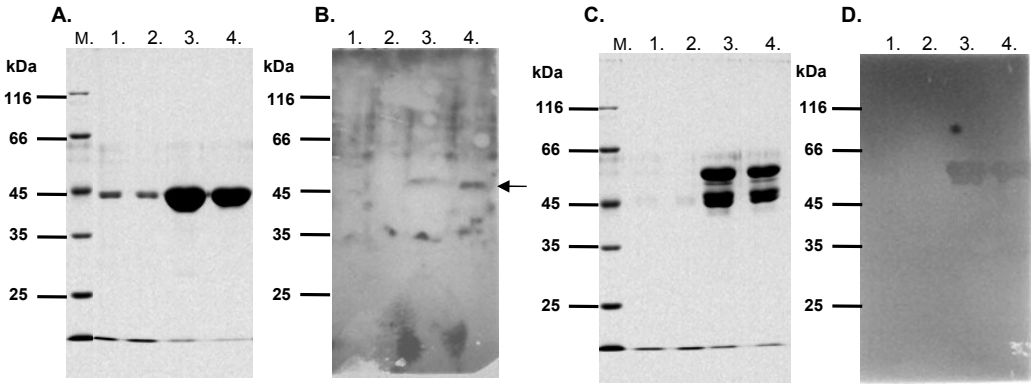

Figure 4.18 Anti-peptide antibody recognition of MBP-*Pf*Ctr211Nt^{TD} and MBP-*Pf*Ctr369Nt^{TD}

10% SDS-PAGE analysis of affinity purified MBP-*Pf*Ctr211Nt^{TD} (**A**) and MBP-*Pf*Ctr369Nt^{TD} (**C**) probed with anti-PMY (**B**) and anti-LQD (**D**) anti-peptide antibodies, respectively. In all panels: lane 1, periplasmic fraction; lane 2, unbound amylose resin eluate; lanes 3 and 4, amylose-affinity purified samples. Molecular mass markers (**M**) are indicated on the left of each image (see materials and methods for details).

4.2.4 Copper binding studies with MBP-*Pb*CtrNt, MBP-*Pf*Ctr211Nt^{TD} and MBP-*Pf*Ctr369Nt^{TD}

The MBP-*Pb*CtrNt aggregate was tested for its ability to bind copper *in vitro* using 10 µM purified recombinant protein incubated with a 20-fold molar excess of copper in the presence or absence of the reducing agent ascorbic acid. Ascorbic acid was added to determine whether the amino terminal domain of the *P. berghei* copper transporter preferentially bound the cuprous (Cu^{+}) or cupric (Cu^{2+}) ion. Following overnight dialysis, bound copper was detected using the copper-specific BCA release assay (Brenner and Harris, 1995). BCA is only capable of forming a detectable purple complex when bound to the cuprous ion, therefore ascorbic acid is included in the assay to ensure copper ion detection (Figure 4.19a) (Brenner and Harris, 1995). This property was utilised to help establish the copper-binding preference of MBP-*Pb*CtrNt. Following copper binding and overnight dialysis, the BCA release assay was conducted with or without a second treatment of ascorbic acid (Figure 4.19b). Thus if ascorbic acid was required for the formation of a purple BCA complex it suggests that Cu^{2+} is preferentially bound. Alternatively, if ascorbic acid supplementation was not required for colour formation then it suggests Cu^{+} is the preferred substrate. With this in mind copper binding to MBP-*Pb*CtrNt was analysed.

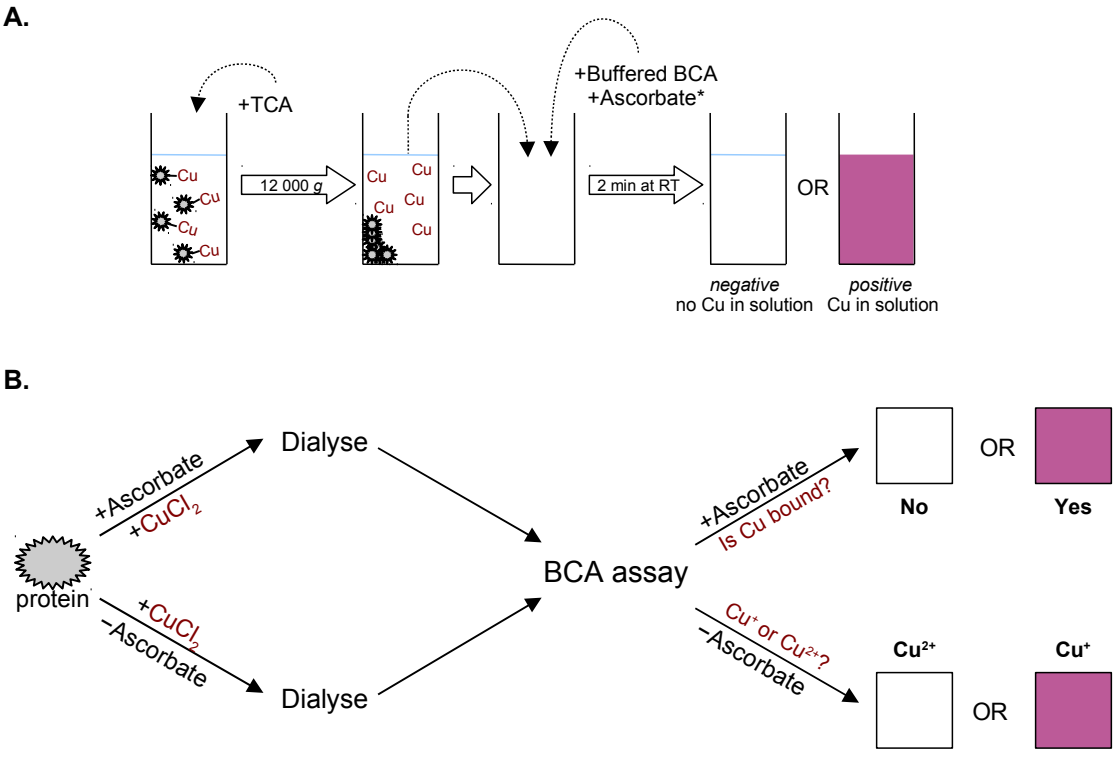

Figure 4.19 Recombinant protein copper binding studies using the BCA release assay for copper detection

A. Standard protocol for the BCA assay, used for the detection of copper in solution. **B**. *In vitro* copper binding to recombinant protein, in the presence or absence of ascorbic acid using a modified BCA assay to determine the oxidation state of protein-bound copper.

Results from the *in vitro* copper-binding experiments indicated that MBP-*Pb*CtrNt had a binding preference for Cu^+ since copper binding appeared to be dependent on the addition of ascorbic acid during incubation with free $CuCl_2$ (Figure 4.20a, **+**). This was supported by omitting ascorbic acid from the BCA release assay, which still resulted in the formation of the purple BCA-Cu^+ complex (Figure 4.20a, **+**, open bar). The exclusion of ascorbic acid from the initial $CuCl_2$ incubation step resulted in a 76% reduction in the amount of BCA-Cu^+ complex formed (Figure 4.20a, **–**), which was statistically significant according to Student's *t*-test (p-value <0.05). These *in vitro* studies were subsequently followed up with an *in vivo* copper binding study. Recombinant MBP-*Pb*CtrNt was expressed in the presence or absence of 0.5 mM $CuCl_2$, which is a concentration of copper salt that does not affect *E. coli* cell growth (Lutsenko *et al*., 1997). Following amylose purification, MBP-*Pb*CtrNt was analysed for binding of copper using the BCA release assay, as described above. As seen in figure 4.20b, copper binds MBP-*Pb*CtrNt *in vivo* with the detection of bound copper appearing dependent upon the addition of extracellular copper. Adding extracellular copper resulted in a statistically significant increase in the amount of copper bound to MBP-*Pb*CtrNt, as determined by Student's *t*-test (p-value <0.05). As with the *in vitro* analysis, the oxidation state of the bound copper was determined by either including (solid bars, Figure 4.20b) or excluding (open bars, Figure 4.20b) ascorbic acid from the BCA release assay. As with copper binding *in vitro*, the preferred oxidation state of *in vivo* bound copper appears to be Cu^+ (Figure 4.17). Importantly, in the control experiments for both *in vivo* and *in vitro* conditions, copper did not show significant levels of binding to the MBP carrier protein (Figure 4.20). These results suggest the amino terminal domain of the *P. berghei* copper transport protein binds copper. Although MBP-*Pb*CtrNt appears to be predominantly aggregated, it still appears to possess a native-like fold allowing for metal coordination.

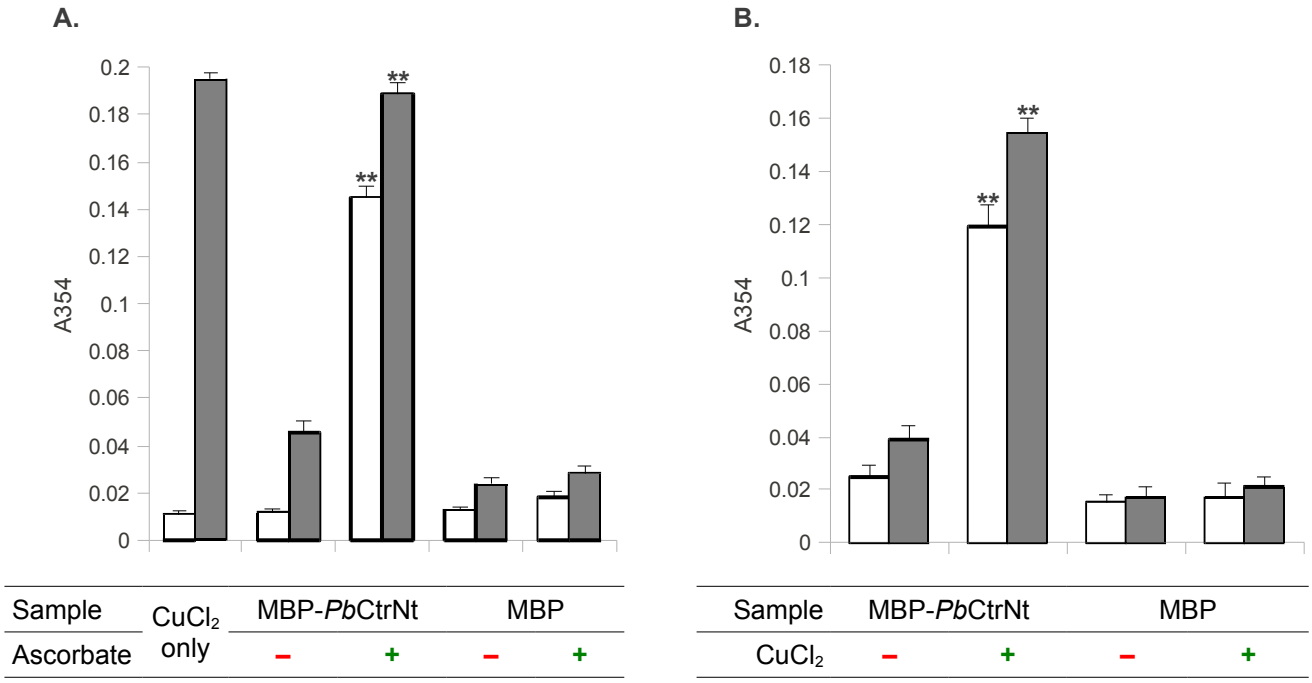

Figure 4.20 Copper binding to MBP-*Pb*CtrNt *in vitro* and *in vivo*

A 10 µM affinity-purified MBP-*Pb*CtrNt or MBP was incubated with $CuCl_2$ in the presence (+) or absence (–) of ascorbic acid *in vitro*. The BCA release assay was used to detect copper with (solid bars) or without (open bars) the addition of ascorbic acid. The BCA-Cu^+ complex was detected at 354 nm. The concentration of the copper standard ($CuCl_2$ only) was equimolar to the amount of protein used. **B** 0.5 mM $CuCl_2$ was added to the cell growth medium after the induction of recombinant protein expression. Following affinity purification, copper bound *in vivo* was detected by the BCA release assay with (solid bars) or without (open bars) the addition of ascorbic acid. As before the BCA-Cu^+ complex was detected at 354 nm. ** denotes statistical significance, as determined by Student's *t*-test (p-value <0.05). Results are means ± S.E. of triplicate measurements from each duplicate dialysis bag.

For *in vitro* copper binding studies with MBP-*Pf*Ctr211Nt^{TD} and MBP-*Pf*Ctr369Nt^{TD}, the conditions used were the same as those used for MBP-*Pb*CtrNt. Protein-bound copper was again detected using the copper-specific BCA release assay (Brenner and Harris, 1995), with or without a second treatment of ascorbic acid following copper binding and overnight dialysis (Figure 4.19b). The data indicated that both MBP-*Pf*Ctr211Nt^{TD} and MBP-*Pf*Ctr369Nt^{TD} bound copper *in vitro* with an apparent preference for Cu^+ (Figure 4.21a). The exclusion of ascorbic acid from the initial $CuCl_2$ incubation step resulted in relatively low levels of bound copper for both recombinant proteins (Figure 4.21a, –). On the other hand, the inclusion of ascorbic acid to the $CuCl_2$ incubation step resulted in an ~80% increase of copper levels bound to MBP-*Pf*Ctr211Nt^{TD} and ~70% increase for MBP-*Pf*Ctr369Nt^{TD}. Both these increases were found to be statistically significant, as determined by Student's *t*-test (p-value <0.05). The omission of ascorbic acid from the BCA release assay also supports a preference for Cu^+, since this still results in the formation of the purple BCA-Cu^+ complex for both proteins (Figure 4.21a, +, open bar).

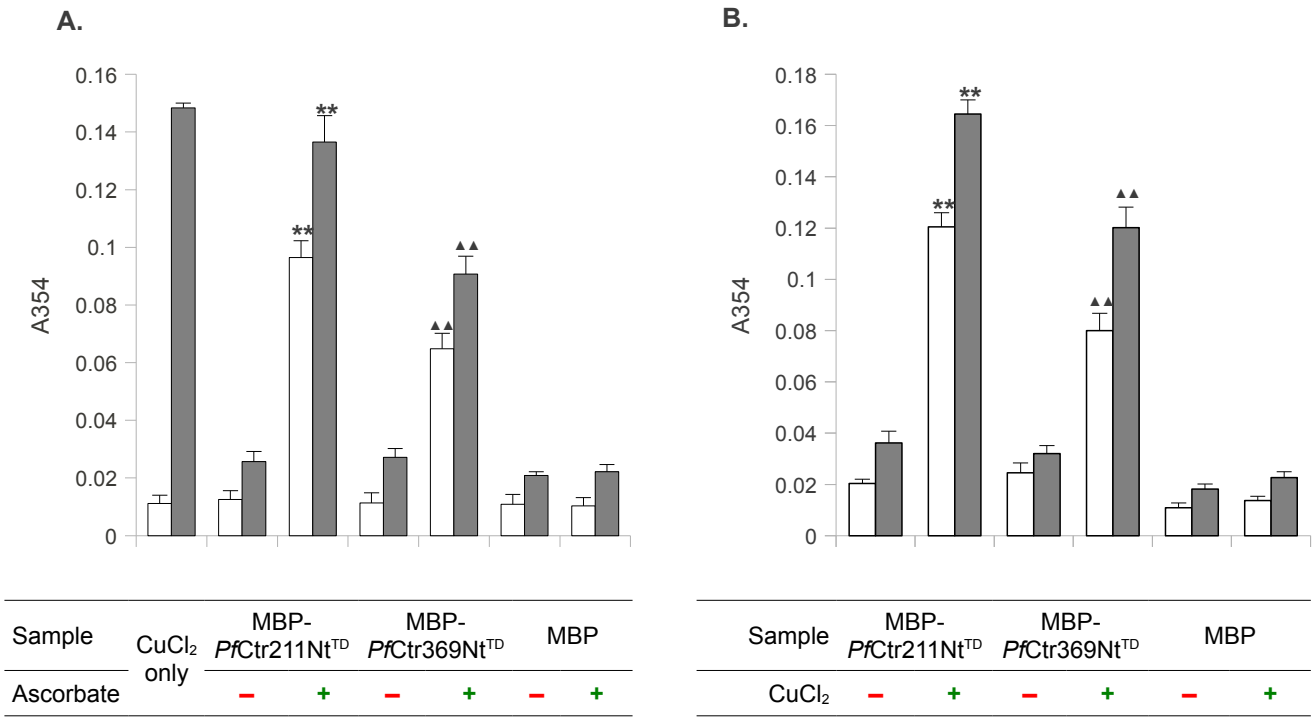

Figure 4.21 Copper binding to MBP-*Pf*Ctr211Nt^{TD} and MBP-*Pf*Ctr369Nt^{TD} *in vitro* and *in vivo*

A 10 µM of affinity-purified MBP-*Pf*Ctr211Nt^{TD}, MBP-*Pf*Ctr369Nt^{TD} or MBP was incubated with $CuCl_2$ in the presence (**+**) or absence (**–**) of ascorbic acid *in vitro*. The BCA release assay was used to detect copper with (solid bars) or without (open bars) the addition of ascorbic acid. The BCA-Cu^+ complex was detected at 354 nm. The concentration of the copper standard ($CuCl_2$ only) was equimolar to the amount of protein used. **B** 0.5 mM $CuCl_2$ was added to the cell growth medium after the induction of recombinant protein expression. Following affinity purification, copper bound *in vivo* was detected by the BCA release assay with (solid bars) or without (open bars) the addition of ascorbic acid. As before the BCA-Cu^+ complex was detected at 354 nm. ****** (for MBP-*Pf*Ctr211Nt^{TD}) and **▲▲** (for MBP-*Pf*Ctr369Nt^{TD}) denote statistical significance, as determined by Student's *t*-test (p-value <0.05). Results are means ± S.E. of triplicate measurements from each duplicate dialysis bag.

Following *E. coli* growth and protein expression, in the presence of 0.5 mM $CuCl_2$, MBP-*Pf*Ctr211Nt^{TD} and MBP-*Pf*Ctr369Nt^{TD} were subsequently amylose purified and analysed for the presence of copper. Both recombinant proteins were found to bind copper *in vivo*, with detectable copper levels dependent on the addition of extracellular copper (Figure 4.21b). The increase in the amount of copper bound to MBP-*Pf*Ctr211Nt^{TD} and MBP-*Pf*Ctr369Nt^{TD} *in vivo* when extracellular copper was added, was found to be statistically significant (p-value <0.05). As with the *in vitro* analysis, the oxidation state of the bound copper was determined by including (Figure 4.21b, grey bars) or omitting (Figure 4.21b, open bars) ascorbic acid from the BCA release assay. For both MBP-*Pf*Ctr211Nt^{TD} and MBP-*Pf*Ctr369Nt^{TD} Cu^+ appeared to be bound *in vivo*; however, it appeared to form a smaller proportion of the total bound copper, particularly for MBP-*Pf*Ctr211Nt^{TD}. This result did, however, indicate a similarity between copper binding *in vitro* and *in vivo.* As before, control experiments for the *in vivo* and *in vitro* conditions indicated copper did not bind to the carrier protein MBP (Figure 4.21).

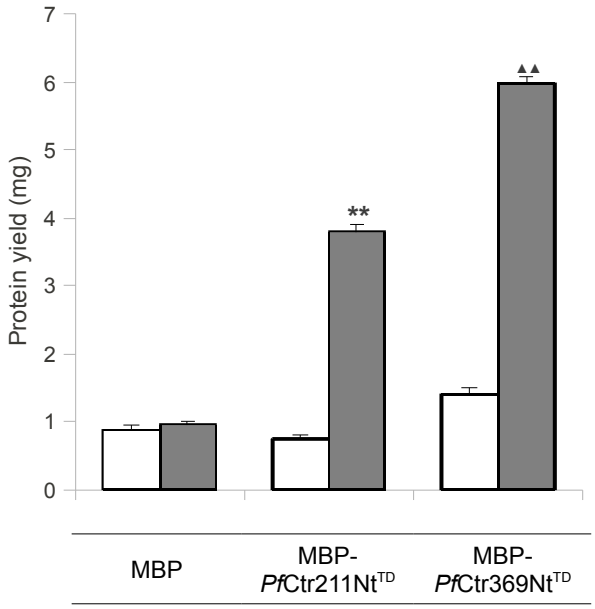

Figure 4.22 MBP-*Pf*Ctr211Nt^{TD} and MBP-*Pf*Ctr369Nt^{TD} protein yields

E. coli host cells were grown in the absence (open bars) or presence (solid bars) of extracellular $CuCl_2$ and the yields of affinity purified recombinant protein determined. The MBP carrier protein alone was included as a control. ****** (for MBP-*Pf*Ctr211Nt^{TD}) and ▲▲ (for MBP-*Pf*Ctr369Nt^{TD}) denote statistical significance, as determined by Student's *t*-test (p-value <0.05).

Analysis of copper binding *in vivo* established the ability of the amino terminal domain of each of the *P. falciparum* copper transport proteins to bind copper in a cellular environment. As previously mentioned, the detection of a significant concentration of bound copper appeared dependent on the presence of extracellular copper. A consequence of adding extracellular copper to the *E. coli* growth medium was a statistically significant increase (p-value <0.05) in the yield of both recombinant *P. falciparum* proteins (Figure 4.22). A similar phenomenon was not observed for the cytoplasmically expressed *P. berghei* protein (data not shown). Under standard conditions the *P. falciparum* recombinant protein yields were found to be poor, particularly for MBP-*Pf*Ctr211Nt^{TD} with an average yield of 0.74 mg per litre of culture, whilst MBP-*Pf*Ctr369Nt^{TD} had a slightly improved yield of 1.53 mg per litre of culture. However, expression in the presence of 0.5 mM $CuCl_2$ significantly improved these yields with an approximate 5-fold increase for MBP-*Pf*Ctr211Nt^{TD} to 3.76 mg per litre of culture and a 4-fold increase for MBP-*Pf*Ctr369Nt^{TD} to 5.98 mg per litre of culture(Figure 4.22). When expressed under the same culture conditions, a comparative analysis for MBP alone indicated minimal alteration to protein yield when $CuCl_2$ was added to the growth medium (Figure 4.22).

Previously it has been demonstrated that peptides representative of the copper transport protein's methionine motifs bind Cu^+ with methionine-only coordination (Jiang *et al.*, 2005). In that study, the oxidation rate of ascorbic acid was used to demonstrate the ability of the

methionine peptides to bind Cu^{+}. Ascorbic acid is stable to aerial oxidation in the absence of metal ions, but the presence of iron or copper ions catalyse its oxidative degradation via equations 1 and 2 (Figure 4.23) (Jiang *et al.*, 2005). Oxidative degradation results in a loss of ascorbate's characteristic, pH-dependent absorption band between 245 and 265 nm (Buettner, 1988). This is therefore a convenient spectroscopic signal for the presence of catalytic metal ions in solution. The pH-dependent oxidation rate of the reaction is first-order, with respect to both the ascorbate monoanion ($HAsc^{-}$) and the metal ion. The oxidation rate is, however, known to decrease in the presence of metal chelators with slower oxidation rates indicative of more stable chelates (Khan and Martell, 1967). Chelators that favour Cu^{2+} slow reaction rates by making equation 1 rate-limiting, whilst chelators that stabilise Cu^{+} shift the rate-limiting step to equation 2 (Figure 4.23). This effect was previously demonstrated for the copper-catalysed oxidation of ascorbate in aqueous acetonitrile (Mi and Zuberbühler, 1992). Similarly the spectroscopic signal, provided by the ascorbate UV-vis assay, was used to demonstrate the ability of methionine peptides to bind Cu^{+} (Jiang *et al.*, 2005). For the current study, the ascorbate UV-vis assay was used to analyse the ability of MBP-*Pf*Ctr211Nt^{TD} and MBP-*Pf*Ctr369Nt^{TD} to bind copper *in vitro*. This assay was also employed to gain further insight into the preferred oxidation state of bound copper.

Equation 1: $HAsc^{-} + Cu^{2+} \rightarrow HAsc^{\bullet -} + Cu^{+}$

Equation 2: $Cu^{+} \xrightarrow{O_2} Cu^{2+}$

Figure 4.23 Equations representing the copper-catalysed oxidative degradation of ascorbic acid

The effect the recombinant proteins had on copper-catalysed ascorbic acid oxidation was examined by monitoring the loss of absorbance, at 255 nm, of a 120 µM ascorbic acid solution at pH 4.5. This particular pH was selected for several reasons. First, the oxidation rate of ascorbic acid increases with increased concentration of $HAsc^{-}$, which has a pK_a of 4.1, therefore using elevated pH values can amplify unwanted errors. Second, the hydrolysis of Cu^{2+} is minimal at this lower pH (Jiang *et al.*, 2005). Last and perhaps most important, hCtr1-transfected human cells show increased copper uptake at a low extracellular pH (Lee *et al.*, 2002). As expected, the freshly prepared ascorbic acid control showed a constant absorbance at 255 nm (A_{255}) over a period of 300 seconds, indicative of the stability of the solution (Figure 4.24, ■). When 8 µM $CuCl_2$ was added, the A_{255} signal was found to decrease highlighting the catalytic oxidation of ascorbic acid by copper (Figure 4.24, ▼). The oxidation of ascorbic acid was, however, inhibited by the addition of 5 µM purified MBP-*Pf*Ctr211Nt^{TD} (Figure 4.24, ▲) or MBP-*Pf*Ctr369Nt^{TD} (Figure 4.24, ►). The presence of either recombinant protein results in only a slight decrease in ascorbic acid stability over time, compared to the dramatic decrease when

$CuCl_2$ was added. This result indicates that both MBP-*Pf*Ctr211Nt^{TD} and MBP-*Pf*Ctr369Nt^{TD} chelate copper in solution, thus preventing its participation in the redox cycle (Figure 4.23). Although this assay is not definitive of the copper species being preferentially bound by each protein, it is likely to be Cu^+ based on the *in vitro* and *in vivo* copper-binding studies (Figure 4.21). Thus it is highly likely that equation 2 is the rate-limiting step of the redox cycle (Figure 4.23).

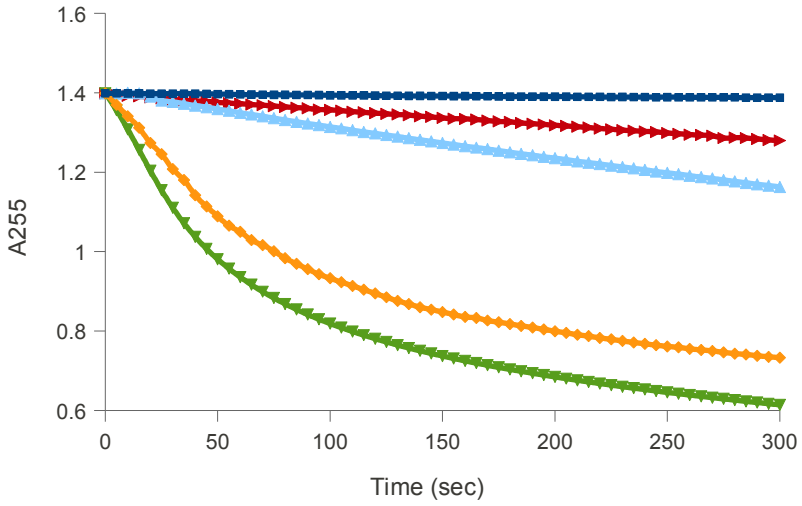

Figure 4.24 Copper-catalysed oxidative degradation of ascorbic acid in the presence of MBP-*Pf*Ctr211Nt^{TD} and MBP-*Pf*Ctr369Nt^{TD}

120 µM ascorbic acid (H_2Asc) at pH 4.5 (■). Addition of 8 µM $CuCl_2$ to the H_2Asc solution (▼). MBP-*Pf*Ctr211Nt^{TD} (▲), MBP-*Pf*Ctr369Nt^{TD} (►) or MBP (♦) were added to the $CuCl_2/H_2Asc$ solution.

4.3 Discussion

Both prokaryotes and eukaryotes require copper as an essential enzyme co-factor for survival. It was similarly determined that *P. falciparum* requires intracellular copper for transition from the ring to trophozoite stage of parasite development (Rasoloson *et al.*, 2004). Characterisation of a *P. falciparum* P-type ATPase copper efflux protein further supported the presence of a parasite intracellular copper pool (Rasoloson *et al.*, 2004). However, the mechanism by which the malaria parasite acquires and transports extracellular copper into its cytosol is unknown. One possible mechanism is via a dedicated parasite copper transport protein. A BLASTp search of the *Plasmodium* database (PlasmoDB), coupled with an *in silico*-based analysis, identified putative copper transport protein sequences in eight species of the *Plasmodium* parasite (Chapter 3). Using rodent-infecting and *P. falciparum* parasites as model organisms, the presence of a parasite copper transporter coding sequence was confirmed. Additionally, a recombinant form of the transporter's amino terminus was shown to bind copper *in vitro* and *in*

vivo.

4.3.1 Confirmation of a *Plasmodium* spp. copper transport protein coding sequence

Bioinformatics tools provide a useful means by which to predict the function of a hypothetical protein. However, protein function and structural properties can only be confidently inferred through biochemical and cell biological experimentation (Birkholtz *et al.*, 2008). Using rodent-infecting parasites and *P. falciparum* as reference organisms, the malaria parasite was probed for the presence of an open reading frame (ORF) encoding a putative copper transporter. In this regard, copper transporter ORF's were PCR amplified from the *P. yoelii* (PY00413), *P. berghei* (PBANKA_130290) and *P. falciparum* (PF14_0211 and PF14_0369) genomes. For *P. yoelii*, an 1800bp amplicon was obtained from genomic DNA (Figure 4.1a) corresponding with a full-length ORF containing two introns and three exons. Amplicon identity was supported by nested PCR (Figure 4.1b) and *Bam*HI restriction digestion (Figure 4.1c). Although a full-length *P. berghei* ORF was not similarly amplified from genomic DNA, a region of the ORF predicted to encode the transporter's amino terminus was amplified by RT-PCR (Figure 4.1d) and the amplicon sequenced. The sequenced product was almost identical to the published PlasmoDB sequence (Figure 4.2), thus supporting the presence of a putative copper transporter ORF in the genome of rodent-infecting malaria parasites. RT-PCR amplification also confirmed that the targeted ORF was transcribed by *P. berghei* for native protein expression.

The *P. falciparum* genome is predicted to encode two putative copper transporters (Chapter 3). Other *Plasmodium* parasite species are also predicted to encode two transporters, except *P. yoelii* whose second predicted transporter's amino acid sequence largely lacks characteristic copper transporter features. The *P. yoelii* genome was, however, only partially sequenced and hence not fully assembled, which may have contributed to errors in gene annotation (Vaughan *et al.*, 2008). This seems likely since the related *P. berghei* genome is predicted to encode two putative copper transporters (PBANKA_130290 and PBANKA_102150) of which only one was PCR amplified (PBANKA_130290). To confirm the presence of two *P. falciparum* copper transporter ORF's, each was targeted for PCR amplification using sequence-specific primers. The two respective full-length *P. falciparum* ORFs are predicted to be 423 bp for PF14_0211 and 920 bp for PF14_0369, with similar sized PCR amplicons obtained from *P. falciparum* genomic DNA (Figure 4.3). PCR amplification and sequencing of a portion of the ORF predicted to encode each respective protein's amino terminus showed a close resemblance to the sequences retrieved from the PlasmoDB (Figure 4.4).

4.3.2 Identification of a native murine malaria parasite copper transport protein

Determining the subcellular location of a native protein can be achieved using a protein-specific antibody-based approach (Martin *et al.*, 2009a). Anti-peptide antibodies were therefore generated (Section 4.2.2.1) and used to identify and localise the native parasite protein. In the first instance the murine malaria parasite model was used for protein localisation. Copper transporters characterised to date have been shown to localise to the cell membrane (Dancis *et al.*, 1994; Lee *et al.*, 2002; Mackenzie *et al.*, 2004; Riggio *et al.*, 2002). To obtain copper the parasite transporters are likely to be membrane localised, as suggested by the identification of three predicted transmembrane domains in the parasite copper transport protein sequences (Figure 3.3). Analysis of fractionated *P. yoelii*-infected mouse red blood cell lysate on a western blot, probed with the specific anti-CSD antibody, identified a 32kDa protein band in the insoluble “membrane” fraction that was absent from the soluble fraction (Figure 4.7). Additional protein bands below the 32kDa band could be the result of protein degradation. The addition of protease inhibitors did not alter this observation.

Immunolocalisation studies, using fluorescent microscopy, indicated that the *P. yoelii* copper transporter was associated with a parasite membrane (Figure 4.8b). Considering the anti-CSD antibodies can also recognise the *P. berghei* copper transporter, the possibility exists that the parasites used for this study actually represented the *berghei* species. Unfortunately both the parasite species and protein location could not be confirmed since antibodies against a specific membrane marker protein were not available for this study. The pattern of fluorescence obtained for the putative copper transport protein was, however, noticeably different from the pattern obtained for the cytoplasmic control protein, lactate dehydrogenase (LDH) (Figure 4.8a), suggesting different locations. Further experimental evidence is, however, required to confirm the specific location of the putative copper transport protein. This could be achieved through co-localisation experiments using a membrane marker protein for confocal microscopy or via immunogold labelling for transmission electron microscopy. An alternative to antibody-based detection is to attach a fluorescent tag to the carboxyl terminus of the copper transporter, for example. Parasites would then be transfected with this construct and the localisation of the target protein tracked throughout the parasite's life cycle.

4.3.3 Recombinant expression of the amino terminus of a putative *P. berghei* copper transport protein

The coding domain of the *P. berghei* copper transport protein's amino terminus was amplified by RT-PCR, cloned and used for recombinant protein expression. The ability of this protein to bind copper would suggest a role for the whole protein in copper transport. This assumption is

based on the finding that the amino terminus of other copper transport proteins studied, is involved in the initial acquisition and transport of the cuprous ion (De Feo *et al.*, 2009; Larson *et al.*, 2010; Nose *et al.*, 2006). Initial attempts to express the recombinant *P. berghei* amino terminus (*Pb*CtrNt) made use of the pET23a vector. The expressed protein was, however, found to be targeted to insoluble inclusion bodies (Table 4.1), which is undesirable given the inherent difficulties faced with protein refolding *in vitro*. Fusion of the amino terminal domain to a soluble carrier protein was therefore explored. Soluble fusion partners, such as glutathione S-transferase (GST) and maltose binding protein (MBP), can improve folding of inherently insoluble, unstable or unfolded proteins (Kapust and Waugh, 1999; Makrides, 1996; Nallamsetty and Waugh, 2007). The carrier protein is thought to rapidly adopt a native conformation thereby promoting the correct folding of downstream units (Baneyx, 1999).

As with the expression of His_6-*Pb*CtrNt (pET23a), expression of GST-*Pb*CtrNt produced an insoluble product (Table 4.1). On the other hand, fusion to the MBP carrier protein produced a soluble product targeted to the cell cytoplasm (pMal-c2), although some of the protein was still found as an insoluble sample (Figure 4.10). Additionally, the expressed product appeared largely degraded or truncated, as evidenced by multiple protein bands below the desired 61kDa product. The addition of protease inhibitors, during lysate preparation, suggested degradation did not occur following cell lysis (data not shown). This indicated that product truncation and/or degradation may have occurred during protein synthesis in the host cell cytoplasm. A strategy used to avoid this problem is expression of a target protein in a host strain bearing mutations to native protease genes (Baneyx, 1999). *E. coli* BL21 cells lack the *lon* and *ompT* genes, which encode proteases catalysing the endoproteolytic cleavage of damaged and recombinant proteins (GST handbook). Expression using this strain made no observable improvement (Figure 4.11). The presence of high molecular weight multimers in all purified samples was another concern. These protein multimers are formed from MBP-*Pb*CtrNt, as indicated by anti-MBP (Figure 4.11) and specific antibody blots (data not shown). Expressing problematic recombinant proteins by fusion to a soluble carrier partner, such as MBP, can be accompanied by large molecular weight aggregates as a result of carrier protein-induced solubilisation (Kapust and Waugh, 1999; Nominé *et al.*, 2001a; Sachdev and Chirgwin, 1999; Zanier *et al.*, 2007).

In an effort to reduce MBP-*Pb*CtrNt degradation and multimer formation various alterations to culture and purification conditions were examined (Table 4.2). Variations to temperature, pH and cell density can affect proteolytic activity, protein secretion and the levels of protein production in *E. coli* expression systems (Makrides, 1996). Reducing the growth temperature is known to help limit the *in vivo* aggregation of recombinant proteins and improve production of

soluble protein (Gräslund *et al.*, 2008; Vasina and Baneyx, 1997). This is presumed to be due to slower rates of protein production, thereby allowing newly transcribed recombinant protein time to fold correctly (Vera *et al.*, 2007). In addition, the composition of the cell growth medium should be carefully formulated and monitored, since it too can have significant metabolic effects on the cells and protein production (Makrides, 1996). In this study, changes to nutrient broth composition made no improvement to the MBP-*Pb*CtrNt banding pattern (Table 4.2). The recombinant expression of other malarial parasite proteins at reduced growth temperatures has proven beneficial (Flick *et al.*, 2004; Jalah *et al.*, 2005). For example, expression of soluble *P. falciparum* LDH at 15°C increased expression levels (Berwal *et al.*, 2008). Growth at 15°C made little improvement to MBP-*Pb*CtrNt expression (Table 4.2). Recombinant protein production is also affected by cell density. Induction of expression is usually initiated in mid-to-late log phase, which can be identified by a culture having an optical density between 0.4 and 0.6, at 600 nm. At post-log phase, recombinant protein production can be affected by a limited availability of dissolved oxygen and increased carbon dioxide levels (Makrides, 1996). Expression of GST-*Pf*EMP1 domains post-log phase was, however, found to improve protein production (Flick *et al.*, 2004). A similar observation was not made for MBP-*Pb*CtrNt (Table 4.2).

A critical step in recombinant protein purification is the preparation of the bacterial lysate. Optimal conditions maximise cell lysis and affect the cell fraction to which the recombinant protein is extracted, while minimizing oxidation and proteolysis (Gräslund *et al.*, 2008). The lysis buffer typically consists of a strong buffering species to overcome the effects of the bacterial lysate, high ionic strength to enhance protein solubility and stability plus a reducing agent to prevent protein oxidation (Gräslund *et al.*, 2008). The conditions used for cell lysis and protein purification were systematically tested for their effects on the quality of purified MBP-*Pb*CtrNt. Different buffers, pH's and the addition of detergents, redox reagents and chaotropic agents were tested (Table 4.2), with protein aggregates only disrupted under reducing conditions in the presence of 8 M urea (Figure 4.12). Previous studies with human papillomavirus (HPV) E6 oncoprotein, as a MBP-fusion (MBP+E6), identified that protein aggregation most likely occurred *in vivo* during protein expression (Nominé *et al.*, 2001b). These aggregates were only solubilised using harsh denaturing conditions suggesting that the interactions maintaining MBP+E6 aggregates were probably similar to those found in precipitates of misfolded proteins and bacterial inclusion bodies (Nominé *et al.*, 2001b).

The amino acid residues likely to contribute to aggregate formation are the cysteine residues, of which *Pb*CtrNt has eight (Figure 4.13a). This is likely to have affected heterologous expression since the bacterial cytoplasm has a strong reducing potential and thus few cytoplasmic proteins with disulfide bonds (Fahey *et al.*, 1977). This property generally

translates into the misfolding of heterologous proteins whose tertiary structure depends, in part, on disulfide bond formation (Makrides, 1996). The problem can be overcome by exporting the target protein from the cytoplasm to the oxidising environment of the bacterial cell periplasm (Baneyx, 1999). Attempts at this approach, by fusing *Pb*CtrNt to MBP having a periplasmic *malE* leader sequence, proved unsuccessful (data not shown), which may be due to the presence of a predicted amino-terminal signal sequence in the inserted gene.

Molecular exclusion chromatography (MEC) was used to fractionate the multiple MBP-*Pb*CtrNt products. MBP-*Pb*CtrNt was, however, found to elute in the void volume of Sephacryl S-100 and S300 resins (Figure 4.14), thereby suggesting a significant number of MBP-*Pb*CtrNt monomers aggregate in the cell cytoplasm to form “soluble” inclusion bodies. A similar observation was made for MBP-E6 expression (Nominé *et al.*, 2001b; Zanier *et al.*, 2007) and although the protein aggregated due to misfolding, it was still found to be able to bind zinc ions with a similar stoichiomery to that of the native protein. This suggested the recombinant protein was synthesised with a native-like fold, thus enabling correct coordination of the metal centre (Zanier *et al.*, 2007). MBP-*Pb*CtrNt was therefore assessed for copper binding *in vitro* and *in vivo* with bound copper detected by the copper-specific BCA release assay (Brenner and Harris, 1995). MBP-*Pb*CtrNt bound copper under both examined conditions (Figure 4.20) with an apparent binding preference for the cuprous ion (Cu^{+}). However, considering the misfolded nature of MBP-*Pb*CtrNt, these results were cautiously interpreted since other structural studies were not carried out.

4.3.4 Recombinant expression of the amino termini of two *P. falciparum* copper transport proteins

Plasmodium parasite gene sequence features that affect recombinant expression include signal peptides, transmembrane domains, rare codons, the presence of introns and the AT-richness of the genome (Mehlin *et al.*, 2006; Sørensen and Mortensen, 2005a; Vedadi *et al.*, 2007). The predicted amino terminal signal peptide was not removed from *Pb*CtrNt, which could explain the problems experienced with His_6-*Pb*CtrNt expression (Table 4.1) and with the ineffective targeting of MBP-*Pb*CtrNt to the cell periplasm. The two *P. falciparum* copper transporter amino terminal domains were therefore cloned and expressed with the exclusion of a predicted signal peptide. However, when expressed as pMal-c2 constructs, both MBP-*Pf*Ctr211Nt^{TD} and MBP-*Pf*Ctr369Nt^{TD} produced a similar result to that obtained for cytoplasmically expressed MBP-*Pb*CtrNt (Figure 4.15). This suggested it was a sequence feature of the partner protein that was responsible for protein aggregation. For *Pb*CtrNt, this sequence feature was suggested to be the presence of multiple cysteine residues. *Pf*Ctr211Nt^{TD} has two such cysteine residues

(Figure 4.13b) whilst *Pf*Ctr369Nt^{TD} has five (Figure 4.13c), with a higher number of cysteine residues seeming to correlate with an increase in high molecular weight protein aggregates. Most bacterial proteins that require stable disulfide bonds are in fact exported (Thornton, 1981) since the oxidising environment of the cell periplasm facilitates the correct folding of these proteins (Makrides, 1996). Targeted expression of MBP-*Pf*Ctr211Nt^{TD} and MBP-*Pf*Ctr369Nt^{TD} to the periplasm was therefore examined and was found to significantly reduce aggregate formation and protein proteolysis, although some product truncation was still evident (Figure 4.17).

4.3.5 Copper binding to MBP-*Pb*CtrNt, MBP-*Pf*Ctr211Nt^{TD} and MBP-*Pf*Ctr369Nt^{TD}

Similar to MBP-*Pb*CtrNt, copper binding studies using MBP-*Pf*Ctr211Nt^{TD} and MBP-*Pf*Ctr369Nt^{TD} indicated that both proteins bound copper *in vitro* and *in vivo* (Figure 4.21) with an apparent preference for the cuprous ion. Copper is presumed to be coordinated to methionine motifs (MxM or MxxM) present in each of these *Plasmodium* proteins. These motifs have been demonstrated to be essential for the function of the yeast and human copper transporters when extracellular copper is limited (Eisses and Kaplan, 2005; Guo *et al.*, 2004; Puig *et al.*, 2002a). The amino terminus of the yeast copper transporter contains eight such methionine motifs, but only the last methionine of the eighth motif is essential for function (Puig *et al.*, 2002a). This particular methionine has been found to be conserved in other characterised copper transporters and is located 20 amino acids from the first transmembrane domain. Analysis of the two *P. falciparum* copper transporters identified one MxxM motif in *Pf*Ctr211Nt^{TD} and one MxM motif in *Pf*Ctr369Nt^{TD} (Figure 4.13). Based on hydropathy plots (Figure 3.3) it was established that the last methionine of each of these motifs was located 20 amino acids from the first predicted transmembrane domain. This suggests that this motif may be involved in copper coordination. However, the involvement of other residues in copper coordination cannot be excluded. This is of particular importance since a number of cysteine and histidine residues are also present in the amino-terminal sequences of the *Plasmodium* copper transporters. Both cysteine and histidine residues have been implicated in metal ion coordination in other proteins (Davis and O'Halloran, 2008; Eisses and Kaplan, 2005).

In contrast to the *P. falciparum* proteins, the amino terminal domain of the *P. berghei* copper transporter contains two MxM motifs. The second of these two motifs contains a methionine residue 20 amino acids from the first predicted transmembrane domain, therefore implicating this motif in copper coordination. However, copper coordination to the other methionine motif, or to histidine and cysteine residues, cannot be excluded. Preliminary electron spin resonance data, from MBP-*Pb*CtrNt copper binding studies, suggested that copper was coordinated by

two histidines, a cysteine and methionine residue (data not shown). Identification of the specific residues involved in copper coordination to the *Plasmodium* proteins requires the use of more sophisticated techniques such as protein crystallisation or nuclear magnetic resonance (NMR) spectroscopy. These techniques could also be used to confirm the folded state of each recombinant protein, which would help determine the importance of correct protein folding to copper coordination.

When expressed in the presence of copper, the final yield of MBP-*Pf*Ctr211Nt^{TD} and MBP-*Pf*Ctr369Nt^{TD} was significantly increased (Figure 4.22). A similar phenomenon was, however, not observed when MBP-*Pb*CtrNt was expressed in the presence of copper. This observation could perhaps be accounted for by the fact that MBP-*Pb*CtrNt appears to aggregate in the *E. coli* host cell. However, the fact that MBP-*Pb*CtrNt was still capable of binding copper *in vivo* (Figure 4.20b), despite its aggregation, suggests other factors influenced these differences. One likelihood is the differing copper requirements of the cellular compartments to which the respective proteins were targeted, namely the cytoplasm and periplasm. Almost all bacterial copper proteins, such as multi-copper oxidases, amine oxidases and lysine oxidases are found in the bacterial periplasm or excreted extracellularly (Rensing and Grass, 2003). It has even been proposed that *E. coli* cells do not require copper for cytoplasmic enzymes and only require copper for periplasmic or inner membrane enzymes, such as Cu,Zn-superoxide dismutase or cytochrome-c oxidase (Bagai *et al.*, 2008). Since copper is required in the periplasm, efficient regulatory mechanisms are essential (Macomber *et al.*, 2007). This is perhaps best highlighted by studies of two periplasmic proteins thought to be involved in copper homoeostasis, namely PcoA and PcoC. Mutation of either protein interferes with copper resistance (Brown *et al.*, 1995) whilst gene deletion causes copper hypersensitivity (Huffman *et al.*, 2002).

Due to the oxidising environment of the bacterial periplasm, tight control of copper ensures this metal ion cannot freely enter redox chemistry to produce harmful reactive oxygen species (Puig *et al.*, 2002b). Under standard laboratory growth conditions, this implies there would be limited copper available in the periplasm for copper binding proteins that are not required for *E. coli* metabolic function. Consequently, MBP-*Pf*Ctr211Nt^{TD} and MBP-*Pf*Ctr369Nt^{TD} expression is perhaps limited to ensure native *E. coli* copper-dependent proteins can function normally under these growth conditions. However, if excess extracellular copper is added to the growth medium, MBP-*Pf*Ctr211Nt^{TD} and MBP-*Pf*Ctr369Nt^{TD} protein yield is improved (Figure 4.22) by alleviating the copper-related metabolic stress from the *E. coli* cells. The lack of an increase in protein yield for cytoplasmically expressed MBP-*Pb*CtrNt, could perhaps be related to the fact that few cytoplasmic *E. coli* proteins require copper as an essential cofactor (Macomber *et al.*,

2007). Thus the cytoplasmic expression of MBP-*Pb*CtrNt would place less stress on *E. coli* cellular metabolism under standard growth conditions, resulting in similar yields in the presence or absence of extracellular copper.

In mammalian and yeast cells the favoured redox state of copper for transfer and transport, is the reduced cuprous ion (Cu^{+}) (Hassett and Kosman, 1995; Puig *et al.*, 2002a). This is thought to be due to the fact that Cu^{+} is more exchange labile than Cu^{2+} thereby facilitating its transfer between two binding sites (Jiang *et al.*, 2005; Rees and Thiele, 2007). Considering the highly reactive nature of Cu^{+} in an oxidising environment, the challenge is to safely sequester these ions prior to transport across the lipid bilayer. The methionine motifs present in the extracellular amino terminus of the copper transporter family are thought to provide this desired coordination environment (Jiang *et al.*, 2005; Puig *et al.*, 2002a). Methionine only coordination of Cu^{+} has been established through a unique study using a synthesized methionine motif peptide (MTGMKGMS). Inhibition of copper-catalysed ascorbic acid oxidation, by this peptide, suggested it chelated Cu^{+} thereby preventing it from participating in the redox cycle (Figure 4.23). This data, combined with similar experiments using peptide variants lacking methionines as well as electrospray mass spectra, strongly supported methionine-specific coordination of Cu^{+} (Jiang *et al.*, 2005). The affinity with which these motifs bound copper (~2.5 μM) was also found to be compatible with biological copper uptake, which is between 1 and 5 μM in a variety of organisms (Puig and Thiele, 2002). These methionine motifs were therefore suggested to be required by copper transport proteins for extracellular copper acquisition and transport across the membrane.

The two *P. falciparum* copper transporter amino termini are each predicted to contain a single methionine motif (Figure 4.13). This motif is presumed to be involved in copper binding, as suggested from the *in vitro* and *in vivo* studies. The ability of the recombinant *P. falciparum* amino termini to inhibit copper-catalysed ascorbic acid oxidation was examined and indicated that both MBP-*Pf*Ctr211Nt^{TD} and MBP-*Pf*Ctr369Nt^{TD} inhibited ascorbic acid oxidation (Figure 4.24). Considering the dynamics of the redox cycle (Figure 4.23), this result suggested that each protein coordinated the Cu^{+} ion. Therefore, the ability of these recombinant proteins to readily bind copper combined with protein localisation studies (Figure 4.8) supports a physiological role for the *Plasmodium* copper transporters (Chapter 3). Nevertheless, cation uptake and/or functional complementation studies will be necessary to confirm the directional transport of copper by these parasite proteins.

CHAPTER 5

The *Plasmodium* spp. putative Cox17 copper metallochaperone: Recombinant protein copper binding studies

5.1 Introduction

The redox activity of copper has been harnessed for catalysis by a broad range of enzymes. These enzymes are critical to a number of cellular biochemical and regulatory functions in microbes, plants and animals (Kim *et al.*, 2008; Lutsenko, 2010). However, it is this same redox property that allows copper to generate free radicals if left unregulated within a cell. This has therefore resulted in the development of sophisticated cellular mechanisms for the acquisition, distribution and regulation of copper (Dameron and Harrison, 1998; Kim *et al.*, 2008; Leary *et al.*, 2009). These mechanisms involve copper transporters, metallochaperones and molecules that chelate copper in biologically inert complexes. Excess cytosolic copper is exported from cells via copper efflux proteins belonging to the P-type ATPase family of transporters. The importance of these cellular pathways is best highlighted by human diseases and pathophysiologies resulting from defects in copper homoeostasis (Bertinato and L'Abbe, 2004; Kim *et al.*, 2008). These diseases include Menkes and Wilson's disease, caused by genetic defects (Camakaris *et al.*, 1999; Shim and Harris, 2003), and Alzheimer's and Parkinson's disease, resulting from alterations in copper balance (Hung *et al.*, 2010) Considering the biochemical role of copper, it is expected that humans and human pathogens share a similar cellular requirement of copper for growth, proliferation and development (Kim *et al.*, 2008).

Following copper entry into the cytosol of eukaryotic cells, it is delivered to target proteins via soluble Cu^{+}-binding proteins known as copper chaperones (Rosenzweig, 2002). It is unclear how chaperones obtain their cargo, but appears to involve direct interaction with the copper transport protein (Xiao *et al.*, 2004). It is currently understood that there are three cellular pathways that require copper chaperones. These pathways involve copper shuttling to: cytosolic Cu,Zn-superoxide dismutase, metal transporting P-type ATPases and mitochondria (Boal and Rosenzweig, 2009). Of these three pathways, the mitochondrial pathway appears to be the most complex (Lutsenko, 2010). Copper delivery to the mitochondrion is essential, since the copper-requiring protein cytochrome-c oxidase is localised there. Copper is essential for cytochrome-c oxidase function and is aided in its assembly by the copper metallochaperone Cox17 (Glerum *et al.*, 1996; Punter and Glerum, 2003). Cox17 was also suggested to contribute to copper delivery to the mitochondrion (Beers *et al.*, 1997).

The suggestion that Cox17 was involved with copper shuttling was based on its localisation to

both the cytosol and mitochondrial intermembrane space (Beers *et al.*, 1997) coupled with its copper binding properties (Heaton *et al.*, 2001; Srinivasan *et al.*, 1998). This idea was, however, disputed by the finding that cytochrome-c oxidase deficiency, in *cox17Δ* yeast cells, could be functionally complemented by restricting Cox17 location to the mitochondrial intermembrane space (Maxfield *et al.*, 2004). In addition, *cox17Δ* cells still maintain similar mitochondrial copper levels to those observed in wild-type cells. This therefore suggested that Cox17 was not an obligate mitochondrial copper transporting metallochaperone. Searches for additional metallochaperones led to the observation that the bulk of mitochondrial copper is localised within the matrix in a soluble, low molecular weight complex termed CuL (Cobine *et al.*, 2004). Subsequent studies identified that CuL was also abundant in the cytosol as a copper-free ligand (Cobine *et al.*, 2006b). It was therefore proposed that Cu^{+} binding to apo-CuL in the cytosol triggers translocation of the anionic CuL complex to the mitochondrion, thereby delivering copper (Leary *et al.*, 2009). Although this model is distinct from the other metallochaperone systems in the cytosol, it does not exclude the importance of the copper metallochaperones identified as essential for cytochrome-c oxidase assembly, namely Cox17, Cox11 and Sco1 (Lutsenko, 2010).

Catalytically active cytochrome-c oxidase is assembled via numerous steps, requiring over 30 accessory proteins (Cobine *et al.*, 2006a). Of particular importance to cytochrome-c oxidase activity is Cox17-mediated copper delivery to Sco1 and Cox11 for subsequent insertion into the cytochrome-c oxidase Cu_A and Cu_B sites, respectively (Cobine *et al.*, 2006a). The indispensability of Cox17 function is highlighted by embryonic lethality in *COX17* null mice (Takahashi *et al.*, 2002). The highly conserved and essential nature of Cox17 and its cellular role suggests novel Cox17 candidate proteins would be similarly essential to their host cells. A Cox17 homologue was identified in the proteome of the *Plasmodium* parasite, with its metabolic role supported by the identification of putative proteins required for the assembly of a parasite cytochrome-c oxidase complex (Table 3.1). The aim of this study was to clone and recombinantly express the *P. yoelii* and *P. falciparum* Cox17 proteins to measure copper binding *in vitro* and *in vivo*.

5.2 Results

5.2.1 Confirmation of a native *Plasmodium* Cox17 coding domain

The initial identification of a putative parasite Cox17 coding domain made use of the rodent-infecting malaria parasite model. *P. falciparum* was subsequently used to corroborate these results. *P. yoelii* Cox17 is predicted to be encoded by an open reading frame of 201bp, whilst the *P. falciparum* Cox17 open reading frame is predicted to be 204bp. However, due to

constraints in the designing of the reverse primer, the expected sizes of the *P. yoelii* and *P. falciparum* PCR amplicons was 192bp and 195bp, respectively. For both parasites a PCR amplicon of approximately 200 bp was amplified from genomic DNA (Figure 5.1). The 3bp difference between these two amplicons would not be discernible by agarose gel analysis. The LDH control was amplified as an 835bp product from the genomic DNA of both parasite species (Figure 5.1). Additional controls included DNA isolated from uninfected BALB/c mouse blood (Figure 5.1a) or no DNA template (Figure 5.1b). Both reactions returned negative results.

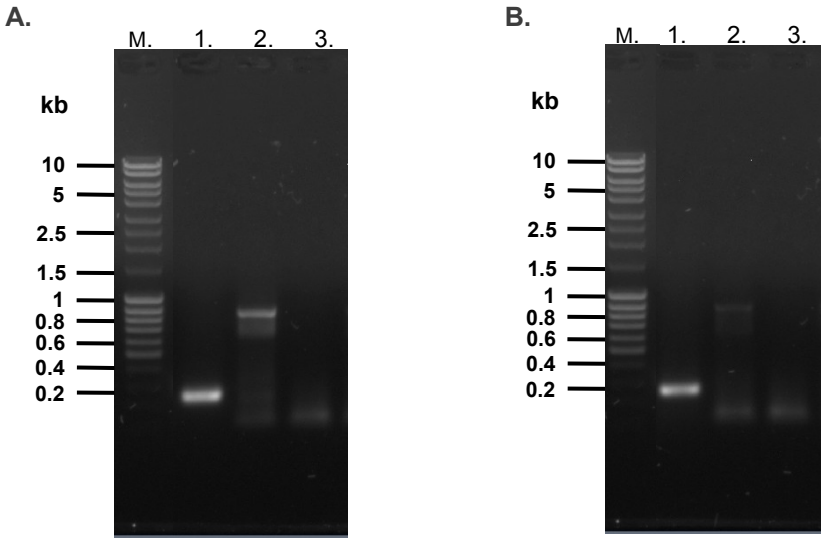

Figure 5.1 PCR amplification of the *P. yoelii* and *P. falciparum* Cox17 coding domains

The *P. yoelii* (**A**) and *P. falciparum* (**B**) Cox17 coding domains were PCR amplified from genomic DNA and analysed on a 1% agarose gel. Lane 1, Cox17; lane 2, LDH control; lane 3, negative control. Molecular mass markers (**M**) are on the left of each gel (see materials and methods for details).

To confirm the identity of the amplicons, the Cox17 PCR products were ligated into the pGEM®-T vector and sequenced. Alignment of the sequencing data with the corresponding PlasmoDB sequences indicated a 100% sequence identity for both PCR products (Figure 5.2). As expected, translation of these sequenced products yielded amino acid sequences with 100% identity to the PlasmoDB sequences (data not shown).

A.

```
PyCox17_vect      ATGGGATTAGGTTTAACTAAGCCATTAAATACAACTGAGGAAAGTAAAACGTGTGCAAAA 60
PyCox17_plas      ATGGGATTAGGTTTAACTAAGCCATTAAATACAACTGAGGAAAGTAAAACGTGTGCAAAA 60
                  ************************************************************

PyCox17_vect      AAAAAGAAAATATGTTGTGTATGCTTAGATACAAAAAAATTAAGAGATGAATGTATTGTT 120
PyCox17_plas      AAAAAGAAAATATGTTGTGTATGCTTAGATACAAAAAAATTAAGAGATGAATGTATTGTT 120
                  ************************************************************

PyCox17_vect      AATTTAGGAGAAGAACAATGTAAGAAATATATTAATGATCATAATCAGTGCCTAAGAAAT 180
PyCox17_plas      AATTTAGGAGAAGAACAATGTAAGAAATATATTAATGATCATAATCAGTGCCTAAGAAAT 180
                  ************************************************************

PyCox17_vect      GAAGGGTTTGAT 192
PyCox17_plas      GAAGGGTTTGAT 192
                  ************
```

B.

```
PfCox17_vect      ATGGGTATGAGCTTGAACAAACCAATAAATAACACGAATGAAGCAAATAAAGGAGAAGTT 60
PfCox17_plas      ATGGGTATGAGCTTGAACAAACCAATAAATAACACGAATGAAGCAAATAAAGGAGAAGTT 60
                  ************************************************************

PfCox17_vect      AAAAAAAAAAAAATTTGTTGTGTTTGTTTAGAAACCAAAAAGTTAAGAGATGAATGTATT 120
PfCox17_plas      AAAAAAAAAAAAATTTGTTGTGTTTGTTTAGAAACCAAAAAGTTAAGAGATGAATGTATT 120
                  ************************************************************

PfCox17_vect      GTTAAATTGGGGGAAGAGCAGTGTAAGAAATTTATCGATGATCATAATAAATGTTTAAGG 180
PfCox17_plas      GTTAAATTGGGGGAAGAGCAGTGTAAGAAATTTATCGATGATCATAATAAATGTTTAAGG 180
                  ************************************************************

PfCox17_vect      AGTGAAGGTTTTGAT 195
PfCox17_plas      AGTGAAGGTTTTGAT 195
                  ***************
```

Figure 5.2 Alignment of the sequenced *P. yoelii* and *P. falciparum* Cox17 amplicons with PlasmoDB sequences

P. yoelii (PyCox17_vect) (**A**) and *P. falciparum* (PfCox17_vect) (**B**) Cox17 amplicons were aligned with sequences retrieved from PlasmoDB (PyCox17_plas and PfCox17_plas, respectively) using ClustalW**.**

5.2.2 Anti-peptide antibody production for parasite Cox17 protein detection

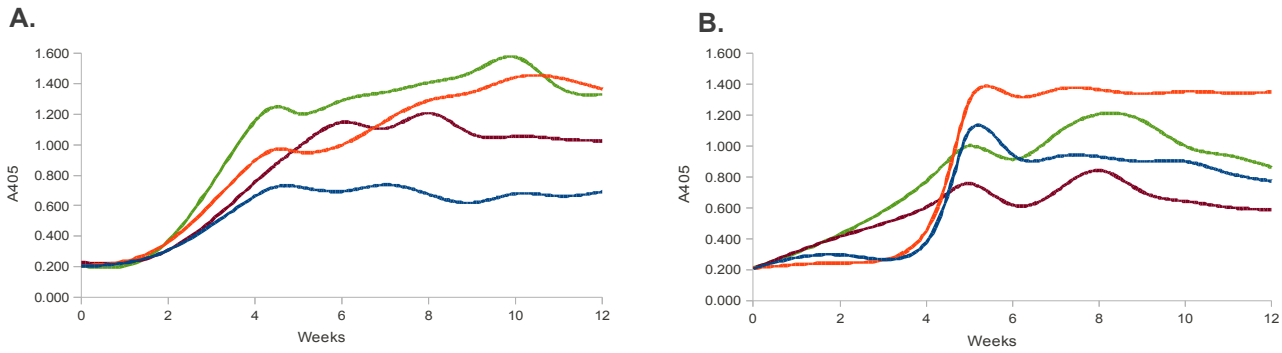

Figure 5.3 Anti-peptide antibody responses against peptides selected from the *P. yoelii* (KTC) and *P. falciparum* (NKG) Cox17 metallochaperones

Anti-peptide antibody production against the KTC (**A**) and NKG (**B**) peptides was monitored by ELISA over a 12 week period. In all panels peptide-specific antibody production is shown for chicken 1 (—) and chicken 2 (—). Also shown is the antibody production against the rabbit albumin carrier for chicken 1 (—) and chicken 2 (—).

For the detection of either native or recombinant *P. yoelii* and *P. falciparum* Cox17 metallochaperones, antibodies were generated against peptides from each protein. Details of peptide selection are described in Section 3.2.8 (KTC for *P. yoelii* and NKG for *P. falciparum*). Antibody titres against each peptide were monitored by ELISA over a 12-week period, with responses to both the KTC (Figure 5.3a) and NKG (Figure 5.3b) peptides showing some minor differences between chickens. For these two peptides, antibody production was detectable from week three with a peak after week four. Antibody production then either plateaus or decreases to the end of week twelve. Anti-peptide antibody titres showed similar trends to antibodies generated against the anti-rabbit albumin carrier protein (Figure 5.3). Antibodies were isolated from egg yolks, pooled and affinity purified on a peptide-specific matrix. Bound antibodies were eluted from the matrix (Figure 5.4) and pooled for each peptide. The final yield for the Cox17 antibodies was 5.7 mg for anti-KTC and 9.0 mg for anti-NKG antibodies. Attempts to detect the native *P. yoelii* and *P. falciparum* Cox17 metallochaperones, using the respective antibodies, were unsuccessful in both blotting and immunoprecipitation experiments (data not shown).

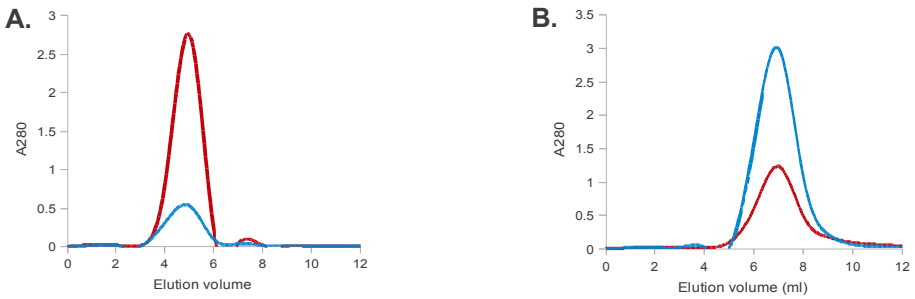

Figure 5.4 Affinity purification profiles for anti-*P. yoelii* (KTC) and -*P. falciparum* (NKG) Cox17 antibodies

Representative purification profiles of antibodies raised against the KTC (**A**) and NKG (**B**) peptides are shown above. Shown in all panels are the purification profiles for antibodies purified from eggs collected 4 to 8 weeks post-inoculation of chicken 1 (—) and chicken 2 (—).

5.2.3 Recombinant expression of *P. yoelii and P. falciparum* Cox17

Using recombinant *P. yoelii* and *P. falciparum* Cox17, the *in vitro* and *in vivo* copper binding ability of each protein was to be examined. The BCA release assay was again used to detect bound copper (Brenner and Harris, 1995). Preparation of the parasite Cox17 expression constructs followed the strategy outlined for expression of the amino terminal domain of the parasite copper transport proteins (Figure 4.9). Following PCR amplification of the *P. yoelii* and *P. falciparum* Cox17 coding domains (Figure 5.1), the PCR products were gel purified and ligated into a pGEM®-T cloning vector. These constructs were transformed into *E. coli* JM109 cells, positive colonies identified and the plasmid isolated. The *P. yoelii* Cox17 insert was excised by *Eco*RI and *Not*I digestion, whilst the *P. falciparum* insert was excised by *Bam*HI and *Not*I digestion. Each insert was gel purified and ligated into a pET expression vector digested with the corresponding restriction enzymes. Initial attempts at recombinant expression of His_6-*Py*Cox17 and His_6-*Pf*Cox17 made use of the pET23a and pET28a vectors transformed into *E. coli* BL21(DE3) cells.

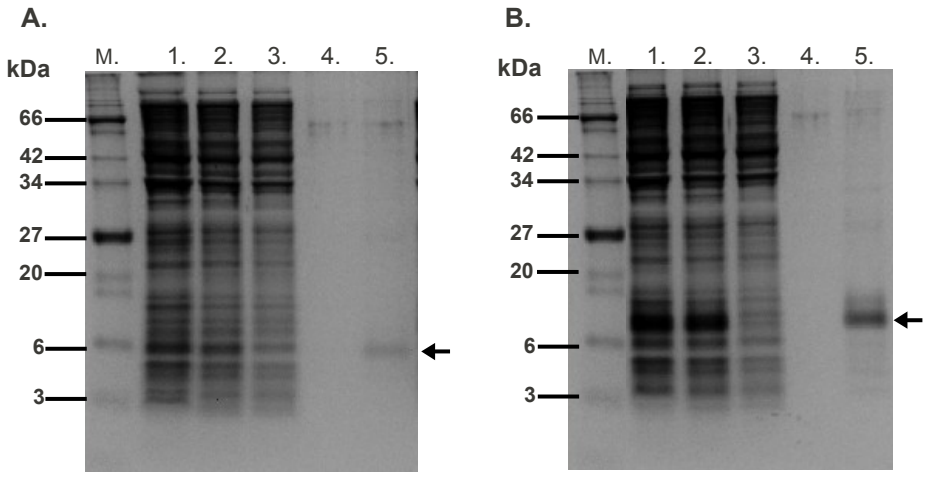

Figure 5.5 Pilot expression and small-scale purification of recombinant His_6-*Py*Cox17

His_6-*Py*Cox17 expressed from the pET23a (**A**) and pET28a (**B**) vectors. All samples were analysed by 10% Tricine-SDS-PAGE. In A and B: lane 1, total cell protein; lane 2, soluble fraction; lane 3, unbound protein fraction; lane 4, resin wash eluate and lane 5, Ni-NTA bound protein. Molecular mass markers (**M**) are on the left of each gel (see materials and methods for details).

In initial screening, His_6-*Py*Cox17 was expressed as a soluble protein by both the pET23a and pET28a vectors (Figure 5.5), whilst His_6-*Pf*Cox17 expression was not detected (data not shown). Small-scale experiments with the pT-*Py*Cox17 constructs suggested higher expression levels for the pET28a construct (Figure 5.5b). This difference was not apparent in larger scale preparations, hence the pET23a construct was selected for further studies. The pET23a-expressed product was approximately 11.6kDa in size (Figure 5.5a), which is larger than its predicted size but is a similar finding to that reported for purified yeast Cox17 (Beers *et al.*, 1997).

Table 5.1 Confirmation of *Pf*Cox17 amplicon ligation into expression vectors

	Insert presence confirmed by:		
	*Bam*HI digestion	PCR	
		pET primers	*Pf*Cox17-specific
pET23a	✔	✔	✔
pET28a	✔	✔	✔
pGex-4T-1	✔	✔	✔

Reasons for the apparent lack of His_6-*Pf*Cox17 expression by the pET vectors were not understood. Ligation of the *Pf*Cox17 coding domain into the two pET vectors was confirmed by *Bam*HI digestion, PCR using pET- and *Pf*Cox17-specific primers (Table 5.1), and sequencing the amplicon (Figure 5.2b). Altering the fermentation conditions made no difference to His_6-*Pf*Cox17 expression (data not shown). A new *Pf*Cox17 expression construct was therefore prepared using the pGex-4T-1 vector, producing a GST-fusion protein.

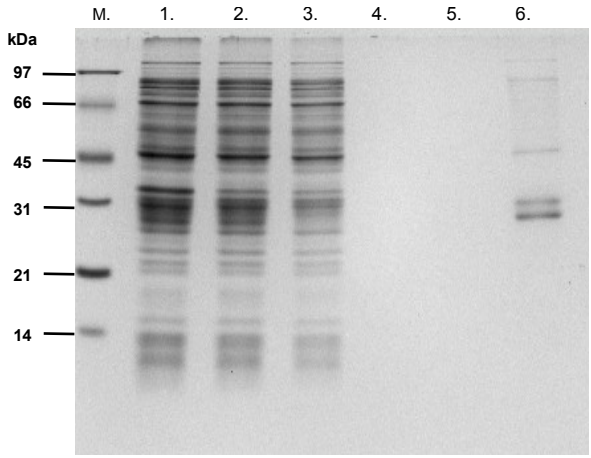

Figure 5.6 Pilot expression and small-scale purification of recombinant GST-*Pf*Cox17

12.5% SDS-PAGE analysis of GST-*Pf*Cox17 expression. Lane 1, total cell protein; lane 2 soluble fraction; lane 3, unbound protein fraction; lanes 4 and 5, resin wash eluate; lane 6, glutathione agarose-bound protein. Molecular mass markers are on the left of each gel (see materials and methods for details).

GST-*Pf*Cox17 expression required that the *Pf*Cox17 coding sequence was excised from a pGEM®-T cloning vector by *Bam*HI and *Not*I digestion, gel purified and ligated into a *Bam*HI-*Not*I digested pGex-4T-1 expression vector. The construct was then transformed into *E. coli* BL21 host cells and screened for the expression of the GST-*Pf*Cox17 fusion protein. Successful ligation was confirmed by *Bam*HI digestion and PCR amplification (Table 5.1). GST-*Pf*Cox17 was expressed as a soluble protein and purified by small-scale glutathione-agarose affinity chromatography (Figure 5.6). The two prominent expression products were approximately 33.5kDa and 30.3kDa in size, respectively, where the larger of the two corresponded to the predicted size for GST-*Pf*Cox17. The smaller protein may be a truncated product. The BL21 host cells used are protease deficient suggesting the smaller proteins are unlikely to be the result of proteolysis (Figure 5.6).

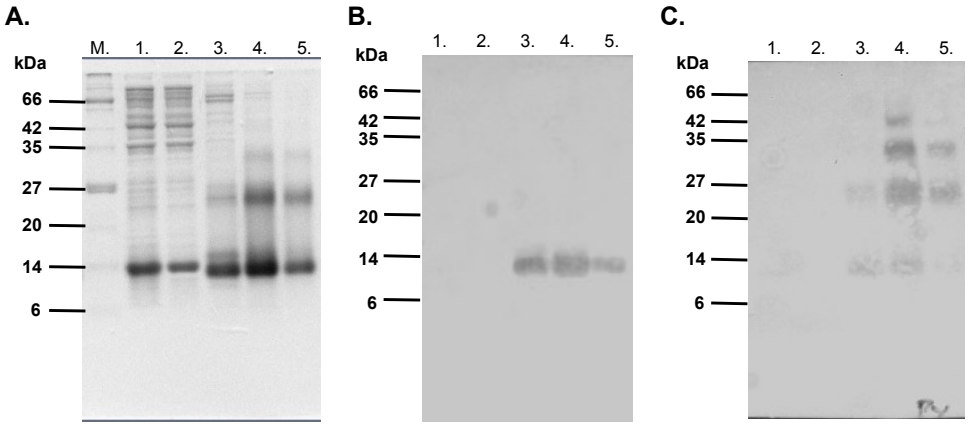

Figure 5.7 Recombinant expression and affinity purification of His_6-*Py*Cox17

10% Tricine-SDS-PAGE analysis of affinity purified His_6-*Py*Cox17 (**A**), detected with an anti-His_6 antibody (**B**) and anti-KTC anti-peptide antibody (**C**) following blotting to nitrocellulose. Lane 1, soluble cell lysate; lane 2, unbound protein fraction; lanes 3 – 5, protein eluate from Ni-NTA affinity matrix. Molecular mass markers (**M**) are on the left of each gel (see materials and methods for details).

For the expression of His_6-*Py*Cox17 it was found that induction with 0.4 mM IPTG, for 4 hours, at 37°C was optimal, whilst for GST-*Pf*Cox17 induction with 0.5 mM IPTG, for 4 hours, at 37°C was optimal (data not shown). Each construct was then prepared for large-scale expression and purification of the recombinant protein. Following cell lysis, each recombinant protein was affinity purified using the Ni-NTA matrix for His_6-*Py*Cox17 (Figure 5.7) and glutathione-agarose for GST-*Pf*Cox17 (Figure 5.8). His_6-*Py*Cox17 yields were 3.95 mg and GST-*Pf*Cox17 6.87 mg protein per 500 ml of culture. The identity of each recombinant protein was confirmed by western blot. Purified His_6-*Py*Cox17 was detected by both an anti-His_6 and anti-KTC anti-peptide antibody (Figure 5.7) and GST-*Pf*Cox17 was detected by an anti-GST and anti-NKG anti-peptide antibody (Figure 5.8). The His_6-*Py*Cox17 bands of a higher molecular weight than the monomeric species are likely to represent multimers. Although less evident, GST-*Pf*Cox17 also produced multimeric species (Figure 5.8).

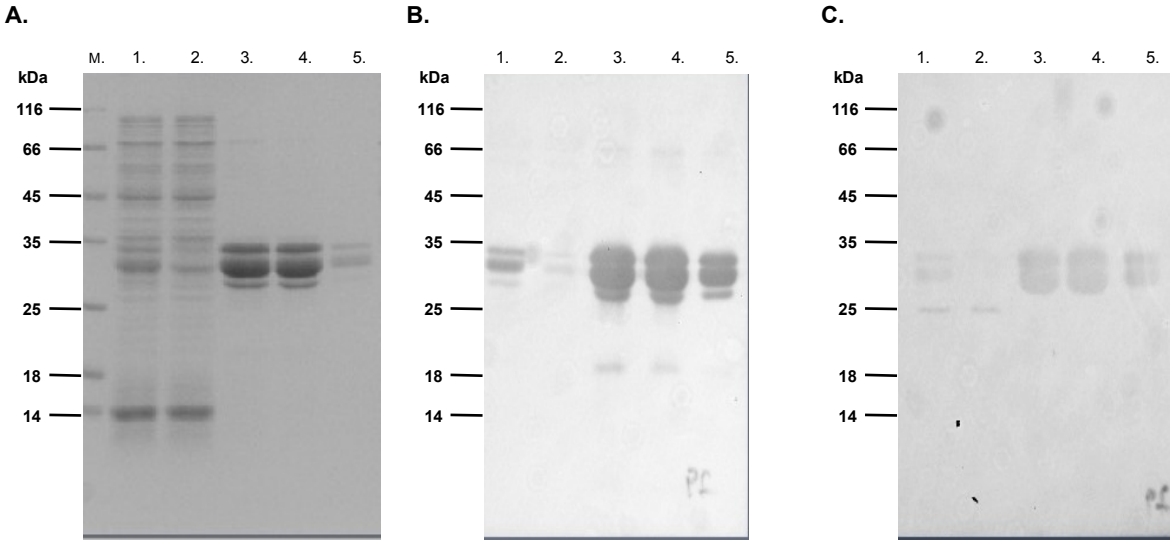

Figure 5.8 Recombinant expression and affinity purification of GST-*Pf*Cox17

12.5% SDS-PAGE analysis of affinity purified GST-*Pf*Cox17 (**A**), detected by an anti-GST antibody (**B**) and anti-NKG (**C**) anti-peptide antibody following blotting to nitrocelulose. Lane 1, soluble cell lysate; lane 2, unbound protein fraction; lanes 3 – 5, protein eluate from glutathione-agarose affinity matrix. Molecular mass markers (**M**) are on the left of each gel (see materials and methods for details).

5.2.4 Copper binding studies with His_6-*Py*Cox17 and GST-*Pf*Cox17

Recombinant *S. cerevisiae* and *H. sapiens* Cox17 have been reported to bind copper *in vivo* (Heaton *et al.*, 2001; Srinivasan *et al.*, 1998; Takahashi *et al.*, 2002; Voronova *et al.*, 2007a). Similar experiments have been undertaken for His_6-*Py*Cox17 and GST-*Pf*Cox17. Briefly, for the *in vitro* study of copper binding, 10 µM purified recombinant protein was incubated with a 20-fold molar excess of copper in the presence of DTT and ascorbic acid, which acts as the reducing agent. Ascorbic acid was included to ensure that copper is reduced and maintained in the cuprous state, whilst DTT promotes the partial reduction of the labile Cox17 disulfide bond

(Banci *et al.*, 2008b). These conditions were used to emulate the reducing environment of the cell cytosol. Following overnight dialysis, protein-bound copper was detected using the copper-specific BCA release assay (Brenner and Harris, 1995). The BCA release assay was conducted on duplicate samples with or without the inclusion of ascorbic acid (Figure 5.9, solid and open bars, respectively) to identify the oxidative state of the bound copper. Similar to the previous results (Chapter 4), both His_6-*Py*Cox17 and GST-*Pf*Cox17 could be reconstituted with Cu^+ *in vitro* as seen following protein incubation with $CuCl_2$ in the presence of DTT and ascorbic acid (Figure 5.9a, **+**). The binding of the Cu^+ ion, to both recombinant proteins, was supported by omitting ascorbic acid from the BCA release assay, which resulted in the formation of a detectable purple BCA-Cu^+ complex (Figure 5.9a, **+**, open bars).

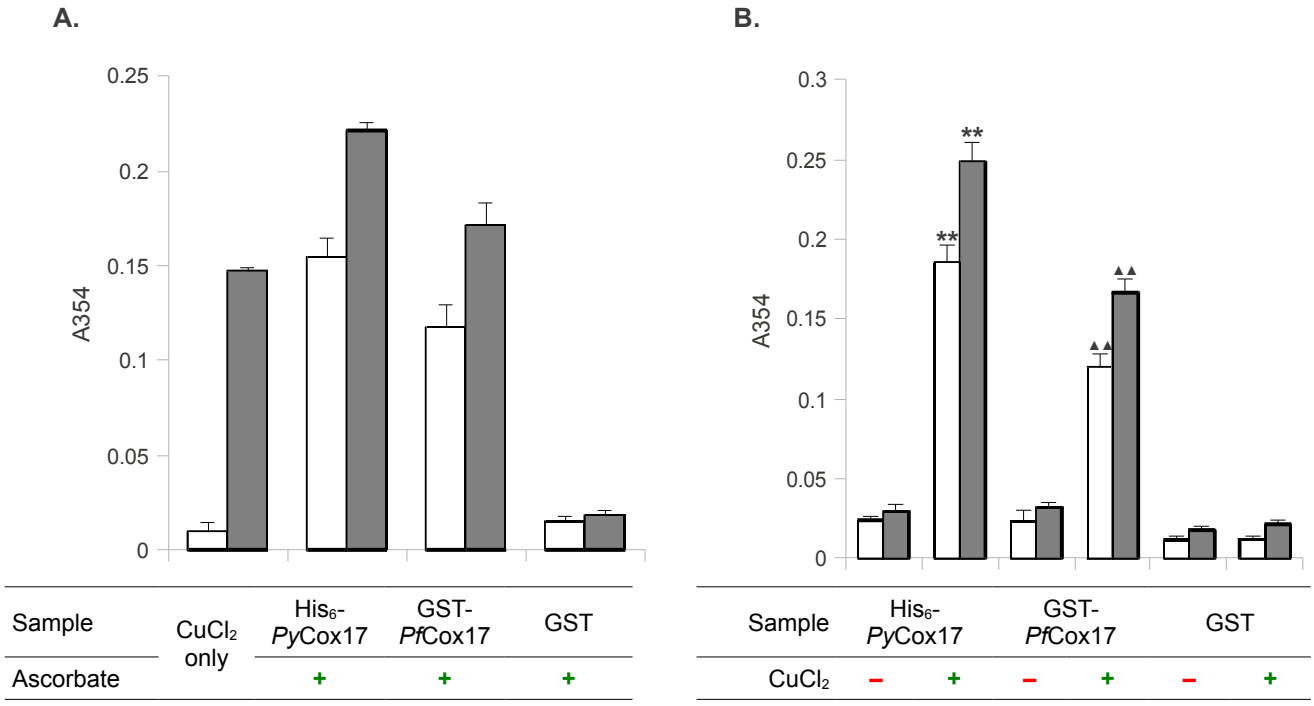

Figure 5.9 Copper binding to His_6-*Py*Cox17 and GST-*Pf*Cox17 *in vitro* and *in vivo*

Copper binding was analysed **A** *in vitro* and **B** *in vivo*. (**A**) 10 µM affinity purified protein was incubated with $CuCl_2$ in the presence (**+**) of ascorbic acid. The standard BCA release assay was altered to test for bound copper in the presence (solid bars) or absence (open bars) of ascorbic acid. The BCA-Cu^+ complex was detected at 354 nm. The concentration of the copper standard ($CuCl_2$ only) was equimolar to the amount of protein used. (**B**) 0.5 mM $CuCl_2$ was added to the cell growth medium after induction of recombinant protein expression. Following affinity purification bound copper was detected by the BCA release assay with (solid bars) or without (open bars) the addition of ascorbic acid and the BCA-Cu^+ complex detected at 354 nm. ****** (for His_6-*Py*Cox17) and ▲▲ (GST-*Pf*Cox17) denote statistical significance as determined by Student's *t*-test (p-value <0.05). Results are means ± S.E. of triplicate measurements from each duplicate dialysis bag.

Copper binding to His_6-*Py*Cox17 and GST-*Pf*Cox17 was also evaluated *in vivo.* As before (Chapter 4), copper binding *in vivo* was determined by expressing the two recombinant proteins in the presence or absence of 0.5 mM $CuCl_2$. Bound copper was detected using the BCA release assay. Following affinity purification and dialysis, His_6-*Py*Cox17 and GST-*Pf*Cox17 were

shown to bind copper *in vivo* (Figure 5.9b), with the addition of extracellular copper producing a statistically significant increase in the amount of copper detected (p-value <0.05). The oxidation state of the bound copper was determined by including (Figure 5.9b, solid bars) or omitting (Figure 5.9b, open bars) ascorbic acid from the BCA release assay. His_6-*Py*Cox17 and GST-*Pf*Cox17 bound Cu^+ *in vivo* (Figure 5.9b). Interestingly, when the *in vitro* and *in vivo* data are compared, a similar amount of copper was found to be bound to these two proteins under the two conditions tested (Figure 5.9). Copper did not bind to the GST carrier protein (Figure 5.9) thereby indicating that copper binding was specific to the *Pf*Cox17 partner protein.

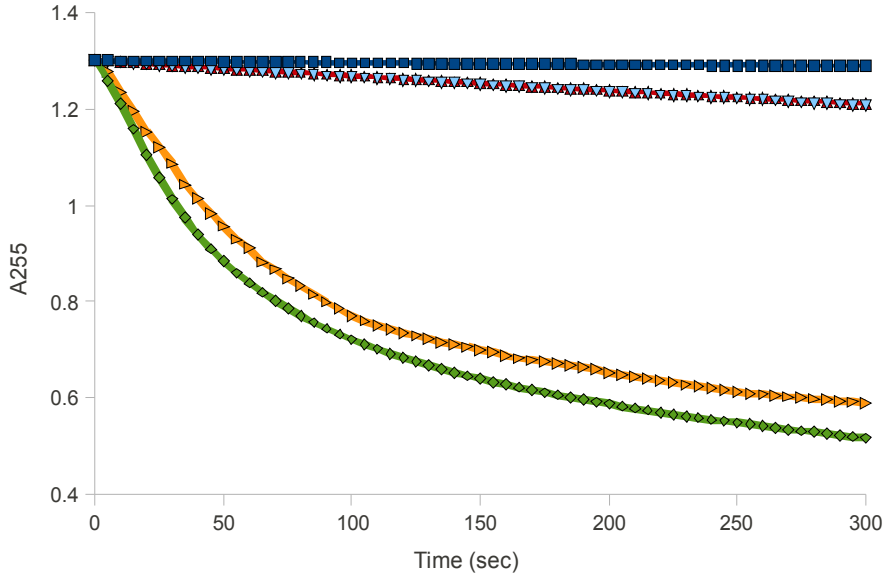

Figure 5.10 Copper-catalysed oxidation of ascorbic acid is inhibited by His_6-*Py*Cox17 and GST-*Pf*Cox17

A 120 µM solution of ascorbic acid (H_2Asc) at pH 4.5 (■). Addition of 8 µM $CuCl_2$ to the H_2Asc solution (♦). His_6-*Py*Cox17 (▼), GST-*Pf*Cox17 (▲) and GST carrier protein (►) added to the H_2Asc-copper solution.

As before, the effect that the recombinant proteins had on copper-catalysed ascorbic acid oxidation was examined by monitoring the loss of absorbance, at 255 nm, of a 120 µM ascorbic acid solution at pH 4.5. This pH was selected for reasons previously described (Section 4.2.4). As expected, the control reaction, with freshly prepared ascorbic acid, showed a persistent absorbance at 255 nm (A_{255}) over a period of 300 seconds, indicative of the stability of the solution to aerial oxidation (Figure 5.10, ■). Upon the addition of 8 µM $CuCl_2$, the A_{255} signal was found to decrease thereby highlighting the catalytic oxidation of ascorbic acid by copper (Figure 5.10, ♦). The copper-catalysed oxidation of ascorbic acid was, however, inhibited by the addition of 5 µM of purified His_6-*Py*Cox17 (Figure 5.10, ▼) or GST-*Pf*Cox17 (Figure 5.10, ▲). The presence of either recombinant protein results in only a slight decrease in ascorbic acid stability over time, compared to the dramatic decrease seen when $CuCl_2$ is added. This indicates that both His_6-*Py*Cox17 and GST-*Pf*Cox17 chelate copper in solution, thus preventing its participation in the redox cycle. Taken together with the previous copper binding results

(Figure 5.9), it is presumed that both proteins chelate the cuprous ion in solution thereby shifting the rate-limiting step to equation 2 of this redox cycle (Figure 4.23). Interestingly, for the ascorbate oxidation assay, His_6-*Py*Cox17 and GST-*Pf*Cox17 produce a very similar result (Figure 5.10). This was in contrast to the differences observed for the *in vitro* and *in vivo* copper-binding assays (Figure 5.9). Overall these studies suggest that both proteins bind Cu^+ in solution. This is in agreement with findings for other Cox17 metallochaperones, such as *S. cerevisiae* Cox17 (Abajian *et al.*, 2004; Beers *et al.*, 1997; Palumaa *et al.*, 2004; Voronova *et al.*, 2007b).

5.3 Discussion

The copper metallochaperone Cox17 was first identified in *S. cerevisiae* as an essential component for cytochrome-c oxidase assembly (Glerum *et al.*, 1996). Cox17 is a small, cysteine-rich protein that has been reported to bind between one and four Cu^+ ions (Abajian *et al.*, 2004; Arnesano *et al.*, 2005; Voronova *et al.*, 2007a). Based on its localisation, Cox17 was initially implicated in shuttling copper from the cytosol to the mitochondrion (Beers *et al.*, 1997). However, this idea was revisited when it was found that Cox17 was still effective in copper delivery to cytochrome-c oxidase when tethered to the mitochondrial intermembrane space (Maxfield *et al.*, 2004). Although the precise mechanism of copper delivery to the mitochondrion is not fully understood, the importance of Cox17 function to yeast and mammalian cell survival is well documented (Glerum *et al.*, 1996; Takahashi *et al.*, 2002). The identification of a putative *Plasmodium* spp. Cox17 metallochaperone sequence (Table 3.1) suggested that malaria parasites might use similar pathways for cytochrome-c oxidase assembly. This was supported by the presence of both Sco1 and Cox11 parasite orthologs (Table 3.1). In this study recombinant *P. yoelii* and *P. falciparum* Cox17 proteins were shown to bind copper.

5.3.1 Confirmation of a putative *Plasmodium* Cox17 copper metallochaperone coding sequence

A putative Cox17 protein sequence was identified in eight species of the *Plasmodium* parasite following a BLASTp screen of PlasmoDB with the *A. thaliana* Cox17 sequence (Section 3.2.4). The presence of essential amino acid residues, in each retrieved sequence, suggested a copper binding role (Figure 3.6). The *P. yoelii* and *P. falciparum* Cox17 coding domains were PCR amplified and sequenced, with each sequence showing 100% identity to the corresponding PlasmoDB sequences (Figure 5.2). Sequencing of the PCR products confirmed the presence of an open reading frame for parasite Cox17. To detect native malarial parasite Cox17, the anti-peptide antibodies generated in this study (Section 5.2.2) were used in immunoprecipitation and blotting experiments. For both *P. yoelii* and *P. falciparum* the detection

of native Cox17 was, however, unsuccessful. Reasons for this remain unknown, but were thought to either pertain to the relative expression levels of parasite Cox17 or to target protein degradation.

Analysis of the putative *P. falciparum* Cox17 metallochaperone gene (PF10_0252) transcription levels show consistent levels throughout the parasite's life cycle (Figure 3.8c). In comparison to the reference protein, lactate dehydrogenase, Cox17 transcription is approximately 5-fold less. The low expression levels may reflect a tight homoeostatic regulation of cellular copper, similar to that observed in other systems (Lutsenko, 2010). However, a consequence of this decreased protein expression is an associated difficulty in detecting the native protein. As mentioned, attempts were made to detect *P. yoelii* and *P. falciparum* Cox17 by immunoprecipitation, similar to the approach previously used for the characterisation of *P. falciparum* protein kinases (Merckx *et al.*, 2003). However, no signal was detected on a western blot of the immunoprecipitate. Although native Cox17 immunoprecipitation was unsuccessful, parasite LDH has been precipitated using this same method in the laboratory as has recombinant His_6-*Py*Cox17 and GST-*Pf*Cox17 (data not shown). For parasite lysate preparation care was also taken with reducing agents, excessive detergent concentrations or extremes in pH that can interfere with antibody-antigen interactions (Immunoprecipitation troubleshooting guide, Stressgen Biotechnologies Corp.).

Protease inhibitors were included in the lysis buffer to reduce proteolysis, which can interfere with target protein detection. The solution structure of *S. cerevisiae* Cox17 established that the protein has a structural organisation with an α-helical hairpin preceded by an unstructured amino terminal segment of approximately 20 amino acids (Abajian *et al.*, 2004). Considering the conservation of essential amino acids within the *Plasmodium* spp. Cox17 sequences (Figure 3.5), it is presumed these proteins would have a similar structure and fold to yeast and human Cox17 as suggested by the homology model of *Pf*Cox17 (Figure 3.6). This makes the amino terminal segment of these proteins particularly prone to degradation, which may then contribute to the lack of parasite Cox17 detection due to a loss of the targeted epitope.

5.3.2 Recombinant expression of the putative *P. yoelii* and *P. falciparum* Cox17 metallochaperones

The function of a hypothetical *Plasmodium* protein is determined using a thorough biochemical analysis (Birkholtz *et al.*, 2008). Isolating sufficient quantities of native protein from malaria parasites, for functional studies, is difficult. The heterologous expression of *P. yoelii* and *P. falciparum* Cox17 was therefore pursued using *E. coli* as the expression host. Interestingly,

despite the sequence similarity of *Py*Cox17 and *Pf*Cox17, expression of these proteins as His-tagged proteins yielded different results. His_6-*Py*Cox17 was successfully expressed from two pET vectors (Figure 5.3), whereas the expression of His_6-*Pf*Cox17 from the same two vectors was unsuccessful. This result perhaps highlights the 'power of orthologues' as described by Vedadi *et al*. (2007). In this study seven Apicomplexan genomes were regarded as a 'super genome'. Heterologous expression of proteins from multiple Apicomplexan genomes yielded at least twice the percentage of purified proteins, crystals and structures than that obtained from *P. falciparum* alone (Vedadi *et al.*, 2007). This therefore suggests that the problem with *Pf*Cox17 expression could be related to certain properties of its coding sequence, such as the presence of rare codons or an A+T bias in the coding sequence (Birkholtz *et al.*, 2008). Recent studies have, however, suggested that the A+T bias in *Plasmodium* sequences has less of an impact on heterologous expression than originally thought (Mehlin *et al.*, 2006; Vedadi *et al.*, 2007).

Rare codons are known to affect heterologous protein expression due to differences in codon usage between the *E. coli* host and heterologous target gene. These differences can impede translation due to the demand for one or more tRNAs that may be rare or lacking in the *E. coli* population (Makrides, 1996). In this regard the presence of AGA and AGG codons, encoding arginine, have proven most problematic (Kurland and Gallant, 1996). Analysis of the *Py*Cox17 and *Pf*Cox17 coding sequences identified an equal number of these particular codons in each sequence. In addition, these arginine codons were located at similar positions in each sequence. Interestingly, when other rare codons were taken into account it was found that the *Py*Cox17 coding sequence contained a higher percentage of these codons. One significant difference between the two coding domains though, is the presence of a doublet of rare codons within the first 10 amino acids of the *Pf*Cox17 sequence and not the *Py*Cox17 sequence. Clusters of rare codons, such as doublets or triplets, can create translational errors. These errors include mistranslational amino acid substitutions, frameshifting events or premature translational termination (Sørensen and Mortensen, 2005a). Dramatic translational errors are generally expressed as a failure to produce a complete canonical copy of a target protein, resulting in the production of truncated products (Kurland and Gallant, 1996). Following GST-*Pf*Cox17 expression, truncation of the full-length fusion protein was observed (Figure 5.8). Considering the same coding sequence was used for His_6-*Pf*Cox17 and GST-*Pf*Cox17 expression, the truncation of GST-*Pf*Cox17 suggests the rare codon doublet may have contributed to the inability to detect His_6-*Pf*Cox17 expression.

Fusion to soluble carrier proteins, such as glutathione S-transferase (GST) and maltose binding protein (MBP), can improve the folding of inherently insoluble, unstable or unfolded proteins

(Kapust and Waugh, 1999; Makrides, 1996; Nallamsetty and Waugh, 2007). In this instance, a GST carrier protein was selected since yeast and mammalian Cox17 have been successfully expressed as GST-fusions (Srinivasan *et al.*, 1998; Takahashi *et al.*, 2002). Fusion of *Pf*Cox17 to GST was found to assist protein expression (Figure 5.8). This supports the suggestion that the elevated expression of an amino-terminal fusion partner can be transferred to a poorly expressing passenger protein as a result of mRNA stabilisation (Sørensen and Mortensen, 2005b). Successful GST-*Pf*Cox17 expression suggests that the presence of a rare codon doublet had little influence on expression since this was still present in the fusion construct. Analysis of affinity purified His_6-*Py*Cox17 (Figure 5.7) and GST-*Pf*Cox17 (Figure 5.8) samples identified the presence of multimeric species. Similar results have been observed for human and yeast Cox17, which exist in a dimeric and tetrameric state that inter-convert in a concentration-dependent manner (Heaton *et al.*, 2001; Voronova *et al.*, 2007a).

5.3.3 Copper binding to His_6-*Py*Cox17 and GST-*Pf*Cox17

Mammalian Cox17, which contains six conserved cysteine residues, can in principle exist in three different oxidation states; the fully oxidised protein with three disulfide bonds ($Cox17_{3S\text{-}S}$), a partially oxidised form with two disulfide bonds ($Cox17_{2S\text{-}S}$) or a fully reduced state where no disulfide bonds ($Cox17_{0S\text{-}S}$) are present (Palumaa *et al.*, 2004; Voronova *et al.*, 2007a). These various forms of Cox17 have been found to differ in their copper binding ability. The partially oxidised state binds a single Cu^+ ion, whereas the fully oxidised state cannot bind copper (Palumaa *et al.*, 2004). On the other hand, the fully reduced form of Cox17 contains six free cysteine residues that cooperatively bind four Cu^+ ions to form a tetracopper-thiolate cluster (Arnesano *et al.*, 2005; Palumaa *et al.*, 2004; Voronova *et al.*, 2007b). Recombinant bacterial expression of human Cox17, in an unaltered cellular redox environment, was found to yield three almost equally populated redox states corresponding to $Cox17_{2S\text{-}S}$, $Cox17_{1S\text{-}S}$ and $Cox17_{0S\text{-}S}$ (Voronova *et al.*, 2007b). Based on copper transfer studies, the preferred cellular redox state of Cox17 appears to be the partially oxidised state, $Cox17_{2S\text{-}S}$ (Banci *et al.*, 2008a). This state can been attained, *in vitro*, by treating purified Cox17 with millimolar concentrations of DTT since Cox17 contains two stable disulfide bonds and one labile bond that is susceptible to reducing agents (Arnesano *et al.*, 2005; Banci *et al.*, 2008b; Voronova *et al.*, 2007a). Purified His_6-*Py*Cox17 and GST-*Pf*Cox17 were therefore treated similarly to promote this redox state ($Cox17_{2S\text{-}S}$) for *in vitro* copper binding studies.

Analysis of *in vitro* copper binding to His_6-*Py*Cox17 and GST-*Pf*Cox17 revealed both proteins could bind copper following protein purification (Figure 5.9a). The differences in copper binding between the His_6-tagged and GST-fusion proteins has also been reported for yeast Cox17

(Heaton *et al.*, 2001; Srinivasan *et al.*, 1998). GST-tagged yeast Cox17 bound two molar equivalents of Cu^{+} (Srinivasan *et al.*, 1998) whilst untagged Cox17 bound three molar equivalents (Heaton *et al.*, 2001). This was suggested to be a result of the obligate dimeric state of GST (Heaton *et al.*, 2001). An important difference between the present study, and those with yeast Cox17, is that copper binding was examined *in vivo* for yeast Cox17. Therefore another explanation for the differences (Figure 5.9a) is that a mixed distribution of protein redox states was created, following DTT treatment, thereby causing differences in copper binding. Alternatively, DTT itself may have leached bound copper from the recombinant protein, similar to what was observed for Cu_4Cox17 when DTT was used at supramillimolar concentrations (Palumaa *et al.*, 2004). A further possibility is that these differences relate to truncated GST-*Pf*Cox17 accounting for part of the 10 μM protein solution. This could have reduced the amount of protein able to bind copper in solution.

His_6-*Py*Cox17 and GST-*Pf*Cox17 were also found to bind copper in a cellular environment (Figure 5.9b). A comparison of the *in vivo* data with the *in vitro* reconstitution of each protein indicated a similar difference between proteins with regard to the amount of copper bound. GST dimerisation may have contributed to these differences, as reported for yeast Cox17, since it can result in a non-native conformer of Cox17 being induced by Cu^{+} binding (Heaton *et al.*, 2001). It is also possible that copper ions bound *in vivo* were lost during purification and dialysis, as reported for native yeast Cox17 purification (Beers *et al.*, 1997). Through a slight modification of the BCA assay it was shown that both recombinant proteins bound the cuprous ion under the two conditions examined. This finding is in agreement with the preferred redox state of copper bound to mammalian and yeast Cox17 (Abajian *et al.*, 2004; Banci *et al.*, 2008b; Beers *et al.*, 1997; Palumaa *et al.*, 2004).

The ascorbic acid oxidation assay has previously been used to demonstrate the copper binding ability of a methionine peptide (Jiang *et al.*, 2005) and was used to demonstrate copper binding to the amino terminal domains of the *P. berghei* and *P. falciparum* copper transporters (Section 4.2.4). Ascorbic acid is stable to aerial oxidation, but the presence of metal ions, such as iron or copper, catalyse its oxidative degradation (Jiang *et al.*, 2005). The oxidation rate of ascorbic acid can be monitored between 245 and 265 nm (Buettner, 1988). Conveniently the oxidation rate of ascorbate is known to decrease in the presence of metal chelators with slower oxidation rates indicative of more stable chelates (Khan and Martell, 1967). Metal chelation by the *Plasmodium* copper transporters was thought to be via methionine motifs present in the protein sequence, but this was not confirmed. *Plasmodium* Cox17 recombinant proteins are predicted to coordinate copper via a similar cysteine motif to that found in yeast Cox17 (Abajian *et al.*, 2004).

The ability of His_6-*Py*Cox17 and GST-*Pf*Cox17 to inhibit copper-catalysed ascorbic acid oxidation was tested *in vitro* (Figure 5.10). Both proteins inhibited ascorbate oxidation and showed a near identical decrease in the oxidation rate. The reduction in the oxidation rate suggests stable chelation of what is presumed to be the cuprous ion. Although the ascorbate UV-vis assay alone does not prove the preferred copper oxidation state for these *Plasmodium* proteins, when analysed in conjunction with the previously described *in vivo* assay it suggests the cuprous ion is the preferred substrate. Given the reducing potential of both the prokaryotic and eukaryotic cell cytoplasm (Schafer and Buettner, 2001) it is predicted that the Cu^+ ion is the likely oxidation state in which copper would be found within the cell (Davis and O'Halloran, 2008). A similar reducing cytoplasmic environment has been identified for the *Plasmodium* parasite (Krnajski *et al.*, 2001). If copper is present in a reduced state within the parasite cytoplasm, it is the likely substrate for cytoplasmic copper-requiring proteins. Parasite Cox17 is presumed to be located in the cytoplasm based on previous findings (Beers *et al.*, 1997).

In the present study *P. yoelii* and *P. falciparum* Cox17 were recombinantly expressed and shown to bind copper, but further protein characterisation is necessary. Firstly, native parasite Cox17 requires localisation using an antibody-mediated approach. This can be achieved using confocal and/or transmission electron microscopy. Alternatively, Cox17 localisation could be determined by attaching it to a fluorescent GFP-tag. Secondly, to assist with establishing protein function, *Plasmodium* Cox17 could be used in a yeast functional complementation system using *cox17Δ* cells. Thirdly, site-directed mutatgenesis could be employed to help identify the amino acid residues important for Cox17 structure and function. A final possibility would be to attempt producing protein crystals of *Plasmodium* Cox17, with and without bound copper, to help establish the protein's copper binding properties in more detail.

CHAPTER 6

General discussion

6.1 Introduction

Malaria is a devastating disease caused by single-celled parasites belonging to the *Plasmodium* genus. *P. falciparum* is responsible for the most severe form of the disease. Not only is malaria a major cause of child mortality in the developing world, but it is also a large contributor to economic hardship in endemic countries, particularly those within sub-Saharan Africa. The complexity of the parasite's life cycle has hindered the development of an effective malaria vaccine, with no commercial vaccine currently available (Crompton *et al.*, 2010). Apart from vaccination with radiation-attenuated *P. falciparum* sporozoites (Hoffman *et al.*, 2002), the most promising vaccine candidate has been the RTS,S vaccine (Casares *et al.*, 2010; Stoute *et al.*, 1997; Sun *et al.*, 2003). With regard to disease control, an additional problem being faced is the emergence of drug-resistant parasite strains. This has led to searches for new antimalarial drug targets, which has been enhanced by the complete sequencing of a number of *Plasmodium* spp. genomes (Carlton *et al.*, 2002; Carlton *et al.*, 2008; Gardner *et al.*, 2002; Pain *et al.*, 2008). Presently, the front-line approach for the treatment of malaria is artemisinin-based combination therapy (World malaria report, 2010).

To prevent malaria transmission, the World Health Organisation (WHO) recommends the use of insecticide-treated bed nets and indoor residual spraying using WHO-approved chemicals including DDT. In endemic countries, indoor residual spraying remains one of the main interventions for reducing and interrupting malaria transmission through vector control (World malaria report 2010). In areas of high disease transmission it is also recommended that intermittent preventative treatment regimes be implemented, particularly for pregnant women. Confirmed cases of uncomplicated *P. falciparum* malaria should be immediately treated with an artemisinin-based drug combination, whilst *P. vivax* infections should be treated with chloroquine where it still remains effective (World malaria report, 2010). For *P. vivax* infections it is also recommended that treatment is combined with a 14-day course of primaquine to prevent relapse. Due to the potential emergence of parasite resistance to artemisinins (Dondorp *et al*., 2009; Noedl *et al*., 2008), artemisinin-based monotherapies are being withdrawn from the market to be replaced by combination therapies (World malaria report 2010). Monitoring the efficacy of currently employed antimalarials is important for reducing the spread of drug resistance, however, there is still a pressing need for novel drug and drug target identification. In this regard, a class of parasite proteins gaining increased attention are the membrane transport proteins (Kirk and Saliba, 2007; Martin *et al*., 2009a; Staines *et al*., 2010).

In a related protozoan parasite, *Theileria parva*, a membrane-bound protein (the polymorphic immunodominant molecule) has been established as a potential diagnostic and therapeutic target (Toye *et al.*, 1996). In the current study, a *Plasmodium* ortholog to this protein was identified and found to possess features suggestive of a role as a copper transport protein (Chapter 3). In yeast and mammalian cells the copper transport protein functions to acquire extracellular copper and transport it into the cell (Kim *et al.*, 2008; Lutsenko, 2010). This transporter plays an important role since copper is an essential micronutrient for all living organisms. Considering the importance of copper transport, it would stand to reason that inhibiting a putative *Plasmodium* parasite copper transporter could prove effective for targeted drug inhibition. Supporting this idea was the finding that the intracellular copper chelator, neocuproine, inhibits *P. falciparum* growth *in vitro* (Rasoloson *et al.*, 2004). However, limited information is currently available regarding *Plasmodium* parasite proteins involved in copper homeostasis. The identification of a parasite mechanism for copper excretion (Rasoloson *et al.*, 2004), suggested an opposing mechanism for copper acquisition is likely to exist. A mechanism not yet considered for this process, is copper acquisition via a dedicated copper transport protein. Therefore the primary aim of the present study was to identify and characterise a *Plasmodium* parasite copper transport protein and in addition, it was endeavoured to identify and characterise an associated copper metallochaperone.

6.2 Identification of *Plasmodium* parasite copper-requiring protein orthologs

Sequencing the *P. falciparum* genome (Gardner *et al*., 2002) has enabled a great deal of research that was previously not possible. One such example is the establishment of a protozoan parasite structural genomics project (www.sgpp.org). The availability of the *P. falciparum* genome sequence has the potential to reveal novel drug targets as well as genes important for parasite biology and pathogenesis. Of the approximately 5,300 *P. falciparum* genes identified, comparatively few have been confirmed to code for protein (Mehlin *et al.*, 2006; Singh *et al.*, 2010; Tuteja, 2007). However, only a couple of these protein-encoding genes are suggested to encode proteins that interact with copper (Kita *et al.*, 1998; Rasoloson *et al.*, 2004). In the study by Rasoloson and colleagues (2004), a BLASTp search of PlasmoDB Version 4.0 identified candidate copper metallochaperone orthologs for *P. falciparum* cytochrome-c oxidase and CuP-ATPase. In the present study, a similar BLASTp search, of PlasmoDB Version 7.1, identified the same Cox17 metallochaperone candidate as well as additional co-metallochaperones required for the assembly of mitochondrial cytochrome-c oxidase (Table 3.1) (Cobine *et al.*, 2006a; Horng *et al.*, 2004). In addition, orthologs of the copper-dependent enzyme S-adenosyl-homocysteine hydrolase as well as cytochrome-c

oxidase subunits I, III, Vb and VIb were identified (Table 3.1). Identification of these copper-dependent protein orthologs support the likelihood that the *Plasmodium* parasite requires intracellular copper for its metabolism. However, how the parasite acquires extracellular copper remains uncharacterised.

A BLASTp search of PlasmoDB, with the sequence of the *T. parva* polymorphic immunodominant molecule, identified a candidate copper transport protein sequence in the genomes of eight *Plasmodium* parasite species. An *in silico* analysis of these sequences (Section 3.2.2) identified features characteristic of known copper transporters (Figures 3.1 and 3.2), thereby supporting the possibility that these proteins play a role in parasite copper acquisition. Within yeast cells it was initially assumed that, following copper acquisition, intracellular copper ions were shuttled from the copper transport protein to mitochondrial cytochrome-c oxidase via Cox17 (Beers *et al.*, 1997; Glerum *et al.*, 1996). Although this simple mechanism has since been disputed (Cobine *et al.*, 2006a; Leary *et al.*, 2009; Lutsenko, 2010), the importance of Cox17 to cytochrome-c oxidase assembly remains well documented (Glerum *et al.*, 1996; Takahashi *et al.*, 2002). Identification of a putative *Plasmodium* parasite Cox17 metallochaperone sequence, as well as its associated co-metallochaperones, suggests a similar parasite mechanism for copper loading into cytochrome-c oxidase. To support this possibility the Cox17 sequences were subject to an *in silico* analysis (Section 3.2.4). From this study, characteristic Cox17 sequence features were identified in each retrieved *Plasmodium* sequence (Figure 3.5), thereby supporting the likelihood that this protein functions as a metallochaperone required for cytochrome-c oxidase assembly. In an effort to confirm native expression of the parasite copper transporter and Cox17 metallochaperone, anti-peptide antibodies were raised for use in immunofluorescence and western blotting studies.

6.3 Production of anti-peptide antibodies used for the detection of a *Plasmodium* copper transporter and Cox17 metallochaperone

The availability of the published amino acid sequences for *P. falciparum* and murine malaria parasites enabled the selection of immunogenic peptides from the copper transporter and Cox17 metallochaperone. Peptides were selected using an epitope prediction algorithm (Cármenes *et al.*, 1989) and anti-peptide antibodies were produced in chickens (Figure 4.5 and Figure 5.3). The use of synthetic peptides for antibody production is a useful approach when the native protein cannot be easily isolated and/or purified to homogeneity (Saravanan and Kumar, 2009). Studies carried out in our laboratory have shown that synthetic peptides, coupled to a carrier protein, induce an immunogenic response in chickens producing up to 30 mg of affinity purified anti-peptide antibodies. Chicken antibodies have also been successfully

used for the characterisation of several *P. falciparum* protein kinases (Dorin *et al.*, 2005; Merckx *et al.*, 2003) and lactate dehydrogenase (Hurdayal *et al.*, 2010). The antibodies raised in this study, detected a murine malaria parasite copper transporter in parasite lysates as well as by immunofluorescence microscopy. Detection of the metallochaperone was, however, unsuccessful. Similarly, detection of the *P. falciparum* copper transporter and metallochaperone was unsuccessful in both western blotting and fluorescent microscopy formats. Detection of a murine malaria parasite copper transporter confirms native parasite expression of this protein and supports the possibility of there being a dedicated parasite mechanism for copper acquisition. Localisation of this protein, to what appears to be a parasite membrane, was in agreement with the prediction that the identified protein is an integral membrane protein. This does, however, require confirmation using either co-localisation experiments, transmission electron microscopy or perhaps via transfection studies with a fluorescently tagged protein.

6.4 Recombinant expression of the amino terminal domain of the putative *Plasmodium* spp. copper transporter and full-length Cox17 metallochaperone

An *in silico* analysis of the putative *Plasmodium* parasite copper transporter and Cox17 metallochaperone sequences identified conserved features important for copper binding. For the copper transporter sequences these included important methionine motifs within the extracellular amino terminal domain, whilst the Cox17 proteins were found to contain a conserved CysCysXaaCys copper-binding motif (Figure 3.6). Previous studies, with similar proteins or selected domains thereof, have established the possibility of reconstituting a purified recombinant protein with copper *in vitro* or testing its ability to bind copper *in vivo* by adding copper to the cell growth medium (Heaton *et al.*, 2001; Jensen *et al.*, 1999; Lutsenko *et al.*, 1997; Palumaa *et al.*, 2004; Srinivasan *et al.*, 1998). The successful recombinant expression of the *P. falciparum* CuP-ATPase amino terminal domain, in *E. coli* cells, coupled with the ability of this protein to bind copper *in vitro* and *in vivo* (Rasoloson *et al.*, 2004), supported the use of a similar approach to examine the copper binding ability of the recombinant amino terminal domain of a putative *Plasmodium* sp. copper transporter and full-length putative Cox17 metallochaperone.

Initial attempts at expressing the amino terminal domain of the putative *P. berghei* copper transport protein yielded an insoluble product (Table 4.1). This was overcome by fusing the amino terminal domain to the maltose binding protein (MBP), however, the expressed product appeared to aggregate within the *E. coli* cell cytoplasm. This was likely to be a result of *Pb*CtrNt's high cysteine residue content (Figure 4.13a). This problem was predicted to be overcome by targeting protein expression to the oxidising environment of the cell periplasm, but

this was unsuccessful. This was thought to be due to the presence of a signal sequence in *Pb*CtrNt, which has been reported to interfere with the recombinant expression of *Plasmodium* parasite proteins (Mehlin *et al.*, 2006; Vedadi *et al.*, 2007). These problems were largely overcome when expressing truncated amino terminal domains of two putative *P. falciparum* copper transporters, which specifically lacked the predicted signal peptide. For these proteins, the removal of the predicted signal peptide appeared to assist with targeted protein expression to the *E. coli* cell periplasm (Figure 4.16). Expression within the *E. coli* periplasm appeared to assist the folding of both *P. falciparum* proteins since an absence of high molecular weight aggregates was noted (Figure 4.17). A similar phenomenon, where recombinant protein expression has been assisted, was observed for other cysteine-rich *P. falciparum* proteins when fused to MBP and expressed in the cell periplasm (Outchkourov *et al.*, 2008; Planson *et al.*, 2003).

As with the amino terminal domain of the copper transport protein, both a murine malaria parasite and *P. falciparum* putative Cox17 metallochaperone orthologs were recombinantly expressed. Interestingly, the expression of a His_6-tagged *P. yoelii* Cox17 ortholog was successful whilst the expression of a similarly tagged *P. falciparum* Cox17 ortholog was not detectable. Reasons for this were not clear, but the result appeared to support the notion of utilising the “power of orthologs” for the successful recombinant expression of Apicomplexan parasite proteins (Vedadi *et al.*, 2007). Fusion of *P. falciparum* Cox17 to a GST carrier protein did, however, result in successful recombinant protein expression. Considering no alterations were made to the *P. falciparum* Cox17 coding sequence, the successful expression of GST-*Pf*Cox17 was unexpected since His_6-tagged *Pf*Cox17 did not express. This result did, however, support the idea that fusion to a soluble carrier protein, such as GST, can improve the expression and folding of inherently insoluble, unstable or unfolded proteins (Kapust and Waugh, 1999; Makrides, 1996; Nallamsetty and Waugh, 2007). An alternative approach to improve recombinant *Pf*Cox17 expression could be to utilise a codon optimised coding sequence. The use of synthetic, codon-optimised *Plasmodium* genes has so far improved the quality and quantity of other heterologously expressed recombinant *Plasmodium* proteins (Chowdhury *et al.*, 2009; Flick *et al.*, 2004; Mehlin *et al.*, 2006; Vedadi *et al.*, 2007), suggesting a similar result might be achievable for *Pf*Cox17. Alternatively, recent studies suggest that co-expression with *P. falciparum* heat shock protein 70 (*Pf*Hsp70) can improve the heterologous production of malarial parasite proteins (Stephens *et al.*, 2011).

6.5 Copper binding to a recombinant amino terminal domain of the putative *Plasmodium* spp. copper transporter and Cox17 copper metallochaperone

The copper binding capacity of each recombinant protein being studied, was tested *in vitro* and *in vivo*. Protein-bound copper was detected using the copper-specific bicinchoninic acid assay (Brenner and Harris, 1995). Each of the purified recombinant proteins was capable of binding copper *in vitro*. These studies also suggested that the amino terminal domain of the putative *Plasmodium* parasite copper transporters had a binding preference for the cuprous ion (Figure 4.20a and Figure 4.21a), which was similarly observed for the metal binding domain of *Pf*CuP-ATPase (Rasoloson *et al.*, 2004). Furthermore, a similar preference for the cuprous ion has been observed for yeast and mammalian copper transporters (Hassett and Kosman, 1995; Puig *et al.*, 2002a). The recombinant amino terminal domains MBP-*Pb*CtrNt, MBP-*Pf*Ctr211Nt^{TD} and MBP-*Pf*Ctr369Nt^{TD} were also observed to bind the cuprous ion *in vivo* (Figure 4.20b and Figure 4.21b). Since Cox17 is predicted to be intracellular (Beers *et al.*, 1997), the reducing environment of the cytosol suggests copper would naturally be present in the reduced, cuprous state. Copper binding studies with the recombinant *Plasmodium* Cox17 proteins established that they too were capable of binding copper both *in vitro* and *in vivo*. For recombinant fusion proteins, control copper binding studies with the respective carrier proteins (MBP or GST) confirmed that copper binding was specific for the fused parasite proteins. These results therefore support the presence of a dedicated *Plasmodium* spp. copper transport protein and elaborate on the uncharacterised pathways for intracellular copper distribution in the parasite.

6.6 Proposed mechanism for *Plasmodium* parasite copper acquisition

The presence of important functional copper transport protein motifs in the putative *Plasmodium* copper transporters (Figure 3.1 and Figure 3.2) suggests they are membrane bound and play a similar role to yeast and mammalian copper transporters. Association of a putative murine malaria parasite copper transporter with what appears to be a parasite membrane (Figure 4.8) supports this possibility. Furthermore, it was established that a recombinant form of the amino terminal domain of the *Plasmodium* parasite's copper transporter could bind copper (Figure 4.20 and Figure 4.21), which has similarly been observed for the human copper transporter ortholog (De Feo *et al.*, 2009; Jiang *et al.*, 2005; Larson *et al.*, 2010). However, it is still necessary to confirm the location, orientation and direction of transport for the *Plasmodium* copper transporter. Establishing protein location, in particular, will assist in elucidating protein function since it is predicted that each of the two putative *P. falciparum* copper transporters are targeted to different organelles (Figure 6.1). Considering the similarities identified between the *Plasmodium* transporters and other characterised copper transporters, two potential mechanisms for parasite copper acquisition are proposed (Figure 6.1).

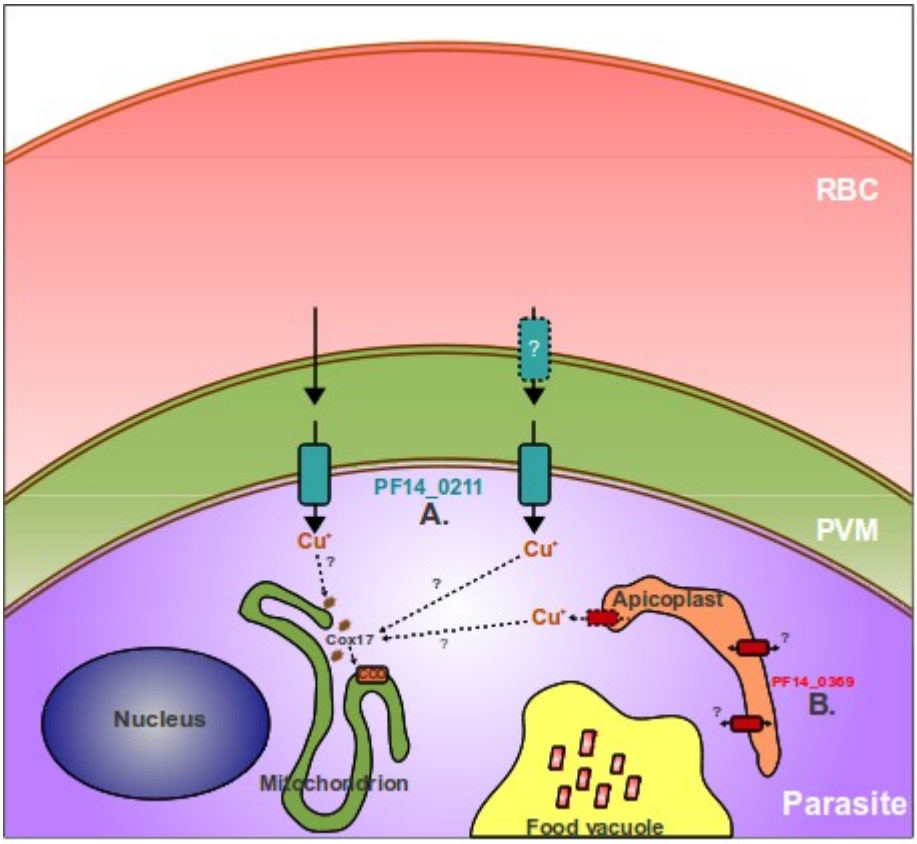

Figure 6.1 Proposed mechanism for *P. falciparum* copper acquisition

Following invasion of the red blood cell (RBC), the *Plasmodium* parasite is encapsulated within the parasitophorous vacuole membrane (PVM). Two putative copper transporters are predicted to be transcribed by *P. falciparum*, PF14_0211 and PF14_0369. PF14_0211 is predicted to be in a parasite membrane (**A**), whilst PF14_0369 is predicted to be in an apicoplast membrane (**B**). The Cox17 metallochaperone is predicted to load copper into cytochrome-c oxidase, which is thought to be associated with the mitochondrion (van Dooren *et al*., 2006). Unknown transport or transfer steps are marked with a question mark (?).

A number of *Plasmodium* parasite transport proteins are targeted to the surface of the parasite, whilst others are localised to the membranes of the parasite apicoplast, mitochondrion, digestive vacuole and organelles of the secretory pathway. The likely cellular destination(s) of a given transporter can be inferred by signals present in its protein sequence and/or by its close similarity to a transport protein of known cellular location (Martin *et al.*, 2005; Martin *et al.*, 2009a). Analysis of the two putative *P. falciparum* copper transporters identified a signal peptide in both proteins, whilst an apicoplast transit peptide was also identified in PF14_0369. This suggests PF14_0211 is targeted to the parasite plasma membrane, whereas PF14_0369 is targeted to the apicoplast (Figure 6.1). Although targeting of PF14_0211 to the parasite membrane seems most likely, it cannot be excluded that PF14_0211 might also be targeted to the parasitophorous vacuole membrane. This is a possibility since the signal/s for targeting membrane proteins to the parasitophorous vacuole membrane remain unknown (Martin *et al.*,

2009a). Should PF14_0211 be localised to the vacuolar membrane, it would presumably transport copper from the erythrocyte cytosol into the parasitophorous vacuole for the parasite (Figure 6.1). However, it is currently believed that only high-capacity, low-selectivity channels are located in the vacuolar membrane to render it freely permeable to low-molecular-weight solutes (Desai *et al.*, 1993; Martin *et al.*, 2009a). Since these solutes could include copper, it is possible that PF14_0211 location in the vacuolar membrane is unnecessary, suggesting this transporter could be exclusively in the parasite plasma membrane.

The *P. falciparum* apicoplast is a plastid bound by four membranes that is homologous and conceptually similar to the plant chloroplast, which was derived from a modified cyanobacterium in a eukaryotic host cell (Lim and McFadden, 2010; Ralph *et al.*, 2004). The apicoplast is essential for parasite survival (Goodman *et al.*, 2007; Vaughan *et al.*, 2009) and contains several plastid-derived biochemical pathways (Lim and McFadden, 2010). A striking feature of the apicoplast is its close association with the parasite mitochondrion (Bannister *et al.*, 2000; van Dooren *et al.*, 2006). This association is thought to be conducive to substrate exchange (Ralph *et al.*, 2004), but the majority of the membrane-bound transporters required for such processes remain to be identified (Lim and McFadden, 2010; van Dooren *et al.*, 2006). In the present study it was proposed that one of the *P. falciparum* copper transporters (PF14_0369) is located in an apicoplast membrane (Figure 6.1). Reasons for this association remain elusive, particularly since the membrane orientation and direction of transport remain unknown. However, the possibility exists that the parasite apicoplast acts as a site for copper storage, similar to the *Chlamydomonas* chloroplast (Merchant *et al.*, 2006). This therefore implies that, depending on its orientation, the PF14_0369 copper transporter could either function to redistribute stored copper for intracellular use or alternatively acquire surplus cellular copper for storage. However, it is perhaps more likely that PF14_0369 functions in copper redistribution since in the *Chlamydomonas* chloroplast, for example, copper is acquired through the action of two independent P-type ATPases whilst copper transporter-type proteins are thought to mobilise stored copper (Merchant *et al.*, 2006; Shcolnick and Keren, 2006). Considering the close association between the apicoplast and mitochondrion it is plausible that, if copper were stored in the apicoplast, PF14_0369 could provide a more direct route of copper delivery to Cox17 for subsequent insertion into cytochrome-c oxidase.

Regardless of their specific loctions, it is presumed that both PF14_0211 and PF14_0369 would transport copper across the membrane via a passive mechanism, similar to that suggested for the human copper transporter (Lee *et al.*, 2002). Another similarity likely to exist between the human and putative *Plasmodium* copper transporters, is that copper is transported

across the membrane in its reduced, cuprous form. This probability was based on the data obtained from copper binding studies with MBP-*Pf*Ctr211Nt^{TD} and MBP-*Pf*Ctr369Nt^{TD} (Figure 4.21). Once copper is transported across the relevant parasite membrane(s) and into the cytosol, it is presumably distributed to target proteins by intracellular metallochaperones. Although the majority of these target proteins and metallochaperones remain to be identified, a putative *Plasmodium* parasite Cox17 metallochaperone ortholog was identified in the present study and shown to bind copper (Figure 5.9). Supporting a parasite requirement for this metallochaperone was the *in silico* identification of parasite cytochrome-c oxidase complex orthologs. In yeast and mammalian cells, Cox17 is required for copper delivery to cytochrome-c oxidase for its activation in the mitochondrion (Kim *et al.*, 2008; Lutsenko, 2010). However, in yeast and mammalian cells, the mechanism by which copper is delivered to the mitochondrion still requires further elucidation (Lutsenko, 2010). This therefore limits the similarities that can be drawn between the mammalian and corresponding parasite mechanisms, apart from the fact that Cox17 is likely to be required for copper delivery to the cytochrome-c oxidase complex (Figure 6.1).

6.7 Conclusions and future direction

The pressing need for new antimalarial chemotherapeutics has resulted in an expanded search for novel targets. However, the demand for new drugs continues to outstrip efforts in development (Mehlin *et al.*, 2006). In the present study, it was suggested that targeted inhibition of *Plasmodium* parasite proteins required for copper homeostasis could prove effective in arresting parasite growth. Drug-targeted inhibition of proteins involved in copper homoeostasis would likely disrupt copper-dependent metabolic pathways within the parasite, thereby inhibiting growth. Such an effect has been observed following treatment of a *P. falciparum* culture with the intracellular copper chelator neocuproine (Rasoloson *et al.*, 2004). However, considering the general importance of copper to all living organisms, as well as the conservation of copper binding motifs in proteins from eukaryotes to prokaryotes (Andreini *et al.*, 2008), it seems likely that developing a specific inhibitor of *Plasmodium* parasite copper-dependent proteins would be difficult. However, it may be possible to utilise the transport mechanism of the copper transporter for the delivery of a drug compound. This suggestion is based on the finding that the uptake of platinum containing anti-cancer drugs, such as cisplatin and oxaliplatin, is mediated by the copper transport protein in human cells (Holzer *et al.*, 2006; Howell *et al.*, 2010; Larson *et al.*, 2009). By utilising a similar approach, it could perhaps be possible to target the malaria parasite, but considering the sequence similarity between the parasite and human copper transporters this too could prove difficult.

Results from the present study provide an insight into the existence of additional pathways for copper homoeostasis in the malaria parasite. However, the directional transport of each putative copper transporter and its specific location in the parasite remains to be determined. It is also necessary to determine the kinetics of these transporters if they are to be considered as either viable drug transporters or targets in their own right. Similarly, the binding kinetics and cellular location of the putative parasite Cox17 copper metallochaperone requires confirmation and further characterisation. In both instances, protein location could be determined by immunolocalisation and electron microscopy (Agarwal *et al.*, 2011; Martin *et al.*, 2009a; Rasoloson *et al.*, 2004), whilst protein function could be inferred through a mutational analysis or by implementing a yeast complementation assay (Lee *et al.*, 2000; Zhou and Gitschier, 1997). Copper transport kinetics could also be established by using transfected *Xenopus laevis* oocytes (Martin *et al.*, 2005; Staines *et al.*, 2010). The potential importance of each protein to the parasite could be inferred from gene knock-out studies using transgenic parasites, as has been done for parasite cysteine repeat modular proteins 3 and 4 (Douradinha *et al.*, 2011) and lipoic acid protein ligase A1 (Günther *et al.*, 2009). Interpreting results from these studies does, however, warrant a note of caution considering that a large proportion of the *Mycoplasma genitalium* genome is dispensable for survival (Hutchison *et al.*, 1999). Resolving these features would provide further insight into the transport and shuttling mechanisms of these proteins and suggest whether or not they are similar to those identified in yeast and mammalian systems. Although the results of this study established the copper binding ability of parasite proteins involved in copper homoeostasis, further work is clearly required to determine their potential as novel drug targets.

References

Abajian, C., Yatsunyk, L.A., Ramirez, B.E. and Rosenzweig, A.C. (2004). Yeast Cox17 solution structure and copper(I) binding. *The Journal of Biological Chemistry* **279**, 53584-53592.

Agarwal S., Kern S., Halbert J. *et al*. (2011). Two nucleus-localized CDK-like kinases with crucial roles for malaria parasite erythrocytic replication are involved in phosphorylation of splicing factor. *Journal of Cellular Biochemistry* **112**, 1295-1310.

Aller, S.G., Eng, E.T., De Feo, C.J. and Unger, V.M. (2004). Eukaryotic Ctr copper uptake transporters require two faces of the third transmembrane domain for helix packing, oligomerization, and function. *The Journal of Biological Chemistry* **279**, 53435-53441.

Aller, S.G. and Unger, V.M. (2006). Projection structure of the human copper transporter Ctr1 at 6-Å resolution reveals a compact trimer with a novel channel-like architecture. *Proceedings of the National Academy of Sciences of the United States of America* **103**, 3627-3632.

Andreini C., Banci L., Bertini I. *et al*. (2008). Occurrence of copper proteins through the three domains of life: a bioinformatic approach. *Journal of Proteome Research* **7**, 209-216.

Arnesano, F., Balatri, E., Banci, L., Bertini, I. and Winge, D.R. (2005). Folding studies of Cox17 reveal an important interplay of cysteine oxidation and copper binding. *Structure* **13**, 713-722.

Atha, D.H. and Ingham, K.C. (1981). Mechanism of precipitation of proteins by polyethylene glycols. Analysis in terms of excluded volume. *The Journal of Biological Chemistry* **256**, 12108-12117.

Bagai, I., Rensing, C., Blackburn, N.J. and McEvoy, M.M. (2008). Direct metal transfer between periplasmic proteins identifies a bacterial copper chaperone. *Biochemistry* **47**, 11408-11414.

Baldauf, S.L., Roger, A.J., Wenk-Siefert, I. and Doolittle, W.F. (2000). A kingdom-level phylogeny of eukaryotes based on combined protein data. *Science* **290**, 972-977.

Banci, L., Bertini, I., Ciofi-Baffoni, S., Leontari, I., Martinelli, M., Palumaa, P. *et al*. (2007). Human Sco1 functional studies and pathological implications of the P174I mutant. *Proceedings of the National Academy of Sciences of the United States of America* **104**, 15-20.

Banci, L., Bertini, I., Ciofi-Baffoni, S., Hadjiloi, T., Martinelli, M. and Palumaa, P. (2008a). Mitochondrial copper(I) transfer from Cox17 to Sco1 is coupled to electron transfer. *Proceedings of the National Academy of Sciences of the United States of America* **105**, 6803-6808.

Banci, L., Bertini, I., Ciofi-Baffoni, S., Janicka, A., Martinelli, M., Kozlowski, H. *et al*. (2008b). A structural-dynamical characterization of human Cox17. *The Journal of Biological Chemistry* **283**, 7912-7920.

Banci L., Bertini I., Ciofi-Baffoni S. *et al*. (2010). Affinity gradients drive copper to cellular destinations. *Nature* **465**, 645-648.

Baneyx, F. (1999). Recombinant protein expression in *Escherichia coli. Current Opinion in Biotechnology* **10**, 411-421.

Bannister, L.H., Hopkins, J.M., Fowler, R.E., Krishna, S. and Mitchell, G.H. (2000). A brief illustrated guide to the ultrastructure of *Plasmodium falciparum* asexual blood stages. *Parasitology Today* **16**, 427-433.

Barros, M.H., Johnson, A. and Tzagoloff, A. (2004). Cox23, a homologue of Cox17, is required for cytochrome oxidase assembly. *The Journal of Biological Chemistry* **279**, 31943-31947.

Beers, J., Glerum, D.M. and Tzagoloff, A. (1997). Purification, characterization, and localization of yeast Cox17p, a mitochondrial copper shuttle. *The Journal of Biological Chemistry* **272**, 33191-33196.

Bender A., van Dooren G.G., Ralph S.A. *et al*. (2003). Properties and prediction of mitochondrial transit peptides from *Plasmodium falciparum. Molecular and Biochemical Parasitology* **132**, 59-66.

Bertinato, J. and L'Abbe, M.R. (2004). Maintaining copper homeostasis: regulation of copper-trafficking proteins in response to copper deficiency or overload. *The Journal of Nutritional Biochemistry* **15**, 316-322.

Bertinato, J., Swist, E., Plouffe, L.J., Brooks, S.P. and L'Abbe M, R. (2008). Ctr2 is partially localized to the plasma membrane and stimulates copper uptake in COS-7 cells. *The Biochemical Journal* **409**, 731-740.

Bertinato J., Cheung L., Hoque R. *et al*. (2010). Ctr1 transports silver into mammalian cells. *Journal of Trace Elements in Medicine and Biology* **24**, 178-184.

Berwal, R., Gopalan, N., Chandel, K., Prasad, G.B.K.S. and Prakash, S. (2008). *Plasmodium falciparum*: enhanced soluble expression, purification and biochemical characterization of lactate dehydrogenase. *Experimental Parasitology* **120**, 135-141.

Birkholtz, L., van Brummelen, A.C., Clark, K., Niemand, J., Marechal, E., Llinas, M. *et al*. (2008). Exploring functional genomics for drug target and therapeutics discovery in plasmodia. *Acta Tropica* **105**, 113-123.

Boal, A.K. and Rosenzweig, A.C. (2009). Structural biology of copper trafficking. *Chemical Reviews* **109**, 4760-4779.

Brady, R.L. and Cameron, A. (2004). Structure-based approaches to the development of novel anti-malarials. *Current Drug Targets* **5**, 137-149.

Breman, J.G., Alilio, M.S. and Mills, A. (2004). Conquering the intolerable burden of malaria: what's new, what's needed: a summary. *The American Journal of Tropical Medicine and Hygiene* **71**, 1-15.

Brenner, A.J. and Harris, E.D. (1995). A quantitative test for copper using bicinchoninic acid. *Analytical Biochemistry* **226**, 80-84.

Brown, N.L., Barrett, S.R., Camakaris, J., Lee, B.T. and Rouch, D.A. (1995). Molecular genetics and transport analysis of the copper-resistance determinant (pco) from *Escherichia coli* plasmid prj1004. *Molecular Microbiology* **17**, 1153-1166.

Buettner, G.R. (1988). In the absence of catalytic metals ascorbate does not autoxidize at ph 7: ascorbate as a test for catalytic metals. *Journal of Biochemical and Biophysical Methods* **16**, 27-40.

Bujnicki, J.M., Prigge, S.T., Caridha, D. and Chiang, P.K. (2003). Structure, evolution, and inhibitor interaction of S-Adenosyl-L-Homocysteine hydrolase from *Plasmodium falciparum. Proteins* **52**, 624-632.

Burns, J.M.J., Parke, L.A., Daly, T.M., Cavacini, L.A., Weidanz, W.P. and Long, C.A. (1989). A protective monoclonal antibody recognizes a variant-specific epitope in the precursor of the major merozoite surface antigen of the rodent malarial parasite *Plasmodium yoelii. Journal of Immunology* **142**, 2835-2840.

Camakaris, J., Voskoboinik, I. and Mercer, J.F. (1999). Molecular mechanisms of copper homeostasis. *Biochemical and Biophysical Research Communications* **261**, 225-232.

Carlton, J.M., Angiuoli, S.V., Suh, B.B., Kooij, T.W., Pertea, M., Silva, J.C. *et al*. (2002). Genome sequence and comparative analysis of the model rodent malaria parasite *Plasmodium yoelii yoelii. Nature* **419**, 512-519.

Carlton, J.M., Adams, J.H., Silva, J.C., Bidwell, S.L., Lorenzi, H., Caler, E. *et al*. (2008). Comparative genomics of the neglected human malaria parasite *Plasmodium vivax. Nature* **455**, 757-763.

Cármenes, R.S., Freije, J.P., Molina, M.M. and Martin, J.M. (1989). Predict7, a program for protein structure prediction. *Biochemical and Biophysical Research Communications* **159**, 687-693.

Carr, H.S. and Winge, D.R. (2003). Assembly of cytochrome-c oxidase within the mitochondrion. *Accounts of Chemical Research* **36**, 309-316.

Carr, H.S., George, G.N. and Winge, D.R. (2002). Yeast Cox11, a protein essential for cytochrome-c oxidase assembly, is a Cu(I)-binding protein. *The Journal of Biological Chemistry* **277**, 31237-31242.

Casares, S., Brumeanu, T. and Richie, T.L. (2010). The RTS,S malaria vaccine. *Vaccine* **28**, 4880-4894.

Chacinska, A., Pfannschmidt, S., Wiedemann, N., Kozjak, V., Sanjuán Szklarz, L.K., Schulze-Specking, A. *et al*. (2004). Essential role of Mia40 in import and assembly of mitochondrial intermembrane space proteins. *The EMBO Journal* **23**, 3735-3746.

Cheng, Q., Cloonan, N., Fischer, K., Thompson, J., Waine, G., Lanzer, M. *et al*. (1998). Stevor and rif are *Plasmodium falciparum* multicopy gene families which potentially encode variant antigens. *Molecular and Biochemical Parasitology* **97**, 161-176.

Chowdhury, D.R., Angov, E., Kariuki, T. and Kumar, N. (2009). A potent malaria transmission blocking vaccine based on codon harmonized full length Pfs48/45 expressed in *Escherichia coli. PLoS ONE* **4**, e6352.

Chun, P.W., Fried, M. and Ellis, E.F. (1967). Use of water-soluble polymers for the isolation and purification of human immunoglobulins. *Analytical Biochemistry* **19**, 481-497.

Claverie, J.M. and Notredame, C. (2003). Bioinformatics for dummies. Wiley, New York.

Coetzer, T.H.T. (1985) Preparation and characterisation of antibodies against mouse Ig (all classes). Internal report, Bioclones (Pty.) Ltd. Immunology Group, Stellenbosch.

Cobine, P.A., Ojeda, L.D., Rigby, K.M. and Winge, D.R. (2004). Yeast contain a non-proteinaceous pool of copper in the mitochondrial matrix. *The Journal of Biological Chemistry* **279**, 14447-14455.

Cobine, P.A., Pierrel, F. and Winge, D.R. (2006a). Copper trafficking to the mitochondrion and assembly of copper metalloenzymes. *Biochimica et Biophysica Acta* **1763**, 759-772.

Cobine, P.A., Pierrel, F., Bestwick, M.L. and Winge, D.R. (2006b). Mitochondrial matrix copper complex used in metallation of cytochrome oxidase and superoxide dismutase. *The Journal of Biological Chemistry* **281**, 36552-36559.

Cox-Singh, J., Hiu, J., Lucas, S.B., Divis, P.C., Zulkarnaen, M., Chandran, P. *et al*. (2010). Severe malaria - a case of fatal *Plasmodium knowlesi* infection with post-mortem findings: a case report. *Malaria Journal* **9**, 10.

Creedon, K.A., Rathod, P.K. and Wellems, T.E. (1994). *Plasmodium falciparum* S-Adenosylhomocysteine hydrolase. cDNA identification, predicted protein sequence, and expression in *Escherichia coli. The Journal of Biological Chemistry* **269**, 16364-16370.

Crompton, P.D., Pierce, S.K. and Miller, L.H. (2010). Advances and challenges in malaria vaccine development. *The Journal of Clinical Investigation* **120**, 4168-4178.

Dameron, C.T. and Harrison, M.D. (1998). Mechanisms for protection against copper toxicity. *The American Journal of Clinical Nutrition* **67**, 1091S-1097S.

Dancis, A., Haile, D., Yuan, D.S. and Klausner, R.D. (1994). The *Saccharomyces cerevisiae* copper transport protein (Ctr1p). Biochemical characterization, regulation by copper, and physiologic role in copper uptake. *The Journal of Biological Chemistry* **269**, 25660-25667.

Davis, A.V. and O'Halloran, T.V. (2008). A place for thioether chemistry in cellular copper ion recognition and trafficking. *Nature Chemical Biology* **4**, 148-151.

De Feo, C.J., Aller, S.G., Siluvai, G.S., Blackburn, N.J. and Unger, V.M. (2009). Three-dimensional structure of the human copper transporter hCtr1. *Proceedings of the National Academy of Sciences of the United States of America* **106**, 4237-4242.

De Feo, C.J., Mootien, S. and Unger, V.M. (2010). Tryptophan scanning analysis of the membrane domain of Ctr-copper transporters. *The Journal of Membrane Biology* **234**, 113-123.

Desai S.A., Krogstad D.J. and McCleskey E.W. (1993). A nutrient-permeable channel on the intraerythrocytic malaria parasite. *Nature* **362**, 643-646.

Diaz, F. (2010). Cytochrome-c oxidase deficiency: patients and animal models. *Biochimica et Biophysica Acta* **1802**, 100-110.

Dondorp, A.M., Nosten, F., Yi, P., Das, D., Phyo, A.P., Tarning, J. *et al*. (2009). Artemisinin resistance in *Plasmodium falciparum* malaria. *The New England Journal of Medicine* **361**, 455-467.

Dorin, D., Semblat, J.P., Poullet, P., Alano, P., Goldring, J.P., Whittle, C. *et al*. (2005). PfPK7, an atypical MEK-related protein kinase, reflects the absence of classical three-component MAPK pathways in the human malaria parasite *Plasmodium falciparum. Molecular Microbiology* **55**, 184-196.

Douradinha B., Augustijn K.D., Moore S.G. *et al*. (2011). *Plasmodium* cysteine repeat modular proteins 3 and 4 are essential for malaria parasite transmission from the mosquito to the host. *Malaria Journal* **10**, 71.

Eckstein-Ludwig, U., Webb, R.J., Van Goethem, I.D.A., East, J.M., Lee, A.G., Kimura, M. *et al*. (2003). Artemisinins target the SERCA of *Plasmodium falciparum. Nature* **424**, 957-961.

Eisses, J.F. and Kaplan, J.H. (2002). Molecular characterization of hCtr1, the human copper uptake protein. *The Journal of Biological Chemistry* **277**, 29162-29171.

Eisses, J.F. and Kaplan, J.H. (2005). The mechanism of copper uptake mediated by human Ctr1: a mutational analysis. *The Journal of Biological Chemistry* **280**, 37159-37168.

Ekland, E.H. and Fidock, D.A. (2008). *In vitro* evaluations of antimalarial drugs and their relevance to clinical outcomes. *International Journal for Parasitology* **38**, 743-747.

Emanuelsson, O., Brunak, S., von Heijne, G. and Nielsen, H. (2007). Locating proteins in the cell using Targetp, Signalp and related tools. *Nature Protocols* **2**, 953-971.

Emini, E.A., Hughes, J.V., Perlow, D.S. and Boger, J. (1985). Induction of Hepatitis A virus-neutralizing antibody by a virus-specific synthetic peptide. *Journal of Virology* **55**, 836-839.

Escalante, A.A. and Ayala, F.J. (1994). Phylogeny of the malarial genus *Plasmodium*, derived from rRNA gene sequences. *Proceedings of the National Academy of Sciences of the United States of America* **91**, 11373-11377.

Escalante A.A. and Ayala F.J. (1995). Evolutionary origin of *Plasmodium* and other apicomplexa based on rRNA genes. *Proceedings of the National Academy of Sciences of the United States of America* **92**, 5793-5797.

Fahey, R.C., Hunt, J.S. and Windham, G.C. (1977). On the cysteine and cystine content of proteins. Differences between intracellular and extracellular proteins. *Journal of Molecular Evolution* **10**, 155-160.

Ferguson-Miller, S. and Babcock, G.T. (1996). Heme/copper terminal oxidases. *Chemical Reviews* **96**, 2889-2908.

Flick, K., Ahuja, S., Chene, A., Bejarano, M.T. and Chen, Q. (2004). Optimized expression of *Plasmodium falciparum* erythrocyte membrane protein 1 domains in *Escherichia coli. Malaria Journal* **3**, 50.

French, C., Keshavarz-Moore, E. and Ward, J.M. (1996). Development of a simple method for the recovery of recombinant proteins from *Escherichia coli* periplasm. *Enzyme and Microbial Technology* **19**, 332-338.

Frevert, U., Sinnis, P., Cerami, C., Shreffler, W., Takacs, B. and Nussenzweig, V. (1993). Malaria circumsporozoite protein binds to heparan sulfate proteoglycans associated with the surface membrane of hepatocytes. *The Journal of Experimental Medicine* **177**, 1287-1298.

Friedman S. and Kaufman S. (1965). 3,4-Dihydroxyphenylethylamine beta-hydroxylase. physical properties, copper content, and role of copper in the catalytic activity. *The Journal of Biological Chemistry* **240**, 4763-4773.

Galinski, M.R. and Barnwell, J.W. (2009). Monkey malaria kills four humans. *Trends in Parasitology* **25**, 200-204.

Gamo, F., Sanz, L.M., Vidal, J., de Cozar, C., Alvarez, E., Lavandera, J. *et al.* (2010). Thousands of chemical starting points for antimalarial lead identification. *Nature* **465**, 305-310.

Gardner, M.J., Hall, N., Fung, E., White, O., Berriman, M., Hyman, R.W. *et al*. (2002). Genome sequence of the human malaria parasite *Plasmodium falciparum. Nature* **419**, 498-511.

Georgatsou, E., Mavrogiannis, L.A., Fragiadakis, G.S. and Alexandraki, D. (1997). The yeast Fre1p/Fre2p cupric reductases facilitate copper uptake and are regulated by the copper-modulated Mac1p activator. *The Journal of Biological Chemistry* **272**, 13786-13792.

Glerum, D.M., Shtanko, A. and Tzagoloff, A. (1996). Characterization of Cox17, a yeast gene involved in copper metabolism and assembly of cytochrome oxidase. *The Journal of Biological Chemistry* **271**, 14504-14509.

Gokhale, N.H., Padhye, S.B. and Billington, D.C.E.A. (2001). Synthesis and characterisation of copper(II) complexes of pyridine-2-carboxamidrazones as potent antimalarial agents. *Inorganica Chemica Acta* **349**, 23-29.

Gokhale, N.H., Padhye, S.B., Croft, S.L., Kendrick, H.D., Davies, W., Anson, C.E. *et al*. (2003). Transition metal complexes of buparvaquone as potent new antimalarial agents. Synthesis, X-ray crystal-structures, electrochemistry and antimalarial activity against *Plasmodium falciparum. Journal of Inorganic Biochemistry* **95**, 249-258.

Gokhale, N.H., Shirisha, K., Padhye, S.B., Croft, S.L., Kendrick, H.D. and McKee, V. (2006). Metalloantimalarials: Synthesis, X-ray crystal structure of potent antimalarial copper(II) complex of arylazo-4-hydroxy-1,2-naphthoquinone. *Bioorganic & Medicinal Chemistry Letters* **16**, 430-432.

Goldring, J. and Coetzer, T.H.T. (2003). Isolation of chicken immunoglobulins (IgY) from egg yolk. *Biochemistry and Molecular Biology Education* **31**, 185-187.

Goodman C.D., Su V. and McFadden G.I. (2007). The effects of anti-bacterials on the malaria parasite *Plasmodium falciparum. Molecular and Biochemical Parasitology* **152**, 181-191.

Gräslund, S., Nordlund, P., Weigelt, J., Hallberg, B.M., Bray, J., Gileadi, O. *et al*. (2008). Protein production and purification. *Nature Methods* **5**, 135-146.

GST gene fusion system handbook. Amersham Biosciences. Code number: 188-1157-58. Edition AA.

Guex, N. and Peitsch, M.C. (1997). Swiss-model and the Swiss-pdb viewer: an environment for comparative protein modelling. *Electrophoresis* **18**, 2714-2723.

Günther S., Matuschewski K. and Müller S. (2009). Knockout studies reveal an important role of *Plasmodium* lipoic acid protein ligase A1 for asexual blood stage parasite survival. *PLoS ONE* **4**, e5510.

Guo, Y., Smith, K., Lee, J., Thiele, D.J. and Petris, M.J. (2004). Identification of methionine-rich clusters that regulate copper-stimulated endocytosis of the human Ctr1 copper transporter. *The Journal of Biological Chemistry* **279**, 17428-17433.

Hakim, S.L., Sharifah Roohi, S.W.A., Zurkurnai, Y., Noor Rain, A., Mansor, S.M., Palmer, K. *et al*. (1996). *Plasmodium falciparum*: increased proportion of severe resistance to chloroquine and high rate of resistance to sulfadoxine-pyrimethamine in peninsular Malaysia after two decades. *Transactions of the Royal Society of Tropical Medicine and Hygiene* **90**, 294-297.

Hall, N., Karras, M., Raine, J.D., Carlton, J.M., Kooij, T.W., Berriman, M. *et al*. (2005). A comprehensive survey of the *Plasmodium* life cycle by genomic, transcriptomic, and proteomic analyses. *Science* **307**, 82-86.

Halliwell, B. and Gutteridge, J.M. (1984). Oxygen toxicity, oxygen radicals, transition metals and disease. *The Biochemical Journal* **219**, 1-14.

Harlow, E. and Lane, D. (1988). Antibodies - a laboratory manual. Cold Spring Harbour Laboratory, New York. 288-293.

Hassett, R. and Kosman, D.J. (1995). Evidence for Cu(II) reduction as a component of copper uptake by *Saccharomyces cerevisiae*. *The Journal of Biological Chemistry* **270**, 128-134.

Hatano, S., Nishi, Y. and Usui, T. (1982). Copper levels in plasma and erythrocytes in healthy Japanese children and adults. *The American Journal of Clinical Nutrition* **35**, 120-126.

Hay, S.I., Guerra, C.A., Gething, P.W., Patil, A.P., Tatem, A.J., Noor, A.M. *et al*. (2009). A World malaria map: *Plasmodium falciparum* endemicity in 2007. *PLoS Medicine* **6**, 286-302.

Heaton, D., Nittis, T., Srinivasan, C. and Winge, D.R. (2000). Mutational analysis of the mitochondrial copper metallochaperone Cox17. *The Journal of Biological Chemistry* **275**, 37582-37587.

Heaton, D.N., George, G.N., Garrison, G. and Winge, D.R. (2001). The mitochondrial copper metallochaperone Cox17 exists as an oligomeric, polycopper complex. *Biochemistry* **40**, 743-751.

Hiser, L., Di Valentin, M., Hamer, A.G. and Hosler, J.P. (2000). Cox11p is required for stable formation of the Cu(b) and magnesium centers of cytochrome-c oxidase. *The Journal of Biological Chemistry* **275**, 619-623.

Hoffman, S.L., Goh, L.M.L., Luke, T.C., Schneider, I., Le, T.P., Doolan, D.L. *et al*. (2002). Protection of humans against malaria by immunization with radiation-attenuated *Plasmodium falciparum* sporozoites. *The Journal of Infectious Diseases* **185**, 1155-1164.

Holzer, A.K., Manorek, G.H. and Howell, S.B. (2006). Contribution of the major copper influx transporter Ctr1 to the cellular accumulation of cisplatin, carboplatin, and oxaliplatin. *Molecular Pharmacology* **70**, 1390-1394.

Hopp, T.P. and Woods, K.R. (1983). A computer program for predicting protein antigenic determinants. *Molecular Immunology* **20**, 483-489.

Horng, Y., Cobine, P.A., Maxfield, A.B., Carr, H.S. and Winge, D.R. (2004). Specific copper transfer from the Cox17 metallochaperone to both Sco1 and Cox11 in the assembly of yeast cytochrome-c oxidase. *The Journal of Biological Chemistry* **279**, 35334-35340.

Howell, S.B., Safaei, R., Larson, C.A. and Sailor, M.J. (2010). Copper transporters and the cellular pharmacology of the platinum-containing cancer drugs. *Molecular Pharmacology* **77**, 887-894.

Hua, H., Georgiev, O., Schaffner, W. and Steiger, D. (2010). Human copper transporter Ctr1 is functional in *Drosophila*, revealing a high degree of conservation between mammals and insects. *Journal of Biological Inorganic Chemistry* **15**, 107-113.

Huffman, D.L., Huyett, J., Outten, F.W., Doan, P.E., Finney, L.A., Hoffman, B.M. *et al*. (2002). Spectroscopy of Cu(II)-PcoC and the multicopper oxidase function of PcoA, two essential components of *Escherichia coli* Pco copper resistance operon. *Biochemistry* **41**, 10046-10055.

Hung, Y.H., Bush, A.I. and Cherny, R.A. (2010). Copper in the brain and Alzheimer's disease. *Journal of Biological Inorganic Chemistry* **15**, 61-76.

Hurdayal, R., Achilonu, I., Choveaux, D., Coetzer, T.H.T. and Goldring, J.PD. (2010). Anti-peptide antibodies differentiate between plasmodial lactate dehydrogenases. *Peptides* **31**, 525-532.

Hutchison C.A., Peterson S.N., Gill S.R. *et al*. (1999). Global transposon mutagenesis and a minimal *Mycoplasma* genome. *Science* **286**, 2165-2169.

Ingham, K.C. (1984). Protein precipitation with polyethylene glycol. *Methods in Enzymology* **104**, 351-356.

Ittarat, W., Pickard, A.L., Rattanasinganchan, P., Wilairatana, P., Looareesuwan, S., Emery, K. *et al*. (2003). Recrudescence in artesunate-treated patients with *falciparum* malaria is dependent on parasite burden not on parasite factors. *The American Journal of Tropical Medicine and Hygiene* **68**, 147-152.

Iwata, S., Ostermeier, C., Ludwig, B. and Michel, H. (1995). Structure at 2.8 Å resolution of cytochrome-c oxidase from *Paracoccus denitrificans. Nature* **376**, 660-669.

Jalah, R., Sarin, R., Sud, N., Alam, M.T., Parikh, N., Das, T.K. *et al*. (2005). Identification, expression, localization and serological characterization of a tryptophan-rich antigen from the human malaria parasite *Plasmodium vivax. Molecular and Biochemical Parasitology* **142**, 158-169.

Janin, J. and Wodak, S. (1978). Conformation of amino acid side-chains in proteins. *Journal of Molecular Biology* **125**, 357-386.

Jensen, P.Y., Bonander, N., Horn, N., Tumer, Z. and Farver, O. (1999). Expression, purification and copper-binding studies of the first metal-binding domain of Menkes protein. *European Journal of Biochemistry* **264**, 890-896.

Jiang, J., Nadas, I.A., Kim, M.A. and Franz, K.J. (2005). A Mets motif peptide found in copper transport proteins selectively binds Cu(I) with methionine-only coordination. *Inorganic Chemistry* **44**, 9787-9794.

Joubert, F., Harrison, C.M., Koegelenberg, R.J., Odendaal, C.J. and de Beer, T.A.P. (2009). Discovery: An interactive resource for the rational selection and comparison of putative drug target proteins in malaria. *Malaria Journal* **8**, 178.

Kampfenkel, K., Kushnir, S., Babiychuk, E., Inze, D. and Van Montagu, M. (1995). Molecular characterization of a putative *Arabidopsis thaliana* copper transporter and its yeast homologue. *The Journal of Biological Chemistry* **270**, 28479-28486.

Kaplan, J.H. and Lutsenko, S. (2009). Copper transport in mammalian cells: special care for a metal with special needs. *The Journal of Biological Chemistry* **284**, 25461-25465.

Kapust, R.B. and Waugh, D.S. (1999). *Escherichia coli* maltose-binding protein is uncommonly effective at promoting the solubility of polypeptides to which it is fused. *Protein Science* **8**, 1668-1674.

Karplus, P.A. and Schulz, G.E. (1985). Prediction of chain flexibility in proteins. *Die Naturwissenschaften* **72**, 212-213.

Kelly, J.M., McRobert, L. and Baker, D.A. (2006). Evidence on the chromosomal location of centromeric DNA in *Plasmodium falciparum* from etoposide-mediated topoisomerase-II cleavage. *Proceedings of the National Academy of Sciences of the United States of America* **103**, 6706-6711.

Khan, M.M. and Martell, A.E. (1967). Metal ion and metal chelate catalyzed oxidation of ascorbic acid by molecular oxygen. II. Cupric and ferric chelate catalyzed oxidation. *Journal of the American Chemical Society* **89**, 7104-7111.

Kim, B.E., Nevitt, T. and Thiele, D.J. (2008). Mechanisms for copper acquisition, distribution and regulation. *Nature Chemical Biology* **4**, 176-185.

Kirk, K. (2004). Channels and transporters as drug targets in the *Plasmodium*-infected erythrocyte. *Acta Tropica* **89**, 285-298.

Kirk K. and Saliba K.J. (2007). Targeting nutrient uptake mechanisms in *Plasmodium. Current Drug Targets* **8**, 75-88.

Kita K., Watanabe Y., Takeo S. *et al*. (1998). Mitochondrial respiratory chain of malaria parasite. *The Tokai Journal of Experimental and Clinical Medicine* **23**, 89-90.

Klomp, A.E., Tops, B.B., Van Denberg, I.E., Berger, R. and Klomp, L.W. (2002). Biochemical characterization and subcellular localization of human copper transporter 1 (hCtr1). *The Biochemical Journal* **364**, 497-505.

Klomp, A.E., Juijn, J.A., van der Gun, L.T., van den Berg, I.E., Berger, R. and Klomp, L.W. (2003). The N-terminus of the human copper transporter 1 (hCtr1) is localized extracellularly, and interacts with itself. *The Biochemical Journal* **370**, 881-889.

Koenderink, J.B., Kavishe, R.A., Rijpma, S.R. and Russel, F.G.M. (2010). The ABC's of multidrug resistance in malaria. *Trends in Parasitology* **26**, 440-446.

Kooij, T.W., Carlton, J.M., Bidwell, S.L., Hall, N., Ramesar, J., Janse, C.J. *et al*. (2005). A *Plasmodium* whole-genome synteny map: Indels and synteny breakpoints as foci for species-specific genes. *PLoS Pathogens* **1**, e44.

Krishna, S., Webb, R. and Woodrow, C. (2001). Transport proteins of *Plasmodium falciparum*: defining the limits of metabolism. *International Journal for Parasitology* **31**, 1331-1342.

Krnajski, Z., Gilberger, T.W., Walter, R.D. and Müller, S. (2001). The malaria parasite *Plasmodium falciparum* possesses a functional thioredoxin system. *Molecular and Biochemical Parasitology* **112**, 219-228.

Krogh A., Larsson B., von Heijne G. *et al*. (2001). Predicting transmembrane protein topology with a hidden Markov model: application to complete genomes. *Journal of Molecular Biology* **305**, 567-580.

Kuo, Y.M., Zhou, B., Cosco, D. and Gitschier, J. (2001). The copper transporter Ctr1 provides an essential function in mammalian embryonic development. *Proceedings of the National Academy of Sciences of the United States of America* **98**, 6836-6841.

Kurland, C. and Gallant, J. (1996). Errors of heterologous protein expression. *Current Opinion in Biotechnology* **7**, 489-493.

Kyes, S.A., Rowe, J.A., Kriek, N. and Newbold, C.I. (1999). Rifins: a second family of clonally variant proteins expressed on the surface of red cells infected with *Plasmodium falciparum. Proceedings of the National Academy of Sciences of the United States of America* **96**, 9333-9338.

Kyes, S., Horrocks, P. and Newbold, C. (2001). Antigenic variation at the infected red cell surface in malaria. *Annual Review of Microbiology* **55**, 673-707.

Laemmli, U.K. (1970). Cleavage of structural proteins during the assembly of the head of bacteriophage T4. *Nature* **227**, 680-685.

LaGier, M.J., Zhu, G. and Keithly, J.S. (2001). Characterization of a heavy metal ATPase from the apicomplexan *Cryptosporidium parvum. Gene* **266**, 25-34.

Larson, C.A., Blair, B.G., Safaei, R. and Howell, S.B. (2009). The role of the mammalian copper transporter 1 in the cellular accumulation of platinum-based drugs. *Molecular Pharmacology* **75**, 324-330.

Larson, C.A., Adams, P.L., Jandial, D.D., Blair, B.G., Safaei, R. and Howell, S.B. (2010). The role of the N-terminus of mammalian copper transporter 1 in the cellular accumulation of cisplatin. *Biochemical Pharmacology* **80**, 448-454.

Lavaran, A. (1881). *Compt'es Rendus de lAcademie des Sciences*.

Le Roch, K.G., Zhou, Y., Blair, P.L., Grainger, M., Moch, J.K., Haynes, J.D. *et al*. (2003). Discovery of gene function by expression profiling of the malaria parasite life cycle. *Science* **301**, 1503-1508.

Leary, S.C., Winge, D.R. and Cobine, P.A. (2009). "Pulling the plug" on cellular copper: the role of mitochondria in copper export. *Biochimica et Biophysica Acta* **1793**, 146-153.

Lee, J., Prohaska, J.R., Dagenais, S.L., Glover, T.W. and Thiele, D.J. (2000). Isolation of a murine copper transporter gene, tissue specific expression and functional complementation of a yeast copper transport mutant. *Gene* **254**, 87-96.

Lee, J., Prohaska, J.R. and Thiele, D.J. (2001). Essential role for mammalian copper transporter Ctr1 in copper homeostasis and embryonic development. *Proceedings of the National Academy of Sciences of the United States of America* **98**, 6842-6847.

Lee, J., Pena, M.M., Nose, Y. and Thiele, D.J. (2002). Biochemical characterization of the human copper transporter Ctr1. *The Journal of Biological Chemistry* **277**, 4380-4387.

Lee, S., Howell, S.B. and Opella, S.J. (2007). NMR and mutagenesis of human copper transporter 1 (hCtr1) show that Cys-189 is required for correct folding and dimerization. *Biochimica et Biophysica Acta* **1768**, 3127-3134.

Lee, K., Divis, P.C.S., Zakaria, S.K., Matusop, A., Julin, R.A., Conway, D.J. *et al*. (2011). *Plasmodium knowlesi*: reservoir hosts and tracking the emergence in humans and macaques. *PLoS Pathogens* **7**, e1002015.

Lim L. and McFadden G.I. (2010). The evolution, metabolism and functions of the apicoplast. *Philosophical Transactions of the Royal Society of London. Series B, Biological Sciences* **365**, 749-763.

Linder, M.C. and Hazegh-Azam, M. (1996). Copper biochemistry and molecular biology. *The American Journal of Clinical Nutrition* **63**, 797S-811S.

Lode, A., Kuschel, M., Paret, C. and Rödel, G. (2000). Mitochondrial copper metabolism in yeast: interaction between Sco1p and Cox2p. *FEBS Letters* **485**, 19-24.

Lutsenko, S., Petrukhin, K., Cooper, M.J., Gilliam, C.T. and Kaplan, J.H. (1997). N-terminal domains of human copper-transporting adenosine triphosphatases (the Wilson's and Menkes disease proteins) bind copper selectively *in vivo* and *in vitro* with stoichiometry of one copper per metal-binding repeat. *The Journal of Biological Chemistry* **272**, 18939-18944.

Lutsenko, S. (2010). Human copper homeostasis: a network of interconnected pathways. *Current Opinion in Chemical Biology* **14**, 211-217.

Ma, C. and Chang, G. (2004). Structure of the multidrug resistance efflux transporter EMRe from *Escherichia coli. Proceedings of the National Academy of Sciences of USA* **101**, 2852-2857.

Mabaso, M.L., Sharp, B. and Lengeler, C. (2004). Historical review of malarial control in Southern Africa with emphasis on the use of indoor residual house-spraying. *Tropical Medicine & International Health* **9**, 846-856.

Mackenzie, N.C., Brito, M., Reyes, A.E. and Allende, M.L. (2004). Cloning, expression pattern and essentiality of the high-affinity copper transporter 1 (Ctr1) gene in Zebra fish. *Gene* **328**, 113-120.

Macomber, L., Rensing, C. and Imlay, J.A. (2007). Intracellular copper does not catalyze the formation of oxidative DNA damage in *Escherichia coli. Journal of Bacteriology* **189**, 1616-1626.

Maharaj, R., Mthembu, D.J. and Sharp, B.L. (2005). Impact of DDT re-introduction on malaria transmission in KwaZulu-Natal. *South African Medical Journal* **95**, 871-874.

Makrides, S.C. (1996). Strategies for achieving high-level expression of genes in *Escherichia coli. Microbiological Reviews* **60**, 512-538.

Marti, M., Good, R.T., Rug, M., Knuepfer, E. and Cowman, A.F. (2004). Targeting malaria virulence and remodelling proteins to the host erythrocyte. *Science* **306**, 1930-1933.

Martin, R.E., Henry, R.I., Abbey, J.L., Clements, J.D. and Kirk, K. (2005). The 'permeome' of the malaria parasite: an overview of the membrane transport proteins of *Plasmodium falciparum. Genome Biology* **6**, R26.

Martin, R.E., Ginsburg, H. and Kirk, K. (2009a). Membrane transport proteins of the malaria parasite. *Molecular Microbiology* **74**, 519-528.

Martin, R.E., Marchetti, R.V., Cowan, A.I., Howitt, S.M., Bröer, S. and Kirk, K. (2009b). Chloroquine transport via the malaria parasite's chloroquine resistance transporter. *Science* **325**, 1680-1682.

Maude, R.J., Woodrow, C.J. and White, L.J. (2010). Artemisinin antimalarials: preserving the "magic bullet". *Drug Development Research* **71**, 12-19.

Maxfield, A.B., Heaton, D.N. and Winge, D.R. (2004). Cox17 is functional when tethered to the mitochondrial inner membrane. *The Journal of Biological Chemistry* **279**, 5072-5080.

Mehlin, C., Boni, E., Buckner, F.S., Engel, L., Feist, T., Gelb, M.H. *et al*. (2006). Heterologous expression of proteins from *Plasmodium falciparum*: results from 1000 genes. *Molecular and Biochemical Parasitology* **148**, 144-160.

Mercer, J.F. (2001). The molecular basis of copper-transport diseases. *Trends in Molecular Medicine* **7**, 64-69.

Merchant S.S., Allen M.D., Kropat J. *et al*. (2006). Between a rock and a hard place: trace element nutrition in *Chlamydomonas. Biochimica et Biophysica Acta* **1763**, 578-594.

Merckx, A., Le Roch, K., Nivez, M., Dorin, D., Alano, P., Gutierrez, G.J. *et al*. (2003). Identification and initial characterization of three novel cyclin-related proteins of the human malaria parasite *Plasmodium falciparum. The Journal of Biological Chemistry* **278**, 39839-39850.

Mesecke, N., Terziyska, N., Kozany, C., Baumann, F., Neupert, W., Hell, K. *et al*. (2005). A disulfide relay system in the intermembrane space of mitochondria that mediates protein import. *Cell* **121**, 1059-1069.

Meshnick, S.R., Scott, M.D., Lubin, B., Ranz, A. and Eaton, J.W. (1990). Antimalarial activity of diethyldithiocarbamate: potentiation by copper. *Biochemical Pharmacology* **40**, 213-216.

Mi L. and Zuberbühler A.D. (1992). Cuprous complexes and dioxygen. Part 12. Rate law and mechanism of the copper-catalyzed oxidation of ascorbic acid in aqueous acetonitrile. *Helvetica Chimica Acta* **75**, 1547-1556.

Miller, L.H., Baruch, D.I., Marsh, K. and Doumbo, O.K. (2002). The pathogenic basis of malaria. *Nature* **415**, 673-679.

Moore, D.V. and Lanier, J.E. (1961). Observations on two *Plasmodium falciparum* infections with an abnormal response to chloroquine. *The American Journal of Tropical Medicine and Hygiene* **10**, 5-9.

Muregi, F.W. and Ishih, A. (2010). Next-generation antimalarial drugs: hybrid molecules as a new strategy in drug design. *Drug Development Research* **71**, 20-32.

Murthy A.S., Mains R.E. and Eipper B.A. (1986). Purification and characterization of peptidylglycine alpha-amidating monooxygenase from bovine neurointermediate pituitary. *Journal of Biological Chemistry* **261**, 1815-1822.

Nallamsetty, S. and Waugh, D.S. (2007). A generic protocol for the expression and purification of recombinant proteins in *Escherichia coli* using a combinatorial His_6-maltose binding protein fusion tag. *Nature Protocols* **2**, 383-391.

Narum, D.L., Kumar, S., Rogers, W.O., Fuhrmann, S.R., Liang, H., Oakley, M. *et al*. (2001). Codon optimization of gene fragments encoding *Plasmodium falciparum* merzoite proteins enhances DNA vaccine protein expression and immunogenicity in mice. *Infection and Immunity* **69**, 7250-7253.

Nobrega, M.P., Bandeira, S.C.B., Beers, J. and Tzagoloff, A. (2002). Characterization of Cox19, a widely distributed gene required for expression of mitochondrial cytochrome oxidase. *The Journal of Biological Chemistry* **277**, 40206-40211.

Noedl, H., Se, Y., Schaecher, K., Smith, B.L., Socheat, D., Fukuda, M.M. (2008). Evidence of artemisinin-resistant malaria in Western Cambodia. *The New England Journal of Medicine* **359**, 2619-2620.

Nominé, Y., Ristriani, T., Laurent, C., Lefèvre, J.F., Weiss E and Travé, G. (2001a). A strategy for optimizing the monodispersity of fusion proteins: application to purification of recombinant HPV-E6 oncoprotein. *Protein Engineering* **14**, 297-305.

Nominé, Y., Ristriani, T., Laurent, C., Lefèvre, J.F., Weiss E and Travé, G. (2001b). Formation of soluble inclusion bodies by HPV-E6 oncoprotein fused to maltose-binding protein. *Protein Expression and Purification* **23**, 22-32.

Nose, Y., Rees, E.M. and Thiele, D.J. (2006). Structure of the Ctr1 copper trans'PORE'ter reveals novel architecture. *Trends in Biochemical Sciences* **31**, 604-607.

Nunes, M.C., Goldring, J.P.D., Doerig, C. and Scherf, A. (2007). A novel protein kinase family in *Plasmodium falciparum* is differentially transcribed and secreted to various cellular compartments of the host cell. *Molecular Microbiology* **63**, 391-403.

O'Halloran T.V. and Culotta V.C. (2000). Metallochaperones, an intracellular shuttle service for metal ions. *The Journal of Biological Chemistry* **275**, 25057-25060.

Olliaro, P.L. and Yuthavong, Y. (1999). An overview of chemotherapeutic targets for antimalarial drug discovery. *Pharmacology & Therapeutics* **81**, 91-110.

Ooi, C.E., Rabinovich, E., Dancis, A., Bonifacino, J.S. and Klausner, R.D. (1996). Copper-dependent degradation of the *Saccharomyces cerevisiae* plasma membrane copper transporter Ctr1p in the apparent absence of endocytosis. *The EMBO Journal* **15**, 3515-3523.

Outchkourov, N.S., Roeffen, W., Kaan, A., Jansen, J., Luty, A., Schuiffel, D. *et al*. (2008). Correctly folded pfs48/45 protein of *Plasmodium falciparum* elicits malaria transmission-blocking immunity in mice. *Proceedings of the National Academy of Sciences of the United States of America* **105**, 4301-4305.

Punter F.A. and Glerum D.M. (2003). Mutagenesis reveals a specific role for Cox17p in copper transport to cytochrome oxidase. *The Journal of Biological Chemistry* **278**, 30875-30880.

Pain, A., Böhme, U., Berry, A.E., Mungall, K., Finn, R.D., Jackson, A.P. *et al*. (2008). The genome of the simian and human malaria parasite *Plasmodium knowlesi. Nature* **455**, 799-803.

Palumaa, P., Kangur, L., Voronova, A. and Sillard, R. (2004). Metal-binding mechanism of Cox17, a copper chaperone for cytochrome-c oxidase. *The Biochemical Journal* **382**, 307-314.

Perkins S.L. and Schall J.J. (2002). A molecular phylogeny of malarial parasites recovered from cytochrome b gene sequences. *The Journal of Parasitology* **88**, 972-978.

Planson, A., Guijarro, J.I., Goldberg, M.E. and Chaffotte, A.F. (2003). Assistance of maltose binding protein to the *in vivo* folding of the disulfide-rich C-terminal fragment from *Plasmodium falciparum* merozoite surface protein 1 expressed in *Escherichia coli. Biochemistry* **42**, 13202-13211.

Polson, A., Coetzer, T., Kruger, J., von Maltzahn, E. and van der Merwe, K.J. (1985). Improvements in the isolation of IgY from the yolks of eggs laid by immunized hens. *Immunological Investigations* **14**, 323-327.

Predki, P.F. and Sarkar, B. (1992). Effect of replacement of "zinc finger" zinc on estrogen receptor DNA interactions. *The Journal of Biological Chemistry* **267**, 5842-5846.

Puig, S. and Thiele, D.J. (2002). Molecular mechanisms of copper uptake and distribution. *Current Opinion in Chemical Biology* **6**, 171-180.

Puig, S., Lee, J., Lau, M. and Thiele, D.J. (2002a). Biochemical and genetic analyses of yeast and human high affinity copper transporters suggest a conserved mechanism for copper uptake. *The Journal of Biological Chemistry* **277**, 26021-26030.

Puig S., Rees E.M. and Thiele D.J. (2002b). The ABCD's of periplasmic copper trafficking. *Structure* **10**, 1292-1295.

Pukrittayakamee, S., Chotivanich, K., Chantra, A., Clemens, R., Looareesuwan, S. and White, N.J. (2004). Activities of artesunate and primaquine against asexual- and sexual-stage parasites in *falciparum* malaria. *Antimicrobial Agents and Chemotherapy* **48**, 1329-1334.

Punter, F.A. and Glerum, D.M. (2003). Mutagenesis reveals a specific role for Cox17p in copper transport to cytochrome oxidase. *The Journal of Biological Chemistry* **278**, 30875-30880.

Rae, T.D., Schmidt, P.J., Pufahl, R.A., Culotta, V.C. and O'Halloran, T.V. (1999). Undetectable intracellular free copper: the requirement of a copper chaperone for superoxide dismutase. *Science* **284**, 805-808.

Ralle, M., Lutsenko, S. and Blackburn, N.J. (2004). Copper transfer to the N-terminal domain of the Wilson disease protein (ATP7b): X-ray absorption spectroscopy of reconstituted and chaperone-loaded metal binding domains and their interaction with exogenous ligands. *Journal of Inorganic Biochemistry* **98**, 765-774.

Ralph S.A., van Dooren G.G., Waller R.F. *et al*. (2004). Tropical infectious diseases: metabolic maps and functions of the *Plasmodium falciparum* apicoplast. *Nature Reviews. Microbiology* **2**, 203-216.

Rasoloson, D., Shi, L., Chong, C.R., Kafsack, B.F. and Sullivan, D.J. (2004). Copper pathways in *Plasmodium falciparum* infected erythrocytes indicate an efflux role for the copper p-ATPase. *The Biochemical Journal* **381**, 803-811.

Rathore D., Wahl A.M., Sullivan M. *et al*. (2001). A phylogenetic comparison of gene trees constructed from plastid, mitochondrial and genomic DNA of *Plasmodium* species. *Molecular and Biochemical Parasitology* **114**, 89-94.

Rees, E.M. and Thiele, D.J. (2004). From aging to virulence: forging connections through the study of copper homeostasis in eukaryotic microorganisms. *Current Opinion in Microbiology* **7**, 175-184.

Rees, E.M., Lee, J. and Thiele, D.J. (2004). Mobilization of intracellular copper stores by the Ctr2 vacuolar copper transporter. *The Journal of Biological Chemistry* **279**, 54221-54229.

Rees, E.M. and Thiele, D.J. (2007). Identification of a vacuole-associated metalloreductase and its role in Ctr2-mediated intracellular copper mobilization. *The Journal of Biological Chemistry* **282**, 21629-21638.

Reininger L., Billker O., Tewari R. *et al*. (2005). A NIMA-related protein kinase is essential for completion of the sexual cycle of malaria parasites. *The Journal of Biological Chemistry* **280**, 31957-31964.

Rensing, C. and Grass, G. (2003). *Escherichia coli* mechanisms of copper homeostasis in a changing environment. *FEMS Microbiology Reviews* **27**, 197-213.

Riggio, M., Lee, J., Scudiero, R., Parisi, E., Thiele, D.J. and Filosa, S. (2002). High affinity copper transport protein in the lizard *Podarcis sicula*: Molecular cloning, functional characterization and expression in somatic tissues, follicular oocytes and eggs. *Biochimica et Biophysica Acta* **1576**, 127-135.

Rissler, M., Wiedemann, N., Pfannschmidt, S., Gabriel, K., Guiard, B., Pfanner, N. *et al*. (2005). The essential mitochondrial protein ERV1 cooperates with Mia40 in biogenesis of intermembrane space proteins. *Journal of Molecular Biology* **353**, 485-492.

Rodrigues, M.H.C., Cunha, M.G., Machado, R.L., Ferreira, O.C.J., Rodrigues, M.M. and Soares, I.S. (2003). Serological detection of *Plasmodium vivax* malaria using recombinant proteins corresponding to the 19-kDa C-terminal region of the merozoite surface protein-1. *Malaria Journal* **2**, 39.

Rosenthal, P.J. (2003). Antimalarial drug discovery: old and new approaches. *The Journal of Experimental Biology* **206**, 3735-3744.

Rosenzweig A.C. (2001). Copper delivery by metallochaperone proteins. *Accounts of Chemical Research* **34**, 119-128.

Rosenzweig, A.C. (2002). Metallochaperones: bind and deliver. *Chemistry & Biology* **9**, 673-677.

Ross, R. (1899). Life history of the parasites of malaria. *Nature* **60**, 322.

Sachdev, D. and Chirgwin, J.M. (1999). Properties of soluble fusions between mammalian aspartic proteinases and bacterial maltose-binding protein. *Journal of Protein Chemistry* **18**, 127-136.

Sachs, J. and Malaney, P. (2002). The economic and social burden of malaria. *Nature* **415**, 680-685.

Sambrook, J., Fritsch, E.F. and Maniatis, T. (1989a). Enzymes used in molecular cloning. In *Molecular cloning: A laboratory manual*. C. Nolan (Ed.). 5.3 - 5.90.

Sambrook, J., Fritsch, E.F. and Maniatis, T. (1989b). Plasmid vectors. In *Molecular cloning: A laboratory manual*. C. Nolan (Ed.). 1.3 - 1.105.

Sanni, L.A., Fonseca, L.F. and Langhorne, J. (2002). Mouse models for erythrocytic-stage malaria. *Methods in Molecular Medicine* **72**, 57-76.

Saravanan, P. and Kumar, S. (2009). Diagnostic and immunoprophylactic applications of synthetic peptides in veterinary microbiology. *Microbiology Research* **1**, 1-6.

Schafer, F.Q. and Buettner, G.R. (2001). Redox environment of the cell as viewed through the redox state of the glutathione disulfide/glutathione couple. *Free Radical Biology & Medicine* **30**, 1191-1212.

Schägger, H. (2006). Tricine-SDS-PAGE. *Nature Protocols* **1**, 16-22.

Schushan, M., Barkan, Y., Haliloglu, T. and Ben-Tal, N. (2010). Carbonα-trace model of the transmembrane domain of human copper transporter 1, motion and functional implications. *Proceedings of the National Academy of Sciences of the United States of America* **107**, 10908-10913.

Sharp, P.A. (2003). Ctr1 and its role in body copper homeostasis. *The International Journal of Biochemistry & Cell Biology* **35**, 288-291.

Shcolnick S. and Keren N. (2006). Metal homeostasis in Cyanobacteria and chloroplasts. Balancing benefits and risks to the photosynthetic apparatus. *Plant Physiology* **141**, 805-810.

Shields G.S., Markowitz H., Klassen W.H. *et al*. (1961). Studies on copper metabolism. XXXI. Erythrocyte copper. *The Journal of Clinical Investigation* **40**, 2007-2015.

Shim, H. and Harris, Z.L. (2003). Genetic defects in copper metabolism. *The Journal of Nutrition* **133**, 1527S-31S.

Sibley, C.H., Hyde, J.E., Sims, P.F., Plowe, C.V., Kublin, J.G., Mberu, E.K. *et al*. (2001). Pyrimethamine-sulfadoxine resistance in *Plasmodium falciparum*: what next?. *Trends in Parasitology* **17**, 582-588.

Singh, S.P., Khan, F. and Mishra, B.N. (2010). Computational characterization of *Plasmodium falciparum* proteomic data for screening of potential vaccine candidates. *Human Immunology* **71**, 136-143.

Smithius, F.M., Monti, F., Grundi, M., Zaw Oo, A., Kyaw, T.T., Phe, O. *et al*. (1997). *Plasmodium falciparum*: sensitivity *in vivo* to chloroquine, pyrimethamine/sulfadoxine and mefloquine in Western Myanmar. *Transactions of the Royal Society of Tropical Medicine and Hygiene* **91**, 468-472.

Sørensen, H.P. and Mortensen, K.K. (2005a). Advanced genetic strategies for recombinant protein expression in *Escherichia coli. Journal of Biotechnology* **115**, 113-128.

Sørensen, H.P. and Mortensen, K.K. (2005b). Soluble expression of recombinant proteins in the cytoplasm of *Escherichia coli. Microbial Cell Factories* **4**, 1.

Srinivasan, C., Posewitz, M.C., George, G.N. and Winge, D.R. (1998). Characterization of the copper chaperone Cox17 of *Saccharomyces cerevisiae. Biochemistry* **37**, 7572-7577.

Srivastava, P., Arif, A.J., Singh, C. and Pandey, V.C. (1997). N-Acetyl penicillamine a protector of *Plasmodium berghei* induced stress organ injury in mice. *Pharmacological Research* **36**, 305-307.

Staines, H.M., Derbyshire, E.T., Slavic, K., Tattersall, A., Vial, H. and Krishna, S. (2010). Exploiting the therapeutic potential of *Plasmodium falciparum* solute transporters. *Trends in Parasitology* **26**, 284-296.

Stephens L.L., Shonhai A. and Blatch G.L. (2011). Co-expression of the *Plasmodium falciparum* molecular chaperone, PfHsp70, improves the heterologous production of the antimalarial drug target GTP-cyclohydrolase I, PfGCHI. *Protein Expression and Purification* **77**, 159-165.

Stoute, J.A., Slaoui, M., Heppner, D.G., Momin, P., Kester, K.E., Desmons, P. *et al*. (1997). A preliminary evaluation of a recombinant circumsporozoite protein vaccine against *Plasmodium falciparum* malaria. RTS,S malaria vaccine evaluation group. *The New England Journal of Medicine* **336**, 86-91.

Sun, P., Schwenk, R., White, K., Stoute, J.A., Cohen, J., Ballou, W.R. *et al*. (2003). Protective immunity induced with malaria vaccine, RTS,S is linked to *Plasmodium falciparum* circumsporozoite protein-specific $CD4^+$ and $CD8^+$ T-cells producing IFN-gamma. *Journal of Immunology* **171**, 6961-6967.

Takahashi, Y., Kako, K., Kashiwabara, S., Takehara, A., Inada, Y., Arai, H. *et al*. (2002). Mammalian copper chaperone Cox17p has an essential role in activation of cytochrome-c oxidase and embryonic development. *Molecular and Cellular Biology* **22**, 7614-7621.

Tapiero, H., Townsend, D.M. and Tew, K.D. (2003). Trace elements in human physiology and pathology. Copper. *Biomedicine & Pharmacotherapy* **57**, 386-398.

Templeton T.J., Iyer L.M., Anantharaman V. *et al*. (2004). Comparative analysis of Apicomplexa and genomic diversity in eukaryotes. *Genome Research* **14**, 1686-1695.

Thompson, J.D., Higgins, D.G. and Gibson, T.J. (1994). Clustal W: Improving the sensitivity of progressive multiple sequence alignment through sequence weighting, position-specific gap penalties and weight matrix choice. *Nucleic Acids Research* **22**, 4673-4680.

Thornton, J.M. (1981). Disulphide bridges in globular proteins. *Journal of Molecular Biology* **151**, 261-287.

Towbin, H., Staehelin, T. and Gordon, J. (1979). Electrophoretic transfer of proteins from polyacrylamide gels to nitrocellulose sheets: procedure and some applications. *Proceedings of the National Academy of Sciences of the United States of America* **76**, 4350-4354.

Toye, P., Nyanjui, J., Goddeeris, B. and Musoke, A.J. (1996). Identification of neutralization and diagnostic epitopes on PIM, the polymorphic immunodominant molecule of *Theileria parva. Infection and Immunity* **64**, 1832-1838.

Travassos, M.A. and Laufer, M.K. (2009). Resistance to antimalarial drugs: molecular, pharmacologic, and clinical considerations. *Pediatric Research* **65**, 64R-70R.

Tren, R. and Bate, R. (2004). Policy analysis: South Africa's war against malaria – lessons for the developing world. Cato Institute, Washington D.C.

Tsukihara, T., Aoyama, H., Yamashita, E., Tomizaki, T., Yamaguchi, H., Shinzawa-Itoh, K. *et al*. (1996). The whole structure of the 13-subunit oxidized cytochrome-c oxidase at 2.8 Å. *Science* **272**, 1136-1144.

Turgut-Balik, D., Akbulut, E., Shoemark, D.K., Celik, V., Moreton, K.M., Sessions, R.B. *et al*. (2004). Cloning, sequence and expression of the lactate dehydrogenase gene from the human malaria parasite, *Plasmodium vivax. Biotechnology Letters* **26**, 1051-1055.

Tusnády G E and Simon I. (2001). The HMMTOP transmembrane topology prediction server. *Bioinformatics* **17**, 849-850.

Tuteja, R. (2007). Malaria - an overview. *The FEBS Journal* **274**, 4670-4679.

van den Berghe, P.V.E., Folmer, D.E., Malingré, H.E.M., van Beurden, E., Klomp, A.E.M., van de Sluis, B. *et al*. (2007). Human copper transporter 2 is localized in late endosomes and lysosomes and facilitates cellular copper uptake. *The Biochemical Journal* **407**, 49-59.

van den Ende, J. and van Gompel, A. (1997). Clinical aspects of malaria. Organizzazione per la Cooperazione Sanitaria Internazionale, Bologna. 79-96.

van Dooren G.G., Stimmler L.M. and McFadden G.I. (2006). Metabolic maps and functions of the *Plasmodium* mitochondrion. *FEMS Microbiology Reviews* **30**, 596-630.

van Lin, L.H., Pace, T., Janse, C.J., Birago, C., Ramesar, J., Picci, L. *et al*. (2001). Interspecies conservation of gene order and intron-exon structure in a genomic locus of high gene density and complexity in *Plasmodium. Nucleic Acids Research* **29**, 2059-2068.

Vasina, J.A. and Baneyx, F. (1997). Expression of aggregation-prone recombinant proteins at low temperatures: a comparative study of the *Escherichia coli* cspa and tac promoter systems. *Protein Expression and Purification* **9**, 211-218.

Vaughan, A., Chiu, S., Ramasamy, G., Li, L., Gardner, M.J., Tarun, A.S. *et al*. (2008). Assessment and improvement of the *Plasmodium yoelii yoelii* genome annotation through comparative analysis. *Bioinformatics* **24**, i383-9.

Vaughan A.M., O'Neill M.T., Tarun A.S. *et al*. (2009). Type II fatty acid synthesis is essential only for malaria parasite late liver stage development. *Cellular Microbiology* **11**, 506-520.

Vedadi, M., Lew, J., Artz, J., Amani, M., Zhao, Y., Dong, A. *et al*. (2007). Genome-scale protein expression and structural biology of *Plasmodium falciparum* and related Apicomplexan organisms. *Molecular and Biochemical Parasitology* **151**, 100-110.

Vera, A., González-Montalbán, N., Arís, A. and Villaverde, A. (2007). The conformational quality of insoluble recombinant proteins is enhanced at low growth temperatures. *Biotechnology and Bioengineering* **96**, 1101-1106.

Voronova, A., Kazantseva, J., Tuuling, M., Sokolova, N., Sillard, R. and Palumaa, P. (2007a). Cox17, a copper chaperone for cytochrome c oxidase: Expression, purification, and formation of mixed disulphide adducts with thiol reagents. *Protein Expression and Purification* **53**, 138-144.

Voronova, A., Meyer-Klaucke, W., Meyer, T., Rompel, A., Krebs, B., Kazantseva, J. *et al*. (2007b). Oxidative switches in functioning of mammalian copper chaperone cox17. *The Biochemical Journal* **408**, 139-148.

Warhurst, D.C. and Williams, J.E. (1996). Laboratory diagnosis of malaria. *Journal of Clinical Pathology* **49**, 533-538.

Welling, G.W., Weijer, W.J., van der Zee, R. and Welling-Wester, S. (1985). Prediction of sequential antigenic regions in proteins. *FEBS Letters* **188**, 215-218.

White, N.J. (1992). Pathophysiology of malaria. Academic Press, London. 83-173.

White, N.J. (2008). The role of anti-malarial drugs in eliminating malaria. *Malaria Journal* **7 Suppl 1**, S8.

Winter, V.J., Cameron, A., Tranter, R., Sessions, R.B. and Brady, R.L. (2003). Crystal structure of *Plasmodium berghei* lactate dehydrogenase indicates the unique structural differences of these enzymes are shared across the *Plasmodium* genus. *Molecular and Biochemical Parasitology* **131**, 1-10.

Winzeler, E.A. (2008). Malaria research in the post-genomic era. *Nature* **455**, 751-756.

World Health Organisation. (2009). World malaria report, 2009. WHO Press, Geneva .

World Health Organisation. (2010). World malaria report 2010. WHO Press, Geneva .

Xiao, Z. and Wedd, A.G. (2002). A C-terminal domain of the membrane copper pump Ctr1 exchanges copper(I) with the copper chaperone Atx1. *Chemical Communications*, 588-589.

Xiao, Z., Loughlin, F., George, G.N., Howlett, G.J. and Wedd, A.G. (2004). C-terminal domain of the membrane copper transporter ctr1 from *Saccharomyces cerevisiae* binds four Cu(I) ions as a cuprous-thiolate polynuclear cluster: Sub-femtomolar Cu(I) affinity of three proteins involved in copper trafficking. *Journal of the American Chemical Society* **126**, 3081-3090.

Yamauchi, L.M., Coppi, A., Snounou, G. and Sinnis, P. (2007). *Plasmodium* sporozoites trickle out of the injection site. *Cellular Microbiology* **9**, 1215-1222.

Zanier, K., Nominé, Y., Charbonnier, S., Ruhlmann, C., Schultz, P., Schweizer, J. *et al*. (2007). Formation of well-defined soluble aggregates upon fusion to MBP is a generic property of E6 proteins from various human *Papillomavirus* species. *Protein Expression and Purification* **51**, 59-70.

Zhou, B. and Gitschier, J. (1997). HCtr1: a human gene for copper uptake identified by complementation in yeast. *Proceedings of the National Academy of Sciences of the United States of America* **94**, 7481-7486.

Zhou, H., Cadigan, K.M. and Thiele, D.J. (2003). A copper-regulated transporter required for copper acquisition, pigmentation, and specific stages of development in *Drosophila melanogaster. The Journal of Biological Chemistry* **278**, 48210-48218.